

Intelligent Decision Support for Business Workflow Adaptation due to Subjective Interruption

Kohei Sugawara(1)¹ and Hamido Fujita(2)

(1) Sangikyo Corporation 4509, Ikebe-cho, Tsuzuki-ku, Yokohama, 224-0053, Japan, e-mail: sugawarak@sangikyo.co.jp

(2) Iwate Prefectural University, Faculty of Software and Information Science, 152-52 Aza-Sugo, Takizawa, Iwate-gun, Iwate, 020-0193, Japan, e-mail: issam@iwate-pu.ac.jp

Abstract: Interruption is occurred by partial participation of workflows with adding new activity to a worker. A concerned worker to the interrupted workflow must restructure task assignment to improve consumed operating time by interruption. An opportunity of decision making is occurred to the workers to select appropriate tasks. However, pre-assignment of tasks to workers includes an expectation of superior decision maker to a training of an inexperienced worker. In order to avoid overmuch improvement to the interrupted workflow, the alternatives for shortening operating time of tasks is computed by TOPSIS method. Although positive ideal solution and negative ideal solution in conventional TOPSIS method are based on objective attributes, subjective completion time of pre-assigned tasks that are positive ideal solution in this model is depending on subjective attributes of the worker. Therefore, this research proposes a novel extension of positive and negative ideal solution of TOPSIS method by aggregating based on subjective fuzzy attributes of the worker and objective attributes of tasks. The approach is examined on simple case study showing that the work is promising on providing solution to handle interruption on carried work in runtime.

Keywords: Interruption; Workflow; Decision making; Subjective attributes; TOPSIS

¹ This research is done through the 1st author enrollment as Doctor student, the results achieved is part of the Doctor dissertation at Iwate Prefectural University, Japan supervised by Prof. Hamido Fujita.

1 Introduction

In a working environment, opportunity of decision making by worker is occurred to generate higher profit or to eliminate severe loss. Herbert A. Simon defined three decision making processes that are Intelligence Activity, Design Activity and Choice Activity [1]. According to this definition, the worker who is a decision maker for operating assigned tasks must retrieve information to formulate alternatives by analyzing context of related tasks. The worker chooses appropriate decision after evaluating developed alternatives. Context of target tasks selected by the worker consists of objective attributes that are gettable several innate profits by task operation and costs to achieve pre-assigned objective. The worker selects appropriate task according to multi criteria of objective attributes that each task has. Tasks for getting profits are assigned to the workers depending on objective of organization as criteria for appropriate task selection of the worker by superior decision maker who could be manager, project leader or customer. Assigned tasks to the workers are structured to get profits for belonging organization of the workers by steps as workflow through consideration of experts. The worker has subjective attributes for task operation based on worker's profile such as experience or operational skill. Degree of expected profits by operating task is changed by applying subjective attributes of the worker to objective attributes of task through task assignment. Expected profits for the organization by assigning tasks are increased by improving work efficiency of current work or forthcoming work. Work efficiency of current work is improved by reducing labor cost that is engagement time of the worker to the assigned task while keeping achievement of the task. Completion time of task as engagement time of the worker is shortened by assigning experienced worker. Although the completion time of task by inexperienced worker is longer than experienced worker, applicable experience for forthcoming similar task is accumulated with time by engaging to the task. Therefore, shortening time for improvement of work efficiency in current task and experience to forthcoming work are trade-off. Weights of each criterion for the appropriate task selection are affected dynamically by an external interference to the worker. The external interference to the worker generates new activity to current workflow of the worker. Corragio (1990) defines an interruption as an "externally-generated, randomly occurring, discrete event that breaks continuity of cognitive focus on a primary task" [2]. Interruption of operation continuity by the worker on the workflow is occurred by invoking new or updates another task of the worker. In other words, interruption is occurred by partial participation of multiple workflows. Interruption would produce positive or negative effect to the worker and the current workflow. Interruption is formalized through two parametric views that are time and context. The time parametric view of interruption is related to operating time of the generated task and completion time of interrupted workflow. The degree of positive or negative effect to forward the current workflow can be represented by normalizing time of the interruption. The context parametric view of interruption

is related to operation and process to the current workflow. The context of the generated task by interruption is analyzed to formulate alternatives based on influenced elements of interruption. Although interruption by non-task such as taking rest or enjoying hobby has positive effect to efficiency of the current workflow by improving mental or physical tiredness, any interruption generates negative effect to the current workflow in time parametric view point. Starting time of subsequent tasks on the interrupted workflow is delayed by consuming time for the interruption. Each weight of criteria for selecting appropriate task is changed to improve the delay of the current workflow by re-assigning tasks of inexperienced worker to experienced worker. There are many approaches for improving work efficiency by handling resources of workers such as job scheduling problem or flow shop scheduling [3], [4]. Although conventional scheduling problem approaches can optimize work efficiency by scheduling, reduction of experience for inexperienced workers due to assigning tasks to experienced worker are not discussed. Task assignment for improvement of too higher efficiency decreases work opportunity of inexperienced worker. The expected profits of pre-assignment for forthcoming work are reduced by the negative effect of interruption and overmuch improvement by re-assigning tasks. In order to minimize the payoff of expected profit for forthcoming work, the appropriate task selection of the worker in interruption must approximate to the expected profit by pre task assignment as an ideal task selection through the superior decision maker. Leaving time (disengagement) of the current workflow due to interruption generates negative effects to short term memory of the interrupted worker because of forgetting the task of workflow. Memory of the interrupted worker for the interrupted work is reduced with time. Relation of both time and degree of decreasing memory is represented by Ebbinghaus's Forgetting Curve [5]. Negative effect of the lacked working memory is appeared when past task is resumed from added tasks. By leaving from the interrupted work, usable time for the interrupted workflow is consumed and accuracy of decision making for the interrupted work is decreased [6]. Experienced worker can decide appropriate task according to own judgment heuristics [7]. The accuracy of decision making by experienced worker also is reduced after long time interruption. Therefore, the authenticity of experienced worker's decision making for selecting appropriate tasks of the current workflow is decreased by interruption. Previously, authors discussed about decision support system algorithm for generated task by estimating interruption context according to working history and by using knowledge mining [8]. The previously proposed system assists operation of new task to reduce time consuming for interruption by recommending appropriate alternatives. In addition to the above issue, concerned workers of the interrupted workflow must restructure operation for the workflow according to the effected situation by interruption. The section 2 is shown the outline of the proposed approach for supporting decision making of appropriate task selection of worker.

2 Proposed Approach

Decision making, for the appropriate task selection in interruption, is improvement of affected work efficiency to the current workflow caused by interruption. Effective alternatives for concerned workers of the interrupted workflow can be ranked according to multi criteria for related tasks, for example through AHP (Analytical Hierarchical Process) [9] or other techniques [10] [11]. The attributes for weighting criteria in the interruption model are classified into two aspects; objective attributes and subjective attributes that are based on nature of the attributes. The objective attributes for weighting the criteria means static objective of organizations. A worker who is employed by organization is oriented to objective of the organization by company strategy. The objective of organization is aggregation of multi criteria attributes for stakeholders in a company. The criteria of task assignment by superior decision maker include work efficiency of workers for benefit of the organization and training for workers that leads to organization benefits in its progress. Meanwhile, the subjective attributes means dynamic changing work environment that consists of fuzzy elements of workers and tasks. Since completion time of tasks are depending on assigned worker's operational skill to task, the situation of interruption for operating workflow is consisted by using the subjective attributes of workers for related tasks. Therefore, the proposed weights of multi criteria are computed by aggregating the objective attributes for tasks aligned on the subjective attributes of workers. The interrupted workers must select appropriate task in dynamic work changing environment within the objective of organization. In addition, the concerned workers to the interrupted workflow must avoid the overmuch improvement to keep the expected profit for organization. There are following multi criteria decision making techniques for approaching alternatives to positive ideal solution. TOPSIS method (Technique for Order of Preference by Similarity to Ideal Solution) [12] can compute best solution to the worker in this situation by setting an ideal objective of an organization as positive ideal solution. Although VIKOR method (Vlse Kriterijumska Optimizacija Kompromisno Resenje) [13] also can rank by using positive ideal solution and negative ideal solution, appropriate alternatives in interruption must distance the negative ideal solution to keep the expected profit of inexperienced worker. Fuzzy TOPSIS [14] can extend crisp values of positive and negative ideal solution in traditional TOPSIS by weighting criteria as objective attributes. The objective attributes of the organization is aggregation of subjective attributes that is dependable on worker's experience (extracted from works preferences). Therefore, this research proposes a novel extension of positive and negative ideal solutions of TOPSIS method by aggregation based on subjective fuzzy attributes of the worker. There are approaches for setting ideal solution by aggregating individual decision making as group decision [15], [16]. Although consensus for appropriate decision making can be improved by including individual decisions as group decision, the proposed approach does not require multiple decisions because the ideal solution in

interruption is computed based on the subjective attributes of workers. Alternatives for appropriate task selection in interruption must improve delay of workflow to achieve by deadline of the workflow. There is an approach to reduce the number of AGVs (automated guided vehicles) in container terminals without effect on completion time of workflow [17]. Cost of AGVs in this approach is reduced by computing appropriate order of the container quay crane and AGVs' operation on the basis of modeling by using the pseudo-analysis. Concerned workers in interruption already have tasks for achieving workflow by deadline. Therefore, appropriate order of tasks for improving delay as alternatives must include individual difference of concerned workers' skills as subjective attributes. The consumed time for the current workflow due to interruption can be improved by supporting tasks of inexperienced worker by the experienced worker as formulated alternatives. The improvable subjective completion time of inexperienced worker's task is changed according to degree of supporting worker's experience. Therefore, the proposed alternatives for appropriate task selection in interruption are formulated by computing subjective completion time of task based on experience of workers. The scores of proposed alternatives for positive or negative ideal solution are computed by estimating expected experience of workers in task operation. Each expected experience of alternatives is computed based on proportion of engagement of experienced worker for improving the consumed time by interruption. Operating time of the inexperienced worker is shortened by asking related information for operating task to the experienced worker without gathering information by oneself. Although the subjective completion time of inexperienced worker is shortened by increasing engaging time of the experienced worker for the task of the inexperienced worker, expected experience of workers by pre-assignment as positive ideal solution is decreased by reducing working opportunity of the inexperienced worker. Therefore, appropriate alternatives for the expected experiences by pre-assignment are ranked according to reduced expected experiences to achieve required engaging time of supporting worker for tasks of the interrupted worker. The distance of proposed alternatives to the positive ideal solution is approached by reducing the engaging time of experienced worker for the task of inexperienced worker. The engaging time for supporting each task is changed based on subjective completion time of the experienced workers for each task. The subjective completion time of the supporting worker for improving negative effect by interruption is shortened by giving related information to the task from documentation of the experienced worker to the supporting worker. Document for knowhow is reflected by experience of document creator. Expertise of the document to the task is extracted according to similarity of the context of the task and the document. The expected experience of alternatives is reduced by shortening the subjective completion time of each task of the interrupted worker with the similar document. Since the distance of the positive ideal solution's score and the score of alternatives is shortened by reducing the required engaging time of supporting worker for the tasks of the interrupted worker, the ranking of

appropriate task selection for shortening negative effect of interruption is changed depending on degree of improvement for the tasks by the similar document. In order to recommend appropriate task selection within the negative effect to the workflow caused by interruption, proposed approach utilizes TOPSIS method to rank appropriate alternatives for the interrupted worker by aggregating objective attributes of task and subjective attributes of worker with objective attributes of related documentations. In our approach the workflow is given. Our purpose is to have the execution of the work be kept or optimized based on the interruptions context project by attributes consider as either objective or subjective ones.

2.1 Definition of Target Tasks

Workflow is an optimized representation of steps to achieve work objective by expert worker and specified in optimal manner based on business policy and etc. These steps are ordered as task by eliminating negative cause such as loss of time, duplicative process and so on. The divided task by steps is an action for achieving simple objective task as input of the other task. Task that needs results of the other task as input is ordered after completing the related task. Tasks that have no input or output relations can be reallocated in parallel. The parallel tasks on workflow can be assigned to multiple workers or multiple project members for operating tasks simultaneously. The task on the workflow is activity that needs to be accomplished within defined period of time or by deadline. Objective of each task is achieved by completing operation of worker before the deadline of each task. The length of usable time for the task operation of worker is up to the deadline of the task from the completion time of prior task. The task that has deadline of short period is ordered earlier than task of long period deadline. Entire deadline of the workflow is defined by aggregating estimated completion time of each task. Even if there is similar task in the workflow, order of these tasks is sequential based on different operating period. The order of tasks in the workflow can be changed by keeping the completion time of each task related deadlines. Therefore, selectable tasks for improving work efficiency by the concerned workers to the interrupted workflow are tasks that have finished the related prior tasks as inputs without including already finished tasks. Figure 1 shows matrix for pre-assignment (*PreA*) by the superior decision maker. Number of rows in the matrix of pre-assignment means assigned workers to same workflow. Each operating time (*Ot*) of task according to deadline of the task and operable time period of the assigned worker is substituted to each columns of assigned worker. The coordinates of non-assigned tasks has value of zero.

$$PreA = \begin{pmatrix} Ot_{11} & \cdots & Ot_{1h} \\ \vdots & & \vdots \\ Ot_{g1} & \cdots & Ot_{gh} \end{pmatrix} \quad \begin{array}{l} g = \text{number of workers to the workflow} \\ h = \text{number of tasks to the workflow} \end{array}$$

Figure 1

Matrix for pre-assignment by superior decision maker

2.2 Relation of Time and Experience

Subjective completion time of task is changed depending on tasks' context and experience of workers. The context of task can be classified as physical work and mental work. The physical work is an activity based on physical condition of worker such body related problems, or muscular tension or physical change in office or working space. The physical part of the work is related to the objective attributes of task based an organization's objectives represented as criteria. Meanwhile, the mental work is an activity of information gathering for the steps of the task operation that lead to efficient physical work. Operating time for the mental work is related to searching and analyzing time based on individual experience of workers as subjective attributes. Experienced worker can shorten the time for the mental work by utilizing information for the steps of the task operation based on accumulated experience through a past task operation as knowledge. Workers acquire multiple types of experiences for the mental work depending on context of task through the task operation. The context of task is represented as a set of objective attributes by weighting of operating time of task to each type of experience. Impact for each type of experience on operating time of task can be weighted as fuzzy membership by experienced worker. The membership function of task for each type of experience is shown in following.

$$\sum_{i=1}^l \mu_w(i) = 1.0 \quad \begin{array}{l} \mu_w(i) = \text{weight of each type of experience} \\ l = \text{number of related experiences for task} \end{array} \quad (1)$$

Each value of accumulating experience with a time is evaluated as objective attributes of task by linguistic value of experienced worker. Amount of individual knowledge for workers as the subjective attributes is accumulated by multiplying defined weights of experience ($\mu_w(i)$) and operating time of task. Accumulation of experience is higher for inexperienced worker according to learning curve [18]. In other words, expected experience for experienced worker from task operation is smaller than inexperienced worker. Subjective expected profit by task for each experience ($SPf(i)$) is computed as in the following expression.

$$SPf(i) = \frac{(Ot_{gh} * \mu w(i))}{(Ot_{gh} * \mu w(i)) + We(i)} \quad i = \text{type of experience} \quad (2)$$

$$We(i) = We(i) + SPf(i) \quad We(i) = \text{accumulated experience of worker} \quad (3)$$

Operating time (Ot) for each task is defined by task assignment based on deadline of each task and operable period of workers. The subjective expected profit ($SPf(i)$) for experiences of the task assigned worker is decreased by increasing the past accumulated experiences ($We(i)$) of the worker. Therefore, enhancement of operating task is maximized by assigning tasks of workflow to the inexperienced worker. The time for operating task has essential core time (ct) and improvable time by the experienced worker. The core time (ct) means essential engagement of the worker to the task that includes physical execution or waiting such as running time of machine. Experienced worker can shorten the time for engagement of thinking that includes information gathering for task achievement by utilizing their expertise. Therefore, the core time (ct) that is impossible to shorten by experience is decided by the experienced worker. The subjective completion time (SCt) of task that is changed by amount of experiences of the task assigned worker is computed by crossing the above defined objective attributes of the task to experience. Small expected experience from the task operation means the task assigned worker has related large amount of experience to the task. Impact ($iSPf$) of the time for the engagement of thinking is computed by averaging each subjective expected profit ($SPf(i)$) for the task assigned worker. Following expression represents the subjective completion time (SCt) of the task with the worker.

$$iSPf = \left(\sum_{i=1}^l SPf(i) \right) / l \quad l = \text{number of related experiences for task} \quad (4)$$

$$SCt = ct + (iSPf * (Ot_{gh} - ct)) \quad ct = \text{core time for task operation} \quad (5)$$

The subjective completion time other than the core time is computed by multiplying the impact ($iSPf$) of subjective profits for the task assigned worker to the shortened operating time by experienced worker. The shortened operating time is computed by subtracting the core time from pre-assigned operating time (Ot) based on deadline of the task. Therefore, the subjective completion time (SCt) is maximized by assigning the task to inexperienced worker for the task.

2.3 Setting Positive Ideal Solution and Negative Ideal Solution

Positive ideal solution for decision making of improving work efficiency by TOPSIS method is extracted from expected profits of workers by pre-assignment in the proposed approach. Decision of superior worker who assigned tasks is reflected to avoid the task selection of overmuch improvement for the current

workflow by extracting from pre-assignment as positive ideal solution. Consensus of alternatives for improving effect of interruption is defined by aggregating the weighting of experienced worker and pre task assignment by superior decision maker of the current workflow. Target tasks for improving negative effect of interruption as alternatives on decision making are the confined tasks that have same deadline. The score of positive ideal solution (*PS*) is computed as objective attributes by aggregating each subjective profit for experience of each worker from the target tasks by pre-assignment. Figure 2 shows matrix of the positive ideal solution (*PS*) and negative ideal solution (*NS*) in interruption.

$$PS = \begin{pmatrix} E_{11} & \cdots & E_{1l} \\ \vdots & & \vdots \\ E_{k1} & \cdots & E_{kl} \end{pmatrix} \quad NS = \begin{pmatrix} E'_{11} & \cdots & E'_{1l} \\ \vdots & & \vdots \\ E'_{k1} & \cdots & E'_{kl} \end{pmatrix}$$

$$E_{kl} = \sum_{i=1}^n SPf_1(i) \quad \begin{array}{l} k = \text{number of concerned workers for interruption} \\ l = \text{number of related experiences for task} \\ n = \text{number of target tasks assigned to worker} \end{array}$$

$$E'_{kl} = \sum_{i=1}^n SPf_2(i) \quad \begin{array}{l} SPf_1(i) \text{ is based on pre-assignment} \\ SPf_2(i) \text{ is based on shortest total completion time} \end{array}$$

Figure 2

Matrix of positive ideal solution and negative ideal solution

The expected profits (E_{kl}) of each experience to the task assigned workers are computed by aggregating same experience type of pre-assigned tasks that have same deadline. The number of concerned workers for interruption is selected according to the deadline of assigned tasks on the same workflow. In order to avoid overmuch improvement for the current workflow by restructuring of task assignment, the expected profits (E'_{kl}) of task assignment that have shortest total subjective completion time of related workers within possible combination of task assignment in the interruption is computed as negative ideal solution (*NS*). Number of combinations for the possible task assignment is computed according to the number of workers and deadline of selectable tasks. Therefore, the alternatives that have total expected profits for forthcoming task than pre-assignment are included as improvement for the interruption.

2.4 Context of Task and Documentation

The context of task in proposed approach consists of the terms for classifying each type of experiences and the weighted values of profit to each experience as scalar value. Context of document that is created by experienced worker can be represented based on the used keywords for linguistic classification of the type of experience (μw). Experts conclude the main criteria for workflow, and evaluate

attributes in pair wise fashion based on their strategy etc. The context of document in knowledge base can be represented as vector by counting term frequency of each keyword to compute the relative importance weight of criteria. Therefore relevancy of the target tasks and document of experienced workers are computed with using terms as common features by comparing correlation of two vectors that are the context of the task and the context of the document. The correlation of the two vectors are compared to compute multiple terms of the two vectors on monotonic property by using cosine distance [19]. Figure 3 shows calculation of similarity by cosine distance.

$$\begin{aligned} \vec{p} &= \{\mu w(1), \mu w(2), \dots, \mu w(j)\} \\ \vec{q} &= \{Tm(1), Tm(2), \dots, Tm(j)\} \\ \begin{aligned} p &= \text{vector of the context of task} \\ q &= \text{vector of the context of document} \\ j &= \text{number of common terms} \end{aligned} \end{aligned} \quad \text{Cos}(\vec{p}, \vec{q}) = \frac{\sum_{i=1}^j (\mu w(i) * Tm(i))}{\sqrt{\sum_{i=1}^j (\mu w(i))^2} * \sqrt{\sum_{i=1}^j (Tm(i))^2}}$$

Figure 3

Computing similarity by cosine distance

The vector p consists of proportion of weighted profit for the task ($\mu w(j)$) by classifying named experiences. $Tm(j)$ of the vector q for the documents are normalized to create the vector for analyzing by using term frequency meaning according to terms of the context of task. The similarity of two vectors is higher by approaching score of cosine distance to 1.0.

2.5 Formulating Alternatives with TOPSIS

Appropriate alternatives for ideal expected profits by pre-assignment are formulated based on the subjective completion time of selectable tasks and generated task by interruption. Formulated alternatives must be able to negate to the expected consumed time (ECt) by interruption. The expected consumed time (ECt) is computed by computing the subjective completion time of the generated task by interrupted worker.

$$ECt = ct + (iSPf * (Ot' - ct)) \quad (6)$$

Operating time (Ot') for the generated task by interruption is an operable period of the interrupted worker by deadline of the task. Each worker who is concerned to the target tasks in interruption has subjective flexible time ($SFt(i)$) for usable another tasks based on deadline of pre-assigned tasks and each subjective completion time. Total flexible time ($TSFt(k)$) of the interrupted worker who has multiple tasks can be used for the expected consumed time (ECt) by interruption.

$$SFt(i) = Ot_{gh} - SCt(n) \quad (7)$$

$$TSFt(k) = \sum_{j=1}^n SFt(i) \quad \begin{array}{l} k = \text{number of concerned workers for interruption} \\ n = \text{number of target tasks assigned to worker} \end{array} \quad (8)$$

Achievement of tasks on the current workflow is failed by exceeding the expected consumed time (ECt) from total flexible time ($TSFt(k)$) of the interrupted worker. The subjective flexible time ($SFt(n)$) of each worker also can be utilized to support interrupted worker's tasks. The exceeding time ($EECt$) of the interrupted worker is improved by consuming operating time of the other task within the subjective flexible time of the other worker. Therefore, alternatives ($Alt(x)$) for improving the expected consumed time (ECt) by interruption are formulated based on the supporting time of another worker for improving the exceeding time of the interrupted worker. The required time (Rt) for supporting the interrupted worker is computed based on proportion of exceeding time ($EECt$) for interrupted worker and the impact of subjective profits ($iSPf$) for the experience of supported task by the workers.

$$EECt = ECt - TSFt(k) \quad (ECt > TSFt(k)) \quad (9)$$

$$EECt : iSPf(s) = Rt : iSPf'(s) \quad (10)$$

$$Rt = EECt * \frac{iSPf'(s)}{iSPf(s)} \quad \begin{array}{l} iSPf'(s) \text{ by supporting worker} \\ iSPf(s) \text{ by interrupted worker} \end{array} \quad (11)$$

The subjective expected profits ($SPf(s)$) of supported task for interrupted worker by other worker is computed by subtracting the exceeding time ($EECt$) from the subjective completion time ($SCt(s)$) of the interrupted worker for the supported task as operating time. The subjective expected profits ($SPf(i)$) of the other pre-assigned tasks for the interrupted worker is computed by using the subjective completion time ($SCt(i)$) of the interrupted worker. Total expected profits (Eal) for the interrupted worker who is supported by the other worker in alternatives is computed by aggregating expected profits of the pre-assigned tasks within total flexible time ($TSFt(k)$) of the interrupted worker.

$$SPf(s) = \frac{((SCt(s) - EECt) * \mu w(s))}{(SCt(s) * \mu w(s)) + We(s)} \quad \begin{array}{l} (We(i) = We(s) + SPf(s)) \\ s = \text{type of experience for the supported task} \end{array} \quad (12)$$

$$SPf(i) = \frac{(SCt(i) * \mu w(i))}{(SCt(s) * \mu w(s)) + We(s)} \quad (We(i) = We(i) + SPf(i)) \quad (13)$$

$$Eal = SPf(s) + \sum_{i=1}^{n-1} SPf(i) \quad \begin{array}{l} l = \text{number of related experiences for task} \\ n = \text{number of target tasks assigned to interrupted worker} \end{array} \quad (14)$$

Meanwhile, the total subjective expected profits (Ebt) for the supporting worker as the score of alternatives are computed by aggregating the subjective expected profits ($SPf(s)$) of the supporting task and the subjective expected profits ($SPf(i)$) of pre-assigned tasks to the supporting worker. The negative effect of interruption

is improved by utilizing the subjective flexible time (SFt) of the supporting worker as alternatives. Therefore, the total subjective flexible time ($TSFt$) of the supporting worker must be longer than the required time (Rt) for improving the exceeding time ($EECt$) of the interrupted worker. The subjective expected profit ($SPf(s)$) of the supporting worker for supporting task is acquired by computing the required time (Rt) and impact of subjective profits ($iSPf$) for the supported task.

$$SPf(s) = \frac{(Rt * \mu w(s))}{(Rt * \mu w(s)) + We(s)} \quad (15)$$

$$SPf(i) = \frac{((Ot_{gh} - SFt) * \mu w(i))}{((Ot_{gh} - SFt) * \mu w(i)) + We(i)} \quad \begin{array}{l} (SFt < Rt) \\ (Rt = Rt - SFt) \\ (We(i) = We(i) + SPf(i)) \end{array} \quad (16)$$

$$SPf(i) = \frac{((Ot_{gh} - Rt) * \mu w(i))}{((Ot_{gh} - Rt) * \mu w(i)) + We(i)} \quad \begin{array}{l} (SFt > Rt) \\ (We(i) = We(i) + SPf(i)) \end{array} \quad (17)$$

$$E_{bl} = SPf(s) + \sum_{i=1}^n SPf(i) \quad \begin{array}{l} l = \text{number of related experiences for task} \\ n = \text{number of target tasks assigned to interrupted worker} \end{array} \quad (18)$$

The subjective expected profit ($SPf(i)$) of the supporting worker by pre-assignment is decreased by subtracting applied flexible time (SFt) for supporting from operating time (Ot_{gh}) of the pre-assigned task. When the required time (Rt) for supporting the interrupted worker is longer than the subjective flexible time (SFt) of the task, the required time (Rt) is consumed by utilizing the flexible time of the other tasks of the supporting worker. Distance of alternatives and positive ideal solution (PS) on the expected profits (E_{kl}) of each experience to the workers is shortened by shortening the required time (Rt) for the interrupted worker. The required time (Rt) for the interrupted worker is shorted by increasing an impact of subjective profits ($iSPf''$) of the supporting worker for the supported task. The proposed approach shortens the required time (Rt) of the supporting worker for improving the exceeding time ($EECt$) of the interrupted worker by applying similar document to the supporting worker as experiences for task operation according to experiences ($De(n)$) of document creator. Degree of applied experiences of document creator is computed based on a similarity ($Sm(n)$) of tasks and documents. The impact of subjective profits ($iSPf'''$) for shortening the required time (Rt) with the similar document as alternatives are computed as follows.

$$SPf(s) = \frac{(Ot_{gh} * \mu w(s))}{(Ot_{gh} * \mu w(s)) + (We(s) + (De(s) * Sm(s)))} \quad (19)$$

$$iSPf'''(s) = \left(\sum_{i=1}^l SPf(s) \right) / l \quad l = \text{number of related experiences for task} \quad (20)$$

$$Rt' = EECt * \frac{iSPf''(s)}{iSPf(s)} \quad \begin{matrix} iSPf''(s) \text{ by supporting worker with similar document} \\ iSPf(s) \text{ by interrupted worker} \end{matrix} \quad (21)$$

The alternatives with the similar document shorten only engaged time of thinking such as information gathering. Therefore, the experiences of the document creator are not added to the expected profits of alternatives. Figure 4 shows matrix of alternatives for improving the exceeding time (*EECt*) of the interrupted worker. The scores for concerned workers who do not include the interrupted worker and the supporting worker are substituted same value of the positive ideal solution (*PS*) to the matrix of alternatives (*Alt(x)*).

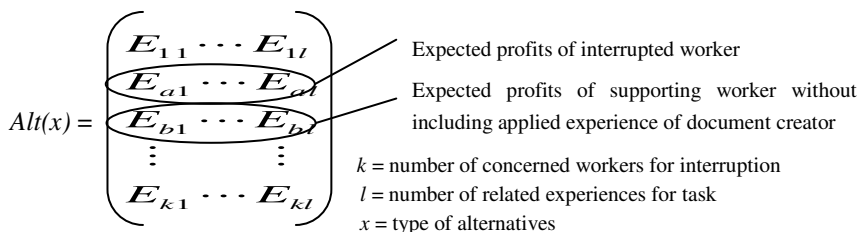


Figure 4
Matrix of alternatives

The formulated alternatives (*Alt(x)*) are ranked by computing scores (*C*) of TOPSIS method based on Euclidean distance of the positive ideal solution (*TDP*) and the negative ideal solution (*TNP*). Each distance of the interrupted worker (*DP(1)*) (*DN(1)*) and the supporting worker (*DP(2)*) (*DN(2)*) to the positive or the negative ideal solution are computed by computing following expressions.

$$DP(1) = \sqrt{\sum_{i=1}^l (E_{kl} - E_{al})^2} \quad DP(2) = \sqrt{\sum_{i=1}^l (E_{kl} - E_{bl})^2} \quad (22)$$

$$DN(1) = \sqrt{\sum_{i=1}^l (E'_{kl} - E_{al})^2} \quad DN(2) = \sqrt{\sum_{i=1}^l (E'_{kl} - E_{bl})^2} \quad (23)$$

$$TDP = \sqrt{\sum_{i=1}^k (DP(k))^2} \quad TDN = \sqrt{\sum_{i=1}^k (DN(k))^2} \quad (24)$$

$$C = \frac{TDN}{TDP + TDN} \quad \begin{matrix} l = \text{number of related experiences for task} \\ k = \text{number of concerned workers for interruption} \end{matrix} \quad (25)$$

3 Case Model of Interruption in Office Work

Interruption of workflow is occurred by overlapping workflows of collaborative work in office work. Concerned workers to the interrupted workflow must improve work efficiency to achieve related tasks. Overmuch improvement must be avoided to keep expected nurture for pre-assigned workers. A system development work is operated with sharing tasks by multiple workers as collaborative work. Workers who have similar role participate to workflow to achieve objective by sharing tasks of the target workflow. The participated workers who have history of developing another system are interrupted by trouble shooting according to user inquiry. The generated activity is operated by interrupted worker till resolving the problem. In order to assist decision making for adaptive task selection in this interruption case, the proposed approach is applied to concerned workers in certain interrupted workflow. Assumed situation model for adaptive task selection in interruption is an actual system development of three workers in a Japanese company. Target three workers who have different working history are developing a sales analysis tool in intra network of the company based on assignment of project leader. The sales analysis tool is developed by using Microsoft Excel with VBA (Visual Basic for Applications). The ranking of adaptive task selection is changed according to the situation of interruption and the subjective attributes of interrupted worker. Firstly, subjective attributes of concerned workers as working experience are computed according to existing working report of two month by using pre-weighted impact of tasks. The focused type of experiences consists of type of computer language, user supporting and specification creation and so on. Table 1 shows sample definitions for weighting impact of experience. The subjective attributes of three target workers are calculated according to working report as Table 2. Each score as the past accumulated experiences ($We(i)$) of each worker in Table 2 is computed by using expression (2)(3) in this paper.

Table 1
Target type of experiences

Type of experiences	Keywords
$We(1)$	Visual Basic
$We(2)$	JavaScript
$We(3)$	HTML
$We(4)$	VBA
$We(5)$	Database
$We(6)$	MS Excel
$We(7)$	User supporting
$We(8)$	Find and fix of bug
$We(9)$	Specification consideration
$We(10)$	System updating
$We(11)$	Document creation

Table 2
The subjective attributes of each worker in two month

	We(1)	We(2)	We(3)	We(4)	We(5)	We(6)	We(7)	We(8)	We(9)	We(10)	We(11)
Worker 1	6.88	9.50	6.75	2.93	7.59	3.60	4.02	4.36	5.91	5.89	4.65
Worker 2	7.38	10.92	6.74	1.00	12.30	1.00	1.00	1.00	7.38	1.00	5.09
Worker 3	1.00	12.13	9.17	2.71	7.18	3.82	1.67	1.00	2.44	1.00	1.00

Worker 1 who has developed first version of the sales analysis tool has experience of web system development. Although Worker 2 has also the experience of the web system development and database development, he is manager who has small experience for VBA development. Worker 3 has experience of supporting development of Worker 1 and he had been trained to develop web application in first month. The positive ideal solution in assumed interruption situation is computed by using each worker's subjective attributes and pre-assignment of tasks. When the interruption is occurred to Worker 1 by adding the task from another workflow as Task 7 due to trouble for another system, operating time for Task 1 and Task 4 of Worker 1 is consumed by generated Task 7. In order to computing appropriate alternatives for improving negative effect of the interruption to Worker 1, the positive ideal solution is computed based on selectable pre-assigned tasks to the concerned workers. Table 3 shows relation of workers and the pre-assigned tasks that have same deadline in assumed interrupted situation. The target workers in this company can work eight hour per day.

Table 3
Relation of pre-assigned tasks

	Operating time	Core time	Assigned worker
Task 1	8.0	5.0	Worker 1
Task 2	8.0	4.0	Worker 2
Task 3	8.0	5.0	Worker 3
Task 4	8.0	4.0	Worker 1
Task 5	8.0	4.0	Worker 2
Task 6	8.0	5.0	Worker 3
Task 7	8.0	5.0	nothing

Table 4 shows scores of weighted tasks by experienced worker. The weights are scored by using fuzzy membership function according to decision of the experienced worker to each task. Task 1 is bug fix activity for improving duplication of inserting data. Task 2 is changing activity of target database for filtering selectable organization function. Task 3 is designing activity for using the system by web browser. Task 4 is improvement activity for showing data quickly on viewer of the system. Task 5 is changing activity of target database for adding data function. Task 6 is design activity for adding data on web browser.

Table 4
Weighted target tasks of same deadline in interruption

	We(1)	We(2)	We(3)	We(4)	We(5)	We(6)	We(7)	We(8)	We(9)	We(10)	We(11)
Task 1	0.1	0.0	0.0	0.0	0.2	0.0	0.2	0.4	0.0	0.1	0.0
Task 2	0.0	0.0	0.0	0.2	0.5	0.3	0.0	0.0	0.0	0.0	0.0
Task 3	0.0	0.1	0.5	0.0	0.1	0.0	0.0	0.0	0.2	0.0	0.1
Task 4	0.0	0.0	0.0	0.5	0.0	0.3	0.0	0.2	0.0	0.0	0.0
Task 5	0.0	0.0	0.0	0.2	0.5	0.3	0.0	0.0	0.0	0.0	0.0
Task 6	0.0	0.1	0.4	0.0	0.1	0.0	0.0	0.0	0.3	0.0	0.1
Task 7	0.1	0.1	0.0	0.0	0.0	0.0	0.4	0.4	0.0	0.0	0.0

The negative effect (ECt) of Task7 to Worker 1 is computed based on the above the subjective attributes of Worker 1 and the objective attributes of Task 7.

$$SPf(1) = \frac{(8.0 * 0.1)}{(8.0 * 0.1) + 6.88} = 0.104 \tag{26}$$

$$SPf(2) = 0.078, \quad SPf(7) = 0.443, \quad SPf(8) = 0.423 \tag{27}$$

$$iSPf = (SPf(1) + SPf(2) + SPf(7) + SPf(8)) / 4 = 0.262 \tag{28}$$

$$ECt = 5.0 + (iSPf * (8.0 - 5.0)) = 5.79 \tag{29}$$

Table 5 shows the computed subjective completion time for each worker according to the subjective attributes of workers and the objective attributes of pre-assigned tasks.

Table 5
Subjective flexible time of pre-assigned tasks

	Completion time	Flexible time	Assigned worker
Task 1	5.66	2.34	Worker 1
Task 2	6.09	1.91	Worker 2
Task 3	5.78	2.22	Worker 3
Task 4	5.66	2.34	Worker 1
Task 5	6.09	1.91	Worker 2
Task 6	5.82	2.18	Worker 3

Therefore, the exceeding time of interrupted worker (Worker 1) is 1.11 hours. The alternatives for appropriate task selection must improve this exceeding time by supporting of other worker.

$$EECt = 5.79 + (2.34 + 2.34) = 1.11 \tag{30}$$

Figure 5 shows the computed matrix of positive ideal solution according to the above pre-assignment of tasks and target worker's subjective attributes.

$$PS = \begin{pmatrix} 0.10, 0.00, 0.00, 0.58, 0.17, 0.40, 0.28, 0.67, 0.00, 0.12, 0.00 \\ 0.00, 0.00, 0.00, 1.11, 0.49, 1.29, 0.00, 0.00, 0.00, 0.00, 0.00 \\ 0.00, 0.12, 0.56, 0.00, 0.20, 0.00, 0.00, 0.00, 0.85, 0.00, 0.80 \end{pmatrix}$$

Figure 5

Matrix of positive ideal solution by pre-assignment

In order to avoid overmuch improvement for the computed exceeding time of Worker 1, each score of the negative ideal solution is computed by using task assignment that is shortest completion time. There are 90 combinations in this situation that three worker operates two tasks from six tasks. The negative ideal solution in Figure 6 is computed by using the task assignment of shortest completion time within 90 combinations.

$$NS = \begin{pmatrix} 0.10, 0.00, 0.00, 0.58, 0.17, 0.40, 0.28, 0.67, 0.00, 0.12, 0.00 \\ 0.00, 0.14, 0.68, 0.00, 0.12, 0.00, 0.00, 0.00, 0.42, 0.00, 0.27 \\ 0.00, 0.00, 0.00, 0.71, 0.70, 0.75, 0.00, 0.00, 0.00, 0.00, 0.00 \end{pmatrix} \begin{matrix} \text{(W1: Task 1, Task 4)} \\ \text{(W2: Task 3, Task 6)} \\ \text{(W3: Task 2, Task 5)} \end{matrix}$$

Figure 6

Matrix of negative ideal solution

The selectable alternatives that can improve 1.11 hours of Worker 1 are four types of supporting in Figure 7. Task 1 and Task 4 of Worker 1 are selectable by Worker 2 and Worker 3. The required time for each worker is changed by supported tasks. Since Worker 2 and Worker 3 have two tasks, the number of alternatives is changed to eight by changing applied flexible time of tasks.

$$\begin{aligned} Rt(T1W2) &= 1.11 * 0.41 / 0.22 = 2.04 & Rt(T4W2) &= 1.11 * 0.71 / 0.42 = 1.89 \\ Rt(T1W3) &= 1.11 * 0.46 / 0.22 = 2.33 & Rt(T4W3) &= 1.11 * 0.53 / 0.42 = 1.42 \end{aligned}$$

Figure 7

Required time for the supported tasks

Table 6 shows each score of alternatives for improving required time of Worker 1. These scores are used to compute the distance of the positive ideal solution and negative ideal solution as Table 7 shown. The appropriate alternative in this situation is Alt(7) that Task 4 of Worker 1 is supported by utilizing flexible time of Task 3 of Worker 3.

Table 6
Scores of alternatives without similar document

	We(1)	We(2)	We(3)	We(4)	We(5)	We(6)	We(7)	We(8)	We(9)	We(10)	We(11)
Alt(1) T1 to T2, T5 of W2	0.06	0.00	0.00	0.49	0.11	0.32	0.18	0.49	0.00	0.07	0.00
	0.03	0.00	0.00	1.05	0.47	1.24	0.29	0.45	0.00	0.17	0.00
	0.00	0.12	0.56	0.00	0.20	0.00	0.00	0.00	0.85	0.00	0.80
Alt(2) T1 to T5, T2 of W2	0.06	0.00	0.00	0.49	0.11	0.32	0.18	0.49	0.00	0.07	0.00
	0.03	0.00	0.00	1.04	0.47	1.22	0.29	0.45	0.00	0.17	0.00
	0.00	0.12	0.56	0.00	0.20	0.00	0.00	0.00	0.85	0.00	0.80
Alt(3) T1 to T3 of W3	0.06	0.00	0.00	0.49	0.11	0.32	0.18	0.49	0.00	0.07	0.00
	0.00	0.00	0.00	1.11	0.49	1.29	0.00	0.00	0.00	0.00	0.00
	0.19	0.11	0.49	0.00	0.23	0.00	0.22	0.48	0.78	0.19	0.73
Alt(4) T1 to T6 of W3	0.06	0.00	0.00	0.49	0.11	0.32	0.18	0.49	0.00	0.07	0.00
	0.00	0.00	0.00	1.11	0.49	1.29	0.00	0.00	0.00	0.00	0.00
	0.19	0.11	0.50	0.00	0.23	0.00	0.22	0.48	0.77	0.19	0.73
Alt(5) T4 to T2 of W2	0.08	0.00	0.00	0.44	0.13	0.27	0.22	0.51	0.00	0.09	0.00
	0.00	0.00	0.00	1.39	0.44	1.49	0.00	0.27	0.00	0.00	0.00
	0.00	0.12	0.56	0.00	0.20	0.00	0.00	0.00	0.85	0.00	0.80
Alt(6) T4 to T5 of W2	0.08	0.00	0.00	0.44	0.13	0.27	0.22	0.51	0.00	0.09	0.00
	0.00	0.00	0.00	1.38	0.44	1.48	0.00	0.27	0.00	0.00	0.00
	0.00	0.12	0.56	0.00	0.20	0.00	0.00	0.00	0.85	0.00	0.80
Alt(7) T4 to T3 of W3	0.08	0.00	0.00	0.44	0.13	0.27	0.22	0.51	0.00	0.09	0.00
	0.00	0.00	0.00	1.11	0.49	1.29	0.00	0.00	0.00	0.00	0.00
	0.00	0.11	0.52	0.21	0.18	0.10	0.00	0.22	0.81	0.00	0.76
Alt(8) T4 to T6 of W3	0.08	0.00	0.00	0.44	0.13	0.27	0.22	0.51	0.00	0.09	0.00
	0.00	0.00	0.00	1.11	0.49	1.29	0.00	0.00	0.00	0.00	0.00
	0.00	0.11	0.52	0.21	0.18	0.10	0.00	0.22	0.81	0.00	0.76

Table 7
Scores and ranking of alternatives without similar document

	<i>TDP</i>	<i>TDN</i>	<i>C</i>	Ranking
Alt(1)	0.624	2.625	0.8080	No.5
Alt(2)	0.626	2.613	0.8067	No.6
Alt(3)	0.659	2.623	0.7993	No.7
Alt(4)	0.660	2.619	0.7987	No.8
Alt(5)	0.512	2.854	0.8479	No.4
Alt(6)	0.504	2.846	0.8495	No.3
Alt(7)	0.420	2.512	0.8572	No.1
Alt(8)	0.421	2.519	0.8569	No.2

However, the ranking of alternatives are changing by applying similar documentation to the supporting workers. When the documents that are written by target workers can be utilized as Table 8 shown, the similarity for the supported tasks is computed to shorten required time for the supporting workers.

Table 8
Proportion of term frequency for documents

	We(1)	We(2)	We(3)	We(4)	We(5)	We(6)	We(7)	We(8)	We(9)	We(10)	We(11)
D1 Written by Worker 1	0.0	0.0	0.0	0.0	0.5	0.0	0.1	0.3	0.0	0.1	0.0
D2 Written by Worker 2	0.4	0.0	0.2	0.0	0.2	0.2	0.0	0.0	0.0	0.0	0.0
D3 Written by Worker 3	0.0	0.5	0.2	0.0	0.3	0.0	0.0	0.0	0.0	0.0	0.0

Table 9
Computed similarity of tasks and documents

	Type of Documents	Smilarity
Task 1	D1	0.82
	D2	0.30
	D3	0.19
Task 2	D1	0.68
	D2	0.49
	D3	0.39
Task 3	D1	0.15
	D2	0.40
	D3	0.52
Task 4	D1	0.16
	D2	0.18
	D3	0.00
Task 5	D1	0.68
	D2	0.49
	D3	0.39
Task 6	D1	0.16
	D2	0.36
	D3	0.49

The required time for supporting workers is changed by applying most similar document. Since the similarity of D1 to Task 1 in Table 9 is high and the experiences of document creator (Worker 1) is high, the required time for Task 1 is reduced longer than Task 4.

$$Rt(T1W2) = 1.11 * 0.19 / 0.22 = 0.95 \quad Rt(T4W2) = 1.11 * 0.67 / 0.42 = 1.80$$

$$Rt(T1W3) = 1.11 * 0.20 / 0.22 = 1.00 \quad Rt(T4W3) = 1.11 * 0.51 / 0.42 = 1.36$$

Figure 8
Required time for the supported tasks with similar document

Table 10 shows changed ranking of alternatives by applying similar document. Despite the score of experience for Worker 3 to Task 1 and Task 4 is higher than Worker 2, the supporting of Worker 2 to Task 1 is best score of alternatives in this situation.

Table 10
Scores and ranking of alternatives with similar document

	<i>TDP</i>	<i>TDN</i>	<i>C</i>	Ranking
Alt(1)	0.415	2.616	0.8632	No.1
Alt(2)	0.416	2.609	0.8626	No.2
Alt(3)	0.417	2.612	0.8624	No.3
Alt(4)	0.417	2.611	0.8622	No.4
Alt(5)	0.501	2.848	0.8504	No.8
Alt(6)	0.494	2.840	0.8519	No.7
Alt(7)	0.411	2.524	0.8599	No.5
Alt(8)	0.412	2.522	0.8596	No.6

Conclusions

The scores of positive ideal solution and negative ideal solution of TOPSIS method is adjusted to the interrupted workflow by aggregating subjective attributes of the worker and objective attributes of the task in this paper. In addition, flexibility of score for alternatives is also extended by applying similar documentation. The proposed approach has indicated that experienced worker is not always appropriate supporter in the improvement of certain interruption. However, even if there are alternatives to get higher profit for the organization with improving the negative impact of interruption, the proposed approach recommends alternatives to the interrupted worker based on the assignment of the superior decision maker. Therefore, the alternatives for assisting decision making in certain interruption by the proposed approach cannot optimize the objective of the pre-assignment by the estimation of the superior decision maker according to the objective of organization. Since the time of the mental work for gathering information from experiences of the worker is increased due to a forgetting with time, the subjective attributes of the worker in this study is not adjusted to actual values by computing reduction of memory for worker's experiences. In order to improve accuracy for computing ranking of alternatives, the impact on shortening task operation with documents must be evaluated by comparing the proposed cosine distance with another data searching approaches. Although the risk of interruption is based on the operation time consumed for the workflow in certain time, uncertain context of interruption must be reasoned for more appropriate supporting the decision making of the interrupted worker as future work. To measure the amount of change by interruption, we provide to handle the interruptions on the running workflow, and how such change fits in the subjective and objective situation of the interrupted worker. This can be represented as fitness function which the direction of our future works. In order to reason the uncertain context of interruption, the predicting approaches based on the other worker's subjective attributes than the proposed experience should be discussed in the future work by using fitness function method, safety measure approach and so on.

References

- [1] Herbert A. Simon, *The Science of the Artificial*, The MIT Press third edition edition (1996)
- [2] L. Corragio, *Deleterious Effects of Intermittent Interruptions on the Task Performance of Knowledge Workers, A Laboratory Investigation*, Unpublished doctoral dissertation, University of Arizona (1990)
- [3] M. Al-Yakoob, H. D. Sherali, *Mixed Integer Programming Models for an Employee Scheduling Problem with Multiple Shifts and Work Locations*, *Annals of Operational Research* 155 (2007) pp. 119-142
- [4] N. Moradi nasab, R. Shafaei, M. Rabiee, M. Mazinani, *Minimization of Maximum Tardiness in a No-Wait TwoSstage Flexible Flow Shop*, *International Journal of Artificial Intelligence* 8 (2012) pp. 166-181
- [5] R. J. Wherry, *The Curve of Forgetting: Its Statistical Application*, *Journal of Educational Psychology*, 23 (1932) pp. 621-624
- [6] Cheri Speier, Joseph S. Valacich, Iris Vessey, *The Influence of Task Interruption on Individual Decision Making: An Information Overload Perspective*, *Decision Sciences* 30 (1999)
- [7] Amos Tversky, Daniel Kahneman, *Judgment under Uncertainty: Heuristics and Biases*, *Science, New Series* 185 (1974) pp. 1124-1131
- [8] K. Sugawara, *Decision Support System for Handling Interruption in Tasks for Workers*, *New Trends in Software Methodologies Tools and Techniques Proceedings of the 11th SoMeT_12* (2012) pp. 273-281
- [9] T. L. Saaty, *The Analytical Hierarchy Process*, New York: McGraw-Hill (1980)
- [10] G. H. Tzeng, C. H. Chiang, C. W. Li, *Evaluating Intertwined Effects in e-Learning Programs: A Novel Hybrid MCDM Model Based on Factor Analysis and DEMATEL*, *Expert Systems with Applications* 32 (2007) pp. 1028-1044
- [11] S. Greco, B. Matarazzo, R. Slowinski, *Rough Sets Methodology for Sorting Problems in Presence of Multiple Attributes and Criteria*, *European Journal of Operational Research* 138 (2002) pp. 247-259
- [12] K. Yoon, C. L. Hwang, *Multiple Attribute Decision Making Methods and Applications*. Springer Verlag, Berlin, Germany (1980)
- [13] S. Opricovic, *Multicriteria Optimization of Civil Engineering Systems*, Faculty of Pennsylvania (1998)
- [14] S. J. Chen, C. L. Hwang, *Fuzzy Multi Attribute Decision Making*, *Lecture Notes in Economics and Mathematical system series 375*, Springer Verlag, New York (1992)

- [15] Z. Yue, An Extended TOPSIS for Determining Weights of Decision Makers with Interval Numbers, *Knowledge-Based Systems* 24 (2011) pp. 146-153
- [16] J. Tian, D. Yu, B. Yu, S. Ma, A Fuzzy TOPSIS Model via Chi-Square Test for Information Source Selection, *Knowledge-Based Systems* 37 (2013) pp. 515-527
- [17] E. Pap, V. Bojanic, M. Georgijevic, G. Bojanic, Application of Pseudo-Analysis in the Synchronization of Container Terminal Equipment Operation, *Acta Polytechnica Hungarica* 8 (2011) pp. 5-21
- [18] Albert Corominas, Jordi Olivellan, Rafael Pastor, A Model for the Assignment of a Set of Tasks When Work Performance Depends, *Int. J. Production Economics* 126 (2010) pp. 335-340
- [19] G. Salton and C. Buckley, Term-Weighting Approaches in Automatic Text Retrieval, *Information Processing & Management* 24 (1988) pp. 513-523

Converting MA-PDDL to Extensive-Form Games

Dániel L. Kovács, Tadeusz P. Dobrowiecki

Department of Measurement and Information Systems, Budapest University of Technology and Economics

Magyar tudósok krt. 2, H-1117, Budapest, Hungary

E-mail: dkovacs@mit.bme.hu, tade@mit.bme.hu

Abstract: This paper presents algorithms for converting multi-agent planning (MAP) problems described in Multi-Agent Planning Domain Definition Language (MA-PDDL) to extensive-form games in order to analyse and solve them with game-theoretic tools in general. MA-PDDL is an attempt to standardize the description of MAP problems similarly to PDDL in the single-agent setting. In this paper MA-PDDL is extended with partial-observability and probabilistic-effects to model more realistic domains. The conversion is fruitful in both ways: 1) extensive-form games can be solved via game-theoretic solution concepts (e.g. Nash-equilibrium) providing solutions to corresponding MAP problems in general, and 2) MA-PDDL problems can be solved via MAP methods providing solutions to corresponding games. Both cooperative and non-cooperative solutions can be achieved.

Keywords: multi-agent; planning; pddl; game theory; partial observability; probabilistic

1 Introduction

This paper presents methods for converting multi-agent planning (MAP) problems [1] described in MA-PDDL (Multi-Agent Planning Domain Definition Language) [2] to extensive-form games [3][4], in order to enable the application of game-theoretic principles (e.g. solution concepts) to MAP problems in general.

PDDL [5] is quasi the standard description language for modeling deterministic, single-agent planning problems. Such problems form the basis of automated planning [6], which is of central importance in Artificial Intelligence (AI) [7] due to it provides practical methods for designing goal- and utility-based intelligent agents, with real-world applications ranging from game playing to control of space vehicles. However PDDL is limited to only one planner, whereas real-world planning problems may involve multiple cooperative or adversary, controllable or non-controllable planner agents with different goals, different capabilities and interacting actions (competing corporations, multiplayer games, electronic

auctions, assisted living, computer networks, robotic soccer, etc.). To model these aspects PDDL was recently extended to the multi-agent setting in [2].

However solving a MAP problem can prove to be quite difficult due to its inherent complexity. It is well known, that single-agent planning in discrete-time is PSPACE-complete even in the propositional case [8] (where conditions within actions are just literals without variables), i.e. propositional single-agent planning is among the hardest problems in PSPACE, and PSPACE contains NP. Now in case of multiple agents the number of actions – and thus complexity – increases exponentially (since all action-combinations of the multiple agents need to be considered in general), not speaking of richer MAP models (including predicates, numeric variables, plan metrics, continuous-time, uncertainty, partial-observability, etc.). This makes MAP intractable for realistic domains in general, and only approximations of the global optima are possible in practice. Thus it comes to no surprise, that currently – in lack of a (quasi)standard MAP problem modeling language – there are no general means for solving MAP problems.

This paper tries to overcome the above issue by proposing a translation of MAP problems to extensive-form games in order to analyze and solve them via game-theoretic methods. MAP problems are described in MA-PDDL, which is an attempt to standardize the description of MAP problems (similarly to PDDL in single-agent planning). Naturally the translation cannot reduce the complexity of converted MAP problems (i.e. solution approximation or shrinking of games [9] may be required for tractability), but at least it opens a way to strategically analyze and solve MAP problems in general. To our knowledge this is the first result in automatically converting MAP problems to game-theoretic models.

Game theory [3][10] describes essentially the same multi-agent situations as MAP (i.e. strategic interaction of agents), thus the conversion of MAP problems to games is relatively straightforward, but game theory also provides a rich repertoire of useful solution concepts that can be applied to MAP problems after the conversion. The solution of a game is usually a set of strategy-combinations, which corresponds to a set of joint-plans in the MAP problem. These solutions may be cooperative or non-cooperative depending on the solution concept used. Extensive-form games are appropriate for both cases even though they are part of non-cooperative game theory. In the non-cooperative case e.g. Nash-equilibrium (NE) [11] or Subgame Perfect NE [12] or Perfect Bayesian Equilibrium [13], while in the cooperative case e.g. Pareto-optimum [10] can be used to find suitable solutions. Cooperation can also be achieved by maximizing social-welfare (i.e. the sum of utilities of agents) or individual utility of agents may reflect their collective preferences, so even non-cooperative solution concepts can lead to cooperative solutions. I.e. the proposed conversion does not limit the cooperation of agents.

Eventually the proposed connection of MA-PDDL and extensive-form games is fruitful in both directions: **(1)** an extensive-form game can be solved via available game-theoretic solution concepts providing solutions to the corresponding MAP

problem and (2) MA-PDDL can provide a much richer model of the same game-theoretic situation, and can be solved via available state-of-the-art MAP methods [1] providing solutions to the corresponding game (converted from MA-PDDL).

The paper is structured as follows: Section 2 introduces the preliminaries of automated planning, PDDL, MA-PDDL and extensive-form games. Section 3 proposes conversion algorithms from MA-PDDL to extensive-form games. First the fully-observable, deterministic case is discussed, then partial-observability and probabilistic-effects are added gradually. At the end of Section 3 a short example illustrates the concept. Finally Section 4 concludes the work and outlines future research directions. Appendix 1-3 provides the additional BNF (Backus-Naur Form) grammar for partial-observability and probabilistic-effects in MA-PDDL.

2 Preliminaries

2.1 Automated Planning

Automated planning [6] is a process of finding a plan of action (e.g. either a totally ordered sequence of actions, or some conditional plan of action) that upon execution is expected to solve a planning problem. A *planning problem* typically defines an *initial state* and desired *goal states* of an environment, i.e. the solution of a planning problem, a *solution plan* should drive the environment from the initial state to a goal state upon execution (hopefully in a minimal number of steps, minimizing the risk and the cost of execution). In case of a deterministic environment with only a single agent the execution of a solution plan should lead to a goal state, however in case the environment is only partially observable to the agent, or it is probabilistic/non-deterministic, or there are multiple autonomous agents in it, then the execution may fail (e.g. an other agent may interfere during execution). So in this case a solution plan should be either prepared for all contingencies or its execution should be monitored and the plan should be repaired on-the-fly. A planning problem may have many or no solutions at all.

2.2 PDDL (Planning Domain Definition Language)

PDDL [5] is the quasi-standard, predicate logic based declarative description language for deterministic, single-agent planning problems. The latest official version of PDDL is 3.1 [14,15]. Each new version of the language adds new, modular features to previous versions. PDDL divides the description of the planning problem in two parts: a *domain-* and a *problem-description*. The domain-description contains those model-elements which are present in every particular problem of the domain, while the problem-description specifies the concrete planning problem at hand within the domain. Thus the *input* of a domain-

independent PDDL-based planner is the domain- and problem-description, while its *output* is a plan that solves the specified planning problem (if it is solvable).

More precisely, the domain-description contains the following: a unique *name*; a list of *requirements* (a list of PDDL-features used); a *type-hierarchy* (classifying *objects*); *constants* (objects present in every problem of the domain); and a list of *predicates* and *actions*. Actions have input *parameters*; *preconditions* (that need to be satisfied in a given state of the environment for the action to be executable); and *effects* (describing the change to the state if the action is executed). Effects of an action can be *conditional* or *continuous*. Moreover, actions may have arbitrary, non-unit *duration*. A domain-description may also include a list of *functions*, *derived predicates* or hard *constraints*. The domain of a function is a Cartesian product of object-types, while its range may be either the set of real numbers or any object-type. A derived predicate is true, if its preconditions are true. Actions may refer to derived predicates in their preconditions. Constraints are statements in modal logic about state-trajectories that must be true for valid *solution plans*.

The problem-description also has a unique *name*; a *reference* to the respective domain-description; a list of all *objects* in the logical universe; an *initial state*; and a specification of *goal states* of the environment. Problem-descriptions can also include a *metric* (a real-valued function for measuring the quality of solution plans); *timed initial literals* (facts becoming true at a given time); and *constraints* similarly to the domain-description, but here they can refer to *preferences* (soft constraints, which should not necessarily be satisfied, but they can be incorporated in the metric). Preferences can also be defined in goal, or in action preconditions.

2.3 MA-PDDL (Multi-Agent PDDL)

MA-PDDL [2] is a minimalistic, modular extension of PDDL3.1, indicated by a new additional PDDL-requirement, `:multi-agent`. It extends PDDL3.1 to allow *planning by and for multiple agents*. *Different agents* may have *different actions*, *different goals* and *different metrics*, unlike in original PDDL. This allows modeling of not just homogeneous, but also heterogeneous agents in either cooperative or competitive scenarios. Moreover, in MA-PDDL the preconditions of actions can directly refer to concurrent actions and thus *actions with interacting effects* can be modeled in general (e.g. when at least 2 agents are needed to execute the lift action to lift a heavy table, or it will remain on the ground, or a third agent may interfere by pushing the table down to the ground), which allows for a more refined model of cooperation and inter-dependence of agents. However, since PDDL3.1 assumes that the environment is deterministic and fully-observable (i.e. every agent can access the value of every state-fluent at every instant and observe every previously executed action), thus by default the same holds in MA-PDDL too. Nonetheless in Section 3.2 and 3.3 these constraints are lifted by extending MA-PDDL with partial-observability and probabilistic effects.

2.4 Game Theoretic Fundamentals

The *normal form* of an *incomplete information game* Γ [16] (the most general non-cooperative game) is a 5-tuple $\Gamma = (N, \{S_i\}_{i \in N}, \{u_i\}_{i \in N}, \{T_i\}_{i \in N}, p)$, where $N = \{1, 2, \dots, n\}$ denotes the set of *agents*; S_i is the finite set of *pure strategies* of $i \in N$ and T_i is the finite set of its *types* of $i \in N$; typically $u_i: S \times T_i \rightarrow \mathbb{R}$ is the real-valued *utility function* of agent i , where $S = \times_{i=1}^n S_i$ is the set of all *strategy-combinations*. Depending on the interpretation and dependence of types, sometimes the utility of an agent may also depend on the type of other agents too, i.e. $u_i: S \times T \rightarrow \mathbb{R}$, where $T = \times_{i=1}^n T_i$ denotes the set of all *type-combinations*.

The goal of an agent is to choose its strategy so as to maximize its own expected utility. The difficulty is that agents choose their strategies simultaneously and independently. Moreover each agent i plays with an *active type*, $t_i \in T_i$, which is revealed only to i , and chosen randomly by Nature (or Chance) at the beginning of each play. p is the *a priori probability distribution* above all type-combinations $t \in T$ according to which Nature chooses active types for agents. A type-combination $t \in T$ is thus realized with probability $p(t)$. If there is only 1 type-combination, i.e. when $|T| = 1$, then Γ is of *complete information*. Otherwise, when $|T| > 1$, Γ is of *incomplete information*. In any case Γ is *common knowledge* among the agents (every agent knows, that every agent knows... Γ).

The *extensive form* of Γ adds the notion of *choice nodes* $\omega \in \Omega$, where Ω is the finite set of all choice nodes with a distinguished *initial choice node*, $\omega_0 \in \Omega$, from where each play of Γ begins. A function $g: \Omega \rightarrow N \cup \{0\}$ can indicate which agent $i = g(\omega)$ chooses an elementary move (or action) in $\omega \in \Omega$ from the finite, non-empty set of its *moves*, A_i (one and only one agent is associated to each $\omega \in \Omega$). Similarly function $h: \Omega \rightarrow 2^{\cup_{i=0}^n A_i} \setminus \{\emptyset\}$ may indicate the set of those moves, $h(\omega) \subseteq A_{g(\omega)}$, which agent $g(\omega)$ can choose in ω (one and only one move can be chosen in each ω). Thus in an incomplete information game $g(\omega_0) = 0$ and $h(\omega_0) = T$ holds, where *agent 0* represents Nature (or Chance).

In any given $\omega \in \Omega$ node, where $g(\omega) = 0$ holds, agent 0 chooses its respective moves randomly according to a probability distribution $s_0(\omega)$, where $s_0: \Omega \rightarrow \Delta(A_0)$ denotes the *stochastic strategy* of agent 0, and $\Delta(A_0)$ is the set of all probability distributions above A_0 . It follows that $s_0(\omega_0) = p$ holds for ω_0 . Eventually each choice node corresponds to a unique sequence of moves of length between 0 and $\kappa \in \mathbb{Z}^+$ (a given maximum), with ω_0 corresponding to the empty sequence \mathcal{E} of length 0. So a play begins initially in ω_0 . Then, after agent $g(\omega_0)$ chooses a move $a_{g(\omega_0)} \in A_{g(\omega_0)}$, the play continues in ω_1 corresponding to the sequence $\langle a_{g(\omega_0)} \rangle$. This continues until the play reaches a sequence $\langle a_{g(\omega_0)}, a_{g(\omega_1)}, \dots, a_{g(\omega_{\kappa-1})} \rangle$. Thus the choice nodes can be connected in a tree-graph G of maximal depth κ with ω_0 being the root-node.

Agents can't necessarily observe all the previous moves of other agents during a play. For this reason *information functions* $P_i: \Omega \rightarrow 2^\Omega \setminus \{\emptyset\}$ are introduced for

each $i = 1, 2, \dots, n$. The information function of agent i associates a non-empty *information set*, $P_i(\omega) \subseteq \Omega$, to each choice node ω , where $i = g(\omega)$. An information set $P_i(\omega)$ denotes the set of those choice nodes that agent i believes to be possible in ω . It is assumed that $\omega \in P_i(\omega)$ holds for every $\omega \in \Omega$ and $i \in N$, and also that $\forall \omega', \omega'' \in P_i(\omega): h(\omega') = h(\omega'')$. Thus the choice nodes inside an information set are indistinguishable for the respective agent. Information sets of agent i are disjoint, forming an *information partition* $\mathbf{P}_i = \bigcup_{\omega \in \Omega, g(\omega)=i} P_i(\omega)$. Now the set of pure strategies S_i of agent $i = 1, 2, \dots, n$ in G is the set of all $s_i: \mathbf{P}_i \rightarrow A_i$ functions, where for $\forall P_i(\omega) \in \mathbf{P}_i$ $s_i(P_i(\omega)) \in h(\omega)$ holds. This finishes the description of the extensive-form of an incomplete information game.

3 Conversion of MA-PDDL to Extensive Form Games

This section presents the main results of the paper: the conversion of fully- and partially-observable, probabilistic MA-PDDL models to extensive-form games.

3.1 Case of Full-Observability

The idea of the conversion is to generate successor states from the initial state of an MA-PDDL problem, *PROB*, in every possible way (i.e. via every applicable action-combination of agents, including `no-op` (no-operation) actions, with every agent executing one action at a time), and then recursively apply the same process to the resulting states altogether k -times, and convert this graph into an extensive-form game. Thus all joint-plans with agents acting effectively $\leq k$ times (maybe even heterogeneously) are found. **Alg. 1** forms the backbone of this method.

Algorithm 1: Convert a fully-observable MA-PDDL description to an extensive-form game

```

1: CONVERT(PROB, k)
2:  $l \leftarrow 0$ 
3:  $N \leftarrow$  AGENT_OBJECTS(PROB)
4:  $n = |N|$ ,  $\kappa = 1 + k \cdot n$ 
5: foreach  $i \in N$ 
6:    $T_i \leftarrow \{t_i \leftarrow$  NEW_TYPE( $\cdot$ ) $\}$ ,  $\mathbf{P}_i \leftarrow \emptyset$ 
7:    $A_i \leftarrow$  ALL_GROUNDED_ACTIONS(PROB,  $i$ )  $\cup \{\text{no-op}\}$ 
8: end-foreach
9:  $\omega_0 \leftarrow$  NEW_CHOICE_NODE( $\cdot$ ),  $g(\omega_0) \leftarrow 0$ ,  $A_0 \leftarrow \{t = (t_1, t_2, \dots, t_n)\}$ ,  $h(\omega_0) \leftarrow A_0$ 
10:  $p(t = (t_1, t_2, \dots, t_n)) \leftarrow 1$ ,  $s_0(\omega_0) \leftarrow p$ 
11:  $\omega_1 \leftarrow$  CHOICE_NODE_FROM_INITIAL_STATE(PROB)
12:  $g(\omega_1) \leftarrow 1$ ,  $h(\omega_1) \leftarrow A_1$ ,  $P_1(\omega_1) \leftarrow \{\omega_1\}$ ,  $\mathbf{P}_1 \leftarrow \mathbf{P}_1 \cup \{P_1(\omega_1)\}$ 
13:  $\Omega \leftarrow \{\omega_0, \omega_1\}$ ,  $G \leftarrow (\Omega, \{(\omega_0, t, \omega_1)\})$ ,  $state\_level_0 \leftarrow \{\omega_1\}$ 
14: while ( $l < k$ )
15:    $l \leftarrow l + 1$ 
16:    $\langle G, \Omega, \{\mathbf{P}_i\}_{i \in N}, \{P_i\}_{i \in N}, state\_level_l \rangle \leftarrow$ 
17:    $\text{ADD\_NEXT\_LEVEL}(\text{PROB}, G, \omega_0, \Omega, \{\mathbf{P}_i\}_{i \in N}, \{P_i\}_{i \in N}, state\_level_{l-1}, \{A_i\}_{i \in N}, n)$ 
18: end-while
19:  $\{S_i\}_{i \in N} \leftarrow$  ENUMERATE_STRATEGIES( $N, \{\mathbf{P}_i\}_{i \in N}, h, \{A_i\}_{i \in N}$ )

```

```

20:  $\{u_i\}_{i \in N} \leftarrow \text{GET\_METRIC\_VALUES}(PROB, N, \{S_i\}_{i \in N}, \{T_i\}_{i \in N}, p, \omega_0, s_0, G, \text{state\_level}_k)$ 
21: return  $\Gamma = (N, \{S_i\}_{i \in N}, \{u_i\}_{i \in N}, \{T_i\}_{i \in N}, p, \Omega, \omega_0, s_0, \{\mathbf{P}_i\}_{i \in N}, \{P_i\}_{i \in N}, \{A_i\}_{i \in N \cup \{0\}}, g, h, \kappa, G)$ 

```

The **CONVERT** method has 2 inputs (#1): *PROB* is a fully-observable, discrete, deterministic MA-PDDL domain- and problem-description, and $k \geq 0$ is a positive integer specifies the number of levels of successor states generated. In case of $n = |N|$ agents the resulting extensive-form game Γ (#21) has a tree-graph *G* of depth $\kappa = 1 + k \cdot n$ (#4), where *N* is the set of agent-objects in *PROB* (#3).

The algorithm first sets a level-counter *l* to zero (#2), then for every agent it initializes the set of types to a one-element set (deterministic MA-PDDL is converted to a complete information game). Information partition \mathbf{P}_i is set to the empty-set for every $i \in N$, and all grounded actions of agent *i* are extracted from *PROB* into respective sets of moves, A_i , including the always executable `no-op` action with no effects (#5-8). Next (#9) the root node of the game-tree, ω_0 , is created, and its actor is set to agent 0, the actions of agent 0 are set to A_0 , and A_0 is allowed in ω_0 . Then (#10) the probability of “action” *t*, $p(t)$, is set to 1, so this distribution governs the stochastic strategy of agent 0 in ω_0 , i.e. $s_0(\omega_0)$ is set to *p*.

Next (#11) the **CHOICE_NODE_FROM_INITIAL_STATE** method creates a new choice node, ω_1 , which corresponds to the initial state of *PROB*. Agent 1 is set to act in ω_1 (#12), allowing any move from A_1 . Line (#12) initializes also the information set $P_1(\omega_1)$ and information partition \mathbf{P}_1 of agent 1. Line (#13) initializes the set of choice nodes, Ω , to include only ω_0 and ω_1 ; and the game-graph *G* to have these nodes as vertices with only one edge – labeled with move *t* –, (ω_0, t, ω_1) , and then also the 0th state-level is initialized to $\{\omega_1\}$.

State-levels are of central importance. They consist of those choice nodes in *G*, which correspond directly to states of the multi-agent environment. The following 5 lines (#14-18) create new state-levels via intermediate action-levels by calling the **ADD_NEXT_LEVEL** method iteratively in a `while`-loop. The detailed pseudocode of the method is shown in Alg. 2. After *k* iterations the `while`-loop exits, and the finalized information partitions of agents, $\{\mathbf{P}_i\}_{i \in N}$, are used to enumerate (#19) all the possible $s_i: \mathbf{P}_i \rightarrow A_i$ functions (for every $i \in N$) to form the sets of pure strategies, $\{S_i\}_{i \in N}$. This is done by the **ENUMERATE_STRATEGIES** method.

The utility of agents is defined explicitly for every possible outcome (i.e. for every strategy-combination). These outcomes are represented with choice-nodes of the last state-level in the game-tree. Each of them corresponds to exactly one *k*-step state/action-trajectory, thus the idea is to simply get the MA-PDDL metric-value of these trajectories from *PROB* for every agent-object, and associate them to the respective choice-nodes. If an agent-object has no metric defined in *PROB*, then its utility is 1, if its goal was achieved during the given trajectory, and 0 otherwise. This way each choice-node in the last state-level will have an *n*-long utility-vector. This is what the **GET_METRIC_VALUES** method does (#20). Finally the algorithm returns the converted game, Γ (#21).

The heart of the above presented **CONVERT** method is the iterative call of the **ADD_NEXT_LEVEL** method, which effectively builds the game-tree, level-by-level (**#16-17**). This method is described in **Alg. 2** below.

Algorithm 2: Add a level to the extensive game-tree of a fully-observable MA-PDDL description

```

1: ADD_NEXT_LEVEL(PROB, G = (V, E),  $\omega_0$ ,  $\Omega$ ,  $\{P_i\}_{i \in N}$ ,  $\{P_i\}_{i \in N}$ , last_state_level,  $\{A_i\}_{i \in N}$ , n)
2: next_state_level  $\leftarrow \emptyset$ 
3: foreach  $\omega \in \textit{last\_state\_level}$ 
4: | action_level1  $\leftarrow \{\omega\}$ , action_leveln+1  $\leftarrow \emptyset$ 
5: | TRACE( $\omega$ )  $\leftarrow \varepsilon$ ,  $\omega' \leftarrow \text{CLONE}(\omega)$ ,  $\Omega \leftarrow \Omega \cup \{\omega'\}$ 
6: | g( $\omega'$ )  $\leftarrow 1$ , h( $\omega'$ )  $\leftarrow A_1$ , P1( $\omega'$ )  $\leftarrow \{\omega'\}$ ,  $P_1 \leftarrow P_1 \cup \{P_1(\omega')\}$ 
7: | for i = 1, i  $\leq n$ , i++
8: | | if i > 1 then Pi  $\leftarrow P_i \cup \{\textit{action\_level}_i\}$  end-if
9: | | if i < n then action_leveli+1  $\leftarrow \emptyset$  end-if
10: | | foreach x  $\in \textit{action\_level}_i$ 
11: | | | if i > 1 then Pi(x)  $\leftarrow \textit{action\_level}_i$  end-if
12: | | | foreach ai  $\in h(x)$ 
13: | | | | if i < n then
14: | | | | | y  $\leftarrow \text{NEW\_CHOICE\_NODE}()$ 
15: | | | | | TRACE(y)  $\leftarrow (\text{TRACE}(x), a_i)$ 
16: | | | | | g(y)  $\leftarrow i + 1$ , h(y)  $\leftarrow A_{i+1}$ 
17: | | | | | else
18: | | | | | | if HAS_CONSISTENT_EXECUTABLE_SUBSET((TRACE(x), ai), PROB,  $\omega_0$ ,  $\omega$ , G) then
19: | | | | | | | y  $\leftarrow \text{CHOICE\_NODE\_FROM\_SUCCESSOR\_STATE}(\omega, (\text{TRACE}(x), a_i), \textit{PROB}, \omega_0, G)$ 
20: | | | | | | | g(y)  $\leftarrow 1$ , h(y)  $\leftarrow A_1$ , P1(y)  $\leftarrow \{y\}$ ,  $P_1 \leftarrow P_1 \cup \{P_1(y)\}$ 
21: | | | | | | | else
22: | | | | | | | | y  $\leftarrow \omega'$ 
23: | | | | | | | | end-if
24: | | | | | | | | end-if
25: | | | | | | | | action_leveli+1  $\leftarrow \textit{action\_level}_{i+1} \cup \{y\}$ 
26: | | | | | | | | V  $\leftarrow V \cup \{y\}$ , E  $\leftarrow E \cup \{(x, a_i, y)\}$ ,  $\Omega \leftarrow \Omega \cup \{y\}$ 
27: | | | | | | | | end-foreach
28: | | | | | | | | end-foreach
29: | | | | | | | | end-for
30: | next_state_level  $\leftarrow \textit{next\_state\_level} \cup \textit{action\_level}_{n+1}$ 
31: end-foreach
32: return (G = (V, E),  $\Omega$ ,  $\{P_i\}_{i \in N}$ ,  $\{P_i\}_{i \in N}$ , next_state_level)

```

The **ADD_NEXT_LEVEL** method has 9 inputs (**#1**): *PROB* is the MA-PDDL description; *G* is the actual game-graph (a set of vertices, *V*, and a set of labeled edges, *E*); ω_0 is the root node of *G*; Ω is the actual set of choice-nodes; $\{P_i\}_{i \in N}$ and $\{P_i\}_{i \in N}$ are actual information partitions and functions of agents respectively; *last_state_level* is the latest state-level; $\{A_i\}_{i \in N}$ is the set of sets of moves of agents; and *n* is the number of agents. First (**#2**) the next state-level is initialized to an empty-set, and then it is gradually built in a **foreach**-loop (**#3-31**), which goes through every $\omega \in \textit{last_state_level}$ node, and grows a sub-tree of moves from it, every move of every agent, starting with agent 1 until agent *n* (**#7-29**).

The levels of sub-trees are called *action-levels*, and the choice nodes of an action-level belong to the same information set (of the respective actor agent), since agents act simultaneously in every instant and thus they cannot observe each other's moves. However each information set at state-levels (where agent 1 acts) consists of one choice node because of *full-observability*. The sub-tree built from ω in the **for**-loop (**#7-29**) has *n* + 1 levels, level 1 being part of *last_state_level* and level *n* + 1 being part of the *next_state_level*. The latter consists of choice

nodes that correspond to successor states of the environment, produced in every possible way from the state corresponding to ω . Inside the `for`-loop a `foreach`-loop (#10-28) goes through every choice node x of action-level i , and inside it a further `foreach`-loop (#12-27) goes through every possible move $a_i \in h(x)$ of agent i supposing that the previous $i - 1$ agents chose action-combination $\text{TRACE}(x)$. $\text{TRACE}(\omega)$ is initially empty. Further choice nodes of the game-tree are updated with the move-path (TRACE) which leads to them from ω .

If $i < n$ (#13-16), then the possible action-combination is not yet ready, so a new choice node y is created in action-level $i + 1$, and its trace, actor and move-set is set. Otherwise, if $i = n$ (#18-24), then $(\text{TRACE}(x), a_i)$ is an n -element action-combination, which may have an executable subset in the state corresponding to ω in light of the generated state-trajectory. This is checked by the **HAS_CONSISTENT_EXECUTABLE_SUBSET** method (#18) in 5 steps: first (i) it collects those actions from $(\text{TRACE}(x), a_i)$ into a set C , which are potentially executable in ω . A single-action is considered *potentially executable* in a state if its pre-conditions are satisfied taking also **Assumption 1** into account.

Assumption 1 (undefined effects). If the executability of a grounded action a in a state requires the concurrent execution (or no execution) of some actions, then if any of those actions are not executed (or executed) concurrently with a , then we assume that a still remains executable, but it will have no effects (empty effects).

Assumption 1 covers the case when an MA-PDDL action is defined to refer to an action in its pre-conditions, but no effects are specified for the case, when that reference is negated. I.e. potential executability of actions is independent from concurrently executed actions in light of Assumption 1.

Next (ii) all single- and joint-actions are identified within C . A *joint-action* within C is a subset of C , where all members either refer to at least one other member in their pre-conditions or the conditions of their *active conditional effects*, or they are referred to by at least one of the other members. Reference to actions may be positive or negative, and the conditional effects are *active* in ω if their conditions are satisfied in ω with actions in C being executed. This produces an unambiguous partition of C . Next (iii) individually inconsistent or not executable elements are removed from that partition. A *single-action is individually consistent* in ω if its active conditions and effects are both consistent on their own in ω . A *joint-action is individually consistent* in ω if its joint active conditions and joint active effects are both consistent on their own in ω in case the actions within the given joint-action are executed simultaneously. Interference of conditions and effects of concurrent discrete actions is not considered. *Individual executability* requires satisfaction of (joint) pre-conditions in ω .

Next (iv) elements with *pairwise inconsistent joint-effects* are removed from the partition. Finally (v) the remaining elements are checked, whether their *joint execution* is allowed by the hard state-trajectory constraints in *PROB*. **If yes**, then these actions form the *consistent and executable subset* of $(\text{TRACE}(x), a_i)$, i.e.

they can be executed, and so the `HAS_CONSISTENT_EXECUTABLE_SUBSET` method returns `true`. Otherwise, **if not**, or if the executable subset is empty, then the return-value is `false`. In case the return-value is `true`, a new choice node y corresponding to the state produced by the consistent and executable subset is added to action-level $n + 1$ (**#19,20,25**). Otherwise a choice node $y = \omega' = \omega$ is put into action-level $n + 1$ (**#5,22,25**). In both cases G and Ω are updated appropriately (**#26**) and action-level $n + 1$ is added to the `next_state_level` (**#30**). This is repeated for every ω in `last_state_level` (**#3-31**) before finishing.

3.2 Case of Partial-Observability

Now MA-PDDL is extended with partial-observability (cf. Appendix 1 and 3). In case of partial-observability information sets at state-levels of the converted game may not be singleton, since there may be state/action-trajectories, where the observation-history (including the observation of actions) is the same for an agent, and thus the choice-nodes corresponding to those trajectories should be members of the same information set. Based on this *Alg.1 needs to be extended* as follows. First the following 3 lines should be inserted between line **#12** and **#13** in Alg. 1.

```

13: foreach  $i \in N$ ,
14: | OBS_HIST( $i, \omega_1$ )  $\leftarrow$  OBS( $i, \omega_1$ ),  $Q_i(\omega_1) \leftarrow \{\omega_1\}$ ,  $\mathbf{Q}_{i,0} \leftarrow \{Q_i(\omega_1)\}$ 
15: end-foreach

```

This `foreach`-loop initializes the observation-history of agent i (for $\forall i \in N$) to a list including only its observations in ω_1 , `OBS`(i, ω_1), which is a set of grounded observations and their value holding in ω_1 . $Q_i(\omega_1)$ is the information-set of agent i in ω_1 (even though agent 1 acts in ω_1), and $\mathbf{Q}_{i,0}$ is the information-partition at state-level 0 of agent i . The `ADD_NEXT_LEVEL` method now has also $\{\mathbf{Q}_{i,l-1}\}_{i \in N}$ and $\{Q_i\}_{i \in N}$ among its inputs, and $\{\mathbf{Q}_{i,l}\}_{i \in N}$ and $\{Q_i\}_{i \in N}$ among its outputs. *Alg.2 is changed* accordingly: first, manipulation of agent 1's information-partition, \mathbf{P}_1 , in line **#6** and **#20** are removed together with the complete line **#8**. Then each reference to any `action_levelm` is replaced with `action_levelm(ω)` to keep track of the possibly distinct sub-trees of each $\omega \in \text{last_state_level}$. Line **#11** is deleted, but the following line is added after line **#6** to initialize the observation-history and information-sets $Q_i(\omega')$ of choice node ω' (clone of ω).

```

7: | foreach  $i \in N$ , OBS_HIST( $i, \omega'$ )  $\leftarrow$  OBS_HIST( $i, \omega$ ),  $Q_i(\omega') \leftarrow \{\omega'\}$  end-foreach

```

To update the observation-histories of agents and to initialize their information sets for a new choice node y corresponding to a successor state, the next 5 lines should be added after line **#20** in the original pseudo-code of Alg.2.

```

20: | | | | | foreach  $j \in N$ ,
21: | | | | | | OBS_HIST( $j, y$ )  $\leftarrow$  OBS_HIST( $j, \omega$ ), ...
22: | | | | | | OBS( $j, \text{INCL\_PROGR\_FACTS}(\omega, (\text{TRACE}(x), a_i), \text{PROB}, \omega_0, G)$ ), ...
23: | | | | | | OBS( $j, y$ ),  $Q_j(y) \leftarrow \{y\}$ 
24: | | | | | end-foreach

```


In line **#22** `INCL_PROGR_FACTS` produces a choice node corresponding to a state, where *progressive facts* about consistent and executable actions of $(\text{TRACE}(x), a_i)$ are added to ω . They are identified as in `HAS_CONSISTENT_EXECUTABLE_SUBSET`. Finally line **#32** in Alg.2 is replaced with the following code-segment.

```

36: foreach i ∈ N
37: | if i > 1
38: | | foreach qi ∈ Qi
39: | | | action_levelsqi ← ∪ω ∈ qi action_leveli(ω)
40: | | | foreach x ∈ action_levelsqi, Pi(x) ← action_levelsqi end-foreach
41: | | | Pi ← Pi ∪ {action_levelsqi}
42: | | end-foreach
43: | end-if
44: | foreach ω, ω' ∈ next_state_level where ω ≠ ω'
45: | | if OBS_HIST(i, ω) == OBS_HIST(i, ω') then
46: | | | if i == 1 then P1(ω) ← P1(ω) ∪ {ω'}, P1(ω') ← P1(ω') ∪ {ω} end-if
47: | | | Qi(ω) ← Qi(ω) ∪ {ω'}, Qi(ω') ← Qi(ω') ∪ {ω}
48: | | end-if
49: | end-foreach
50: | Ri ← ∅
51: | foreach ω ∈ next_state_level
52: | | if i == 1 then P1 ← P1 ∪ {P1(ω)} end-if
53: | | Ri ← Ri ∪ {Qi(ω)}
54: | end-foreach
55: end-foreach
56: return ⟨G = (V, E), Ω, {Pi}i ∈ N, {Ri}i ∈ N, {Qi}i ∈ N, next_state_level)

```

In the `foreach`-loop (**#36-55**), if $i > 1$ (**#37-43**), then those i^{th} action-levels are unified into an information-set P_i of agent i , where the root nodes belong to the same information-set. P_i is updated accordingly. Q_i in line **#38** is $Q_{i,*}$ received as an input of `ADD_NEXT_LEVEL`. In lines (**#44-49**) choice nodes in the next state-level corresponding to states with same observation-history are put in the same information-set. Finally the information-partitions of all agents are finalized in the next state-level (**#50-54**), and it is returned by the method (**#56**).

3.3 Case of Probabilistic Effects

In this section probabilistic elements are assumed to be added to MA-PDDL on top of partial-observability (cf. Appendix 2-3), so the `CONVERT` method in Section 3.2 needs to be modified accordingly. In row (**#4**) the calculation of κ should be: $\kappa = 1 + k \cdot (n + 1)$, since now a dedicated chance-node level is added after each action-tree to represent all the possible probabilistic outcomes. Next, the initialization of types-sets should be replaced with initialization of information-partitions $Q_{i,0} \leftarrow \emptyset$ in row (**#6**). Then in row (**#9**) the initialization of the action-set of agent 0 should be replaced with: $(T, p) \leftarrow \mathbf{P_INITSTATES}(PROB)$, $A_0 \leftarrow T$. Here `P_INITSTATES` generates all the possible grounded initial states of the MA-PDDL problem *PROB*, corresponding to the finite set of type-combinations and their respective probabilities forming the a priori probability distribution p over T . Thus in row (**#10**) the initialization of p is omitted, and row (**#11**) is replaced with:

```

11: (Ω1, inv) ← CHOICE_NODES_FROM_P_INITSTATES(T), Ω ← {ω0} ∪ Ω1, state_level0 ← Ω1, E ← ∅

```

Here the set of choice nodes, Ω_1 , is formed from T . An inverse function, $inv: \Omega_1 \rightarrow T$ is also returned for later use. The set of all nodes, edges and the initial state-level is initialized. Next, row (#12) is deleted, and the next 4 rows before the `while`-cycle are replaced with the following code-segment.

```

12: foreach  $\omega_1 \in state\_level_0$ 
13: |  $g(\omega_1) \leftarrow 1$ ,  $h(\omega_1) \leftarrow A_1$ ,  $P_1(\omega_1) \leftarrow \{\omega_1\}$ ,  $E \leftarrow E \cup \{(\omega_0, t, \omega_1)\}_{inv(\omega_1)=t \in T}$ 
14: | foreach  $i \in N$ ,
15: | | OBS_HIST( $i, \omega_1$ )  $\leftarrow \langle \text{OBS}(i, \omega_1) \rangle$ ,  $Q_i(\omega_1) \leftarrow \{\omega_1\}$ 
16: | end-foreach
17: end-foreach
18:  $G \leftarrow (\Omega, E)$ 
19: foreach  $i \in N$ ,
20: | foreach  $\omega, \omega' \in state\_level_0$  where  $\omega \neq \omega'$ 
21: | | if OBS_HIST( $i, \omega$ ) == OBS_HIST( $i, \omega'$ ) then
22: | | | if  $i == 1$  then  $P_1(\omega) \leftarrow P_1(\omega) \cup \{\omega'\}$ ,  $P_1(\omega') \leftarrow P_1(\omega') \cup \{\omega\}$  end-if
23: | | |  $Q_i(\omega) \leftarrow Q_i(\omega) \cup \{\omega'\}$ ,  $Q_i(\omega') \leftarrow Q_i(\omega') \cup \{\omega\}$ 
24: | | end-if
25: | end-foreach
26: | foreach  $\omega \in state\_level_0$ 
27: | | if  $i == 1$  then  $P_1 \leftarrow P_1 \cup \{P_1(\omega)\}$  end-if
28: | |  $Q_{i,0} \leftarrow Q_{i,0} \cup \{Q_i(\omega)\}$ 
29: | end-foreach
30: end-foreach

```

This initializes information-sets, partitions and observation-histories of all agents at the initial state-level. Next, **ADD_NEXT_LEVEL** should include s_0 in its inputs and outputs; the set of type-sets, $\{T_i\}_{i \in N}$, should be replaced with T both in Γ returned by **CONVERT** and in the inputs of **GET_METRIC_VALUES**. Utilities returned by this method should be of form $u_i: S \times T \rightarrow \mathbb{R}$, and the contents of **ADD_NEXT_LEVEL** in Section 3.2 between rows (#12-30) should be replaced with:

```

12: | | | | if  $i < n$  then
13: | | | | |  $y \leftarrow \text{NEW\_CHOICE\_NODE}()$ ,  $\text{TRACE}(y) \leftarrow (\text{TRACE}(x), a_i)$ 
14: | | | | |  $g(y) \leftarrow i + 1$ ,  $h(y) \leftarrow A_{i+1}$ ,  $E \leftarrow E \cup \{(x, a_i, y)\}$ ,  $Y \leftarrow \{y\}$ 
15: | | | | | else
16: | | | | |  $c \leftarrow \text{NEW\_CHOICE\_NODE}()$ ,  $g(c) \leftarrow 0$ ,  $h(c) \leftarrow A_0$ 
17: | | | | |  $\Omega \leftarrow \Omega \cup \{c\}$ ,  $V \leftarrow V \cup \{c\}$ ,  $E \leftarrow E \cup \{(x, a_i, c)\}$ 
18: | | | | | if HAS_CONSISTENT_EXECUTABLE_SUBSET( $(\text{TRACE}(x), a_i), \text{PROB}, \omega_0, \omega, G)$ ) then
19: | | | | | |  $(Y, p_Y) \leftarrow \text{CHOICE\_NODES\_FROM\_P\_SUCC\_STATES}(\omega, (\text{TRACE}(x), a_i), \text{PROB}, \omega_0, G)$ 
20: | | | | | | foreach  $y \in Y$ ,
21: | | | | | | |  $g(y) \leftarrow 1$ ,  $h(y) \leftarrow A_1$ ,  $P_1(y) \leftarrow \{y\}$ ,  $E \leftarrow E \cup \{(c, y, y)\}$ 
22: | | | | | | | foreach  $j \in N$ ,
23: | | | | | | | | OBS_HIST( $j, y$ )  $\leftarrow \langle \text{OBS\_HIST}(j, \omega), \dots$ 
24: | | | | | | | | |  $\text{OBS}(j, \text{INCL\_PROGR\_FACTS}(\omega, (\text{TRACE}(x), a_i), \text{PROB}, \omega_0, G))$ , ...
25: | | | | | | | | |  $\text{OBS}(j, y)\rangle$ ,  $Q_j(y) \leftarrow \{y\}$ 
26: | | | | | | | end-foreach
27: | | | | | | end-foreach
28: | | | | | | else
29: | | | | | | |  $Y \leftarrow \{\omega'\}$ ,  $p_Y(\omega') \leftarrow 1$ ,  $E \leftarrow E \cup \{(c, \omega', \omega')\}$ 
30: | | | | | | end-if
31: | | | | | |  $s_0(c) \leftarrow p_Y$ 
32: | | | | | | end-if
33: | | | | |  $action\_level_{i+1}(\omega) \leftarrow action\_level_{i+1}(\omega) \cup Y$ ,  $V \leftarrow V \cup Y$ ,  $\Omega \leftarrow \Omega \cup Y$ 

```

This includes management of chance nodes c , added after each n -long action-combination $(\text{TRACE}(x), a_i)$ to represent possible probabilistic outcomes. The set of choice nodes in the next state level corresponding to these outcomes, Y ,

connected to c , is produced by **CHOICE_NODES_FROM_P_SUCC_STATES**. It generates all possible successor states via all possible consistent and executable action-subsets of $(\mathbf{TRACE}(x), a_i)$ as described in the end of Section 3.1, except that the consistency of (joint)actions depends on every variation of their effects.

The **CONVERT** method in Sections 3.1-3.3 is of *constant-time complexity* in the number of possible state/action-trajectories within a finite horizon k , however the number of these trajectories is *super-exponential* in the number of agents., i.e. optimization is needed. The following 4 steps reduce the redundancy of G .

1. From top to bottom each edge of potentially not executable and `no-op` actions should be deleted from G together with their complete sub-graph.
2. If a chance node c has only 1 outgoing edge, then it should be deleted, and its parent action node a should be connected directly to its child state node ω .
3. Starting from the last state-level the cloned ω' nodes should be deleted together with the edges from their parents.
4. If the last remaining outgoing edge of a node is being deleted, then the node should be replaced with the end-vertex of that edge, if it exists. Otherwise, if it is an action-node, it should be deleted with all edges from its parents.

3.4 Example

A *one-card poker problem* is formulated in MA-PDDL based on pp. 37-40 in [10]. It is then converted to an extensive-form game, which is solved, and the solution is projected back to the MA-PDDL level. The example is best read and understood in conjunction with the original definition of MA-PDDL in [2] and Appendix 1-3.

```

(define (domain one-card-poker)
  (:requirements :strips :equality :negative-preconditions :typing :numeric-fluents
    :conditional-effects :partial-observability :probabilistic-effects :multi-agent)
  (:types player) (:constants player1 player2 - player)
  (:predicates (next-role fo ?p - player) (winning-hand-player1 (fo player1)))
  (:functions (income-of fo ?p - player) (investment-of fo ?p - player) (money-in-pot fo))

  (:action raise :agent player1 :parameters ()
    :precondition (next-role player1)
    :effect (and (not (next-role player1))
      (next-role player2)
      (increase (investment-of player1) 1)
      (increase (money-in-pot) 1)))

  (:action fold :agent player1 :parameters ()
    :precondition (next-role player1)
    :effect (and (not (next-role player1))
      (when (not (winning-hand-player1))
        (increase (income-of player2) (money-in-pot)))
      (when (winning-hand-player1)
        (increase (income-of player1) (money-in-pot)))))

  (:action meet :agent player2 :parameters ()
    :precondition (next-role player2)
    :effect (and (not (next-role player2))
      (increase (investment-of player2) 1)
      (when (not (winning-hand-player1))
        (increase (income-of player2) (+ (money-in-pot) 1)))
      (when (winning-hand-player1)
        (increase (income-of player1) (+ (money-in-pot) 1)))))

  (:action pass :agent player2 :parameters ()
    :precondition (next-role player2)
    :effect (and (not (next-role player2))
      (increase (income-of player1) (money-in-pot))))

  (define (problem one-card-poker-probl)
    (:domain one-card-poker)
    (:init (next-role player1)
      (= (money-in-pot) 2)
      (= (income-of player1) 0)
      (= (income-of player2) 0)
      (= (investment-of player1) 1)
      (= (investment-of player2) 1)
      (probabilistic 0.5 (winning-hand-player1)))
    (:goal :condition ())
    (:metric :agent ?p - player
      :utility maximize (- (income-of ?p) (investment-of ?p))))

```

There are 2 agents, `player1` and `player2`, playing a simple poker game. Before the play, both put 1 coin in the pot. Then they both receive their cards. `player1` receives a winning hand with a probability of $\frac{1}{2}$, and then it either *raise* the bid (to 2 coins) or *fold*. If it folds (shows its cards), then if it has a winning hand, then it wins the pot. Otherwise `player2` wins. But if `player1` raises, then `player2` can either *meet* this bid (also put 1 more coin in the pot) or *pass*. If it decides to pass, then `player1` wins the pot. But if `player2` meets, then if `player1` has a winning hand, then `player1` wins the pot. Otherwise `player2` wins the pot.

Both agents try to maximize their profit (i.e. the difference of their income and investment), but `player2` is in a worse position, since it is unable to observe the hand of `player1`. So `player2` decides between meeting or passing by chance.

To solve this problem it is first converted to an extensive-form game. Since Poker is non-cooperative game, a non-cooperative solution concept can be used, e.g.

Perfect Bayesian Equilibrium [13], since the game is of incomplete information. The horizon of the conversion is trivially $k = 2$. There are 2 possible initial states depending on whether `winning-hand-player1` is true with probability $\frac{1}{2}$. A chance node, ω_0 , is created with 2 edges to `state_level_0`. Every action-combination is considered for $k = 2$ steps, and since both decentralized agents have 3 actions (including `no-op`), there are 9 combinations, so a resulting game-graph G with 423 nodes emerges, which can be reduced to 11 nodes by using the optimization steps at the end of Section 3.3 (see. Fig. 1). Finding the PBE of this game leads to a unique mixed NE, according to which `player1` should *raise* if it has a winning hand, otherwise it should *fold* with probability $\frac{2}{3}$ or *raise* (bluff) with probability $\frac{1}{3}$, while `player2` should *meet* with probability $\frac{2}{3}$ or *pass* with probability $\frac{1}{3}$. This is a rational joint-solution of the above non-cooperative MAP problem.

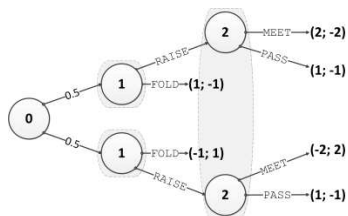


Figure 1

Extensive-form of the one-card poker problem (as shown also in Fig. 2.2 on p. 40 in [10])

The above (reduced) game may seem small, but this is only due to the simplicity of the example. More complex MAP problems can induce much larger games, which may need reduction or solution approximation [9]. Furthermore, the example given was non-cooperative, but MA-PDDL can also describe inherently cooperative situations, e.g. cf. the example in [2], where the only solution is for the self-interested agents to cooperate to achieve their common goal. Thus beyond using cooperative solution concepts, cooperation can be achieved even that way.

Conclusions

Algorithms for converting fully- and partially-observable probabilistic MA-PDDL descriptions to extensive-form games were proposed in order to solve multi-agent planning problems in general. Partial-observability and probabilistic effects were introduced as separate, additional extensions to MA-PDDL. Depending on the multi-agent planning problem at hand and the solution concepts used to solve the resulting game, both cooperative and non-cooperative behavior can be achieved. Limitations include the discrete nature of converted descriptions, and that each agent needs to execute exactly one action at a time. In the future this could be extended to durative cases without the limit on the number of concurrent actions.

Acknowledgement

This work was partially supported by the ARTEMIS JU and the Hungarian National Development Agency (NFÜ) in frame of the R3-COP (Robust & Safe Mobile Co-operative Systems) project.

References

- [1] M. de Weerd, B. Clement: Introduction to Planning in Multiagent Systems, *Multiagent Grid Systems*, 5(4):345-355, 2009
- [2] D. L. Kovacs: A Multi-Agent Extension of PDDL3.1, *Proceedings of the 3rd Workshop on the International Planning Competition (IPC), ICAPS-2012*, Atibaia, Brazil, 25-29 June 2012, pp. 19-27
- [3] J. von Neumann, O. Morgenstern: *Theory of Games and Economic Behavior*, Princeton, 1944
- [4] H. W. Kuhn: Extensive Games and the Problem of Information, in: H. W. Kuhn, A. W. Tucker, eds., *Contributions to the Theory of Games*, Vol. 2, Princeton University Press, Princeton, 1953, pp. 193-216
- [5] D. McDermott et al.: PDDL---The Planning Domain Definition Language, *Tech.Rep., TR-98-003/DCS TR-1165*, Yale Center for CVC, NH, CT, 1998
- [6] M. Ghallab, D. S. Nau, and P. Traverso: *Automated Planning: Theory and Practice*, Morgan Kaufmann, 2004
- [7] S. J. Russell, P. Norvig: *Artificial Intelligence: A Modern Approach* (3rd edition) Prentice Hall, 2010
- [8] T. Bylander: Complexity Results for Planning, *Proc. of 12th International Joint Conference on Artificial Intelligence (IJCAI 91)*, Sydney, New South Wales, Australia, 24-30 August 1991, pp. 274-279
- [9] A. Gilpin: *Algorithms for Abstracting and Solving Imperfect Information Games*, Ph.D. Dissertation, Carnegie Mellon University, Pittsburgh, 2009
- [10] R. B. Myerson: *Game Theory: Analysis of Conflict*, Harvard Univ., 1997
- [11] J. F. Nash: Non-Cooperative Games, *Annals of Maths*, 54:286-295, 1951
- [12] R. Selten: Reexamination of the Perfectness Concept for Equilibrium Points in Extensive Games, *Int. Journal of Game Theory*, 4(1):25-55, 1975
- [13] D. Fudenberg, J. Tirole: Perfect Bayesian Equilibrium and Sequential Equilibrium, *Journal of Economic Theory*, 53:236-260, 1991
- [14] M. Helmert: Changes in PDDL 3.1, *Unpublished Summary from the IPC-2008 Website*, 2008
- [15] D. L. Kovacs: BNF Definition of PDDL3.1, *Unpublished Manuscript from the IPC-2011 Website*, 2011
- [16] J. C. Harsanyi: Games with Incomplete Information Played by Bayesian Players, Part I-III., *Management Science*, 14(3):159-182, 14(5):320-334, 14(7):486-502, 1967-1968
- [17] M. Fox, D. Long: Modelling Mixed Discrete-Continuous Domains for Planning, *Journal of Artificial Intelligence Research*, 27:235-297, 2006

- [18] F. Müller, S. Biundo: HTN-Style Planning in Relational POMDPs Using First-Order FSCs, Proc. of 34th Annual German Conference on Artificial Intelligence (KI 2011), Berlin, Germany, 4-7 October 2011, pp. 216-227
- [19] H. L. S. Younes, M. L. Littman: PPDDL 1.0: an Extension to PDDL for Expressing Planning Domains with Probabilistic Effects, Technical Report, CMU-CS-04-167, Carnegie Mellon University, Pittsburgh, 2004
- [20] F. Teichteil-Königsbuch: Extending PPDDL1.0 to Model Hybrid Markov Decision Processes, Proc. of Workshop on A Reality Check for Plan. and Sched. Under Uncert., ICAPS-08, Sydney, Australia, 15 September 2008
- [21] D. S. Bernstein, R. Givan, N. Immerman, and S. Zilberstein: The Complexity of Decentralized Control of Markov Decision Processes, Mathematics of Operations Research, 27(4):819-840, 2002

Appendix 1. Extending MA-PDDL with partial-observability

Appendix 1-3 is best read in conjunction with the BNF (Backus-Naur Form) grammar of MA-PDDL [2] and PDDL3.1 [15]. A new requirement is *added* to MA-PDDL, `:partial-observability`. To capture partial-observability, the *addition* of the following 6 rules is proposed to the BNF of MA-PDDL.

```
<structure-def> ::= :partial-observability <observation-def>
<observation-def> ::=
    (:observation <observation-symbol>
     [:agent <agent-def>]:multi-agent
     [:parameters (<typed list (variable)>)]
     [:condition <emptyOr (pre-GD)>]
     [:value <emptyOr (observation-value)>])

<observation-symbol> ::= <name>
<observation-value> ::= :numeric-fluents <f-exp>
<observation-value> ::= :numeric-fluents + :continuous-effects <f-exp-t>
<observation-value> ::= :object-fluents <function-term>
```

The above extension has the same semantics as events proposed in [17]. A *grounded observation holds in states where its conditions are satisfied*, but it can't be referred to in conditions or effects of actions or anywhere else. Observations can be used solely by the planners and/or incorporated in conditional plans. For the sake of convenience the following 5 rules are also *added* to the grammar.

```
<atomic formula skeleton> ::= :partial-observability
    (<predicate> <fo> <typed list (variable)>)

<atomic function skeleton> ::= :partial-observability
    (<function-symbol> <fo> <typed list (variable)>)

<fo> ::= fo
<fo> ::= :multi-agent (fo [<name>])
<fo> ::= :multi-agent (fo [<type>])
```

The above 5 rules allow the declaration of full-observability of individual Boolean- and numeric-fluents. An `fo` atom can be placed as the first argument of respective predicate- or function-definitions. The 1st rule for `<fo>` is covers the

single-agent case, but if it is used in the multi-agent case, then every agent(object) can observe the corresponding fluent (always, every value). The other two rules for `<fo>` let us specify the type (or even a union of types) of those agents, which always observe every value. If the type is not given, it is assumed to be `object`.

According to our current knowledge, the only work in literature addressing the addition of partial-observability to PDDL is [18]. It adds observations to the probabilistic extension of PDDL (PPDDL1.0) [19] via the addition of observation-predicates that can be referred to in separate observation-effects of actions. Although this concept is simple, it is not clear enough semantically. The partial-observability extension of MA-PDDL proposed in this paper aims to clarify that.

Appendix 2. Further extending MA-PDDL with probabilistic-effects

Now probabilistic-effects are added to MA-PDDL beyond partial-observability based on PPDDL1.0 [19] and its extension to probability-distributions [20]. First the BNF of the effects of discrete actions should be *modified* to the following.

```

<effect> ::= <p-effect>
<effect> ::= (and <effect>*)
<effect> ::=:conditional-effects (forall (<typed list (variable)>) <effect>)
<effect> ::=:conditional-effects (when <GD> <effect>)
<effect> ::=:distribution-effects (imply <f-comp> <effect>)
<effect> ::=:probabilistic-effects (probabilistic <prob-effect>)
<p-effect> ::= (not <atomic formula(term)>)
<p-effect> ::= <atomic formula(term)>
<p-effect> ::=:numeric-fluents (<assign-op> <f-head> <f-exp>)
<p-effect> ::=:object-fluents (assign <function-term> <term>)
<p-effect> ::=:object-fluents (assign <function-term> undefined)
<p-effect> ::=:rewards (<additive-op> <reward fluent> <f-exp>)
<prob-effect> ::= <probabilistic list effect>+
<prob-effect> ::=:distribution-effects + :numeric-fluents <distribution (f-exp)> <effect>
<probabilistic list effect> ::= <probability> <effect>
<probability> ::= <number>
<probability> ::=:numeric-fluents <f-exp>

```

PPDDL1.0 [19] is different compared to PDDL3.1 [15] in that it allows *when*-statements to be nested directly into each other. This is the only significant difference. This allows for *conditional probabilistic effects*. Beyond this [20] adds *distribution-effects*, which are also included above in a bit optimized form. They are introduced in the Appendix of [20]. The difference here is that they are parametric (thus grounded or lifted). E.g. the following distributions can be used.

```

<distribution (t)> ::= (gaussian t t <random variate>)
<distribution (t)> ::= (exponential t <random variate>)
<distribution (t)> ::= (uniform t t <random variate>)
<distribution (t)> ::= (poisson t <random variate>)

```

PPDDL1.0 also introduced `:rewards` in form of *reward-fluents* which are not part of the state. Moreover, in PPDDL1.0 `<probability>` was only `<number>`, but in [20] it could be already a function-expression. We used the latter. A further *modification* of the MA-PDDL grammar based on [19,20] is the following.


```

<assign-op> ::= <additive-op>
<additive-op> ::= increase
<additive-op> ::= decrease

```

Similarly to [19] reward-fluents are also *added* to the language in form of the below 2 rules. The second rule allows reward-fluents to be defined for specific agents (referred to as constants, variables or object-fluents) in the multi-agent case. The first rule can be used only in the single-agent case.

```

<reward fluent> ::= total-reward
<reward fluent> ::= :multi-agent (total-reward <term>)

```

A novelty in [20] was the addition of probability-distributions to [19]. A key of this addition was the introduction of *random variates*, which are eventually the actual random values of the distributions, that can be referred in functional-expressions in the below form, after *adding* the below 2 rules to the grammar.

```

<f-exp> ::= :distribution-effects <random variate>
<random variate> ::= #<any char>*

```

PPDDL1.0 and its extension in [20] were discrete, but their ideas can be applied in a straightforward manner to the durative case by *adding* the following 10 rules.

```

<da-effect> ::= :probabilistic-effects (probabilistic <prob-da-effect>)
<timed-effect> ::= :continuous-effects + :numeric-fluents + :rewards
                (<additive-op> <reward fluent> <f-exp-t>)

<f-assign-da> ::= :numeric-fluents + :rewards
                (<additive-op> <reward fluent> <f-exp-da>)

<prob-da-effect> ::= <probabilistic list da-effect>+
<prob-da-effect> ::= :distribution-effects + :numeric-fluents
                <distribution (f-exp-da)> <da-effect>
<prob-da-effect> ::= :distribution-effects + :continuous-effects + :numeric-fluents
                <distribution (f-exp-t)> <da-effect>

<probabilistic list da-effect> ::= <da-probability> <da-effect>

<da-probability> ::= <number>
<da-probability> ::= :numeric-fluents <f-exp-da>
<da-probability> ::= :numeric-fluents + :continuous-effects <f-exp-t>

```

Probabilistic- and distribution-effects can now define the value of observations with the *addition* of the below 8 rules.

```

<observation-value> ::= :probabilistic-effects (probabilistic <prob-observation>)

<prob-observation> ::= <probabilistic list observation>+
<prob-observation> ::= :distribution-effects + :numeric-fluents
                <distribution (f-exp)> <observation-value>
<prob-observation> ::= :distribution-effects + :numeric-fluents + :continuous-effects
                <distribution (f-exp-t)> <observation-value>

<probabilistic list observation> ::= <obs-probability> <observation-value>

<obs-probability> ::= <number>
<obs-probability> ::= :numeric-fluents <f-exp>
<obs-probability> ::= :numeric-fluents + :continuous-effects <f-exp-t>

```

In case of continuous-time probabilities are normalized in runtime to guarantee that they comply with the elementary properties of probability distributions.

```

<problem> ::= (define (problem <name>)
                (:domain <name>)
                [<require-def>]
                [<object declaration>]
                <init>
                <goal>+
                [<goal-reward>]:rewards
                [<constraints>]:constraints
                <metric-spec>*:numeric-fluents
                [<length-spec>])

```

Above the *modified* rule for describing problems is shown. The only change beyond the previous changes is the *addition* of goal-rewards, similarly to [19].

```

<goal-reward> ::= (:goal-reward <metric-f-exp>)
<goal-reward> ::=:multi-agent (:goal-reward
                                [:agent <agent-def>]
                                :reward <metric-f-exp>)

```

If the first rule is used in case of `:multi-agent`, then it refers to all agents. Inheritance/polymorphism of goal-rewards is similar to goals and metric in [2].

```

<metric-f-exp> ::=:rewards <reward fluent>
<metric-f-exp> ::= goal-achieved
<metric-f-exp> ::=:multi-agent (goal-achieved <term>)

```

Similarly to [19] the above 3 rules are *added*. The 3rd rule allows the goal-achieved fluent of a specific agent in the metric of any agent. If the 2nd rule is used in MA-case then it is 1 iff the goal of every agent was achieved at least once.

The following collection of rules is based on [20], and *changes* the hitherto description of initial states mainly to optionally include uncertainty.

```

<init-el> ::= <p-init-el>
<init-el> ::=:timed-initial-literals <t-init-el>
<init-el> ::=:probabilistic-effects (probabilistic <prob-init-el>)
<init-el> ::=:conditional-effects (forall (<typed list(variable)>) <effect>)
<p-init-el> ::= <literal(name)>
<p-init-el> ::=:numeric-fluents (= <basic-function-term> <metric-f-exp>)
<p-init-el> ::=:object-fluents (= <basic-function-term> <metric-o-exp>)
<t-init-el> ::= (at <number> <p-init-el>)
<t-init-el> ::= (at <number> (and <p-init-el>*))
<t-init-el> ::=:probabilistic-effects
                (at <number> (probabilistic <t-prob-init-el>))
<t-init-el> ::=:conditional-effects
                (at <number> (forall (<typed list(variable)>) <effect>))
<prob-init-el> ::= <probabilistic list init>+
<prob-init-el> ::=:distribution-effects + :numeric-fluents
                <distribution (metric-f-exp)> <a-init-el>
<probabilistic list init> ::= <init-probability> <a-init-el>
<a-init-el> ::= (and <a-init-el>*)
<a-init-el> ::= <p-init-el>
<a-init-el> ::=:timed-initial-literals <t-init-el>
<a-init-el> ::= (probabilistic <prob-init-el>)
<a-init-el> ::=:conditional-effects (forall (<typed list(variable)>) <effect>)
<t-prob-init-el> ::= <probabilistic list t-init>+
<t-prob-init-el> ::=:distribution-effects + :numeric-fluents
                <distribution (metric-f-exp)> <t-a-init-el>
<probabilistic list t-init> ::= <init-probability> <t-a-init-el>
<t-a-init-el> ::= (and <t-a-init-el>*)
<t-a-init-el> ::= <p-init-el>
<t-a-init-el> ::= (probabilistic <t-prob-init-el>)
<t-a-init-el> ::=:conditional-effects (forall (<typed list(variable)>) <effect>)
<init-probability> ::= <number>
<init-probability> ::=:numeric-fluents <metric-f-exp>

```

Appendix 3. Summary of all additional new MA-PDDL requirements

- `:partial-observability` Allows observations in the domain description. It is compatible with multiple agents and probabilistic effects.
- `:probabilistic-effects` Allows discrete probabilistic elements in the effects of durative and non-durative actions and in initial states.
- `:distribution-effects` Allows probability distributions in probabilistic effects of durative and non-durative actions and in initial states.
- `:rewards` Allows reward fluents in effects of durative and non-durative actions and in the metric. It is compatible with `:multi-agent`.
- `:mdp` = `:probabilistic-effects` + `:rewards`
- `:pomdp` = `:mdp` + `:partial-observability`
- `:dec-mdp` = `:mdp` + `:multi-agent`
- `:dec-pomdp` = `:pomdp` + `:multi-agent`

I.e. MA-PDDL with `partial-observability+probabilistic-effects` can describe DEC-POMDPs (DECentralized Partially Observable Markov Decision Processes) [21].

Modelling Execution Tracing Quality by Means of Type-1 Fuzzy Logic

Tamás Galli, Francisco Chiclana, Jenny Carter, Helge Janicke

Centre for Computational Intelligence, Faculty of Technology, De Montfort University, The Gateway, Leicester, LE1 9BH, United Kingdom

p10553741@myemail.dmu.ac.uk, chiclana@dmu.ac.uk, jennyc@dmu.ac.uk, heljanic@dmu.ac.uk

Abstract: Execution tracing quality is a crucial characteristic which contributes to the overall software product quality though the present quality frameworks neglect this property. In the scope of this pilot study the authors introduce a process to create a model for describing execution tracing as a quality property; moreover, the performance of four different models created is compared. The process and the models presented are capable of capturing subjective uncertainty which is an intrinsic part of the quality measurement process. In addition, the possibility of linking the presented models to software product quality frameworks is also illustrated.

Keywords: software product quality models; execution tracing quality; fuzzy logic; uncertainty

1 Introduction

Execution tracing and logging are frequently used as synonyms in software technology; however, the first one serves the software developers to localize errors in applications, while the second one contributes to administration tasks to check the state of software systems. In the scope of this publication we also use the two phrases as synonyms.

Execution tracing dumps the data about the program state and the path of execution for developers for offline analysis, which helps to investigate error scenarios and follow changes in the state of the application. Thus, execution tracing belongs to dynamic analysis techniques i.e. testing, and investigating live systems which are integral parts of the maintenance activities. Dynamic analysis techniques can be applied only if the software is built and executable. Static and dynamic analysis techniques possess two significant common attributes: (1) they are applied to achieve the same goal to diagnose errors; (2) they generalize from a subset of all possible executions. Each technique has its own particular advantage.

Static analysis can produce sound results however with general properties, which are not precise but these results are accurate and have validity over all possible inputs. Dynamic analysis examines the concrete execution of the program by observing its behaviour, which is precise but the results are not valid for all possible inputs. The literature promotes the synergic use of these techniques [37], [6].

The increasing size and complexity of software systems considering their varying workload makes localizing software errors more difficult. This difficulty is more challenging with regard to the enormous number of software and hardware combinations. Adding execution trace to some key places of the application can drastically reduce the time spent with debugging. Consequently, execution tracing has direct impact on the development and maintenance costs [2].

In addition, debugging is not necessarily a feasible option when (1) applications perform process control, (2) the error is related to parallel processing and race conditions, or (3) performance problems need to be analysed [2], [35]. In the case of distributed, multithreaded applications execution tracing is the only adequate instrument to help with the error analysis as states Laddad in [20]. In the case of embedded applications, which have no user interface, only by means of execution tracing can the developer or system maintainer answer such questions as to what the application is doing [34].

Moreover, execution tracing significantly influences program comprehension, the importance of which arises if the program documentation is deficient or of poor quality. In a study by Fjeldstad and Hamlen [7] it is estimated that the comprehension of existing software systems consumes between 47% and 62% of maintenance resources [25], [31]. An experiment conducted by Karahasanovic and Thomas introduced in [19] categorized the difficulties related to the maintainability of object-oriented applications. Program logic was ranked the first in the source of difficulties. Understanding the program logic belongs to the category of software specific knowledge which can greatly be enhanced by execution tracing, offering a basis for trace visualization and program comprehension [31].

Tracing, logging or constraint checks represent a significant part of the source code of applications. Spinczyk, Lehmann and Urban in [33] state that the ratio of code lines related to monitoring activities reached approximately 25% in their measurements targeted at certain commercial applications. This ratio shows that a significant amount of source code is written to deal with such tasks as execution tracing which in itself is an important quality factor.

In conclusion, the above indicate that execution tracing has significant impact on the analysability of software systems. Moreover, measuring quality is difficult, some properties are easier to measure than others even if they are well defined [27]. Quality frameworks include the description of qualitative properties in quantitative manner and quality measure elements which cannot be measured

directly but only derived. Consequently, the measurement process implicates subjective uncertainty which has also been admitted by the standard ISO/IEC 25021:2007 involved in software product quality by defining the subjective measurement method. In the scope of this article the authors introduce a pilot study to describe execution tracing quality by means of a model which can encompass subjective uncertainty. The model itself does not perform quality assessment but it can be used to define quality targets against which a product can be assessed.

The remainder of this article is structured as follows: Section 2 describes how the quality model pilot was built including identification of inputs, outputs and construction of the knowledge base. Section 3 introduces the validation of the quality model. Section 4 describes the limitations of the pilot study and gives an outlook to the final model while Section 5 introduces related works. We summarise the contributions of our work in Section “Conclusions” and outline the future work in this area.

2 Constructing the Model

The model reflects the results of an empirical research which comprises of two parts: (1) a qualitative part to determine the model’s inputs, i.e. the quality properties on which execution tracing quality depends, and (2) a quantitative part to describe the relationships between the inputs and the output.

The qualitative research results from a brainstorming session and further processing of the output of this session. Brainstorming served as a method of data collection, developed by A. Osborn and made more sophisticated by H. C. Clark as a technique to create, collect, express ideas to a topic [34]. The main principle of the method is formed by two fundamental factors: (1) each group member must have the possibility to express ideas without having to expose them to a critic at first, then (2) the ideas can be developed further by other group members. Consequently, synergistic effects can lead to the triggering of ideas by those already present [33]. Before and after the idea generation phase an ideation phase must take place. Before ideation the participants think over the brainstorming question individually as preparation for the brainstorming [13]. The idea generation is followed by an ideation phase again where evaluation of the collected ideas takes place [34]. The critics towards this method mainly focus on the idea generation phase regardless of ideation that takes place before and after; however, Osborn did not propose brainstorming instead of the ideation but as a supplement to it [13]. In this method the quantity of ideas is not limited. The more ideas that are collected the more probable it is to have qualitative ideas among them. The latter has been questioned in [8], which contradicts the views held in [13] in some respects.

The output of the brainstorming is a list of raw ideas considered to be feasible by the group [34]. This list forms the possible input candidates of the model, which need to undergo further analysis.

The quantitative part of the research formalizes the relationships of the inputs in the output. For collecting this information, experiences of one software developer involved also in software maintenance for several years were scrutinized. The quantitative part of the research needs to use methods to deal with subjective uncertainty. Consequently, fuzzy logic is used to describe the input-output relationships, which also offers tolerance towards imprecision [37].

Fuzzy logic offers basically two theoretical approaches to the problem: type-1 and type-2 fuzzy logic. Type-1 fuzzy logic can consider a certain amount of subjective uncertainty and it usually performs well in process control but shows less positive results in decision making where larger amounts of uncertainty need to be considered. In contrast, type-2 fuzzy logic performs well in both situations but the operations and inference are more complex and computationally more expensive than the operations and inference of type-1 fuzzy logic. In the pilot study described in this paper type-1 fuzzy logic is used [23], [5], [17], [18].

Fuzzy modelling makes it possible to incorporate human expertise in the model directly [14], [4]. Castillo and Melin recommend the following modelling steps [4]:

1. Determining the relevant input and output variables
2. Choosing the type of the fuzzy inference system
3. Determining the number of linguistic terms associated with each input and output variable
4. Designing the fuzzy if-then rules
5. Choosing memberships functions
6. Interviewing human experts to determine the parameters of membership functions
7. Refine the parameters of membership functions

As four fuzzy models have been built and tested in the scope of this pilot study, the above steps were not performed in the same order as they stand in the list. In addition, tuning the membership functions did not take place to be able to compare the performance of the different models with the same membership functions.

2.1 Determining the Inputs and the Output of the Model

The output of the model, i.e. execution tracing quality, originates from the goals of the research; meanwhile, the possible inputs, i.e. quality properties on which execution tracing quality depends, were identified by brainstorming.

The brainstorming group was constructed of software developers and maintainers with several years of experience. The list of feasible ideas collected by the group underwent analysis by two experts who scored the input candidates according to their importance with regard to execution tracing quality. The experts had to distribute the same amount of scores among the items collected i.e. constant sum scaling was applied [22].

The arithmetic means of the scores assigned by experts were calculated. Each input candidate that has been selected as input has a relative importance above 10% according to the judgement of the experts. In this way the chosen inputs of the execution tracing quality model are:

1. Processability

Processability refers to such properties of the execution traces whether (1) the trace possesses appropriate granularity for the examination of the execution path, (2) communication dialogs can uniquely be identified, (3) threads can uniquely be identified, (4) process IDs are traced, (5) error severity is traced, (6) component interfaces can be traced, (7) trace entries are marked with a timestamp with appropriate granularity.

2. Code Coverage

The property code coverage indicates maximally how many per cent of the source code is covered with execution tracing.

3. Configurability

Configurability encompasses how easily and sophisticatedly the execution tracing can be configured. This property includes such judgements whether (1) execution tracing can be set to different levels of granularity, (2) the configuration change in execution tracing requires complex actions from the operators, developers or maintainers, (3) it is possible to configure a performance trace which only traces method invocations at the component boundaries to have less impact on the performance, (4) it is possible to trace in different outputs including file, database, network socket, (5) it is possible to trace in different formats including: plain text, xml, html, proprietary binary, ASN.1 BER, ASN.1 PER.

4. Consequent Naming

Consequent naming refers to the property whether the same events are always traced with the same pattern in the output, including whether (1) exceptions are always designated with the same identifiers, (2) the same level of errors and warnings are consequently used, (3) method entry and exit points are consequently traced.

2.2 Linguistic Variables

The notion of linguistic variables was introduced by L. Zadeh [38]. These variables are able to handle imprecision and offer a basis also for natural language computation. The formalism implemented by these variables and the if-then rules establishes an effective modelling language [37].

Before identifying the appropriate linguistic variables, each input and output needed to undergo partitioning to determine the granularity with which the system has to be described. A high number of partitions makes sophisticated description possible but it also introduces complexity as the number of necessary fuzzy rules needs to be increased. Moreover, incorporating human expertise with a high number of linguistic variables exposes difficulties because contradictions can be introduced in the model in an easy manner. Finding a consensus between the possibility of a sophisticated model description and the reduction of the possibility of introducing contradictions in the model, three input partitions and five output partitions have been defined. The linguistic variables for the defined partitions have been identified in the following way:

Linguistic variables for all inputs: {*poor*, *medium*, *good*}

Linguistic variables for the output: {*very poor*, *poor*, *medium*, *good*, *very good*}

2.3 Membership Functions

Linguistic variables were depicted by means of membership functions to make inference possible. While developing the model for execution tracing quality, two types of membership functions were used: (1) triangular and (2) Gaussian, both types with overlaps as illustrated in Figure 1.

Each membership function maps the interval $[0, 100]$ to the interval $[0, 1]$. The domains of the membership functions can be interpreted as percentage values, while the codomain depicts the degree of membership in the given category.

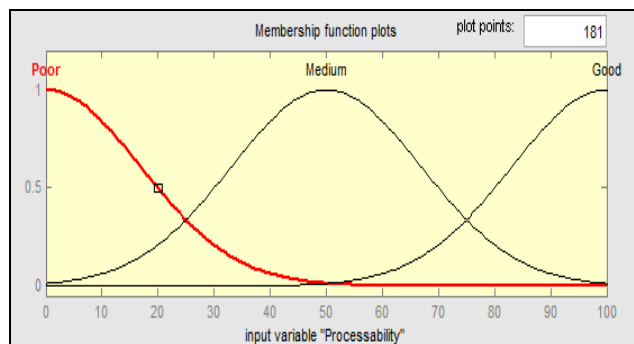


Figure 1
Membership Functions of the Input: Processability

2.4 Knowledge Base for the Model

The knowledge of one expert with regard to execution tracing quality has been described with the formalism offered by the if-then rules and the linguistic variables [37]. The knowledge base is summarized in Table 1. This is not a complete rule set i.e. it does not contain each variation of all linguistic variables of all inputs but a complete rule set is not necessary to achieve appropriate performance. The model was assessed as described in Section 3.

Table 1
Antecedent and Consequent Parts of the Fuzzy Rules

	Antecedent Linguistic Variables are Connected by Logical AND Operation				Consequent
ID	Processability	Code Coverage	Configurability	Consequent Naming	Execution Trace Quality
1.	<i>poor</i>	<i>poor</i>	n.a.	n.a.	<i>very poor</i>
2.	<i>medium</i>	<i>poor</i>	n.a.	n.a.	<i>poor</i>
3.	<i>poor</i>	<i>medium</i>	n.a.	n.a.	<i>poor</i>
4.	<i>medium</i>	<i>medium</i>	<i>poor</i>	<i>poor</i>	<i>poor</i>
5.	<i>medium</i>	<i>medium</i>	<i>poor</i>	<i>medium</i>	<i>medium</i>
6.	<i>medium</i>	<i>medium</i>	<i>medium</i>	<i>medium</i>	<i>medium</i>
7.	<i>medium</i>	<i>medium</i>	<i>good</i>	<i>medium</i>	<i>medium</i>
8.	<i>medium</i>	<i>medium</i>	<i>good</i>	<i>poor</i>	<i>medium</i>
9.	<i>medium</i>	<i>medium</i>	<i>good</i>	<i>good</i>	<i>good</i>
10.	<i>medium</i>	<i>medium</i>	<i>poor</i>	<i>good</i>	<i>medium</i>
11.	<i>good</i>	<i>medium</i>	<i>poor</i>	<i>poor</i>	<i>poor</i>
12.	<i>good</i>	<i>medium</i>	<i>medium</i>	<i>poor</i>	<i>medium</i>
13.	<i>good</i>	<i>medium</i>	<i>good</i>	<i>poor</i>	<i>medium</i>
14.	<i>good</i>	<i>medium</i>	<i>poor</i>	<i>medium</i>	<i>medium</i>
15.	<i>good</i>	<i>medium</i>	<i>medium</i>	<i>medium</i>	<i>medium</i>
16.	<i>good</i>	<i>medium</i>	<i>good</i>	<i>medium</i>	<i>medium</i>
17.	<i>good</i>	<i>medium</i>	<i>poor</i>	<i>good</i>	<i>good</i>
18.	<i>good</i>	<i>medium</i>	<i>medium</i>	<i>good</i>	<i>good</i>
19.	<i>good</i>	<i>medium</i>	<i>good</i>	<i>good</i>	<i>good</i>
20.	<i>good</i>	<i>good</i>	<i>poor</i>	<i>poor</i>	<i>medium</i>
21.	<i>good</i>	<i>good</i>	<i>medium</i>	<i>poor</i>	<i>medium</i>
22.	<i>good</i>	<i>good</i>	<i>good</i>	<i>poor</i>	<i>good</i>
23.	<i>good</i>	<i>good</i>	<i>poor</i>	<i>medium</i>	<i>medium</i>
24.	<i>good</i>	<i>good</i>	<i>medium</i>	<i>medium</i>	<i>medium</i>

25.	<i>good</i>	<i>good</i>	<i>good</i>	<i>medium</i>	<i>good</i>
26.	<i>good</i>	<i>good</i>	<i>poor</i>	<i>good</i>	<i>medium</i>
27.	<i>good</i>	<i>good</i>	<i>medium</i>	<i>good</i>	<i>good</i>
28.	<i>good</i>	<i>good</i>	<i>good</i>	<i>good</i>	<i>very good</i>
29.	<i>medium</i>	<i>good</i>	<i>Good</i>	<i>good</i>	<i>medium</i>
30.	<i>poor</i>	n.a.	n.a.	<i>good</i>	<i>medium</i>
31.	n.a.	<i>poor</i>	n.a.	<i>medium</i>	<i>poor</i>

2.5 Type-1 Fuzzy Inference Techniques

The two most widespread fuzzy methods for inference have been considered: (1) Mamdani's approach and (2) the approach of Takagi-Sugeno-Kang. The Tsukamoto method [28], [14] has been excluded as it requires monotonic consequent membership functions.

2.6 Comparison of the Created Models

For the purpose of comparison, four models were created with the same inputs and output: (1) type-1 fuzzy logic with Mamdani's approach with triangular membership functions, (2) type-1 fuzzy logic with Mamdani's approach with Gaussian membership functions, (3) type-1 fuzzy logic with the approach of Takagi-Sugeno-Kang with triangular membership function, (4) type-1 fuzzy logic with the approach of Takagi-Sugeno-Kang with Gaussian membership functions. In addition, Mamdani's approach was also tested with two different defuzzification techniques: (1) mean of maxima (MOM), and (2) centroid of gravity (COG). The validation charts are presented only for the best performing method which in this context was implemented by the inference mechanism of Takagi-Sugeno-Kang with Gaussian membership functions. The outcomes of the other approaches are briefly introduced below.

The acceptance criteria towards the model and its output can be summarized in the following way:

1. Representation of expert's knowledge
2. Appropriate response for the changes in inputs
3. No oscillation in the output for input changes
4. Full output range needs to be used
5. The smoothness of the output is desired as it satisfies the problem better than fitting 2D planes together which build sharp edges where they join causing drastic responses in the output for small changes at certain points of the input.

2.6.1 Mamdani's Approach

Inference was performed with the min-max method [28]. The model built with Gaussian and triangular membership functions did not show significant differences, nevertheless, the surfaces achieved with Gaussian membership functions were slightly smoother.

The defuzzification methods applied indicated considerable deviations when the inputs reached the limits of the input range: the COG method did not use the full output range in contrast to the MOM method, which used the full output range. The MOM method can cause oscillation in the output [29].

The model built according to Mamdani's approach also shows sharp edges on the surfaces of the validation charts. With triangular membership functions thirty one rules were applied to describe the system and thirty rules were used with Gaussian membership functions for the same purpose.

2.6.2 Approach of Takagi-Sugeno-Kang

In the course of constructing the Takagi-Sugeno-Kang model, zero order functions (constants) were applied in the output range. This approach does not require computationally expensive defuzzification. For obtaining the output values weighted averages were calculated. Inference was performed with the product and probabilistic OR method.

The input Gaussian membership functions in comparison to the triangular ones resulted in more even transients between the different surface areas of the functions constructed from the input variables. The model with triangular membership functions contained thirty rules, meanwhile the model with Gaussian membership functions contained thirty one rules. Fine tuning of both models can be subject of further investigations.

The model built with the approach of Takagi-Sugeno-Kang with Gaussian membership functions provided the best performance compared to the other models on the basis of the above listed acceptance criteria. This inference technique helped to avoid sharp edges on the surfaces of the functions between the input and output variables.

Research also shows that the overlap of the antecedent membership functions determines the smoothness of the output behaviour with this inference method [14]. Further investigation of Jassbi et al. confirms that Takagi-Sugeno-Kang method shows more tolerance towards input noise than Mamdani's method [15], which is an advantageous property in the problem domain of the current research.

3 Validation

As the best results were produced by the Takagi-Sugeno-Kang approach with Gaussian membership functions, the validation of this model is presented in this section. The model possesses four inputs; consequently, six different combinations of the input pairs are possible to depict the influence of the inputs on the output, i.e. on execution tracing quality. Face validity [20] was applied to validate the model. An expert checked whether potential changes in the inputs cause appropriate response changes in the output according to the charts.

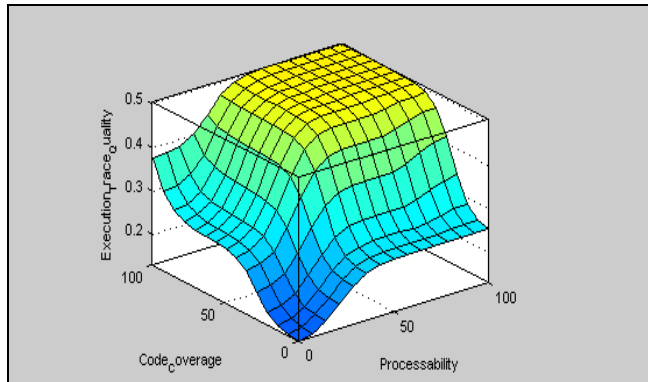


Figure 2

Code Coverage and Processability vs. Execution Trace Quality

Figure 2 shows that the decrease of the inputs “*Processability*” and “*Code Coverage*” below the medium level have a drastic impact on the execution tracing quality which also reflects the expert’s opinion. On the other hand, maximum quality of “*Processability*” and “*Code Coverage*” cannot cause a more than 50% increase in execution tracing quality, which supports the idea that these two inputs in themselves cannot cause the output to reach its maximum value.

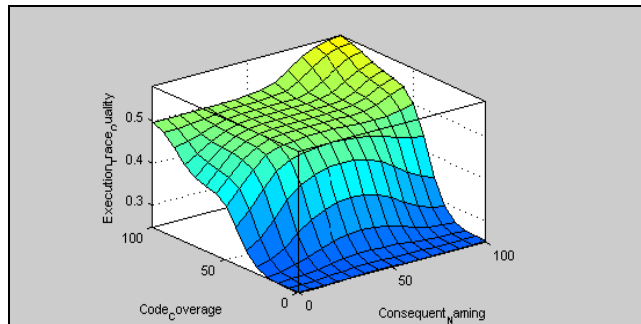


Figure 3

Code Coverage and Consequent Naming vs. Execution Trace Quality

Figure 3 illustrates that “Code Coverage” has a far stronger impact on the output than “Consequent Naming”. The system needs some fine tuning with regard to “Consequent Naming” in the *medium* range as the surface has a slight enhancement which slowly falls back when the value of “Consequent Naming” increases. The maximum of “Code Coverage” and “Consequent Naming” in themselves cannot cause the output to reach its maximum value. The diagram reflects the expert’s opinion.

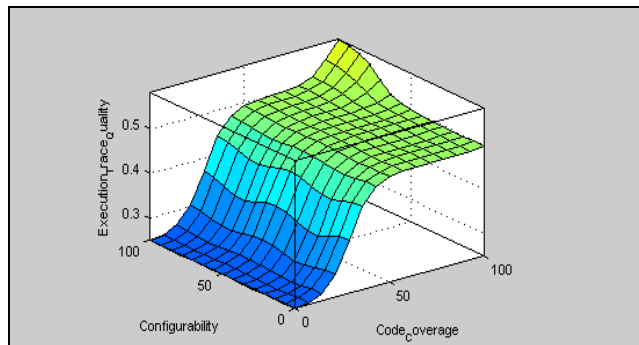


Figure 4

Configurability and Code Coverage vs. Execution Trace Quality

Figure 4 depicts that “Configurability” has a far smaller impact on the execution tracing quality than “Code Coverage”. Significant decrease of the output can be observed if “Code Coverage” is below *medium*, which reflects the expert’s opinion. The maximum quality of “Configurability” and “Code Coverage” without the other inputs cannot cause the output to reach its maximum value.

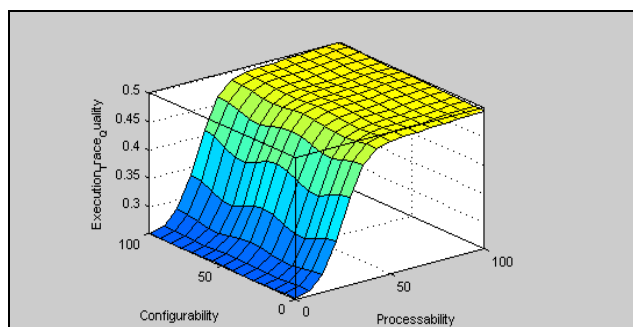


Figure 5

Configurability and Processability vs. Execution Trace Quality

Figure 5 shows that “Processability” contributes more to the execution trace quality than “Configurability”. With regard to the “Processability”-“Configurability” input pair, the diagram shows that “Configurability” has nearly no influence on the output in comparison to “Processability”. The fuzzy rules

need to undergo fine tuning to remove the slight waves from the chart, when “*Configurability*” changes; moreover, “*Configurability*” has little more than zero influence on the output in comparison to “*Processability*”, which has to be reflected by the model.

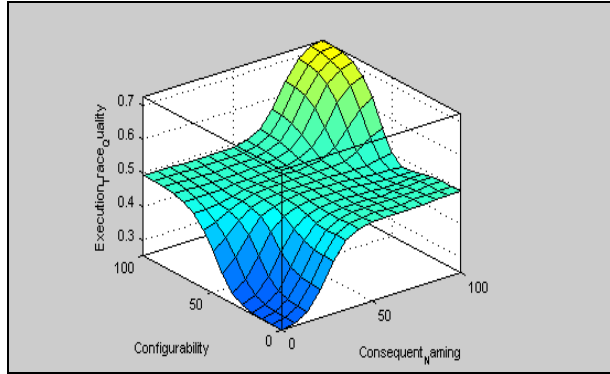


Figure 6

Configurability and Consequent Naming vs. Execution Trace Quality

Figure 6 shows that “*Configurability*” and “*Consequent Naming*” contribute to the output approximately to the same extent. Moreover, in comparison to the previously presented input pairs this combination has the most influence on the output in the *good-good* range. However, even if both inputs carry the highest value, the execution tracing quality is limited i.e. it depends on the other inputs too, as with the previously investigated pairs.

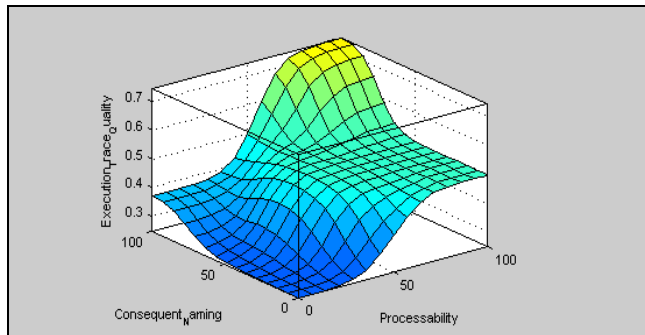


Figure 7

Consequent Naming and Processability vs. Execution Trace Quality

Figure 7 illustrates that both “*Consequent Naming*” and “*Processability*” have strong impacts on the output. The influence of the input pair reaches the same extent on the output as the “*Configurability*”-“*Consequent Naming*” input pair combination. The *medium-medium* ranges require fine tuning to avoid a slight local maximum on this area, depicted on the chart.

Table 2
Summary of the Validation Charts

Summary of the validation charts		
ID	Diagram	Conclusion
1.	From Figure 2. to Figure 7.	Changes of the inputs produce appropriate responses in the output.
2.	Figure 2.	The inputs Code Coverage and Processability have a significant impact on Execution Trace Quality.
3.	Figure 3.	Code Coverage influences Execution Trace Quality to a bigger extent than Consequent Naming.
4.	Figure 4.	Code Coverage influences Execution Trace Quality to a bigger extent than Configurability.
5.	Figure 5.	Processability influences Execution Trace Quality to a bigger extent than Configurability.
6.	Figure 6.	The inputs Consequent Naming and Configurability have approximately the same impact to Execution Trace Quality.
7.	Figure 7.	Processability has a bigger impact on Execution Trace Quality than Consequent Naming.
8.	Figure 7.	The fuzzy rules or the parameters of the membership functions need to undergo fine tuning to avoid the local maximum in the <i>medium-medium</i> range of the input variables Consequent Naming and Processability.

4 Related Works

Canfora, Aggarwal, Nerurkar amongst others have already illustrated how fuzzy mathematics can help to make judgements or predictions in connection with software maintainability [1], [3], [24] or reusability [26], [32]. However, these models cannot help with the assessment of software product quality as a whole because they are not linked to extensive software product quality frameworks like ISO/IEC 25010 [10]. In addition, the maintainability models investigated do not handle execution tracing quality.

Canfora, Cerulo, Troiano in [3] applied fuzzy logic to consider the following particularities in maintainability:

1. The assessment of software maintainability is influenced by qualitative and quantitative data including their subjective uncertainty.
2. Qualitative data which are often gathered by surveys are not always available.

3. The different sub-characteristics of maintainability contribute to the overall maintainability to different extents.

Aggarwal *et al.* discussed in [3] how an integrated metric of maintainability correlated with the time devoted to error corrections, however individually none of the investigated inputs of their model correlated with the time spent on error corrections. The model was constructed by means of type-1 fuzzy logic.

Nerurkar, Kumar, Shrivastava in [26] proposed a model based on type-1 fuzzy logic for reusability of aspect-oriented systems. Singh, Bhatia, Sangwan in [32] examined different soft computing techniques for software reusability assessment. In their publication type-1 fuzzy logic, neural network and adaptive neuro-fuzzy inference were compared for evaluating software reusability.

5 Limitations of the Pilot Study and Outlook to the Final Model

We need to make a distinction between the research methods applied for the pilot model described by this paper and the final model. Both approaches are empirical in nature and comprise of qualitative and quantitative research methods. The qualitative research part determines the inputs of the quantitative research i.e. the quality properties on which execution tracing quality depends in both cases. In addition, the quantitative research determines the impacts of these properties in execution tracing quality.

The reliability of the model strongly depends on the reliability of the data collected. The data of the pilot originate from the output of one brainstorming session processed by two experts in the field; meanwhile, the knowledge base formalises the knowledge of one expert. In contrast, the data of the final model will be based on a well-defined study population: software developers and maintainers will be selected from companies which have at least 50 employees in Hungary. The study population is distributed among 37¹ companies and its size amounts to 6010² individuals. Participants of the brainstorming sessions will be selected from this study population with judgmental sampling [22] for the qualitative research. Several brainstorming sessions will take place until a saturation point is reached or appropriately approached [20]. To implement this, two coders will look for synonyms in the outputs of the brainstorming sessions.

¹ Online database of HBI Online, [Online], 2012, [Accessed: 23.05.2012], Available from: www.hbi.hu, Search criteria: TEAOR'08=6201 and number of employees greater or equal 50

² Source: Hungarian Central Statistical Office, Social Statistics, Labour Market, 2012, [Online], [Accessed: 14.09.2012], Available from: <http://statinfo.ksh.hu/Statinfo/themeSelector.jsp?&lang=en>

Moreover; the data collected will undergo first and second cycle coding to establish the quality properties [30]. Coding also assumes calculating intercoder reliability for the coding process between the coders.

Regarding the quantitative stage, the same study population will be sampled with random multistage sampling to ensure a $p < .05$ statistical significance [22], [9]. The knowledge base, i.e. the rule set, of the model will be constructed from the knowledge gained from the sample by on-line surveying.

Conclusions

The pilot results illustrate that fuzzy modelling can be deployed to create a model for execution tracing quality to encompass the subjective uncertainty associated with the measurements process of software product quality.

In addition, modelling the knowledge of experts manually even if this knowledge is formalised with only thirty rules, introduces the chance for contradictions in the rule base. The number of these contradictions can considerably be reduced if the knowledge of several experts is considered in order to find a consensus and if automatic rule generation is used with adaptive neuro-fuzzy inferencing. Different algorithms for parameter tuning will also be considered [16].

The experimental models furthermore showed that the Gaussian membership functions performed better under the same settings because they contributed to avoiding sharp transients on the three-dimensional validation charts. Moreover, the most preferential smoothness in the output was achieved with the inference of Takagi-Sugeno-Kang while using overlapping Gaussian membership functions. In addition, Mamdani's inference method with the COG or MOM defuzzification techniques could not be applied as it does not satisfy the acceptance criteria introduced.

The pilot has been validated by face validity. For the pilot study the purpose was to test the research methodology and analysis methods to show the feasibility of the approach to model execution tracing quality. For this purpose face validity was sufficient to show that the selected approach is workable and can yield usable results. For the final model of execution tracing quality a more rigorous validation will be required. According to the plans its validity will be based on statistical evidence beside face and content validity [20]. Furthermore, the final model is planned to be constructed by using the adaptive neuro-fuzzy approach (ANFIS) which helps to keep the internal consistency by creating the model on the randomly selected one half of the data and checking it on the other half [14]. Application of ANFIS is also necessary due to automatic processing larger amount of data planned to be collected during the quantitative research. Reliability will also be embedded in the whole process of the research reaching from intercoder reliability to the reliability of the sampling and statistical inference. Moreover, in the qualitative part credibility, transferability, dependability and confirmability

will also be considered [20]. Research methods for the final model are presented in more detail in the previous section.

The present model is a standalone model but it also offers the possibility to be linked to the analysability sub-characteristic of the characteristic maintainability of ISO/IEC 9126-1 [10] or ISO/IEC 25010 software product quality models [10]. Linking the developed model to the standards is possible after formal description of the inputs, required by ISO/IEC 25021 [12], and after applying decomposition according to the internal-external view of the software product quality expressed by the ISO/IEC software product quality models.

Acknowledgement

The authors would like to acknowledge gratefully to all colleagues who participated in the brainstorming session and in the qualification of the input candidates of the model or contributed in any other way to the research.

References

- [1] Aggarwal, K. K., Y. Singh, P. Chandra, and M. Puri. "Measurement of Software Maintainability Using a Fuzzy Model." *Journal of Computer Sciences*, 2005: pp. 537-541
- [2] Buch, I. Park and R. "Improve Debugging and Performance Tuning with ETW." *MSDN Magazine*, [Online], [Accessed: 01.01.2012], Available from: <http://msdn.microsoft.com/en-us/magazine/cc163437.aspx>, 2007
- [3] Canfora, G., L. Cerulo, and L. Troiano. "Can Fuzzy Mathematics enrich the Assessment of Software Maintainability?" *ICEISSAM - Software Audit and Metrics*, 2004: 85-89
- [4] Castillo, O., and P. Melin. *Contributions to Fuzzy and Rough Set Theories and Their Applications, Type-2 Fuzzy Logic: Theory and Applications, Studies in Fuzzyness and Soft Computing*. Vol. 223, Springer, 2010
- [5] Coupland, S., M. Gongora, R. John, and K. Wills. "A Comparative Study of Fuzzy Logic Controllers for Autonomous Robots." *Proceedings of IPMU 2006 Conference*, [Online], [Accessed: 07.12.2011], Available from: <https://www.dora.dmu.ac.uk/handle/2086/184>, 2006
- [6] Ernst, M. D. "Static and Dynamic Analysis: Synergy and Duality." *In Proceedings ICSE Workshop on Dynamic Analysis*, 2003: 24-27
- [7] Fjeldstad, R. K. and W. T. Hamlen, "Application Program Maintenance Study: Report to Our Respondents," *Proceedings GUIDE 48*, Philadelphia, PA, 1983
- [8] Goldenberg, O., and J. Wiley. "Quality, Conformity, and Conflict: Questioning the Assumptions of Osborn's Brainstorming Technique." *The Journal of Problem Solving* 3, No. 2 (2011)

-
- [9] Hunyadi, L., and L Vita. *Statistika II. (Translated Title: Statistics II.)*. Aula Kiado, 2008
- [10] International Organization for Sandardization. "ISO/IEC 25010:2011, Systems and software engineering -- Systems and software Quality Requirements and Evaluation (SQuaRE) -- System and software quality models." 2011
- [11] International Organization for Sandardization. "ISO/IEC 9126-1:2001, Software engineering -- Product quality -- Part 1: Quality model." 2001
- [12] International Organization for Sandardization. "ISO/IEC TR 25021:2007, Systems and software engineering -- Systems and software Quality Requirements and Evaluation (SQuaRE) -- Quality measure elements." 2007
- [13] Isaksen, S. G., and J. P. Gaulin. "A Reexamination of Brainstorming Research: Implications for Research and Practice." *Gifted Chiled Quarterly The Official Journal of the National Association for Gifted Children* 49, No. 4 (2005)
- [14] Jang, J.-S. R., C.-T. Sun, and E. Mizutani. *Neuro-Fuzzy and Soft Computing*. Prentice Hall, 1997
- [15] Jassbi, J., P. J. A. Serra, R. A. Ribeiro, and A. Donati. "A Comparison of Mandani and Sugeno Inference Systems for a Space Fault Detection Application." *Proceedings of World Automation Congress WAC06* (doi: 10.1109/WAC.2006.376033), 2006: 1-8
- [16] Johanyák, Zsolt Csaba, Olga Papp. "A Hybrid Algorithm for Parameter Tuning in Fuzzy Model Identification." *Acta Polytechnica Hungarica*, Vol. 9, No. 6, pp. 153-166, 2012
- [17] John, R., and J. Mendel. "Type-2 Fuzzy Sets Made Simple." *IEEE Transactions on Fuzzy Systems*, 2002: pp. 117-127
- [18] John, R., and S. Coupland. "Extensions to Type-1 Fuzzy Logic: Type-2 Fuzzy Logic and Uncertainty." In *Computational Intelligence: Principles and Practice*, by eds. G. Y. Yen ET AL, 89-102, 2006
- [19] Karahasanovic, A., and R. Thomas. "Difficulties Experienced by Students in Maintaining Object-oriented Systems: An Empirical Study." *Proceedings of the 9th Australasian Conference on Computing Education*, 2007: pp. 81-87
- [20] Kumar, R. *Research Methodology, A Step-by-step Guide for Beginners*. Sage, 2011
- [21] Laddad, R. *AspectJ in Action*. Manning, MEAP, Second Edition, 2009
- [22] Malhotra, N. H. *Marketingkutatas (Translated title: Marketing Research)*. Akademia Kiado, 2009
-

- [23] Mendel, J. "Type-2 Fuzzy Sets: Some Questions and Answers." *IEEE Neural Networks Society*, 2003: 10-13
- [24] Mittal, H., and P. Bhatia. "Software Maintainability Assessment Based on Fuzzy Logic Technique." *ACM SIGSOFT Software Engineering Notes* Volume 34, No. 3 (2009)
- [25] Nelson, M. L. "A Survey of Reverse Engineering and Program Comprehension." *ODU CS 551 - Software Engineering Survey*, 1996
- [26] Nerurkar, N. W., A. Kumar, and P. Shrivastava. "Assessment of Reusability in Aspect-Oriented Systems using Fuzzy Logic." *ACM SIGSOFT Software Engineering Notes* Volume 35, No. 5 (2010)
- [27] Research Triangle Institute. "RTI Project Number 7007.011, The Economic Impacts of Inadequate Infrastructure for Software Testing." [Online], [Accessed: 06.12.2012], Available from: <http://www.nist.gov/director/planning/upload/report02-3.pdf> (U.S Department of Commerce), 2002
- [28] Ross, T. *Fuzzy Logic with Engineering Application*. Wiley, 2010
- [29] Runkler, T. "Selection of Appropriate Defuzzification Methods Using Applicationspecific Properties." *IEEE Transactions on Fuzzy Systems* 5, No. 1 (1997)
- [30] Saldana, J. *The Coding Manual for Qualitative Researchers*. Sage, 2009
- [31] Shi, Z. "Visualizing Execution Traces, Master Thesis." [Online], [Accessed: 17.05.2011], Available from: <http://www.mcs.vuw.ac.nz/comp/graduates/archives/mcompsc/reports/2004/Zhenyu-Shi-final-report.pdf>, 2005
- [32] Singh, Y., P. K. Bhatia, and O. Sangwan. "Software Reusability Assessment Using Soft Computing Techniques." *ACM SIGSOFT Software Engineering Notes* Volume 36, No. 1 (2011)
- [33] Spinczyk, O., D. Lehmann, and M. Urban. "AspectC++: an AOP Extension for C++." *Software Developers Journal*, 2005: pp. 68-74
- [34] Univeristy of Cologne, Methodenpool. "Brainstorming, [Online], [Accessed: 27.07.2012], Available from: http://methodenpool.uni-koeln.de/brainstorming/frameset_brainstorming.html."
- [35] V. Uzelac, A. Milenkovic, M. Burtscher, M. Milenkovic. "Real-time Unobtrusive Program Execution Trace Compression Using Branch Predictor Events." *CASES 2010 Proceedings of the 2010 international conference on Compilers, Architectures and Synthesis for Embedded Systems*, ISBN: 978-1-60558-903-9, 2010

- [36] Young, M. "Symbiosis of Static Analysis and Program Pesting." *In Proc. 6th International Conference on Fundamental Approaches to Software Engineering*, 2003: 1-5
- [37] Zadeh, L. A. "Fuzzy logic = computing with words." *IEEE Transactions on Fuzzy Systems* 4, No. 2 (1996): 103-111
- [38] Zadeh, L. A. "The Concept of a Linguistic Variable and its Application to Approximate Reasoning-II." *Information Sciences*, 1975: 301-357
- [39] Zadeh, L.A. "Fuzzy Sets." *Information and Control*, 1965: pp. 338-355

Doberdó Observation Trail for the Education of Environmental Protection Engineers

Judit Németh-Katona

Óbuda University

Rejtő Sándor Faculty of Light Industry and Environmental Protection Engineering

Doberdó út 6, H-1034 Budapest, Hungary

e-mail: katona.judit@rkk.uni-obuda.hu

Abstract: The objective of this research: To comply a set of field exercises to evaluate environmental conditions with special emphasis on ecological and biological aspects, for the education of environmental engineering and engineering instructor students. Sets of tests to adequately analyze the environment in a complex way are practically non-existent. The few that exist are focused on some particular, narrow area, primarily examining inanimate environmental factors. The majority of these tests are chemical quick tests to detect the presence and level of a specific substance polluting the environment. The results are descriptive observations, merely stating facts, without offering any explanation for the causes of different phenomena, simply providing factual data measured in a particular moment in time. Based merely on these results, it could be hard or impossible to make any responsible suggestion regarding environmental or land development issues.

Keywords: Education for the environment, The Application of Field Exercise in the Education of Environmentalism and Nature Conservation, Observation trail, Biologically qualified environment, Ecologically evaluated conditions

1 Introduction

“Education for the environment”

The survival of life on earth depends on a harmonious equilibrium between human society and the environment. To achieve this balance through the process of sustainable development should be our eternal goal that could be attained only by an increased environmental awareness of people [3].

The necessity of paradigmatic changes has become a matter of life and death in our time. The domain of environmental education has been extended, it is rather “education FOR the environment” [2] [11] [12]. It includes the encouraging of a dedicated, environmentally conscious lifestyle, with constant affirmations, the shaping of behavior, values, attitudes, and emotions, increasing knowledge, and

inspiring actions to prevent any further damage and degradation of the environment [10].

The education for sustainability is based on interpreting the environment as a system. The author focuses on observing living beings, because that is also an indication of the conditions of the inanimate components. The explanation of this statement is that transformations caused by use in a region always result in transformations of living beings on some level, thus the condition of living beings is an indicator of the condition of inanimate components [7].

Environmental field trips concentrating on complex observation of biocenosis can demonstrate causality, and can be operative [4]. [5].

2 Methods

Educational Methods on a Field Trip

The field trip completed together with the students, as an educational learning tool, covered the entire range of pedagogical issues regarding the concepts of sustainability.

The field exercises developed a critical approach based on experimental knowledge, and that improved the students' skills to evaluate, to make decisions, to deal with crisis situations. It promoted problem solving in thinking processes, and increased creativity in actions. By applying experimental knowledge, it produced practical, functional knowledge [8].

As opposed to the declarative communication of information, it emphasized an activity driven, "process" nature of learning, as revealed in the author's researches [1].

The experiences of field exercises confirmed that to comprehend the sustainability of environmental systems, it is not sufficient to rely on unidirectional declaration of theoretical data, or direct verbal communication. It is necessary to apply the knowledge in an actual environment because the preservation of the environment focuses on problems, and actions to solve them [8].

The field trips provided an active and constructive learning environment (promoting self-improvement and collective improvement) where knowledge and educational benefits were achieved by individual and collective experiences through completing tasks. That is why a field trip could be considered the method of direct demonstration and presentation, regarding the method of acquiring knowledge for the basics of the ecological approach [8] (*Figure 1*).



Figure 1

That is why a field trip could be considered the method of direct demonstration and presentation, regarding the method of acquiring knowledge for the basics of the ecological approach (The photo (picture) of the author's)

In the interiorization process, the educational effects (interactions) created by educational factors, and the educational methods resulting in these effects, were quite different on the field trip from the methods of traditional classroom education environment, as revealed by the research.

The primary difference can be found in the methods of organizing activities: On the field, due to the configurations of the terrain, any activity was efficient only when working in smaller groups.

Thus an environmentally conscious value system was developed by the indirect educational methods and impacts of collective activities, and by the influence of emerging customs, behavior and activity models, and convictions of the group.

In the opinion of educational researchers, the problem of applying indirect educational methods is that the results are hard to register [8].

By comparing the results of different groups when completing different tasks and exercises, it was possible not only to determine the level of skills and professional knowledge, but also to measure the degree of personality forming functions achieved.

In the author's experience, when working with groups the project method is the most efficient on the field, because the interiorization of knowledge is achieved as part of, and also the result of a creative process. This supports the idea previously mentioned that field exercises make it possible to measure how effective the indirect educational methods have been [8].

When working on the project, the participants did not simply search for the solution to a particular problem out of context, instead, they observed and analyzed multiple junctions and interconnections. This could not have been accomplished without discussion, arguments, mutual demand and control.

3 Results

Developing Skills of Environmental Awareness by Designing an Observation Trail

The development of information processing methods in evaluating the environment was focused on the potential applications and further elaborations of bioindicators.

Using the sulphur dioxide pollution examination as an example: The amount of sulphur dioxide present can be measured by instruments, but can also be determined by the degree of leaf necrosis of sensitive deciduous trees measured on a scale of experiences, or can also be determined by the presence of lichen species in the area.

The development of educational methods was intended to increase the efficiency of indirect educational methods in a group activity form, and it was accomplished by designing an interactive observation trail.

3.1 Location of Doberdó Observation Trail

The location of the field trip and observation trail project is Budapest's northwest part (Óbuda), between Doberdó street and Kiscelli street, beside Bécsi street (*Figure 2*).

The location is characterized by the polarized and concentrated presence of a great variety of natural features and phenomena within a small, limited area. The location is easy to access from the Óbuda University, is beside it directly.

This location is extremely appropriate to demonstrate environmental qualities from ecological and biological aspects, and to observe and evaluate conditions in an objective manner, which is the very objective of the environmental and nature conservation field exercises. The law regulating the assessment of natural resources defines seven specific areas for the evaluation of conditions. With the exception of two of these areas (condition of agricultural land, and waste management), all other areas (condition of waters, condition of air, condition of living organisms, condition of built components, and level of noise pollution) can be analyzed and evaluated by the observations and exercises described in this presentation at the above mentioned location, thus providing a place of demonstration for field education.



Figure 2

The location of the Doberdó Observation Trail is Budapest' northwest part (Óbuda), between Doberdó street and Kiscelli street. (Comment's figure: Third Region of Budapest, Kiscelli castle's garden; ▲ North; Contour line of Relief is equal 10 metres) (The figure5 is the author's work Budapest based on a map (<http://korlat.bmknet.hu/hun/kiscell/terkep.html> 2007)

3.2 Interactive Observation Trail in the Óbuda

The 12 stations of the observation trail, can be completed with the assistance of a study guide or “information booklet.“ When designing the trail, the educational method was mainly focused on the questions of Where? What? and How? When designating the area, and selecting the topics to be studied, there were two major factors to be considered: The informative value, and the dedication to avoid any harm to the natural resources involved.

Through defined tasks, and relevant explanations the trail provides information about geographical features of the area, about geological and surface processes (*Figure 3*), hydrological values, biocenosis of the area, peculiarities of the vegetation, ecological particulars, and historical cultural values.



Figure 3

Station 6 of The Doberdó Observation Trail; Terrace of Traventino limestone (The photo (picture) of the author's)

The stations are as follows: Opening station (geographical location, marking the boundaries of the region, rules of conduct, itinerary, time frame) (*Figure 4*); the abandoned quarry; talus slope and forest community with linden and ash trees; oak trees; observing Traventino limestone; site of prehistoric fossil; the stone chamber.



Figure 4

Opening station of The Doberdó Observation Trail is beside the Óbuda University; geographical location, marking the boundaries of the region, rules of conduct, itinerary, time frame (The photo (picture) of the author's)

The algorithm introducing the stations in the study guide is as follows:

- Name of station;
- Geographical location of station;
- Phenomena to be observed, natural resources, collecting survey data:
- Description of phenomenon to be observed;

- Tasks;
 - Description of the process of observation or measuring, determining the time and frequency of task, listing the equipments required, suggestions for the type of equipments;
 - Determining the methods of analyzing recorded data (e.g. creating charts or diagrams, comparing photographic and film documents, cartographic representation);
 - Control: Reference to the requirement of evaluating results, interpreting consequences, drawing conclusions, finding explanations.
- Explanation of the emergence and specifics of the phenomenon.
- Summary of results to be expected:
 - As a result of applying methods to process information;
 - As a result of indirect educational methods, accomplished by group activities.

The algorithm is demonstrated on the 1st station of the observation trail:

Station 1: *Abandoned quarry, clay-pit*

Location: The central part for the area, for the observation trail

Phenomena to be observed, natural resources: The study of successions of the vegetation.

Task: Identifying pioneer plant species, and species involved in the climactic forest community in the quarry yard, and the adjacent undisturbed hillside.

Explanation: Succession means the progress of the vegetation. In the quarry yard, due to the disturbance (the mining operations of the quarry), secondary succession can be observed that began when the mining operation was terminated. The area of the quarry was not recultivated, it attained its present condition through the process of natural reforestation. The process of succession is the process of changes in the vegetation in time: Stages of different combinations of species succeed one another, starting from pioneer communities, and ending with climactic communities.

3.3 Methods of Measuring To Qualify the Environment

The tools of education for the environment and nature conservation on a field trip are surveying, measuring, observing, testing.

As the result of my researches, a set of tests was compiled to examine the following: Microclimatic and air quality values, establishing the level of air

pollution by observing bioindicators, testing the reducing effect of vegetation on noise pollution, testing the soil from the ecological aspect, evaluating the condition of natural waters by observing bioindicators, geological and geomorphologic observations, examining characteristics and quality indicators in communities of living organisms [6].

Each test is built on the principle of practical evaluation of the environment: When examining the conditions in a biocenosis, both the qualitative and quantitative biological composition, and also the abiotic factors causing the particular distribution in space and time are taken into consideration as characteristic traits.

Using the microclimatic and air quality examinations regarding the characteristics of the vegetation as an example, this means the observations are not based only on instrumentally measured data (light intensity, temperature, humidity level) but also on surveying and studying the species composing a phytocenosis in different seasons, and by determining the extent of foliage closing, and the degree of exposition on slopes, some cause and effect connections are also revealed.

3.3.1 Examination of the Microclimate and State of the Air on the Basis of the Features of the Vegetation

Examination of periods of sunshine and intensity of light in open and closed surfaces covered with plants

Task. Record of hours of sunlight. Measurement of the strength of direct radiation with the help of lux measure device. Graphic representation of the recorded data (in relation to time) in different periods of the day, in various associations, in areas with various sun expositions and tree-stratum.

Comparison of data of habitats with various tree-stratum but identical exposition, furthermore with various exposition but similar value tree-stratum biotops. Explanation of the differences and interpretation of the consequences.

Anticipated results with application of knowledge-processing (data-processing) methods. The microclimate signifies the climate of smaller areas, which differ significantly from the surrounding area. The relief, exposition of slope, geographical position, soil and vegetation have significant role in their formation. Therefore, the climate is local and may differ significantly from the mezoclimate of the larger surrounding area.

Observation of types of plants with various light- and temperature demand

Task. Compilation of records of types of plants at the same location in early spring, in summer and autumn. Observation of light and temperature features of groups of plants in the living terrains, recording and graphic representation of the daily temperature fluctuation (it is necessary to measure the temperature at least three times daily in various groups, for more precise definition at every hour). The most widely used devices for this examination are station thermometers, which are

also used by meteorologists, which serve for the record of momentary temperature values. The measurement of the temperature fluctuation (extreme values) with a minimum, maximum thermometer of the various groups of trees and turf, as well as the vertical wood levels, the various tree-stratum groups. Interpretation of the measured values. Drafting (preparation) of a comparative diagram for the various associations using measurement data completed at identical point of time, Evaluation and explanation of the results.

Anticipated results with application of knowledge-processing (data-processing) methods. During their evolution plants adapted to various light and temperature conditions. In moderate and cold zones the amount of light and warmth differs significantly with the alteration of seasons and according to the time of day. The quantity of light of the habitat is also influenced by the vegetation. In spring before leaf-opening the turf level of a horn-bean wood receives one-third of the total quantity of light which arrives at the surface (geofiton aspect of early spring). During opening of leaves this value decreases to 1/8th-1/30th of the total quantity of light, while at mid-summer the soil level gets only 1/60th of the light quantity (Szerényi G. 1988).

3.3.2 Examination of the Air Pollution with the Help of Biological Indicators

Observation of sulphur-dioxyde pollution impact on the leaves of sensitive deciduous trees

Task. With the help of a Coverage Scale (*Figure 5*) the value of leave necrosis can be shown by examination of leaves of birch, maple and elm trees, then deduction can be made on the level of sulphur-dioxyde.

Anticipated results with application of knowledge-processing (data-processing) methods. As biological indicators trees can be regarded as sensitive monitors or accumulative monitors.

Sensitive monitors (coniferous, birch, small-leave linden, maple, elm, black elderberry) are very sensitive to air polluting substances, well-visible damage can be observed on the outside.

Leave necrosis means the death of cells and tissues. The impact of the air polluting substance begins on the margin of the leaves, then it continues into the inner surface of the leaves. With the majority of trees the blemishes begin at value of the sulphur-dioxyde air pollution higher than 0,9 ppm.

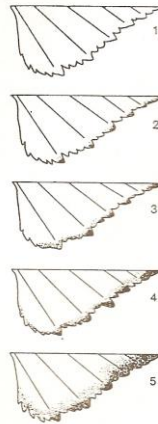


Figure 5

The value of leaf necrosis (Kársz, I. 1992 [8])

Demonstration of air pollution with the help of bark of trees as accumulative indicator

Task. Very careful carving off of a 2 mm thick 2 cm² surface of the bark of fir, maple and/or oak trees, at the height of 1,3 m. The sample should be placed in distilled water for one day, afterwards using a pH measure device the chemical reaction in the liquid should be measured.

Anticipated results with application of knowledge-processing (data-processing) methods. Under the influence of polluting substances accumulative monitors do not demonstrate visible alterations in the short term. However, they accumulate polluting substances in themselves, thus polluting substances can be detected in the bark. The content of heavy metals and sulphur in the bark of trees is proportional with the level of pollution in the area.

Determining air pollution level with the help of lichens

Task. Selection of observation, sample locations at least 300 meters apart from each other in the vicinity of an air polluting source (heavy traffic road, industrial plant, power station). Definition of the available lichen and their marking on a field map, afterwards interpretation of the results, deduction of consequences regarding level of pollution. The interpretation may be done after marking the results on all the sample places on a single map, so the air polluted zones stand out and thus the level of air pollution in the area can be evaluated:

- Lichen deserts, where the content of sulphur dioxide is higher than 0,15 mg/m³
- Straggler zone, where the content of sulphur dioxide is smaller than 0,17 mg/m³ and is greater than 0,15 mg/m³.

- Less polluted zone, where the content of sulphur dioxide is smaller than 0,07 mg/m³ and is greater than 0,05 mg/m³.

Normal or free zones, where the content of sulphur dioxide is 0,05 mg/m³ or lower.

Anticipated results with application of knowledge-processing (data-processing) methods. Lichen are living creatures which originated from the symbiosis of letiferous (fungus) and one-cell blue algae. Letiferous (fungus) is an obligatory parasite and is not capable of living separately from the algae, it cannot be found by itself. Lichen algae lives on photosynthesis, this way the fungus gets organic substances. Regarding their form of growth three types of lichen can be distinguished: lichen living on bark, leaves and bushes.

Lichen can be found on a number of different underlay (stand): soil, rocks, tree-bark, fences, housewalls), they are extremely adaptable and appear everywhere, except in air-polluted areas. Lichen are especially sensitive to high content of sulphur-dioxide and nitrogen-oxide in the air. They also well signal (denote) the presence of hydrogen-fluoride, chlorine, ozone, heavy metals and radi-active isotopes. Their extraordinary sensitivity, and thus their role as indicators for air polluting substances derives from the fact they do not have cuticles, therefore polluting substances easily get into the body of lichen. Their chlorophile content is low, therefore their metabolism, growth, regeneration capacity is limited. Their waterbalance depends entirely on the the air humidity and rain frequency. Their assimilation and regeneration time is quite short. They display activity mainly during rainy autumn and winter time, when the sulphur-dioxide content of the air is considerably higher than in summer. Lichen have been known as air pollution indicators and their presence and state of development has been observed for about 130 years.

Air Quality Index (AQI) can be calculated on the basis of lichen-coverage: the amount of lichen taxon (type, generation) value, and lichen coverage of the surface on the bases of percentage value evaluated 1-10 (0-10%=1 point, 11-20%=2 point, 21-30%=3point...91-100%=10 point).

3.3.3 Ecological Soil Examinations

The role of the chemical structure of the soil in influencing the plant species

Task. Defining the pH value of the soil with the help o fan indicator slip or pH measurement device.

Establishing correlation between the vegetation coverage, diversity of plants and chemical strucre of the soil.

Anticipated results with application of knowledge-processing methods. The chemical structure of the soil is determined by the ratio of the hydrogen and hydroxil ions present in the soil solutions.

According to chemical structure (regarding water pH) types of soil can be categorized in the following way:

pH value under 4,5 - strongly acidic soils

pH value 4,4 -5,5 - acidic soils

pH value 5,5 - 6,5 - mildly acidic soils

pH value 6,5 – 7,5 - chemically neutral soils

pH value 7,5 – 8,2 - soils with mildly base character

pH value 6,2 – 9, 0 - base-character soils

pH value higher than 9, 0 - soils with strong base character

There is a correspondence between the development of various types of vegetation and the pH value of the soil. Soils with pH value 3,5 -4,5 are too acidic for most of the plants. A pH value of about 4,5 is indicated by club moss, and coniferous types (spruce, redwood). Huckle-berries, pine trees, holly, willow-trees, birch denote 5,0 – 6,0 pH value. Most of the plants develop well in 6,5 – 7,0 pH value soils, the main indicators being aspen, ash, beech, red oak and maple. Blackberry, albespine and catalpa indicate pH value 7,0 - 8,0. the range of pH value above 8,5 is unfavourable for most of the plants.

3.3.4 Geological and Geomorphological Observations

Recognition and determination of rocks on the basis of observation of rocks and surface formations (paleontological examination)

Task. Examination and determination of rocks typical for the living place (magmatic, sedimentary, metamorphic). Categorization of sedimentary clastic rock according to the size of particles, differentiation of chemical sedimentary rocks using an acid-dripping method (lime, dolomite), distinguishing deep magmatic rocks on the basis of their mineral content.

Anticipated results with application of knowledge-processing methods. Classification of different types of rock and distinguishing their typical characteristics.

Defining types of surface formations, observation of their typical features

Task. Classification of prominent or flat formations on field upthrust, staired formation, valley, ghat (pass), canon, saddle. Observation of their characteristics, and determining their geographical exposition (with a compass). Correlation between surface formations and surface or subterranean water currents.

Anticipated results with application of knowledge-processing methods. Classification of relief formations, differentiation of their typical features.

3.3.5 Measurement of Noise-Screening Property of Vegetation

Task. Determining the noise-screening influence of the vegetation (the ability of leaves to reflect noise for example at tree-lined roads), graphic representation of the comparative data and interpretation. Making a noise-level map. (*Figure 6*).

Measurement of noise level at different points of the sample area. Defining of points and periods of measurement depending on the type of observation area. In woods it is reasonable to complete the measurement at dawn, in the morning, at dusk and at night. Near common roads it is recommended to measure at every hour and to record the average value of 5-minute measure time. Measurement points should be designated at various distances to the source of noise.

Anticipated results with application of knowledge-processing methods. Noise-moderating influence of the greenery and the distance from the source of noise.

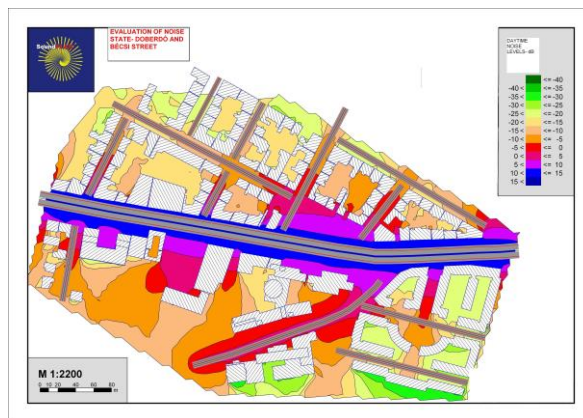


Figure 6

Measurement of noise, evaluation of noise state (Podmaniczky J. 2003, [9])

Conclusions

To sum up our research project: It has been verified that a field trip at a natural, actual location provides an extremely effective educational environment to develop the skills of environmental awareness, to convey information regarding sustainability issues, and to substantiate the holistic approach. Considering these facts, the author suggests that field exercises should be given high priority in the course requirements and curriculum of students majoring as environmental engineers and engineering instructors.

A field trip focusing on the environment and nature conservation is a form of educating and learning, and it can be successfully accomplished by completing the Doberdó Observation Trail designed by the author in the Óbuda.

From the aspect of environmental education, it has a holistic approach, focusing on the main characteristics of the region in a complex manner.

From the aspect of processing information, it emphasizes causality, interpreting the environment as a system. It is a tool to evaluate the environment ecologically and biologically, and to determine conditions objectively, assisted by the set of tasks to analyze the environment in the Doberdó Observation Trail, as described in this presentation.

From the aspect of acquiring knowledge, it is a method of direct demonstration and presentation accomplished in a natural, actual environment.

As a learning process, the field trip focuses on activity, it is an operative learning method based on experience, with preference to working in groups. By elaborating the environmental educational specifics of field exercises, the dissertation contributes to a more effective application of this educating-learning tool in environmental education, also providing a way to measure the efficiency of indirect educational methods.

References

- [1] Gough, Stephen-Scott, William Sustainable Development and Learning London: Routledge Falmer 1-3 2003
- [2] IUCN Commission in Education and Communication Supporting the UN Decade on Education for Sustainable Development IUCN Commission on Education and Communication 2003
- [3] Meadows, Dennis System Thinking in the Higher Education Sustainable Development Conference 21 april, 2005 ELTE University
- [4] Németh Katona, Judit Biologically Qualified Environment, Ecologically Evaluated Conditions Cereal Research Communications 2008/7 pp. 315-318
- [5] Németh Katona, Judit Biologically Qualified Environment, Ecologically Evaluated Conditions, Acta Polytechnica Hungarica, Vol. 5. No.3.2008 pp.101-105
- [6] Németh Katona, Judit Forming an observation trail for the students of environmental protection engineers in order to develop the education of scientific subjects in the field proc. of 4st. Kárpát-medencei International Conference for Development of Environmental Education, Debrecen, 2008. pp. 87-93
- [7] Németh Katona, Judit The reflections with regards to the tragedy of the toxic red sludge disaster of Ajka Proc. of IJCELIT (International Joint Conference on Environmental and Light Industry Technologies), 1st ICDEEE Conference (International Conference for Development of Environmental Engineering Education), Budapest, 2010.11.18-19. ISBN 9786155018084 2010. pp. 59-64
- [8] Németh Katona, Judit The Application of Field Exercise Potentials in the Education of Environmentalism and Nature Conservation, With Continued

Development of These Methods as Studied in the Mariaremete Canyon
Ph.D. Dissertation, University of Western Hungary 2006

- [9] Podmaniczky, József Noise-level map of Doberdó street 2003
- [10] Szabó, Marianne - Kovács, Ádám - Németh Katona, Judit - Lakatos, György Green Nursery Schools Programme 8. International JTEFS/BBCC Conference Sustainable Development Culture Education 2010 05. 17-19 Paris, France
- [11] UNESCO Education for Sustainability From Rio to Johannesburg Lessons learnt from a decade of commitment UNESCO 2002
- [12] United Nations Decade of Education for Sustainable Development 2005-2014, 2004

A Gaussian-mixed Fuzzy Clustering Model on Valence-Arousal-related fMRI Data-Set

Fuqian Shi and Pamela McCauley Bush

Department of Industrial Engineering and Management Systems
University of Central Florida, FL, 32825, USA
E-mail: fuqian.shi@ucf.edu; pamela.mccauleybush@ucf.edu

Abstract: Previous medical experiments illustrated that Valence and Arousal were high corresponded to brain response by amygdala and orbital frontal cortex through observation by functional magnetic resonance imaging (fMRI). In this paper, Valence-Arousal related fMRI data-set were acquired from the picture stimuli experiments, and finally the relative Valence -Arousal feature values for a given word that corresponding to a given picture stimuli were calculated. Gaussian bilateral filter and independent components analysis (ICA) based Gaussian component method were applied for image denoising and segmenting; to construct the timing signals of Valence and Arousal from fMRI data-set separately, expectation maximal of Gaussian mixed model was addressed to calculate the histogram, and furthermore, Otsu curve fitting algorithm was introduced to scale the computational complexity; time series based Valence -Arousal related curve were finally generated. In Valence-Arousal space, a fuzzy c-mean method was applied to get typical point that represented the word relative to the picture. Analyzed results showed the effectiveness of the proposed methods by comparing with other algorithms for feature extracting operations on fMRI data-set including power spectrum density (PSD), spline, shape-preserving and cubic fitting methods.

Keywords: fMRI; Gaussian bilateral filter; Valence-Arousal; power spectrum density; GMM fuzzy c-mean

1 Introduction

Human's emotion was characterized by Valence and Arousal under emotional dimension views. The dimension of Valence ranges from highly positive to highly negative, whereas the dimension of Arousal ranges from calming or soothing to exciting or agitating. Emotional dimension model (EDM) introduced that Valence means the intrinsic attractiveness (positive Valence) or aversiveness (negative Valence) of an event that reflects the extent of positive or negative, and Arousal is a physiological and psychological state of being awake or reactive to stimuli that denotes the degree of excitement or calm [1] [2]. Previous medical experiments

also illustrated the relationship between Valence -Arousal and specific chemical receptive fields in human brain [3] [4], and it was strictly distinguished at the level of regional activation by functional magnetic resonance imaging (fMRI) [5]. A plenty of studies showed that signals detected from many brain regions were applied to predict the subject's behavior during a scanning session of fMRI [6] [7] [8]. P. A. Lewis observed that in terms of different emotions (affective words) under varying degrees of stimuli were relative to the brain specific areas including the orbital frontal cortex, anterior cingulate, insula, amygdala, brain stem and pons and striatum by fMRI technique; it also indicated that the Valence and Arousal were highly correlated with the special area of brain, while "Arousal" was highly correlated with the orbital frontal cortex and "Valence" with the amygdala [9]. Li et al [10] demonstrated the relationship between specific function area of brain and decision-making through fMRI.

There have some tools for fuzzy clustering [11] [12] in fMRI research. For features extraction of fMRI images, CNR (contrast-to-noise ratio) reducing [13], Fourier reconstruction [14], and wavelet [15] were applied in image pre-processing; some scholars also focused on their difference by comparing with Electroencephalogram (EEG) [16] and Heart Rate Variability (HRV) [17]. Particularly, artificial intelligence technologies were applied in fMRI research successfully, the fuzzy c-mean clustering [18] [19] and independent component analysis (ICA) [20] [21], and fMRI visualization works were also crucial for fMRI images' processing [22]. Thereafter, neural networks [23], support vector machine [24], and Markov models [25] were applied in classification of fMRI from different zones of human brain. Analysis tools for fMRI were developed to some mathematical issues, such as fuzzy set, local optimization and preserving mappings algorithms [26]. Features exacted from fMRI were composed of a sequence of data points on a universe space. For calculating the Valence and Arousal response in human's brain, fuzzy c-mean clustering was addressed to solve the problem.

An outline of this paper is as follows. Section 2 introduced fMRI images' pre-processing includes image filter, segmenting, and feature exaction. Section 3 introduced a Gaussian mixed model for fuzzy clustering method on Valence - Arousal related fMRI time series images including fuzzy c-mean clustering and its expectation maximal for Gaussian mixed operations. Section 4 introduced case studies using the proposed method. In Section 5, we discussed the results and gave the comparing analysis with ICA and other feature exaction of fMRI-power spectrum density (PSD). Finally, in Section 6 we gave some conclusion remarks and future works. The framework of this paper was illustrated as in Fig. 1.

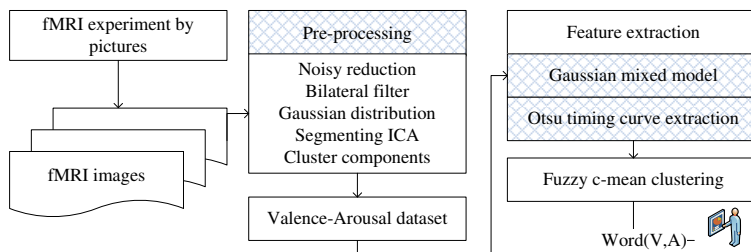


Figure 1

Framework of Valence-Arousal related fMRI time series data-set incorporating Gaussian mixed clustering model

2 fMRI Image Pre-Processing

2.1 fMRI Images' Noisy Reduction

Noisy reduction is the process of removing noise from a signal. All recording devices have traits which make them susceptible to noise, and in this paper, bilateral filter was applied for fMRI images' noisy-reduction. Bilateral filter (BF) is an edge de-noising filter methods that is constituted by two functions, one is to calculate the filter coefficients through a given geometric distance and another is depended on pixel difference. BF has obvious fuzzy-edge effect instead of Gaussian filter. Let $B(X) = k_d^{-1} \int_{-\infty}^{+\infty} \int_{-\infty}^{+\infty} f(\eta) c(\eta - X) d\eta$ be a transform on fMRI images, let k_d be $k_d = \int_{-\infty}^{+\infty} \int_{-\infty}^{+\infty} c(\eta) d\eta$, then the range filtering was calculated by

$$k_r^{-1}(X) \int_{-\infty}^{+\infty} \int_{-\infty}^{+\infty} f(\eta) S(f(\eta) - f(X)) d\eta \quad (1)$$

Photometric pixel similarity was defined as

$$k_r(X) = \int_{-\infty}^{+\infty} \int_{-\infty}^{+\infty} S(f(\eta) - f(X)) d\eta \quad (2)$$

But it is resulted that range filter need to be combined with domain to enforce both geometric and photometric locality that will be defined by

$$k_r^{-1} \int_{-\infty}^{+\infty} \int_{-\infty}^{+\infty} f(\eta) c(\eta - X) S(f(\eta) - f(X)) d\eta \quad (3)$$

and by

$$k_r(X) = \int_{-\infty}^{+\infty} \int_{-\infty}^{+\infty} c(\eta - X) S(f(\eta) - f(X)) d\eta \quad (4)$$

for normalizing. The BF was combined Gaussian distribution in this paper; for bilateral Gaussian filtering, let $c(\eta - X) = e^{-\frac{1}{2} \left(\frac{d(\eta - X)}{\sigma_d} \right)^2}$, where $d(\eta - X) = \|\eta - X\|$ is the Euclidean distance, and the similarity function is calculated by

$$Sim(\eta - X) = e^{-\frac{1}{2} \left(\frac{\delta(f(\eta) - f(X))}{\sigma_r} \right)^2} \quad (5)$$

where $\delta(f(\eta) - f(X)) = |f(\eta) - f(X)|$ is a norm in intensity space. In this paper, fMRI images were filtered by bilateral Gaussian model.

2.2 Cluster Components with Segmenting ICA

While filter and de-noising operation finished, we need to segment the initial fMRI images to locate the Valence and Arousal (Amygdala and orbital frontal cortex) related images' zone in each timing slices. Traditional methods, presented the independent components analysis (ICA) for fMRI segmenting [27] [28] are statistical theory based calculations; and most of them also are based on linear transformation; this transformation of the data or signal was separated into a linear combination of statistically independent non-Gaussian signal source. And ICA also is a special case of the blind signal separation (Blind source separation). Let $X = (x_1, x_2, \dots, x_n)^T$ $S = (s_1, s_2, \dots, s_n)^T$ be two random vectors, the objective is to use a transformation $S = WX$ to maximally independent components S that by function $F(s_1, s_2, \dots, s_n)$ of independence.

3 fMRI Feature Extraction

3.1 Otsu Curve Timing Histogram on fMRI

For extracting features from images of fMRI, some indices need to be calculated from spectrum of those images, and the image histogram was adopted in this paper. Time series based histogram and its statistical indices were selected for

time series prediction by Gaussian mixed fuzzy clustering operations. And the key issue was to output weighted sum of histogram, so Otsu's method [29] was proposed for searching for the threshold that can minimize the intra-class variance and was defined as a weighted sum of variances of the classes. Supposed that $\sigma_{\omega}^2(t) = \sum_i \omega_i(t) \sigma_i^2(t)$, weights ω_i are the probabilities of classes separated

by a threshold t and σ_i^2 variances of these classes. But minimizing the intra-class variance was equal to maximize inter-class variance that proposed by Otsu. we have that $\sigma_b^2(t) = \sigma^2 - \sigma_{\omega}^2(t) = \omega_1(t)\omega_2(t)[\mu_1(t) - \mu_2(t)]^2$ for two classes, where μ_i is the means of each class. And $\omega_1(t)$ was calculated as

$$\omega_1(t) = \sum_{i=0}^{i=t} p(i), \mu_1(t) = \sum_{i=0}^t p(i)x(i),$$

where $x(i)$ is the value at the center of the i -th histogram bin, and the same operation on $\omega_2(t)$.

3.2 Gaussian Mixed Modeling for Fuzzy Clustering

Fuzzy clustering supposed that data elements can belong to more than one cluster under a set of membership levels; and the widely used algorithm is the fuzzy c -means (FCM), which attempts to partition a finite collection of n elements $X = \{x_1, x_2, \dots, x_n\}$ into a collection of c fuzzy clusters with respect to some given criterion. Let $C = \{c_1, c_2, \dots, c_n\}$ be the centers, $U = u_{ij} \in [0, 1]$, $i = 1, 2, \dots, n$, $j = 1, 2, \dots, c$ be partition matrix, where each element u_{ij} represented the degree to how an element x_i belongs to a cluster c_j [30]. So the FCM was to minimize the function:

$$u_k(x) = \left(\sum_j \left(\frac{d(c_k, x)}{d(c_j, x)} \right)^{\frac{2}{m-1}} \right)^{-1} \quad (6)$$

The fuzzifier m determines the level of cluster fuzziness. Fuzzy c -means was a very important tool for image processing in clustering objects in an image that was proposed for fMRI feature extraction.

Let $\delta(\mu_i, \sigma_i)$ be the normal Gaussian distribution, 2-Gaussian mixed model is $M = \alpha_1 \delta(\mu_1, \sigma_1) + \alpha_2 \delta(\mu_2, \sigma_2)$, where $\sum_i \alpha_i = 1$, for calculating and simplify the covariance, let $\sigma = \sigma_1 = \sigma_2$, consider μ_1 we have that

$$\delta(\mu_1, \sigma^2) = \frac{1}{\sqrt{(2\pi)^3}} \sigma^{-1} e^{-\frac{(P-\mu)^T(P-\mu)}{2\sigma^2}} \quad (7)$$

Partial derivative on μ_1 , we have that

$$\begin{aligned} \partial_{\mu_1}(\delta(\mu_1, \sigma^2)) &= \frac{1}{\sqrt{(2\pi)^3}} \partial_{\mu}(\sigma^{-1} e^{-\frac{(x-\mu)^T(x-\mu)}{2\sigma^2}}) \\ &= \frac{1}{\sqrt{(2\pi)^3}} \cdot \left(-\frac{1}{2\sigma^2}\right) \sigma^{-1} \partial_{\mu}((x-\mu)^T(x-\mu)) \\ &= \delta(\mu_1, \sigma^2) \left(\frac{x-\mu_1}{\sigma^2}\right) \end{aligned}$$

and

$$\begin{aligned} \partial_{\sigma}(\delta(\mu_1, \sigma^2)) &= \frac{1}{\sqrt{(2\pi)^3}} \left[(-1)\sigma^{-2} e^{-\frac{(x-\mu_1)^T(x-\mu_1)}{2\sigma^2}} \right] + \\ &\quad \frac{1}{\sqrt{(2\pi)^3}} \sigma^{-1} e^{-\frac{(x-\mu_1)^T(x-\mu_1)}{2\sigma^2}} \left[\frac{(x-\mu_1)^T(x-\mu_1)}{\sigma^3} \right] \\ &= \delta(\mu_1, \sigma^2) \left[\frac{(x-\mu_1)^T(x-\mu_1)}{\sigma^3} - \frac{1}{\sigma^2} \right] \end{aligned}$$

Let estimation parameter matrix be $\theta = [\alpha_1, \alpha_2, \mu_1, \mu_2, \sigma_1^2, \sigma_2^2]$, the object is that

$$L(\theta) = \sum_i \ln\left(\sum_{j=1}^6 \alpha_j \delta(\mu_j, \sigma_j^2)\right) \quad (8)$$

deffrential by μ_j and σ_j on $L(\theta)$ respectively, we have that

$$\partial_{\mu_j}(L(\theta)) = \sum_i \frac{\alpha_j \delta(\mu_j, \sigma_j^2)}{\sum_{j=1}^2 \alpha_j \delta(\mu_j, \sigma_j^2)} \frac{x_i - \mu_j}{\sigma_j^2} \quad (9)$$

let $\varphi_j(P_i) = \frac{\alpha_j \delta(\mu_j, \sigma_j^2)}{\sum_{j=1}^2 \alpha_j \delta(\mu_j, \sigma_j^2)}$, we have that

$$\partial_{\mu_j}(L(\theta)) = \sum_i \varphi_j(P_i) \left(\frac{x_i - \mu_j}{\sigma_j^2} \right)$$

$$\begin{aligned} \partial_{\sigma_j}(L(\theta)) &= \sum_i \frac{\alpha_j \delta(\mu_j, \sigma_j^2)}{\sum_{j=1}^2 \alpha_j \delta(\mu_j, \sigma_j^2)} \left[\frac{(x_i - \mu_j)^T (x_i - \mu_j)^T}{\sigma_j^2} - \frac{1}{\sigma_j^2} \right] \\ &= \sum_i \varphi_j(x_i) \left[\frac{(x_i - \mu_j)^T (x_i - \mu_j)^T}{\sigma_j^2} - \frac{1}{\sigma_j^2} \right] \end{aligned}$$

let the above two equations equal to 0, we have that

$$\hat{\mu}_j = \frac{\sum_i \varphi_j(x_i) x_i}{\sum_i \varphi_j(x_i)}$$

$$\hat{\sigma}^2 = \frac{1}{2} \frac{\sum_i \varphi_j(x_i) (x_i - \mu_j)^T (x_i - \mu_j)}{\sum_i \varphi_j(x_i)}$$

For α_j , under $\sum_j \alpha_j = 1$, by Lagrangian Multiplier (LM), re-defined the object as

$$J = L(\theta) + \lambda \left(1 - \sum_{i=1}^6 \alpha_i \right) = \sum_i \ln \left(\sum_j \alpha_j \delta(\mu_j, \sigma_j^2) \right) + \lambda \left(1 - \sum_{i=1}^6 \alpha_i \right)$$

Diferential by α_j for this new object, we have that

$$\partial_{\alpha_j} J = \sum_i \frac{\delta(6\mu_j, \sigma_j^2)}{\sum_{j=1}^2 \alpha_j \delta(6\mu_j, \sigma_j^2)} - \lambda = \frac{1}{\alpha_j} \sum_i \varphi_j(x_i) - \lambda = 0$$

$$[\tilde{\alpha}_1, \tilde{\alpha}_2] = \left[\frac{1}{\lambda} \sum_i \varphi_1(x_i), \frac{1}{\lambda} \sum_i \varphi_2(x_i) \right]$$

$$\tilde{\alpha}_1 + \tilde{\alpha}_2 = \frac{1}{\lambda} \left[\sum_i (\varphi_1(x_i) + \varphi_2(x_i)) \right] = 1$$

We have $\lambda = 6$, so

$$[\tilde{\alpha}_1, \tilde{\alpha}_2] = \left[\frac{1}{6} \sum_i \varphi_1(x_i), \frac{1}{2} \sum_i \varphi_2(x_i), \dots, \frac{1}{2} \sum_i \varphi_6(x_i) \right]$$

where φ also is function of parameters, and resolved by iterations:

Step 1: let $\theta = [\alpha_1, \alpha_2, \mu_1, \mu_2, \sigma_1^2, \sigma_2^2]$, and given an initial value, in order to achieve convergence, μ_1, μ_2 can be calculated by the clustering method.

Step 2: calculate $\varphi_j(P_i)$.

$$\text{Step 3: calculate } \tilde{\mu}_j = \frac{\sum_i \varphi_j(x_i) x_i}{\sum_i \varphi_j(x_i)}.$$

$$\text{Step 4: calculate } \sigma_j = \frac{1}{6} \frac{\sum_i \varphi_j(x_i) (x_i - \tilde{\mu}_j)^T (x_i - \tilde{\mu}_j)}{\sum_i \varphi_j(x_i)}.$$

$$\text{Step 5: calculate } \alpha_j = \frac{1}{6} \sum_i \varphi_j(x_i).$$

Step 6: let $\tilde{\theta} = [\tilde{\alpha}_1, \tilde{\alpha}_2, \tilde{\mu}_1, \tilde{\mu}_2, \tilde{\sigma}_1^2, \tilde{\sigma}_2^2]$, if $\|\theta - \tilde{\theta}\| < \delta$, δ is a given threshold, then stop the process, or else goto **Step 2**.

4 Case Studies

4.1 Pre-Processing for Time Series-based fMRI Data-Set

A picture (related norm is kindness) stimuli experiment was arranged for acquiring time series fMRI data-set, the stimuli-time was 6s, and fast spin echo (FSE) acquisition anatomical images was adopted for imaging experimental data, and software - SPM8 was applied for space pre-processing and interlayer interference including the elimination of head motion correction, spatial registration and smoothing. The first step is to get clustering-components operations under bilateral filter of fMRI data-set, let α be spatial spread, β be the pixel value spread, γ be the number of components. The results were shown in Fig. 2.

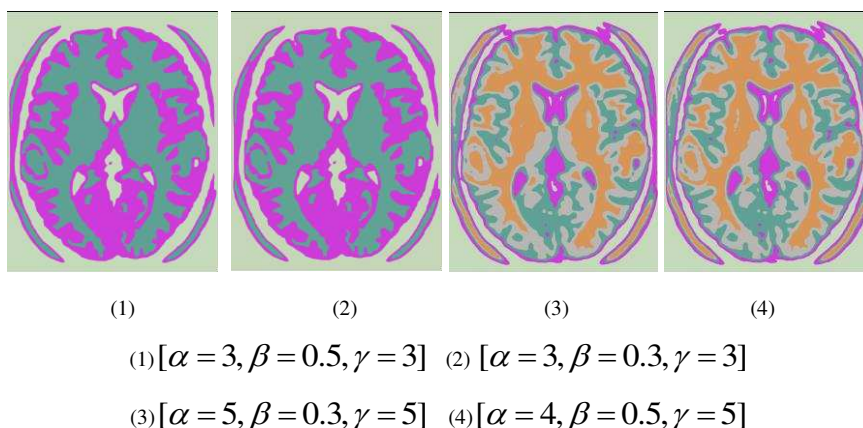
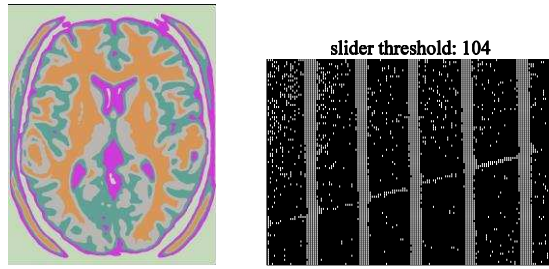


Figure 2

Gaussian components under bilateral filter for fMRI images

4.2 Gaussian-mixed Model under for fMRI Features Extraction

Expectation maximization for Gaussian mixture distributions combining Otsu's methods was applied to fMRI features extraction, and image histogram was calculated (Shown in Fig. 3).



(1) Initial images by filter and colored segmenting (2) operation by slider threshold =104

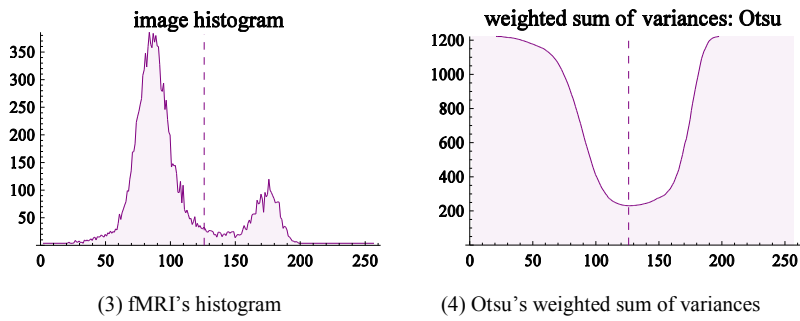


Figure 3

Feature curve exaction by Gaussian mixed model combining Otsu method

4.3 Fuzzy Clustering and Prediction

Valence - Arousal related fMRI curve extraction was finished by the proposed methods in Section 4.2 shown in as Fig. 4 and Fig. 5.

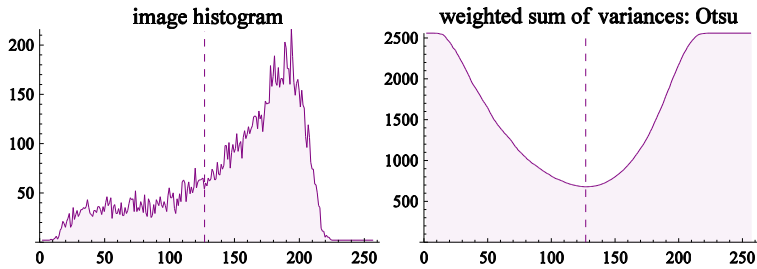


Figure 4

Valence related curve for single slice of fMRI

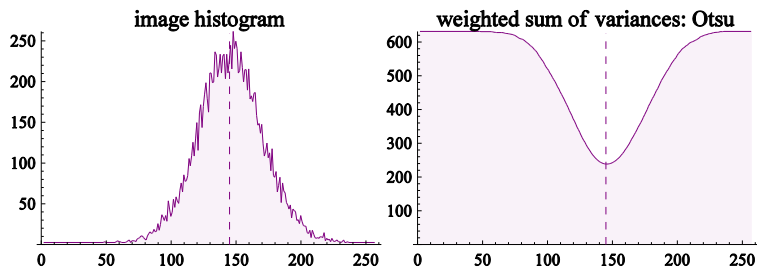


Figure 5

Arousal related curve for single slice of fMRI

From 6s stimuli experiment, we sampling 100 images from Valence related fMRI data-set and 100 from Arousal, and through fuzzy clustering, center point and radius of Valence and Arousal were acquired. For each 0.6 sec time range, the histogram by Otsu weighted was composed of a 100-units time series curve (shown in Fig. 6 and Fig. 7).

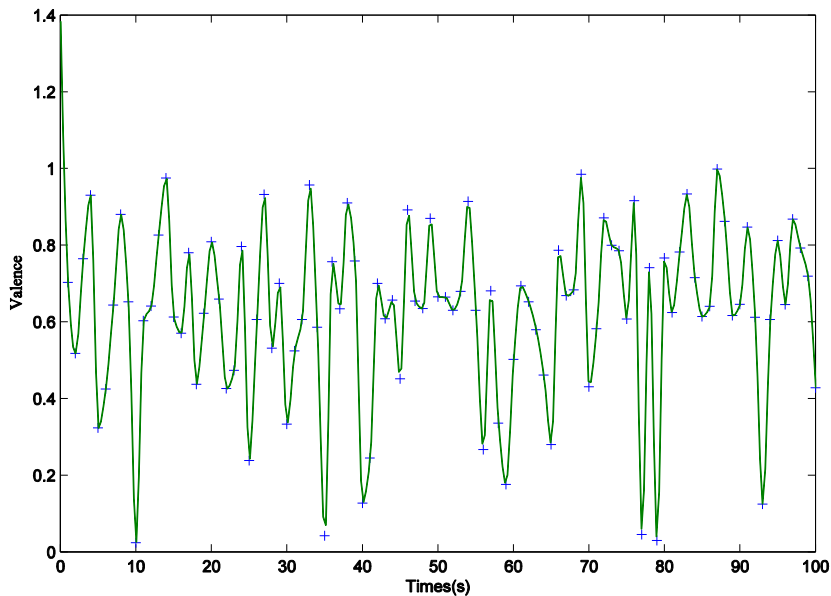


Figure 6

Time series Valence related fMRI images' histogram

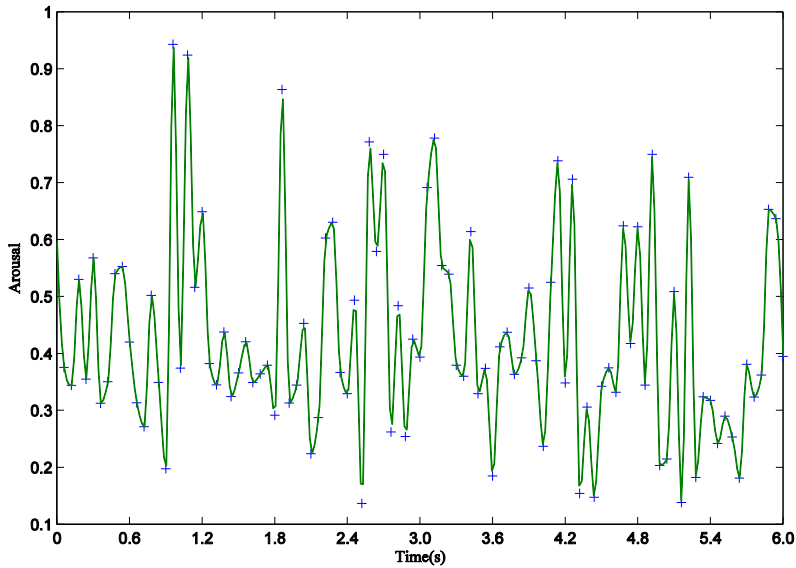


Figure 7

Time series Arousal related fMRI images' histogram

Now, fuzzy c-mean algorithm was started using Matlab 8.0 Fuzzy Logic Toolbox. It starts to suppose mark the mean location of clusters with an initial guess and assigns each point a membership grade for each cluster. We loaded the histogram of Valence-Arousal as 2D plot shown in Fig. 8

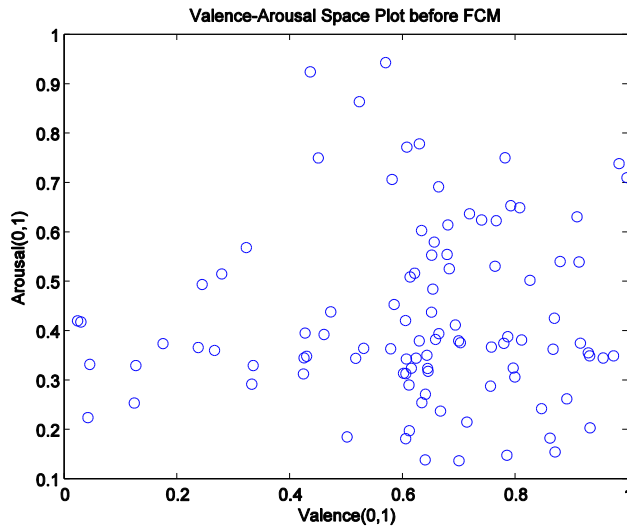


Figure 8

2D plots on histogram of Valence Arousal related fMRI

Running the code as:

```
load fcmva.dat
plot(fcmva(:,1),fcmva(:,2),'o')
[center, U, obj_fcn] = fcm(fcmva, 2);
maxU = max(U);
index1 = find(U(1, :) == maxU);
index2 = find(U(2, :) == maxU);
line(fcmva(index1, 1), fcmva(index1, 2),
line(fcmva(index2,1),fcmva(index2,2),
hold on
plot(center(1,1),center(1,2),'ko','markersize',15,'LineWidth',2)
plot(center(2,1),center(2,2),'kx','markersize',15,'LineWidth',2)
```

We got the objective function under FCM by iterations shown in Fig. 9. And after 20 iterations, we got the clusters ($n=2$) and the center points are $[0.739, 0.426]$ and $[0.360, 0.405]$ shown in Fig. 10.

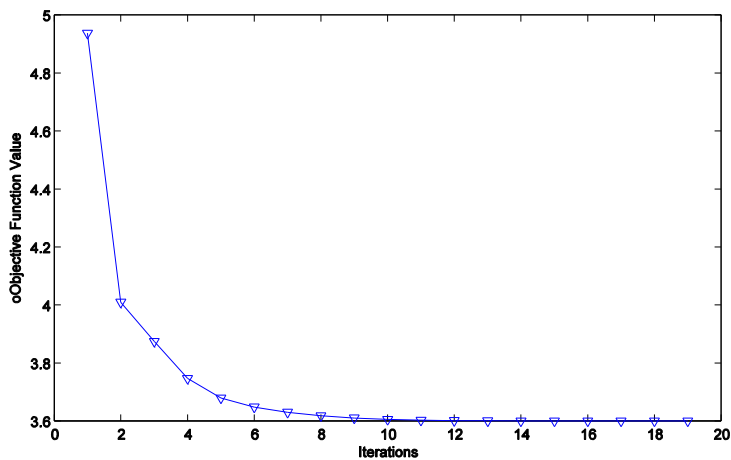


Figure 9
Objective function of FCM by iterations

5 Result Discuss and Comparing Analysis

In this paper, Gaussian mixture fuzzy clustering method was applied to histogram processing of Valence-Arousal related fMRI image, experimental analysis shows the effectiveness of the proposed method. In image pre-processing phase, image segmentation, Expectation Maximization of Gaussian Mixed model were adopted to describe the fMRI histogram. While obtained time series based 100 sample images from the experiment of picture stimuli, Otsu curve fitting method was proposed to extract the histogram, finally to construct the Valence-Arousal timing curve. The objective is to get Valence and Arousal from given picture relative a word that was introduced in Emotional dimensional theory. So we built these points (V, A) in a plane while fuzzy clustering algorithm extracted the typical (V, A) value; by setting the clustering parameters, center point was acquired from data in a relatively short period of time. In previous studies, the usual method was to obtain the image features by calculating image spectrums, such as, amplitude spectrum, frequency spectrum, and the power spectrum density (PSD, describes how the power of a time series based fMRI image was distributed with frequency instead of energy spectral density (ESD), which also describes how the energy of a time series was distributed with frequency [31] [32]). To illustrate the efficiency of the proposed method in this paper, we also calculated the PSD for Valence-Arousal related fMRI (Shown as Fig. 11 and Fig.12). After comparative study, it was indicated that the algorithm complexity of PSD is $O(n^3)$ and histogram proposed in this paper is $O(n^2)$, while Otsu fitting operating also was $O(n^2)$. So for a large number of fMRI data the proposed method in this paper is more effective in fMRI feature extraction by a smaller rate of loss of information.

In other hand, some studies introduced curve fitting methods for image processing, and constructed a fitting curve to describe the characteristics of the fMRI timing signal. We compared spline fitting, shape-preserve fitting and cubic fitting for Valence signal, it was indicated that spline and shape-preserve had smallest errors, but high algorithm complexity. Cubic fitting's error is large and the algorithm is $O(n^3)$. The Valence related fMRI data-set's curve fitting calculation results were shown in Fig. 13.

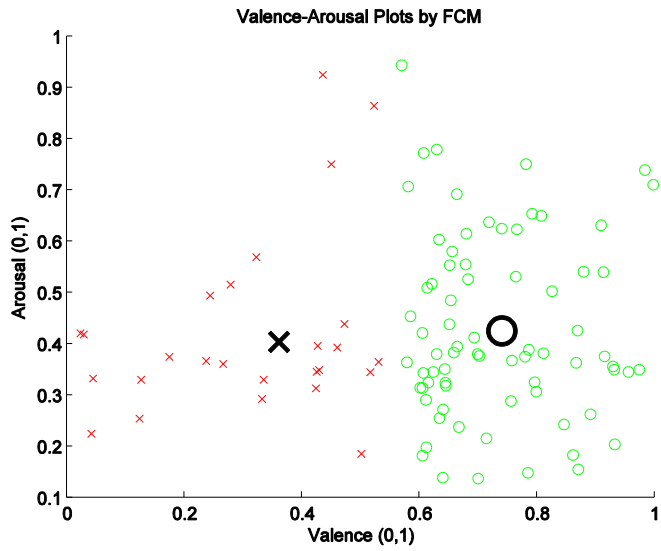


Figure 10
FCM under 2 clusters and the center points

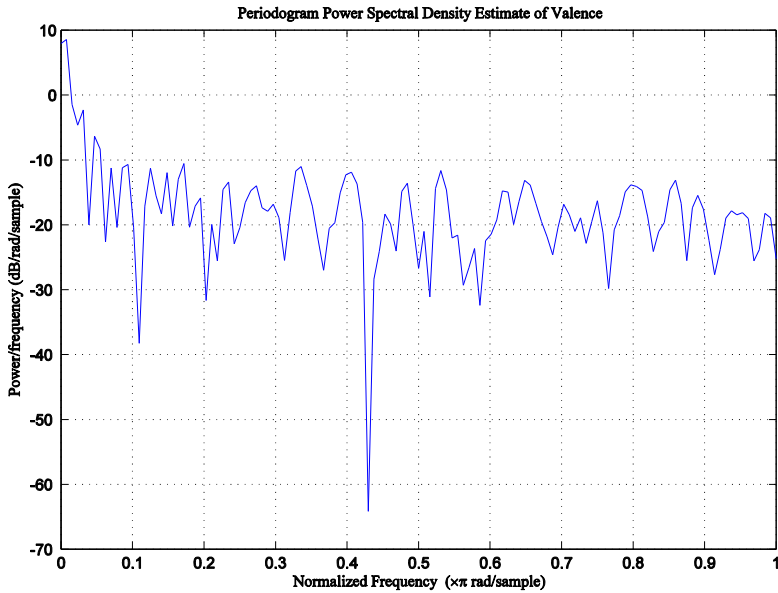


Figure 11
Power spectrum density estimation of Valence

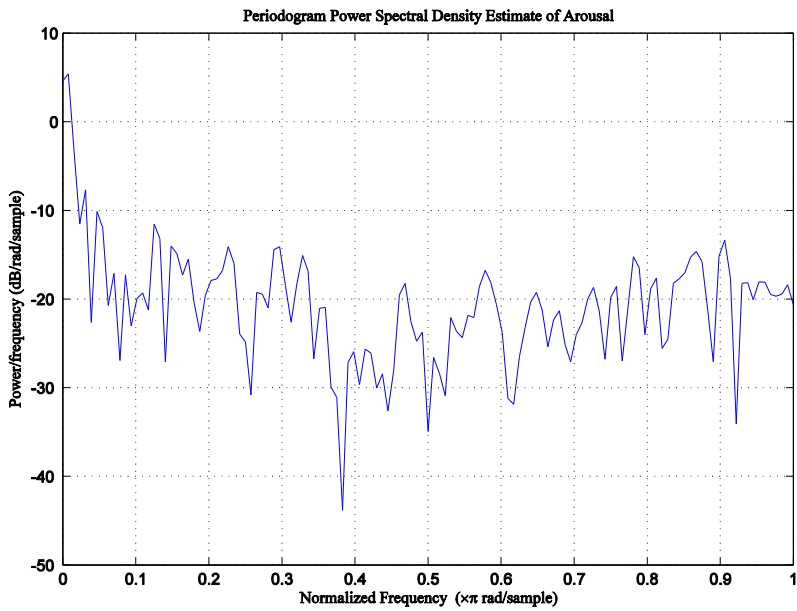


Figure 12

Power spectrum density estimation of Arousal

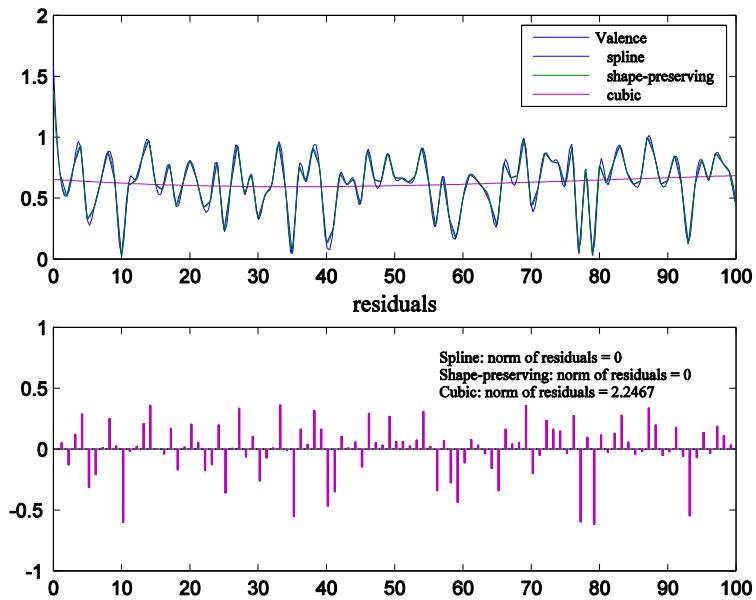


Figure 13

Spline, shape-preserving and cubic fitting operations on Valence

Concluding Remarks and Future Works

In this paper, fMRI images data-set was acquired from fMRI experiments by picture stimuli, the time series based Valence-Arousal related fMRI images were generated. The pre-processing of images included bilateral filter and ICA based components, for extracting features from Valence-Arousal related fMRI images, expectation maximization method for Gaussian mixed model was applied to get histogram and subsequently Otsu curve fitting operation was introduced to generate timing curve for Valence and Arousal. By fuzzy c-mean clustering, the typical Valence and Arousal value relative to a given word (picture stimuli) were acquired. The proposed methods show the effectiveness by comparing with other algorithms such as PSD, curve fitting. The next step is to improve the fMRI experiments by large-scale set of picture stimuli, and the second is to further improve the efficiency processing and the method of feature extraction from fMRI.

Acknowledgement

This work was supported by Natural Science Foundation of Zhejiang Province under Grant No. Y1110322. And the author would like to thank the editors, the anonymous reviewers, and Ms. Thayer El-Dajjani for their most constructive comments and suggestions to improve the quality of the paper.

References

- [1] J. A. Russell. A Circumplex Model of Affect, *J. Pers. Soc. Psychol*, 1980, 39: 1161-1178
- [2] M. M. Bradley. Greenwald, M. K., Petry, M. C. & Lang, P. J., *J. Exp. Psychol. Learn. Mem. Cognit.*, 1992, 18: 379-390
- [3] Michael E Kelly, Christoph W Blau, Karen M Griffin, et al., 3Quantitative Functional Magnetic Resonance Imaging of Brain Activity Using Bolus-Tracking Arterial Spin Labeling, *Journal of Cerebral Blood Flow & Metabolism*, 30 (2010), 913-922
- [4] Prantik Kundu, Souheil J. Inati, Jennifer W. Evans, et al., Differentiating BOLD and Non-BOLD Signals in fMRI Time Series Using Multi-Echo EPI, *NeuroImage*, 60 (2012) 1759-1770
- [5] Yan Fan, Niall W. Duncan, Moritz de Greck, Georg Northoff, Is There a Core Neural Network in Empathy? An fMRI-based Quantitative Meta-Analysis, *Neuroscience and Biobehavioral Reviews*, 35 (2011), 903-911
- [6] E. A. Kensinger and S. Corkin. Two Routes to Emotional Memory: Distinct Neural Processes for Valence and Arousal, *PNAS*, 2004, 101(9): 3310-3315
- [7] E. A. Kensinger and D. L. Schacter. Processing Emotional Pictures and Words: Effects of Valence and Arousal, *Cognitive, Affective, & Behavioral Neuroscience*, 2006, 6(2): 110-116

- [8] Vincent Michel, Alexandre Gramfort, Gaël Varoquaux, et al., A Supervised Clustering Approach for fMRI-based Inference of Brain States, *Pattern Recognition*, 45 (2012), 2041-2049
- [9] P. A. Lewis, H. D. Critchley, P. Rotshtein and R. J. Dolan. Neural Correlates of Processing Valence and Arousal in Affective Words, *Cerebral Cortex* March, 2007, (17): 742-748
- [10] C. Liu , S. Li, *Neuroeconomics: Decision Science for Brain Science, Psychological Science*, 2007, 30 (2) : 482-484 (in Chinese)
- [11] M. Jarmasz, R. L. Somorjai, Exploring Regions of Interest with Cluster Analysis (EROICA) Using a Spectral Peak Statistic for Selecting and Testing the Significance of fMRI Activation Time-Series, *Artificial Intelligence in Medicine*, 25 (2002), 45-67
- [12] Christian Windischberger, Markus Barth, Claus Lamm Fuzzy Cluster Analysis of High-Field Functional MRI Data, *Artificial Intelligence in Medicine*, 29 (2003), 203-223
- [13] R. Baumgartner, L. Ryner, W. Richter, R. Summers, M. Jarmasz, R. Somorjai, Comparison of Two Exploratory Data Analysis Methods for fMRI: Fuzzy Clustering vs. Principal Component Analysis, *Magnetic Resonance Imaging*, 18 (2000), 89-94
- [14] Daniel B. Rowe, Andrew S. Nencka, Raymond G. Hoffmann, Signal and Noise of Fourier Reconstructed fMRI Data, *Journal of Neuroscience Methods*, 159 (2007), 361-369
- [15] Shing-Chung Ngan, Xiaoping Hu, Pek-Lan Khong, Investigating the Enhancement of Template-Free Activation Detection of Event-related fMRI Data Using Wavelet Shrinkage and Figures of Merit, *Artificial Intelligence in Medicine*, 51 (2011), 187-198
- [16] Rami N. Khushaba, Luke Greenacre, Sarath Kodagoda, Jordan Louviere, Sandra Burke, Gamini Dissanayake, Choice Modeling and the Brain: A study on the Electroencephalogram (EEG) of preferences, *Expert Systems with Applications*, 39 (2012), 12378-12388
- [17] Károly Hercegfı, Heart Rate Variability Monitoring during Human-Computer Interaction, *Acta Polytechnica Hungarica*, 2011, 8(5), 205-224
- [18] Hesamoddin Jahanian, Gholam-Ali Hossein-Zadeh, Hamid Soltanian-Zadeh, Babak A. Ardekani, Controlling the False Positive Rate in Fuzzy Clustering Using Randomization: Application to fMRI Activation Detection, *Magnetic Resonance Imaging*, 22 (2004), 631-638
- [19] Alain Smolders, Federico De Martino, NoJl Staeren, Paul Scheunders, Jan Sijbers, Rainer Goebel, Elia Formisano, Dissecting Cognitive Stages with Time-resolved fMRI Data: a Comparison of Fuzzy Clustering and

- Independent Component Analysis, Magnetic Resonance Imaging, 25 (2007), 860-868
- [20] R. Baumgartner, L. Ryner, W. Richter, R. Summers, M. Jarmasz, R. Somorjai, Comparison of Two Exploratory Data Analysis Methods for fMRI: Fuzzy Clustering vs. Principal Component Analysis, Magnetic Resonance Imaging, 18 (2000), 89-94
- [21] Elizabeth Ann Maharaj, Pierpaolo D'Urso, Fuzzy Clustering of Time Series in the Frequency Domain, Information Sciences, 181 (2011), 1187-1211
- [22] R. Baumgartner, R. Somorjai, Graphical Display of fMRI Data: Visualizing Multidimensional Space, Magnetic Resonance Imaging, 19, (2001), 283-286
- [23] Masaya Misaki and Satoru Miyauchi, Application of Artificial Neural Network to fMRI Regression Analysis, NeuroImage, 29 (2006), 396-408
- [24] Xiaomu Song, Alice M. Wyrwicz, Unsupervised Spatiotemporal fMRI Data Analysis Using Support Vector Machines, NeuroImage, 47, (2009), 204-212
- [25] C. Pruneti, N. Vanello, R. Morese, C. Gentili, F. Fontana, E. Ricciardi, C. Fante, M. Paterni, P. Pietrini, M. Guazzelli, L. Landini, E. M. Ferdeghini, Psychophysiological and fMRI Neural Correlates to Stress Response: A Pilot Study, International Journal of Psychophysiology, 69 (2008), 207-241
- [26] O. Lange, A. Meyer-Baese, M. Hurdal, S. Foo, A Comparison between Neural and Fuzzy Cluster Analysis Techniques for Functional MRI, Biomedical Signal Processing and Control, 1 (2006), 243-252
- [27] I. Daubechies, E. Roussos, S. Takerkart, M. Benharrosh, C. Golden, K. D'Ardenne, W. Richter, J. D. Cohen, and J. Haxbya, Independent Component Analysis for Brain fMRI Does Not Select for Independence, PNAS, 2009, 106(26), 10415-10422
- [28] Dominic Langlois, Sylvain Chartier, and Dominique Gosselin, An Introduction to Independent Component Analysis: InfoMax and FastICA algorithms, Tutorials in Quantitative Methods for Psychology, 2010, 6(1), 31-38
- [29] Nobuyuki Otsu (1979). "A Threshold Selection Method from Gray-Level Histograms". IEEE Trans. Sys., Man., Cyber. 9 (1): 62-66
- [30] J C Bezdek, Pattern Recognition with Fuzzy Objective Function Algorithms. Plenum, New York, NY, 1981
- [31] Frédéric Joassin Pierre Maurage, Salvatore Campanella, The Neural Network Sustaining the Crossmodal Processing of human Gender from Faces and Voices: An fMRI Study, NeuroImage, 54 (2011), 1654-1661

- [32] Mohamed L. Seghier, Cathy J. Price, Dissociating Functional Brain Networks by Decoding the Between-Subject Variability, *NeuroImage*, 45 (2009), 349-359

Indoor Air Quality Testing in Low-Energy Wooden Houses: Measurement of Formaldehyde and VOC-s

Csilla Patkó¹, István Patkó², Zoltán Pásztor³

¹ University of West Hungary, Innovation Centre, Bajcsy Zs. út 4, 9400 Sopron, Hungary, csilla.patko@gmail.com

² Óbuda University, Doberdo út 6, 1034 Budapest, Hungary, patko@uni-obuda.hu

³ University of West Hungary, Innovation Centre, Bajcsy Zs. út 4, 9400 Sopron, Hungary, pasztor@fmk.nyme.hu

Abstract: The objective of our study is to determine the indoor air quality of a low-energy wooden house. During the field measurements we detected the presence of formaldehyde ($34 \mu\text{g}/\text{m}^3$), BTX ($35.51 \mu\text{g}/\text{m}^3$), and some materials in the terpene family, limonene ($64.7 \mu\text{g}/\text{m}^3$), and alpha-pinene ($297 \mu\text{g}/\text{m}^3$), in the indoor air. The concentration of the detected TVOC (Total Volatile Organic Compounds) was $2150 \mu\text{g}/\text{m}^3$, which does not significantly differ from European average values. The LCI (Lowest Concentration of Interest) analysis shows that none of the VOCs tested by us are a health risk to the occupants in the building. However, it can be established that the health risk of benzene (0.622) stands out from the tested substances. The health risks of other aliphatic hydrocarbons (0.176) and alpha-pinene (0.198) may be considered identical, but even these do not pose a risk to humans. In order to clarify the sources of the harmful substances further investigations are needed.

Keywords: indoor air quality; VOC; formaldehyde; BTX; terpene; wooden building

1 Introduction

1.1 The Development of Indoor Air Quality Testing

Indoor air quality testing has come to the fore gradually in the past 30 years. The compounds concentrated in the air and entering into reaction with each other have an effect on human health. Formaldehyde and BTX (benzene, toluene, xylene) were the first such volatile organic compounds (VOC) whose harmful, carcinogenic effects were already recognized earlier. A major part of these comes from indoor sources such as human activity and the evaporation of the building

materials of buildings. Several tests have been performed worldwide and there is significant professional literature available about the case studies conducted. As a result several guides and design aids have been created about the effects of harmful substances and their possible sources. Wood, as the ecological building material of the future, is gaining a new role in the design and realization of energy efficient houses.

Clean air is one of the most fundamental conditions of our life. In buildings where people spend most of their days indoor air quality greatly affects their comfort level and state of health [1]. People dealt with unpleasant odours and their effects on health already in the 18th Century. In 1858 a German hygienist, Max von Pettenkoffer defined the maximum value of CO₂ in indoor air (0.1 vol%), which value still has not lost its relevance [2]. In the past 30 years more and more significant studies have been published on this subject. Before 1991 the main subject of indoor air testing was the protection against corrosion of indoor objects and the methods of preserving the condition of these objects.

James N. Pitts, Jr. was the first to identify and measure NO₂ concentration in indoor air. In his book *Chemistry of the Upper and Lower Atmosphere* published in 2000 he already devoted one chapter to indoor air quality testing, which demonstrated the importance of the topic [3].

Another important compound is CO, which is considered toxic to humans in higher concentration. Carbon monoxide is a temporary atmospheric pollutant in some urban areas, chiefly from the exhaust of internal combustion engines (including vehicles, portable and back-up generators, power washers, etc.), but also from incomplete combustion of various other fuels (including wood, coal, charcoal, oil, paraffin, propane, natural gas, and trash). Considering the fact, that new houses are more airtight and the ventilation rates are less, in closed environments the concentration of carbon monoxide can easily rise to lethal levels [28].

In America the testing of indoor harmful substances became the centre of attention in the early 1980s. These tests dealt with the detection and measurement of formaldehyde, radon, asbestos and volatile organic compounds (VOC). Through the development of laboratory technology with the help of more sensitive measurement tools more and more compounds can be detected and defined [4].

Between 1991 and 2000 only about 60 articles appeared on the subject of Indoor Chemistry. However, between 2001 and 2010 nearly 210 articles were published. Nevertheless, the testing of chemical substances in indoor air is still less developed compared to ambient air testing on which approximately 12,000 articles have been published in the past 20 years [5].

1.2 The Purpose of Our Study

In recent years a large number of houses with low energy consumption, so-called energy efficient houses have been built in Hungary. They do not only seek ecological solutions from building energetic points of view, but the choice of ecological materials has also come to the forefront. It is important that the building should not appear in the environment as a foreign body, but it should fit into natural cycles as much as possible.

Our research was the first in Hungary to perform air quality measurements in a newly built wooden structure house which had been constructed as a result of environmentally conscious design and building. This building contains wooden building blocks which are untreated or treated with natural materials. Our study focused on detecting the chemical substances – in the indoor air of the building – which basically affect the indoor air quality.

2 The Theoretical Background of Our Testing

Some countries already have specific emission rates of different materials [6]. In 1992 Seifert classified the volatile organic compounds from building materials into three categories: on the basis of their long term effect on health (such as carcinogenic, mutagenic, teratogenic, allergenic, etc.), short term effects (such as mucous membrane irritation, etc.) and their unpleasant odour. However, this system did not yet take account of the possible emission degradation of the substances present in the atmosphere and its consequences [7, 8].

The guidelines of WHO (World Health Organisation) categorize the harmful substances emitted by the sources [9]. In Germany the Committee for the Health Assessment of Building Materials (AgBB - Ausschuss zur gesundheitlichen Bewertung von Bauprodukten) first defined VOCs from the emission of building products in 2000. Now more than 180 different VOCs can be defined [10].

Several other studies also deal with similar topics such as EnVIE, BUMA, HealthyAir [6]. The objective of this research is to provide architects with available information already in the design phase of buildings about such building materials (masonry blocks, tiles, etc.) that do not emit any harmful substances into the indoor air-space of the building. In the case of new buildings air quality may be best influenced by controlling the sources.

2.1 VOC Sources and Their Impact on Health

VOC is a group of organic substances with boiling points between 50 and 260°C, the best known of which are BTEXS (benzene, toluene, ethyl benzene, xylene and styrene) substances, terpenes (α -pinene, limonene), as well as formaldehyde and acetaldehyde among carbonyl compounds [11]. These are the main pollutants of indoor air with formaldehyde, benzene and acetaldehyde considered carcinogenic [12]. They may be found in almost all air-spaces because most household products contain them, such as paints, varnishes, waxes, conservation materials, solvents of anti-mould agents, detergents and cleaning agents. In the case of new buildings the main source of these substances is the primary emission from the building materials, which may last for several months. After the primary emission certain building materials emit further harmful materials into the air as these materials get older and used. This process is called secondary emission [13].

2.2 Benzene

Benzene is an industrial solvent which is widely used in paints, lacquers and for varnishing [14]. Today it is used as a raw material for producing plastics, resins and detergents. Benzene is present everywhere, for instance also in tobacco smoke. The results of measurements performed in buildings in different European cities have shown that it is not present in new houses in Finland. On the other hand, the highest measured concentration was 109 $\mu\text{g}/\text{m}^3$ according to research [15]. In the latest study published by WHO benzene's carcinogenic effects are still emphasized and so is the possibility of developing acute myeloid leukaemia.

Since there is no exposure limit defined for benzene the risk factor for developing leukaemia at 1 $\mu\text{g}/\text{m}^3$ concentration is 6×10^{-6} during one lifecycle [1].

2.3 Formaldehyde, Acetaldehyde

Their main sources are the adhesives that are used for the production of chipboards, various resins, paints, disinfectants and paper products. They are found in cigarette smoke [16, 17]. They may come from secondary emissions [11]. Possible sources are the stubble pages of furniture. The resin parts of stubble pages are made with the polymerization of formaldehyde monomers. The minimum amount which can cause eye irritation is 0.36 mg/m^3 ; 0.6 mg/m^3 will lead to mild conjunctivitis. A concentration of 0.1 mg/m^3 is the quantity where neither the elderly nor children will suffer any irritation if the duration of exposure is less than 30 minutes. The concentration of formaldehyde indoors can be significantly influenced by the number of air exchanges. [1]

2.4 Terpenes (Limonene and α -pinene)

Limonene is an organic compound classified as a terpene, i.e. it is not synthetic but a real plant extract. It is a colourless liquid at room temperature with a strong smell of oranges. Lemons and other citrus fruit contain limonene in high quantities. It is used as a flavour and fragrance additive in food, household detergents and perfumes [18]. It can cause allergic symptoms such as eye, nose, throat and skin irritation, but generally it is not considered as a harmful substance. The average concentration measured in households is less than $30 \mu\text{g}/\text{m}^3$. This value is largely affected by whether any air fresheners or cleaning agents were used which may contain it in higher concentration [11].

α -pinene is also a natural terpene, which might be emitted by surface-treated wood products, aerosols, paints and water-resistant solvents. It is not a carcinogen, just like limonene, it can only cause irritation. According to literature [19] on average less than $30 \mu\text{g}/\text{m}^3$ is present in indoor air. It is characteristic of both substances that they become easily oxidized due to ozone or other substances containing active oxygen [20].

3 Overview of Case Studies from Professional Literature

In Hungary several eco-epidemiological studies have been made by the National Institute of Environmental Health during the last 15 years. In 1998 several homes were selected in six Hungarian cities, where they measured the indoor air for formaldehyde, NO_2 , benzene, xylene and toluene concentrations. The research was intended to find the source of the substances measured indoors and to find correlations between the state of health of the children living in these homes and indoor air pollution. The tests showed that the NO_2 present in the indoor air came from the kitchen gas cooker ($75 \mu\text{g}/\text{m}^3$), gas convectors ($80 \mu\text{g}/\text{m}^3$) and smoking ($27 \mu\text{g}/\text{m}^3$). Benzene was detected in homes with under floor heating, while formaldehyde was detected in homes built from gas silicate masonry building materials. In addition to instrumental measurements, a questionnaire survey was also conducted among the residents. According to the result of the survey among the interviewed 1768 children 14.2% had symptoms of chronic bronchitis. Plastic floor covering increased allergy symptoms by 66% and congestion by 49%. In prefabricated flats air-conditioners and fitted carpets exponentially increased the number of allergic symptoms. One conclusion of this study was to draw attention to the safe removal of the combustion products of domestic gas appliances, which does not only prevent health risks, but will greatly contribute to preventing mould growth in buildings [21].

In Paris a number of similar studies were also conducted using questionnaires and by taking multiple air samples in the homes. The Laboratoire Santé Publique et Environment Institute of the Université Paris Descartes University conducted environmental surveys to find the indoor sources causing the allergic symptoms of newborn babies. Primarily they measured the aldehyde levels of indoor air for one year in the homes of 196 Parisian new-born babies. During their testing the concentration of formaldehyde of newly built buildings was $19.4 \mu\text{g}/\text{m}^3$. No correlation was found between heating, tobacco smoke and the concentration of formaldehyde. However, it was observed that the concentration of formaldehyde was higher in the summer. $8.9 \mu\text{g}/\text{m}^3$ of acetaldehyde was measured and it was established that indoor nicotine content, relative humidity and carbon dioxide levels affect acetaldehyde concentration. The conclusion was that the concentration of the aldehyde may be reduced by increasing ventilation [22].

In England the testing of the air-space of 876 newly-built homes showed that in the first year the concentration of formaldehyde in the indoor airspace was significant [23].

In Canada by examining 100 newly built homes Gilbert established in his study [24] that the concentration level of formaldehyde in the indoor air was influenced by the furniture or covering made of materials containing wood or melamine.

In South-Korea due to the large number of illnesses caused by the symptoms referred to as Sick Building Syndrome they placed a strong emphasis on indoor air quality in homes. Due to the use of low-quality building materials and insufficient ventilation – which was a consequence of mass constructions – and as a result of thermal insulation the concentration of VOCs significantly increased in the indoor air. The solution was to increase the ventilation of the rooms and use air cleaning agents [25].

4 Formaldehyde and VOC Measurement Method

4.1 Description of the Tested Building

The sampling was performed in a newly built, low energy wooden frame building. The construction was completed in the summer of 2012. It has an area of 120 m^2 , a ground-floor and an attic. Downstairs there are a hall, a living room with a kitchen, a room and a bathroom. From the living room there is a staircase leading up to the gallery, which opens into the room in the attic.

The structure of the building consists of wooden frames and wooden panels with Isocell insulation, which is rendered outside and covered with gypsum fibre panels inside. The interior walls are all solid wood panels without any chemical

treatment. The house is heated with circulating hot air. The air is heated by solar collectors and geothermal heat. In addition, the ground-floor heating is supported by electric under-floor heating in winter. The sampling was performed in the room on the ground-floor, which is 12 m² with a ceiling height of 2.8 m. Two walls of the room are exterior side walls with windows of 84x140 cm, the other two walls are interior wood walls. The floor is covered with stone slabs. The room is unfurnished. The measuring instrument was placed in the middle of the room at a height of 1.2 m.

4.2 On-Site Measurements

The sampling was performed in the building described in Section 4.1 and the samples were analysed by the laboratory of Wessling Hungary Ltd. Active sampling devices were used on the site. During the sampling the physical condition of the indoor airspace was the following: The indoor air temperature was 18°C continuously, the relative humidity was 41%, the indoor, air exchange rate was 2.5 m³/h, which means that during the measurement the windows and doors were closed [27]. In order to ensure the accuracy of laboratory measurements, the physical characteristics of indoor air had been set 24 hours before the sampling. Thus, the sampling was performed in a stationary state.

Two sampling tubes were connected to the active measuring device used for the sampling. One sampling tube was a 200 mg Tenax TA stainless steel tube, 90 mm long, for sampling the VOCs.

Suction duration: 60 min

Suction rate: 100 ml/min

Suctioned air volume: 6000 ml

The other was a formaldehyde sampling tube filled with silica gel coated with 150/300 ml dinitrophenyl-hydrazine:

Suction duration: 240 min

Suction rate: 200 ml/min

Suctioned air volume: 48000 ml

5 Evaluation of Measurement Results

When we determined the VOC content of the samples taken from the indoor air we measured the concentrations of 180 components according to ISO standard 16000-6/2004. The determination of formaldehyde was performed according to

ISO 16000-3/2001. In Table 5.1 we included the measured concentrations of formaldehyde and of those VOC components out of the 180 measurement results whose values were significantly greater than the detection limit. Presumably, these are the substances which determine the quality of indoor air in the building.

The total VOC (TVOC) content was 2150 $\mu\text{g}/\text{m}^3$. The total amount of the concentration of substances in Table 5.1 was 1508.06 $\mu\text{g}/\text{m}^3$.

Table 5.1
Measured concentration of VOC components

Component Name	Concentration [$\mu\text{g}/\text{m}^3$]
Benzene	3.11
Toluene	11.6
1.3-Xylene and 1.4-Xylene	20.8
n-Propylbenzene	1.95
Other aliphatic hydrocarbon (>C8-C16)	1060
Alpha-Pinene	297
Limonene	64.7
Hexanal	48.9
Formaldehyde	34

5.1 LCI (Lowest Concentration of Interest) Analysis

German laws specify that VOC emission from building materials shall be reduced in the long term so much that it should not pose a risk to the health of the occupants in the building. The workgroup of AgBB (Ausschuss zur gesundheitlichen Bewertung von Bauprodukten) created a list of VOCs determining indoor air quality and at the same time gave the concentration limit of VOCs impairing air quality [26, 10]. If the concentration of the tested VOC is below the specified limit, it does not pose a health risk to the occupants in the building.

The degree of health risk is expressed by a ratio; the value of the measured concentration is divided by the limits according to AgBB. If this ratio is <1 , the tested substance does not pose a health risk. If the ratio is >1 , the health risk caused by the substance is proportional to the value of the ratio. Table 5.2 contains the VOCs which we measured, their registration number (CAS), the limit of the concentration (LCI), the measured concentration and their quotient. We were not able to calculate the degree of health risk of formaldehyde. In the last prospective LCI value changes (June 2012) the LCI value for Formaldehyde was under discussion.

Table 5.2
Health risk of measured substances

Name of component	CAS	LCI [$\mu\text{g}/\text{m}^3$]	Measured concentration [$\mu\text{g}/\text{m}^3$]	Measured concentration / LCI
Benzene (VOC)	71-43-2	5	3.11	0.622
Toluene (VOC)	108-88-3	1900	11.6	0.00061
1.3-Xylene and 1.4-Xylene (VOC)	106-42-3; 108-38-3	2200	20.8	0.00094
n- Propylbenzene (VOC)	103-65-1	1000	1.95	0.00019
Other aliphatic hydrocarbon (>C8-C16) (VOC) (d)		6000	1060	0.176
Alpha-Pinene (VOC)	80-56-8	1500	297	0.198
Limonene (VOC)	5898-27-5	1500	64.7	0.043
Hexanal (VOC)	66-25-1	890	48.9	0.054

Table 5.2 shows that none of the VOCs tested by us are a health risk to the occupants in the building. However, it can be established that the health risk of benzene (0.622) stands out from the tested substances. The health risks of other aliphatic hydrocarbons (0.176) and alpha-Pinene (0.198) may be considered identical, but even these do not pose a risk to humans.

Conclusions

Literature study no. [11] deals with the indoor air quality of buildings and publishes relevant data. It specifies the average value of pollutants measured in European cities. The comparison of our measured values and the values of article [11] are given in Table 6.1.

Table 6.1
Comparative values

Name of component	Concentration [$\mu\text{g}/\text{m}^3$]	European average [$\mu\text{g}/\text{m}^3$]	Evaluation
Benzene (VOC)	3.11	14.6	passed
Toluene (VOC)	11.6	4 - 30	passed
1.3-Xylene and 1.4-Xylene (VOC)	20.8	0 - 10	failed
Limonene (VOC)	64.7	0 - 30	failed
Formaldehyde	34	10 - 50	passed

It can be seen from Table 6.1 that the xylene and limonene content of the indoor air measured by us is higher than the average value measured in European cities. This fact does not yet mean that these substances pose a health risk.

We tested indoor air quality in the interior space of a wooden residential building constructed in the area of the University of West Hungary (see Section 4.1). Before our study was designed and implemented we carried out detailed literature search on the subject. We explored the methods used in air quality testing. We compared the results obtained and we drew conclusions from them. Taking these into account we designed the on-site sampling and the laboratory measurements.

On the basis of the laboratory results we determined the health risks of the air to humans in the building tested. We compared the pollutant content of the indoor air space of our building with the measured values of European cities taken from the literature. It can be concluded that the quality of the airspace tested by us does not differ from the European average.

In this article we presented the measured values of VOC emissions. In order to clarify the sources of the harmful substances we are going to do further investigations.

Acknowledgement

This study was supported by the Environmental Analytical Laboratory of Wessling Hungary Ltd. and its employees.

This study was supported by the Environment conscious energy efficient building TAMOP-4.2.2.A-11/1/KONV-2012-0068 project sponsored by the EU and European Social Foundation.

References

- [1] WHO: Guidelines for Indoor Air Quality: Selected Pollutants (2010) Denmark: WHO Regional Office for Europe, ISBN 978 92 890 0213 4
- [2] Wohnbauforschung, AGU: Hutter, H., Moshhammer, H., Wallner, P., IMB: Tappler, P., Twrdik, F., ÖÖI: Dr. Ganglberger, E., Geissler, S., Wenisch, A. (2005) Auswirkungen energiesparender Maßnahmen im Wohnbau auf die Innenraumluftqualität und Gesundheit, Forschungsvorhaben F 1469, 15
- [3] Barbara J. Finlayson-Pitts and James N. Pitts, Jr.: Chemistry of the Upper and Lower Atmosphere, Academic Press, 1999, p. 969
- [4] Weschler, C. J. (2008) Changes in Indoor Pollutants since the 1950s, Atmospheric Environment 43 (2009) 153-169
- [5] Weschler, C. J. (2011) Commemorating 20 Years of Indoor Air - Chemistry in Indoor Environments: 20 Years of Research, Indoor Air 2011; 21: 205-218
- [6] Bluysen, M. P. (2009) Towards an Integrative Approach of Improving Indoor Air Quality, Building and Environment 44 (2009) 1980-1989
- [7] Wolkoff, P., Nielsen, P. (1996) A New Approach for Indoor Climate Labeling of Building Materials--Emission Testing, Modeling, and Comfort

- Evaluation, *Atmospheric Environment* Vol. 30, No. 15, pp. 2679-2689, 1996
- [8] Seifert B. (1992) Guidelines for Material and Product Evaluation. *Ann. N.Y. Acad. Sci.* 641, 125-136
- [9] WHO. Air Quality Guidelines, Global Update 2005, Particulate Matter, Ozone, Nitrogen Dioxide and Sulphur Dioxide (2006) Denmark: WHO Regional Office for Europe, ISBN 92 890 2192 6
- [10] AgBB (2012) Updated List of LCI values 2012 in Part 3, Health-related Evaluation Procedure for Volatile Organic Compounds Emissions (VOC and SVOC) from Building Products; http://www.umweltbundesamt.de/produkte/bauprodukte/archive/agbb_evaluation_scheme_2012.pdf
- [11] Sarigiannis, A. D., Karakitsios, P. S., Gotti, A., Liakos, I. L., Katsoyiannis, A. (2011) Exposure to Major Volatile Organic Compounds and Carbonyls in European Indoor Environments and associated Health; *Environment International* 37, 743-765
- [12] Salthammer, T., Mentese, S., Marutzky, R. (2010) Formaldehyde in the Indoor environment. *Chemical Reviews* 110, 2536-2572
- [13] Wolkoff, P., 1999. How to Measure and Evaluate Volatile Organic Compound Emissions from Building Products. A perspective. *Science of the Total Environment* 227, 197-213
- [14] Holmberg B, Lundberg P. (1985) Benzene: Standards, Occurrence, and Exposure. *Am J Ind Med*; 7:375-83
- [15] Zuraimi MS, Roulet CA, Tham KW, Sekhar SC, Cheong KWD, Wong NH, et al. (2006) A Comparative Study of VOCs in Singapore and European Office Buildings. *Build Environ*; 41:316-32
- [16] Jurvelin J, Vartiainen M, Jantunen M, Pasanen P. (2001) Personal Exposure Levels and Microenvironmental Concentrations of Formaldehyde and Acetaldehyde in the Helsinki Metropolitan Area, Finland. *J Air Waste Manag Assoc*; 51:17-24
- [17] EPA California. U. Accessed in November (2003) OEHHA Office of Environmental Health Hazard Assessment. http://www.oehha.ca.gov/air/chronic_rels/
- [18] Kotzias D, Geiss O, Tirendi S. (2005) The AIRMEX (European Indoor Air Monitoring and Exposure Assessment) Project report. European Commission; <http://web.jrc.ec.europa.eu/project/airmex/index.htm>
- [19] Rehwagen M, Schlink U, Herbarth O. (2003) Seasonal Cycle of VOCs in Apartments. *Indoor Air*; 13:283-91

- [20] Uhdea E, Salthammer T. (2007) Impact of Reaction Products from Building Materials and Furnishings on Indoor Air Quality—a Review of Recent Advances in Indoor Chemistry. *Atmospheric Environment*; 41:3111-28
- [21] Rudnai P., Virágh Z., Vaskövi B.(1999): Egyes lakótéri tényezők szerepe iskolás gyermekek légzőszervi panaszainak és allergiás tüneteinek gyakoriságában. *Egészségtudomány* 43, 196-209
- [22] Dassonville, C., Demattei, C., Laurent, A. -M., Le Moullec, Y., Seta, N., Momas, I. (2009) Assessment and Predictor Determination of Indoor Aldehyde Levels in Paris Newborn Babies_ Homes; *Indoor Air* 2009; 19: 314-323
- [23] Raw, G. J., Coward, S. K., Brown, V. M. and Crump, D. R. (2004) Exposure to Air Pollutants in English Homes, *J. Expo. Anal. Environ. Epidemiol.*, 14 (Suppl 1), S85–S94
- [24] Gilbert, N. L., Gauvin, D., Guay, M., Heroux, M. E., Dupuis, G., Legris, M., Chan, C. C., Dietz, R. N. and Levesque, B. (2006) Housing Characteristics and Indoor Concentrations of Nitrogen Dioxide and Formaldehyde in Quebec City, Canada. *Environ. Res.*, 102, 1-8
- [25] Sun-Sook, K., Dong-Hwa, K., Dong-Hee, C., Myoung-Souk, Y., Kwang-Woo, K. (2006) Comparison of Strategies to Improve Indoor Air Quality at the Pre-Occupancy Stage in New Apartment Buildings; *Building and Environment* 43 (2008) 320-328
- [26] ECA (1997) (European Collaborative Action "Indoor Air Quality and its Impact on Man"): Evaluation of VOC Emissions from Building Products – Solid Flooring Materials. Report No. 18, EUR 17334 EN, European Commission, Joint Research Centre, Environment Institute
- [27] Dr. Menyhárt József: Az épületgépészet kézikönyve (1978) Műszaki könyvkiadó Budapest
- [28] Green W. "An Introduction to Indoor Air Quality: Carbon Monoxide (CO)". United States Environmental Protection Agency. Retrieved 2008-12-16

Mathematical Principles and Optimal Design Solutions to Compensation for the Pendulum Temperature Dilatation

Branislav Popkonstantinović¹, Ljubomir Miladinović², Marija Obadović³, Gordana Ostojčić⁴, Stevan Stankovski⁵

¹ Faculty of Mechanical Engineering, Belgrade, Serbia,
bariton@afrodita.rcub.bg.ac.rs

² Faculty of Mechanical Engineering, Belgrade, Serbia,
lmiladinovic@mas.bg.ac.rs

³ Faculty of Civil Engineering, Belgrade, Serbia,
marijaobradovic.masha@gmail.com

⁴ Faculty of Technical Sciences, Novi Sad, Serbia, goca@uns.ac.rs

⁵ Faculty of Technical Sciences, Novi Sad, Serbia, stevan@uns.ac.rs

Abstract: The paper analyzes the effects of pendulum temperature dilatation on the timepiece running and accounts for the basic mathematical principles that neutralization of these detrimental effects are based upon. Both preliminary and detailed calculations are presented, as well as some design solutions leading to technically acceptable pendulum temperature dilatation. Explanation is given for the design of bimetal gridiron pendulum, wood pendulum with a lead weight, mercury pendulum, and pendulum with an Invar alloy rod.

Keywords: timepiece; dilatation; pendulum; compensation; temperature

1 Introduction

Numerous factors affect the uniform running of a timepiece, however, in both quality and quantity terms the most prominent are those caused by temperature changes. This paper is devoted to the pendulum thermal dilatation, the most detrimental of all detrimental effects, as well as to the explanation of the basic principles that elimination of this effect is based upon. Both preliminary and detailed calculations were performed, resulting in some design solutions to almost perfect compensation for the pendulum temperature dilatation.

Notwithstanding the fact that the problem of thermal compensation of oscillators, especially of clock pendulums, is old more than 200 years, it still represents the respectable subject of research in modern science and technology. Thus, in [1], Popkonstantinović, B. et al. exposed the analytical method for the pendulum thermal compensation considering not only the mass center but also the pendulum mass moment of inertia of the first and second order. Actually, fast and efficient mathematical method as well as the practical constructive solutions is given by which the technically acceptable thermal compensation of the long period compound pendulum can be obtained. Popkonstantinović, B. et al., in [2], explain the design, solid modelling and motion simulation of the remontoire mechanism only by which the influence of a pendulum thermal compensation for the clock accuracy can be significant and observable. K. V. Kislov investigates, in [3], the influence of temperature noise on the linear dimensions variation of new broadband seismometers, clarifies which elements of the device are the most sensitive to the ambient temperature variations and determines the level of noise generated by all the elements. In [4], Agatsuma K. Et al. achieved for the first time a direct measurement of the thermal fluctuation of a pendulum in an off-resonant region using a laser interferometric gravitational wave detector and disclosed the conclusion that the measured thermal noise level corresponds to a high quality factor on the order of 10^5 of the pendulum. Jie Luo et al. introduced, in [5], the weighting function by considering the nonlinear least-squares fitting method and the correlation method, and developed a method to calculate the influence of thermal noise on the period measurement in a torsion pendulum. Consequently, they obtained a rigorous formula of thermal noise limit and uncertainty estimation for the pendulum period measurement. This result is significant for precise determination of the Newtonian gravitational constant using the time-of-swing method. A finite element modeling can be used in many different applications [6, 7]. A. Cumming et al. discuss, in [8], the finite element modeling and associated analysis of the loss in quasi-monolithic silica fiber suspensions for future advanced gravitational wave detectors. They emphasized that the detector suspension thermal noise will be an important noise source at operating frequencies between approximately 10 and 30 Hz, and results from a combination of thermo elastic damping, surface and bulk losses associated with the suspension fibers. They concluded that its effects can be reduced by minimizing the thermo elastic loss and optimization of pendulum dilution factor via appropriate choice of suspension fiber and attachment geometry. In [9], V. E. Dzhashitov and V. M. Pankratov considered the control possibility of interconnected mechanical and thermal processes in nonlinear perturbed dynamic systems for irregular motions and parametric temperature perturbations. It is shown that the choice of thermal parameters and mechanical subsystems as well as the introduction of mechanical control subsystem proportional to the temperature gradient between its elements into the feedback can provide both regularization of oscillations and control of oscillations at parametric temperature perturbations. Jie Luo and Dian-Hong Wang, in [10], considered the environment temperature variation and

unhomogeneity of background gravitational field and proposed an improved correlation method to determine the variation period of a torsion pendulum with high precision. This analysis is significant for the determination of gravitational constant with the time-of-swing method. Woodward P., in [11] and [12], and Matthys R. J., in [13], analyzed various methods and technical solution for pendulum thermal compensation and proposed important practical advices for the design of high precision pendulum clocks. In [14], Andri M. Gretarsson et al. consider the problem of pendulum thermal noise in advanced large interferometers for detecting gravity waves. Peter R. Saulson, in [15], analyzed thermal noise in mechanical experiments and constructed models for the thermal noise spectra of systems with more than one mode of vibration, and evaluated a model of a specific design of pendulum suspension for the test masses in a gravitational-wave interferometer.

2 The Pendulum Temperature Dilatation

Any material, therefore the material that the pendulum is made of, changes its dimensions with a change in temperature. This is the linear temperature dilatation phenomenon described by the formula 1:

$$l = l_0 \cdot (1 + a \cdot (t - t_0)) = l_0 \cdot (1 + a \cdot \theta) \quad (1)$$

In this relation, a is the linear coefficient of temperature (thermal) dilatation, and l and l_0 are the pendulum rod lengths at temperatures t and t_0 . The values of coefficient a [K^{-1}] that defines the relative change of length per unit of basic length and the level of temperature change are given in Table 1 for some materials mentioned in this paper.

If circular error is neglected, the oscillation period of a physical pendulum can be calculated using well-known formulas 2:

$$T \approx 2\pi \sqrt{\frac{J}{g \cdot S}} = 2\pi \sqrt{\frac{\sum m_i r_i^2}{g \cdot \sum m_i r_i}} = 2\pi \sqrt{\frac{l_r}{g}} \quad (2)$$

where J and S are square and static moments of inertia and g is the acceleration of gravity. The formulas indicate clearly that:

$$J = \sum m_i r_i^2 \quad (3)$$

$$S = \sum m_i r_i \quad (4)$$

$$l_r = \frac{\sum m_i r_i^2}{\sum m_i r_i} \quad (5)$$

where m_i and r_i in formulas 3, 4 and 5 are masses and, relative to the suspension point, coordinates of the center of gravity of all the parts of a pendulum, and l_r is the so-called reduced length of a physical pendulum. By definition, it represents the length of a mathematical pendulum that has the same period of oscillation as a specified physical pendulum. The static moment S determines the coordinate of the center of gravity, while the square moment J describes the geometric distribution of masses around the suspension point and the center of gravity of the entire pendulum.

Table 1
Linear coefficient of temperature dilatation for some materials

<i>MATERIAL</i>	$a \cdot 10^{-6} [K^{-1}]$	<i>MATERIAL</i>	$a \cdot 10^{-6} [K^{-1}]$
<i>Invar alloy</i>	1,2	<i>Brass</i>	18-19
<i>Wood of silver fir</i>	4	<i>Lead</i>	28
<i>Steel 0.1%C</i>	12	<i>Zinc</i>	39,7

From the very fact that each line coordinate in the above given formulas is susceptible to temperature dilatations, it follows that the physical pendulum eigenoscillations period changes with temperature change. Illustrative example: a pendulum with a period of $T = 2$ seconds¹, whose rod is made of simple, low-carbon structural steel, loses about 0.5 s a day, with temperature rise of 1 °C. If the temperature rises by 10 °C a day, the clock having such a pendulum is around 36 s late for 7 days of permanent running. Under identical temperature conditions, the clock that has a geometrically equivalent pendulum installed, but with a rod of the wood of silver fir, is only 12 s late for 7 days. The described irregularities in a timepiece running were first noticed by English horologists in the 18th Century, so the earliest attempts to correct the irregularities date back to those days.

3 Principles of Temperature Dilatation Compensation

In their simplest form, the principles of compensation for the effects of stochastic temperature changes on the uniform running of a timepiece are based on the choice of the material that has the lowest linear coefficient of temperature dilatation. The above given example indicates clearly that a silver-fir wood rod,

¹ In horology such a pendulum is traditionally referred to as one second, because pendulums were formerly indicated according to duration of oscillation semi-period.

compared to a steel one, is less susceptible to the temperature influence. That is why those rods on old tower clocks and so-called Vienna regulators² were manufactured from wood. Later, in the 19th Century, with the discovery of the Invar alloy³, this compensation method was improved, but was never perfect enough. More complex design solutions had to be used for astronomical clocks, chronometers, best quality public clocks and even some wall clocks.

To make compensation for the temperature effects as much complete as possible, a pendulum should be manufactured of at least two different types of material. In 1726, Honorable George Graham⁴ of London was the first to make this idea come true. He constructed the so-called mercury pendulum. Mercury is characterized by a high volumetric temperature expansion coefficient ($18 \cdot 10^{-5} \text{ K}^{-1}$) and high density (13.6 kg/m^3), which can be utilized for compensation of the pendulum center of gravity displacement due to its rod thermal dilatation. Fig. 1 shows a typical design solution for the mercury pendulum: a vial of glass or cast iron filled with some amount of mercury. The change in pendulum temperature changes both its rod length and mercury column height in a vial, but in the opposite direction. Detailed calculations can be used to determine the needed mercury column height to compensate for the center of gravity position of the entire pendulum. Final calibration of the mercury column height is performed during the pendulum assembly process by adding mercury drop by drop! In order to have the same temperature at any moment as mercury has, which is an essential prerequisite for compensation, the pendulum rod is always immersed in it.

Although mercury performs good compensation for the pendulum temperature dilatation, its use is restricted by the fact that it is a toxic liquid that pollutes the environment it is discharged into, or evaporates into the atmosphere during accidents. That is the reason why other technical solutions are applied. John Harrison⁵ was the first to use compensation based on steel and brass combination in building his stationary clocks and chronometer H1. It is the so-called gridiron bimetal pendulum, whose conceptual solution is given in Fig. 2. The pendulum support is built of 5 steel and 4 brass parallel and symmetrical rods. They are equal in length and are connected in such a way that steel rods always expand *from* and brass rods *toward* the suspension point.

² Wiener Uhren – precision wall clocks were handmade in the Austro-Hungarian Empire throughout the 19th Century; well-known for accuracy, reliability and beauty of style.

³ Solid solution of 36% nickel in iron (symbol – 64 FeNi); Swiss scientist Charles Edouard Guillaume discovered this alloy in 1896 and was awarded the Nobel Prize in Physics in recognition of his discovery of nickel-steel alloys.

⁴ Honorable George Graham (1673-1751) was one of the most famous English clockmakers who invented the deadbeat escapement. He was made Master of Worshipful Company of Clockmakers in 1722.

⁵ John Harrison was a great English clockmaker and inventor. He built the first marine chronometer, and solved the ‘problem of longitude’.

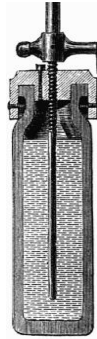


Figure 1

Glass vial of a mercury pendulum

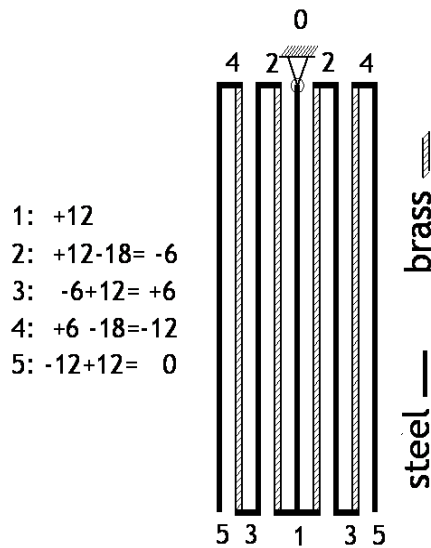


Figure 2

Bimetal gridiron pendulum

As linear coefficient of thermal dilatation for steel is $\alpha_{\text{st}} = 12 \cdot 10^{-6} \text{ K}^{-1}$, and for brass $\alpha_{\text{br}} = 18 \cdot 10^{-6} \text{ K}^{-1}$, the points 1, 2, 3, 4 relative to the gridiron pendulum suspension point have displacements +12, -6, +6 and -12 $\mu\text{m/Km}$, while the points 5 – 5 are not subject to displacement due to temperature change. This solution, the practical realization being presented in Fig. 3, ensures thermal invariance of the position of the pendulum weight center of gravity. However, this is not enough as calculations will demonstrate below. The technical solution is known too. It is based on the same principle as the described gridiron pendulum but it uses steel and zinc coaxial pipes instead of steel and brass rods (Fig. 4). As zinc possesses an extremely high linear coefficient of thermal expansion, compensation is achieved only with one zinc and two steel pipes.



Figure 3

Technical realization of the gridiron pendulum

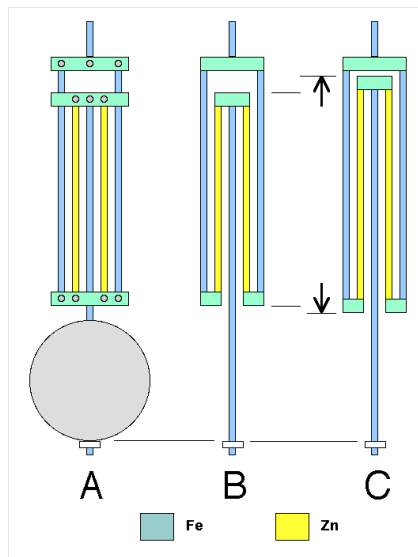


Figure 4

Cross-section of coaxial pipes of the pendulum steel and zinc rod

Very simple and, at the same time, almost the most efficient solution to the compensation for the pendulum thermal dilatation is accomplished by combining wood⁶ and lead. If the pendulum rod is manufactured from the wood of silver fir and the weight from lead pipe of the corresponding length and mass, it is possible to achieve technically perfect temperature compensation for the reduced length of the entire pendulum. First, preliminary and then detailed calculations of such design is the subject of the analysis to follow.

⁶ Wood has first to be protected from harmful effects of moisture!

4 Preliminary Calculations of Thermal Compensation

The wood of silver fir possesses extremely low, while lead high enough linear coefficient of thermal expansion ($a = 4 \cdot 10^{-6} \text{ K}^{-1}$ and $b = 28 \cdot 10^{-6} \text{ K}^{-1}$), therefore their one-fold combination can completely compensate for the pendulum dilatation. Conceptual solution of this coupling is presented in Fig. 5. The pendulum support is a wood rod on the lower part of which a lead pipe is coaxially fixed. The rod expands thermally from the suspension point downward and a lead weight in opposite direction. Preliminary calculations are based on determining the ratio of the rod length to the pipe, thermal displacement of the center of gravity of the entire pendulum being thermally neutralized. From the fact that the position of the pendulum center of gravity is determined by its static moment S , where lengths depend on temperature, there follows:

$$S = m \frac{l_0(1+a\theta)}{2} + M(l_0(1+a\theta) - \frac{L_0(1+b\theta)}{2}); \theta = t - t_0 \quad (6)$$

In this formula 6 as well as in the formulas 7 and 8 below l_0 and L_0 are the lengths of rod and lead pipe at the temperature t_0 ; m , M are rod and pipe masses; a and b are linear coefficients of wood and lead thermal dilatation; $\theta = t - t_0$ is temperature difference.

To make the center of gravity position invariant relative to θ , it is sufficient to annul the thermal gradient of the static moment:

$$\frac{dS}{d\theta} = \frac{m \cdot l_0 \cdot a}{2} + M \cdot l_0 \cdot a - \frac{M \cdot L_0 \cdot b}{2} = 0 \quad (7)$$

As this gradient does not depend on the argument θ , it follows that the influence of displacement position of the pendulum center of gravity will be completely neutralized if the following condition 8 is fulfilled:

$$\lambda = \frac{l_0}{L_0} = \frac{b}{a} \cdot \frac{M}{2M + m} \quad (8)$$

The quality of this compensation will be checked using the example of the clock supplied with the described pendulum, for which it is adopted: $m = 0.4 \text{ kg}$, $M = 20 \text{ kg}$ and $T = 2 \text{ s}$. For 10 days of permanent running, at temperature rise of $\theta = +10 \text{ }^\circ\text{C}$, the clock is -2.16 s late, which is 8 times lower compared to the thermally uncompensated equivalent (-17.28 s). The error residuum stems from the fact that the pendulum oscillation period is not only the function of the center of gravity position but also of the inertia square moment. Its reduction is the subject of the following, more complex calculations.

5 Optimal Solution of Thermal Compensation

Fig. 5 illustrates the origin of error residuum in the timepiece running that has an installed pendulum with thermally compensated center of gravity: compared to the stationary pendulum center of gravity, by changing its original volume due to temperature change, a certain amount of material has changed the square moment of the system inertia. Better quality compensation has to include neutralization of this phenomenon too. Let us start from the formula 9 for a pendulum relative reduced length that is a function of temperature:

$$\frac{l_r}{L_0} = \frac{\frac{1}{12}M(1+b\theta)^2 + \frac{1}{3}m\lambda^2(1+a\theta)^2 + M(\lambda(1+a\theta) - \frac{1}{2}(1+b\theta))^2}{\frac{1}{2}m\lambda(1+a\theta) + M(\lambda(1+a\theta) - \frac{1}{2}(1+b\theta))} \quad (9)$$

The first, second and third term of the numerator in the above formula 9 originates from the square mass moments of inertia, in a row: eigenmoment of a lead pipe, total moment of a rod for the suspension point, and position moment of a lead pipe for the suspension point. The first and second term of the numerator originate from the static moments of inertia of the rod and lead pipe for the suspension point. In this analysis, we establish the condition of annulling the temperature gradient for the pendulum relative reduced length, described by formula 10:

$$\frac{1}{L_0} \cdot \frac{dl_r}{d\theta} = \frac{\frac{2}{3}a\lambda^2m(1+a\theta) + \frac{1}{6}bM(1+b\theta) - 2(\frac{b}{2} - \lambda)M(\lambda(1+a\theta) - \frac{1}{2}(1+b\theta))}{\frac{1}{2}\lambda m(1+a\theta) + M(\lambda(1+a\theta) + \frac{1}{2}(1+b\theta))} - \frac{(\frac{a\lambda}{2} - \frac{b}{2} - a\lambda)M \cdot (\frac{1}{3}\lambda^2m(1+a\theta)^2 + \frac{1}{12}M(1+b\theta)^2 + M(\lambda(1+a\theta) - \frac{1}{2}(1+b\theta))^2)}{(\frac{1}{2}\lambda(1+a\theta) + M(\lambda(1+a\theta) - \frac{1}{2}(1+b\theta)))^2} \quad (10)$$

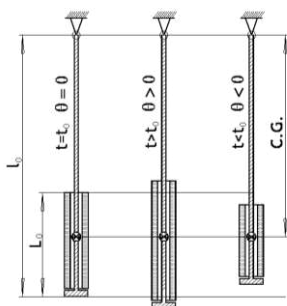


Figure 5

Temperature compensation for the pendulum center of gravity and origin of error residuum

Table 2
Comparison of compensation quality

$\theta [^{\circ}\text{C}]$	NK [s]	KCG [s]	KRL [s]
-30	+54,8416	+6,48685	-0,004220
-20	+34,5607	+4,32520	-0,001876
-10	+17,2802	+2,16292	-0,000469
0	0,0000	0,00000	0,000000
+10	-17,2798	-2,16356	-0,000469
+20	-34,5593	-4,32775	-0,001876
+30	-51,8384	-6,49258	-0.004220

From the fact that temperature gradient of the pendulum reduced length is a function of temperature, there follows an important statement: *it is even theoretically impossible to achieve a complete compensation for the pendulum linear temperature dilatation!* Yet, it is possible to have such a design solution that will reduce thermal disorders of the pendulum eigenoscillations to a minimum. In that regard, it would be the most appropriate to determine the value of the parameters $\lambda = l_0/L_0$ that will annul the gradient $dl_0/d\theta$ for the mean annual temperature of a place of timepiece running. The analysis was carried out using the example of a concrete timepiece supplied, as in a previous case, with a pendulum that the following parameters were adopted for: $m = 0.4 \text{ kg}$, $M = 20 \text{ kg}$ and $T = 2 \text{ s}$. Using the condition⁷ $(dl_0/d\theta) = 0$, and for $\theta = 0 \text{ }^{\circ}\text{C}$, the parameter $\lambda = 3.0128$ was determined, which leads to the pendulum total compensation at $\theta = 0 \text{ }^{\circ}\text{C}$. The lengths of a wood rod l_0 and a lead pipe L_0 are determined from the formula for the physical pendulum eigenoscillations period ($l_0 = 1178.815 \text{ mm}$, $L_0 = 390.569 \text{ mm}$). Table 2 shows error accumulation for three equivalent timepieces, during a 10-day running period, at 7 different temperatures. The first is supplied with an uncompensated pendulum (symbol - NK), the second has a pendulum with a compensated center of gravity (symbol - KCG) according to preliminary calculations, and the third has a pendulum with a compensated gradient of reduced length (symbol – KRL). The results tabulated indicate, first of all, the advantage of compensation for pendulum thermal dilatation, which is based on tempering the temperature gradient of reduced length, over neutralizing the center of gravity thermal displacement. In addition, it is evident that error residuum is always present, but in the last column it is almost negligible and more than acceptable for technical application.

⁷ From this condition there follows the cubic equation for λ that has three real solutions: $\lambda_1 = 0.337667$; $\lambda_2 = 1.12793$; $\lambda_3 = 3.0128$; the last one is technically feasible.

Concluding Remarks

The calculations of thermal gradient tempering of the pendulum relative reduced length, explained and carried out in this paper, can be also directly applied to combined Invar alloy (pendulum rod) and, for example, steel and brass (weight). The issue of non-uniform thermal conductivity, ever present in such technical solutions, is not of practical importance because changes in mean annual, and even daily, air temperatures are extremely slow. If calculations are performed without the help of any electronic aids, the problems of their numerical realization for $(dl,ld\theta) = 0$ are almost insurmountable. It could be the only reason why they were not performed in the 18th and 19th Century, but pendulum thermal compensation was done using tests, or by shortening the weight made of lead pipe. In this paper, all calculations were carried out in the Mathematics 5 application, fast and simply, with the aim to point to the strategy of numerical analysis itself that will make laboratory tests of metric adjustments, always long and expensive, shorter or even redundant.

References

- [1] Popkonstantinović, B., Miladinović, Lj., Stoimenov, M., Petrović, D., Petrović, N., Ostojić, G., Stankovski, S., The Practical Method for Thermal Compensation of Long-Period Compound Pendulum, Indian Journal of Pure & Applied Physics, Vol. 49(10), October 2011, ISSN 0019-5596, pp. 657-664
- [2] Popkonstantinović, B., Miladinović, Lj., Stoimenov, M., Petrović, D., Ostojić, G., Stankovski, S., Design, Modelling and Motion Simulation of the Remontoire Mechanism, Transactions of Famera, XXXV-2, 2011, ISSN 1333-1124, pp. 79-93
- [3] K. V. Kislov, Temperature Variations in Linear Dimensions of Elements of a Broadband Seismometer Perceived by the Latter as Ground Vibration, Seismic Instruments, Volume 46, Number 1, ISSN 1934-7871, Allerton Press, Inc. distributed exclusively by Springer Science+Business Media LLC, 2010, pp. 21-26
- [4] Agatsuma K, Uchiyama T, Yamamoto K, Ohashi M, Kawamura S, Miyoki S, Miyakawa O, Telada S, Kuroda K, Direct Measurement of Thermal Fluctuation of High-Q Pendulum, Physical review letters, ISSN 0031-9007, 2010
- [5] Jie Luo, Cheng-Gang Shao and Dian-Hong Wang, Thermal Noise Limit on the Period of a Torsion Pendulum, Classical and Quantum Gravity, Volume 26, ISSN 1361-6382, IOP Publishing, 2009
- [6] Tiberiu Tudorache, Mihail Popescu, FEM Optimal Design of Wind Energy-based Heater, Acta Polytechnica Hungarica Vol. 6, No. 2, 2009, pp. 55-70

- [7] Fevzi Kentli, Hüseyin Çalik, Matlab-Simulink Modelling of 6/4 SRM with Static Data Produced Using Finite Element Method, *Acta Polytechnica Hungarica*, Vol. 8, No. 6, 2011, pp. 23-42
- [8] A Cumming, A Heptonstall, R Kumar, W Cunningham, C Torrie, M Barton, K A Strain, J Hough and S Rowan, *Finite Element Modelling of the Mechanical Loss of Silica Suspension Fibres for Advanced Gravitational Wave Detectors*, *Classical and Quantum Gravity*, ISSN 0264-9381, IOP Publishing, 2009
- [9] V. E. Dzhashitov and V. M. Pankratov, On the Possibility of Control of Interconnected Mechanical and Thermal Processes in Nonlinear Temperature - Perturbed Dynamic Systems, *Journal of Computer and Systems Sciences International*, ISSN 1555-6530, MAIK Nauka/Interperiodica distributed exclusively by Springer Science+Business Media LLC., 2009, pp. 481-488
- [10] Jie Luo and Dian-Hong Wang, An Improved Correlation Method for Determining the Period of a Torsion Pendulum, ISSN 0034-6748, *Review of Scientific Instruments*, Vol. 79, 094705, 2008
- [11] Woodward P., Woodward on Time (Group 5: Pendulum and Their Suspensions; 1. Compensation of Pendulums; 3. A bimetallic compensator), ISBN 0-95096216-3, Bill Taylor and British Horological Institute, UK, 2006
- [12] Woodward P., My Own Right Time – An Exploration of Clockwork Design (2. Theory and practice; 13. Error correction), ISBN 978-0-19-856522-2, Oxford University Press, New York, 2003
- [13] Matthys R. J., *Accurate Clock Pendulums*, Oxford University Press, USA, 2004
- [14] Andri M. Gretarsson, Gregory M. Harry, Steven D. Penn, Peter R. Saulson, William J. Startin, Sheila Rowan, Gianpietro Cagnoli and Jim Hough, Pendulum Mode Thermal Noise in Advanced Interferometers: A Comparison of Fused Silica Fibers and Ribbons in the Presence of Surface Loss, *Physics Letters A*, Volume 270, Issues 3-4, ISSN 0375-9601, ScienceDirect, Elsevier, 2000. pp. 108-114
- [15] Peter R. Saulson, Thermal Noise in Mechanical Experiments, *Physical Review D*, ISSN 05562821, Volume 42, Issue 8, American Physical Society, 1990, pp. 2437-2445

Morphological Dilation as Fractal Scaling in Roughness Measurement

Peter Bakucz

Óbuda University, Institute of Mechatronics and Vehicle Engineering
Népszínház u. 8, 1081 Budapest, Hungary
e-mail: bakucz.peter@bkg.uni-obuda.hu

Rolf Krüger-Sehm

Physikalisch-Technische Bundesanstalt (PTB), Fachbereich 5.1
Bundesallee 100, 38116 Braunschweig, Germany
e-mail: rolf.krueger-sehm@ptb.de

Abstract: In this work we propose, that the morphological dilation acts as fractal filters rebuilding white noise roughness surfaces into fractal 1/fm noise surfaces. The fractality indicates that the dilation does not have characteristic length scale, and the structuring element follows power-law distribution. Yashchuk's binary pseudo-random grating standard has been dilated with spherical and free form tips between 50 nm and 2000 nm and two scaling regions are referred to the tip diameter versus scaling exponent diagram. The first one in the smaller tip diameter region has a fast slope and the second one in the intermediate and larger tip diameter has a gradual slope. The results show that the dilated surfaces arise from the activity of at least two dynamical systems.

Keywords: Roughness; Morphological Filtering; Fractals

1 Introduction

The roughness signal is constructed through the detection of an interaction between the tip apex and measurement surface features, thence the signal mainly affected by the tip-defined dynamical systems [1] [2] [3].

The real surface could be determined first by measuring the height distribution of the surface (tip convolution or morphological dilation) and second by deconvolving the tip effect with morphological erosion [4]. These processes provide the complete mathematical description of a fabrication procedure within the framework of the mathematical morphology [5]. However, an engineering

surface is an example of a specific structure in the sense that the profile of a surface is irregular, i.e. has no characteristic scale [6] [7].

The purpose of this work is to investigate the morphological dilation operation on the Yashchuk binary pseudo random grating white noise surface [8]. The inherent power spectral density of a white noise is an identical function, independent of spatial frequency. The fractal scaling behavior of the morphological dilation suggests that the operation is scale-free in the sense, that changing the lengthscale associated with dilation results also has a fractal scaling form. Comparing the power spectral densities of the dilated surface, shows how strong the dilation attenuates the surface on each length scales and additionally the structuring element can be characterized.

2 Power Spectra

Variations in the height of an engineering surface can be described with the periodogram, which is the square of the coefficients in a Fourier series representation and measures the average variation of the surface at different frequencies (Fig. 1). The periodogram can be computed for the entire surface at once, or segments of the surface can be averaged together to form the power spectral density (PSD). A widely used PSD is based on the covariance method [10].

If touching engineering surface points are uncorrelated, then the PSD will be constant as a function of wave number, i.e. white noise. If touching points are correlated relative to points far separated the PSD will be considerable at subordinate wavelengths and small short wavelengths [15] [16].

In this work we show, that the morphological dilation operation scales as fractal filter in which the white noise power spectrums are rebuilt into fractal $1/f^m$ spectrums. In $1/f^m$ signal, the spectral power of fluctuations is reversely balanced to their frequency. Surfaces referenced any $1/f^m$ scaling therefore fulfil a multiscale relationship, because fluctuations at any wavelength are engaged in large fluctuations at longer wavelengths, and these, in turn, are engaged in larger fluctuations on longer lengthscales.

3 An Approximate Power Function for Tip Distribution

We characterize the dilation with a 9 point's spherical tip and free form tips (9 and 12 points) (Fig. 1). The tip diameter is defined between the 0th and the 9th (12th) points. We used 21 tips, diameters between 50 nm – 2000 nm.

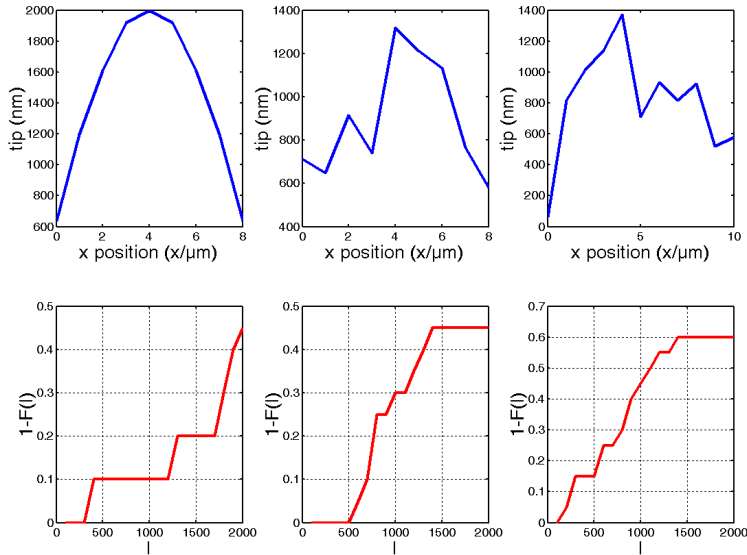


Figure 1

Spherical-, and 9-, 12 points free-form structuring elements (upper) and their distribution functions ($F(l)$)

The dilated surface points reflect the tip around the point weighted by their fractional contribution to the unfiltered input. Mathematically this means that the dilated output ($g_{dil}(n)$) at any value $n \in (0, 1, \dots, N)$ is the convolution of the input $g_{input}(n)$ and the tip $g_{tip}(l)$. ($l \in (-v, \dots, 0, \dots, v)$ v is tip radius.)

$$g_{dil}(n) = \int_{-v}^v g_{tip}(l) g_{input}(n-l) dl = \max_{l \in \{-v, \dots, v\}} \{g_{input}(n-l) + g_{tip}(l)\} \quad \text{for } n = 0, 1, \dots, N - 2 * v - 2 \quad (1)$$

where N is number of measured surface values.

From Eq (1) one can see, if the distribution of the tip is broad compared to the wavelength of the input surface, the filtering will be averaged but the fluctuations attenuated. The shorter the wavelength of the input compared to the tip distribution, the powerfuller this characterization by averaging processes. On the contrary, variations on length scales that are long related to the tip distribution will be transferred through the dilatation without meaningful extension.

By the convolution theorem, Eq (1) indicates

$$C_{dil}(f) = C_{tip}(f)C_{input}(f) \quad \text{and} \quad |C_{dil}(f)|^2 = |C_{tip}(f)|^2 |C_{input}(f)|^2 \quad (2)$$

Here $C_{dil}(f), C_{tip}(f), C_{input}(f)$ are the Fourier spectrums of $g_{dil}(l), g_{tip}(l)$ and $g_{input}(n-l)$ and $|C_{dil}(f)|^2, |C_{tip}(f)|^2, |C_{input}(f)|^2$ are their PSD. When the input surface is white noise, the $|C_{input}(f)|^2$ is approximately constant, and the PSD of the tip is roughly balanced to the PSD of filtered surface: $|C_{dil}(f)|^2 \propto |C_{tip}(f)|^2$.

The scaling behaviour, shown in (Fig. 2 right), is compatible with the assumption that the tip distribution power spectrum has a power decrease $|C_{tip}(f)|^2 \propto \frac{1}{f^m}$.

It is equally clear that this power decrease must break down for large l , because otherwise the tip distribution would become infinite.

An approximate distribution function $F(l)$ that is integrable at large l could be expressed with the gamma function ($\Gamma()$):

$$F(l) = \frac{l^{\alpha-1}}{\beta^\alpha \Gamma(\alpha)} e^{-\frac{l}{\beta}} \quad (3)$$

where β is a scale parameter and $\alpha = 1 - m$ is a shape parameter [12].

Eq. 3. indicates a power spectrum of the form:

$$|C_{tip}(f)|^2 = (1 + 4\pi^2 f^2 \beta^2)^{-\alpha} \quad (4)$$

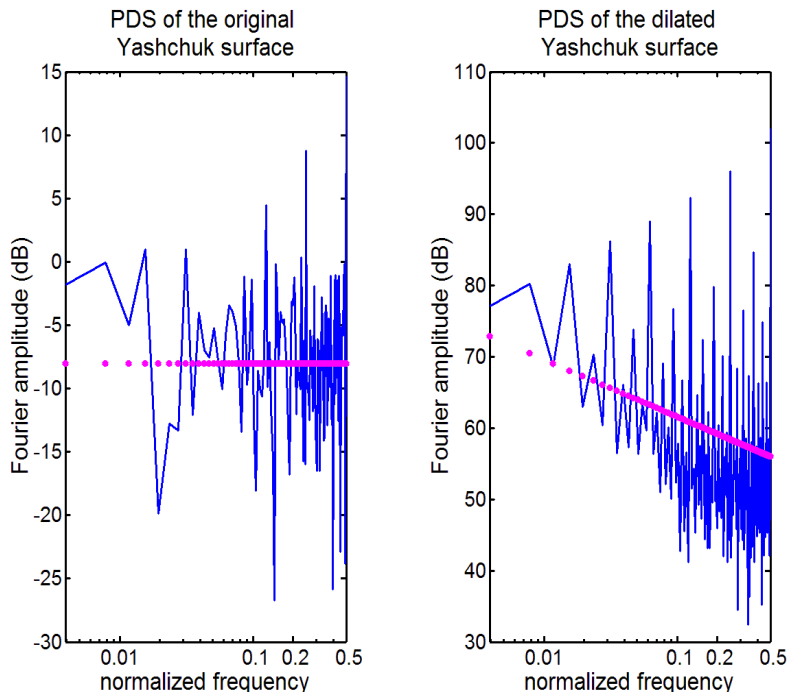


Figure 2

Binary pseudo-random grating standard (Yashchuk surface) of 2^8 samples (normalized, left).
 Periodogram with least-squares fitting for the Yashchuk surface (middle), Periodogram with least-squares fitting for the 400 nm spherical tip dilated Yashchuk surface (right).

The PSD for the spherical-, and free-form 400 nm tips can be seen on Fig. 3. We used the exponential function fit (circle line) and Eq. (4) gamma function fit (star line) for the PSD signal (solid line). The PSD of the dilated surfaces with its fractal behavior could be better approximated by the gamma function. This is obviously the consequence of the localization of the gamma function, since the function “whiten” the surfaces. For the dilated surfaces at low frequencies the dilation operator behaves as a fractional differentiator.

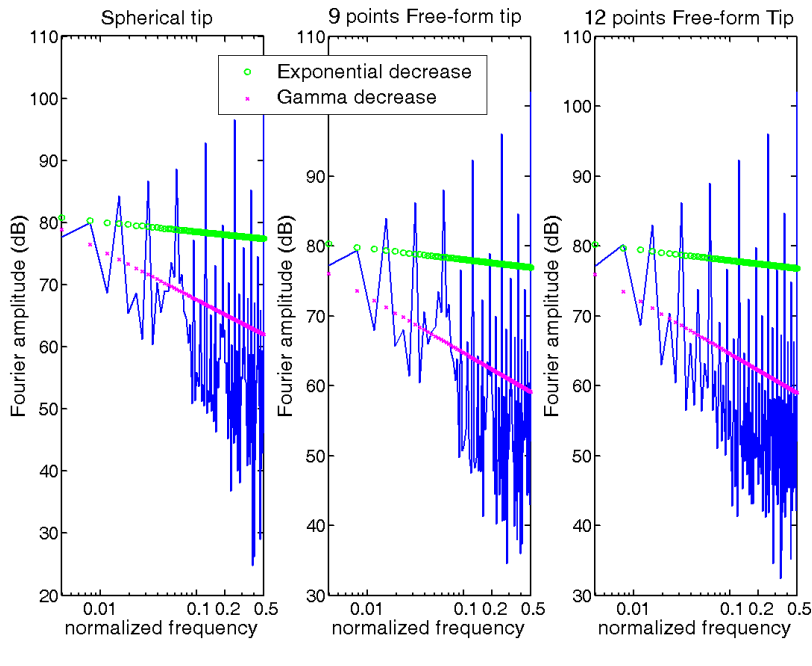


Figure 3

PSD of the dilated Yashchuk surface (solid line). Exponential function fit (circle line), gamma function fit (star line). The tip diameters are 400 nm.

4 Effects of Tipsize

It may be of interest to analyze the tip diameter corresponding the scaling parameter m .

Figure 4 is a plot of the relationship corresponding the scaling exponent and the tip diameter for spherical (solid line), 9 points free form (dashed line), and 12 points free form tips (dashdot line).

One can see two parts (scaling regions I and II) where the sign and the value of the slope are different. The slope of the lower region (300-700 nm for free form tips and 500-800 nm for spherical tip) decreases and the gradient of the upper region (700-2000 nm and 800-2000 nm) decreases as the tip diameter increases.

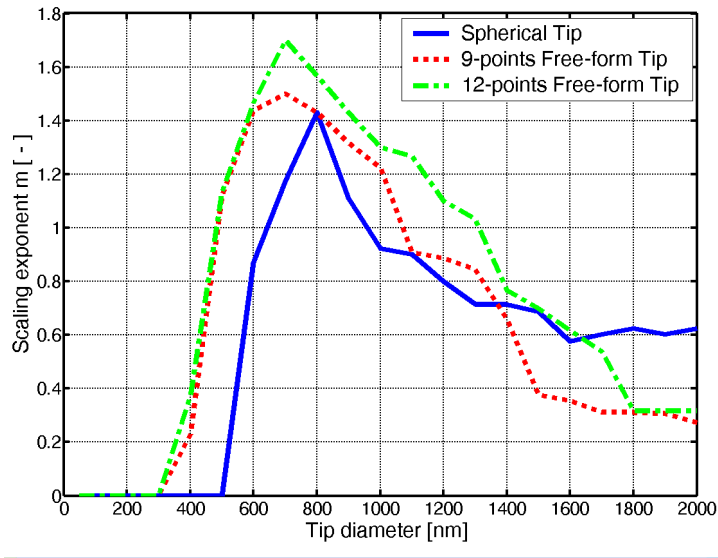


Figure 4

Scaling exponent vs. tip diameter relationship for spherical (solid line), 9 points free form (dotted line), and 12 points free form tips (dashdot line)

The scaling regions are result from the secular relation between nearby points of the surface and the points of the tip and the scaling regions are related to internal variations of Yashchuk surface.

In the Figure 5 the PSD of the two regimes are presented using covariance estimate. The similar scaling relations are observed for the free form tips.

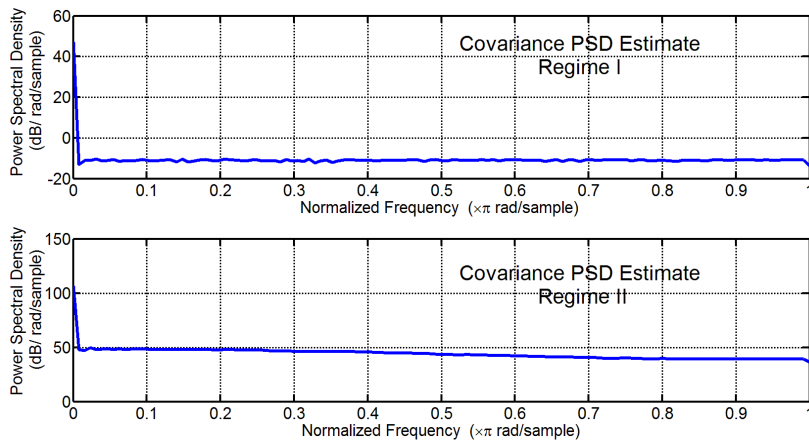


Figure 5

Covariance PSD of the two regimes diluted by 21 different spherical tips

The scaling regions have also been appeared in analyzing the dynamic of the dilated system with Kolmogorov entropy K . (Figure 6). The K describes a degree of chaoticity of system and gives the mean property of information loss about a phase point. In the statistical physics $K = 0$ in an deterministic space, K is infinite in a random space, and $0 < K < 1$ is in a chaotic space. (More detailed see in [13]).

For the scaling region I the slope of Kolmogorov entropy vs. tip diameter diagram of the dilated surfaces are between 0.27 ± 0.09 and 0.15 ± 0.06 , respectively. In the scaling region I is the system chaotic.

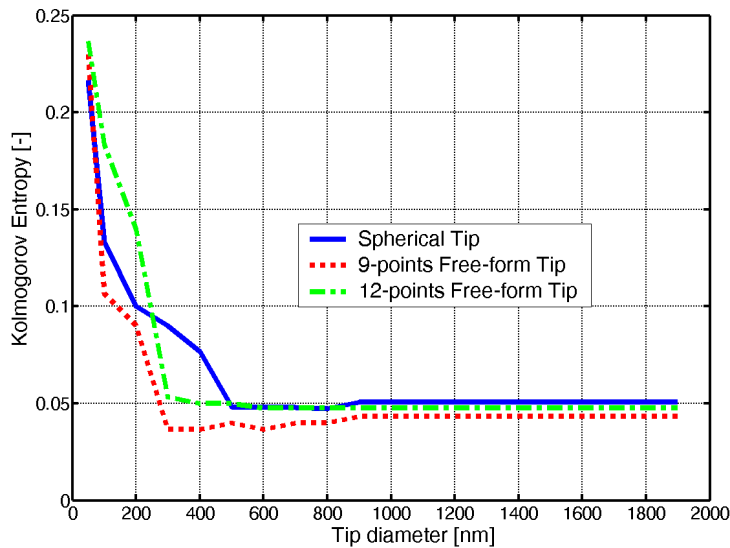


Figure 6

Kolmogorov Entropy for spherical (solid line), 9 points free form (dotted line), and 12 points free form tips (dashdot line)

The scaling region II with the constant near 0 slope in the scaling exponent system are revealed in the ranges of larger tip diameter. The information loss of this region shows that the system is fixed (Table 1).

Table 1

Slope of the Kolmogorov entropy vs. tip diameter diagram for the different scaling regions

	scaling region I	scaling region II
Spherical tip	0.27 ± 0.09	0.05 ± 0.001
9 points free form tip	0.21 ± 0.03	0.05 ± 0.002
12 points free form tip	0.15 ± 0.06	0.04 ± 0.002

Conclusions

The affiliation between the PSD of the Yashchuk binary pseudo-random grating standard and the output dilated surfaces at each wavelength reflects how powerful the dilation changes the tip distribution space on each lengthscale. The power spectra of the dilated surfaces show fractal $1/f^m$ scaling; this indicates that dilation is acting as fractal filter, rebuilding the inputs into $1/f^m$ noise outputs with m scaling exponent. The scaling behaviour is directly related to the input standard lengthscale distribution. If the distribution is comprehensive to the wavelength of the tip distribution, then the fluctuation will be standardized and discouraged.

The relationship between the dilated signal and its PSD can be extracted, and the tip distribution can be determined. The fractal $1/f^m$ scaling is consistent with the tip distribution ($F(l)$) using the gamma function. The dilated tip PSD can present both long-term character of scans and short-term character to scans consequently the gamma distribution is an appropriate categorizing of the scaling behaviour and the tip distribution seen at the dilatation of the Yashchuk surface.

Analyzing the tip diameter versus scaling exponent diagram one can see two parts (scaling regions) where the sign and the value of the slope are different.

The scaling regions are result from the secular relation between nearby points of the surface and the points of the tip and the scaling regions are related to internal variations of Yashchuk surface: for the scaling region I is the system chaotic and the information loss of the scaling region II shows that the system here is already fixed [14].

References

- [1] Palásti-Kovács B, Néder Z, Czifra Á, Váradi K (2004) Microtopography Changes in Wear Process, in Acta Polytechnica Hungarica, Issue 1, No. 1
- [2] Danzebrink H-U, Koenders L, Wilkening G, Yacoot A and Kunzmann H (2006) Advances in Scanning Force Microscopy for Dimensional Metrology *Ann. CIRP* **55** 841–79
- [3] Fekete G, Horváth S, Czifra Á (2007) Microgeometry Tests of 'Contradictory' Surfaces with Various Evaluation Techniques, in Acta Polytechnica Hungarica, Issue 4, Number 4
- [4] Giardina C. R. and Dougherty E. R. (1988) Morphological Methods in Image and Signal Processing. Englewood Cliffs, NJ, Prentice Hall
- [5] Balagurunathan Y. and Dougherty E. (2003) Morphological Quantification of Surface Roughness. *Opt. Eng.* **42**(6). 1795-1804
- [6] Bakucz P. et al (2008) Influence of the Atomic Force Microscope Tip on the Multifractal Analysis of Rough Surfaces. *Rev. of Scientific Instruments* **79** 073703

- [7] Raja J. et al. (2002) Recent Advances in Separation of Roughness, Waviness and form. *Precision Engineering*. 5247. 1-14
- [8] Yashchuk V. V., McKinney W. R. and Takács P. Z. (2007) Binary Pseudo-Random Grating as a Standard Test Surface for Measurement of Modulation Transfer Functions of Interferometric Microscopes. SPIE Optics and Photonics 2007 "Advances in Metrology for X-Ray and EUV Optics II" San Diego, August 30, 2007 Proceedings of SPIE 6704-7
- [9] Brown C. A. and Savary G. (1998) Scale-Sensitivity, Fractal Analysis and Simulations. *International Journal of Machine Tools and Manufacturing*. 38. 5-6 1998. 633-637
- [10] Marple, S. L (1987) *Digital Spectral Analysis*, Englewood Cliffs, NJ, Prentice-Hall, Chapter 7
- [11] Stoica, P., and R. L. (1997) *Moses, Introduction to Spectral Analysis*, Prentice-Hall
- [12] Bain, L. 1983: In *Encyclopedia of Statistical Sciences*. (ed. Kotz, S and Johnson, N. L.) 292-298. Wiley, New York
- [13] Eckman J. and Ruelle, P. D. (1985) Ergodic Theory of Chaos and Strange Attractors *Rev. Mod. Phys.*, 57, 617
- [14] Dai G, Jung L., Pohlenz F., Danzebrink H. U., Krüger-Sehm R., Hasche K., and Wilkening G. (2004) Measurement of Micro Roughness Using a Metrological Large Range Scanning Force Microscope. *Mes. Sci and Technology*. 15. 2004. 2039-2046
- [15] Czerkas S, Dziomba T and Bosse H 2005 Comparison of Different Methods of SFM Tip Shape Determination for Various Characterisation Structures and Types of Tip *Nanoscale Calibration Standards and Methods* ed G Wilkening and L Koenders (Weinheim: Wiley-VCH) ISBN 3-527-40502-X
- [16] Yacoot A, Koenders L and Wolff H (2007) An Atomic Force Microscope for the Study of Tip Sample Interactions and their Effects on Dimensional Metrology *Meas. Sci. Technol.* **18** 350-9
- [17] Binnig G, Quate C F, Gerber C (1986) Atomic Force Microscope. *Physical Review Letters*. **56(9)**, 930-933
- [18] Burnham N A, Colton R J (1989) Measuring the Nanomechanical Properties and Surface Forces of Materials Using an Atomic Force Microscope. *J. Vac. Sci. Technol* **A7**, 2134-2135
- [19] Bushan, B. (2004) *Springer Handbook of Nanotechnology*. Springer

Real-Time and High Precision 3D Shape Measurement Method

Takeshi Hashimoto, Takayuki Suzuki

Shizuoka University, Dept. of Electrical & Electronics Engineering, 5-1, 3-chome Johoku, Naka-ku, Hamamatsu, 432-8561, Japan,
tethash@ipc.shizuoka.ac.jp, f0230108@ipc.shizuoka.ac.jp

Hidemichi Aoshima

SUZUKI Motor Corporation, 300 Takatsuka-cho, Minami-ku, Hamamatsu, 432-8611, Japan

András Rövid

Óbuda University, John von Neumann Faculty of Informatics, Bécsi út 96/B, 1034 Budapest, Hungary, rovid.andras@nik.uni-obuda.hu

Abstract: In this paper, a unique 3D shape measurement method for measurement of nearly plain car body parts is proposed. The main advantage of the system is the high accuracy (about 0.1 mm), the high flexibility and the real-time processing. The primary application of the method is the 100% inspection of press formed car parts in the factory since in these cases the high accuracy and the real-time feature are indispensability. In order to achieve suitable measurement accuracy the camera specifications were carefully inspected. As result, a new type of gray-level marker and a new technique was proposed by the authors for compensating the time variability of marker central points in the camera images. In order to achieve real-time processing, the correspondence matching was devised. Furthermore, since the proposed method is based on processing camera images, i.e. the detection of feature-points on the target (such as screw holes) is also supported. The measured feature-points can easily be compared to CAE data.

Keywords: 3D shape measurement; real-time; high-precision; car parts

1 Introduction

High precision 3D measurement stands for a key issue in many applications. Although there are various kind of 3D measurement devices on the market, their improvement and adaptation to the requirements of specific applications are highly welcome as for instance for vehicle frame and vehicle body inspection, turbine blade inspection [12], for various kind of medical applications [11], etc.

As few examples of most widely used 3D measurement approaches utilizing image data, the structured light based ones as well as methods based on laser strip projection and fringe analysis [1] [2] [4] can be mentioned. Furthermore, there are also various hardware based solutions, e.g. Time of Flight (TOF) cameras [3] [10], as well as approaches based on stereo imaging without the use of pattern projection. The main bottleneck of the latter approach is the accuracy of the correspondence point-matching. The utilization areas of such systems are especially those ones which do not require high accuracy and robustness. Since all the existing realizations differ in several features, their utilization depends on the application requirements. Beside the above mentioned techniques one can find in the literature other interesting approaches, as well [9].

The primary aims related to the development of 3D measurement techniques are to achieve high accuracy as well as to ensure quick and easy measurement. To achieve high accuracy many factors have to be taken into account during the development, e.g. CCD (CMOS) image sensor noise, lens distortion, working distance, image resolution, quantization error of image sensors, etc. The latter one was considered as an unavoidable error in 3D measurement and has been studied and modeled by the authors. Although the error caused by the quantization is not reasonable in general, by high precision measurement its impact may be significant, therefore its reduction plays crucial role. The influence of the other above mentioned error sources may be reduced and compensated by various known techniques [6-8].

This paper describes a unique 3D shape measurement method. In the framework of the research, the main aim was to achieve an accuracy of few dozen microns and ensure the real-time measurement based on pattern projection combined with a multi-camera system. Furthermore, an additional objective was to ensure the acquisition of large objects - targets having the size of a car door or even larger - at once by maintaining the accuracy and measurement speed at similar level (the minimum of the achieved measurement error was 0.05 mm). The impact of the quantization error has been taken into account which has been efficiently reduced by a new technique described later in the upcoming sections. The primary application of the proposed approach is the 100% inspection of the press formed car parts in the factories. Furthermore, the method can advantageously be applied to observe variations on the cliff during the motion of the vehicle. Trough the analyses of the obtained time series, the short-term failure of the cliff may be predicted. In these cases, the high accuracy and the real-time measurement are indispensable.

Conventional 3D shape measurement systems produce dense point clouds. By the proposed method, the feature-points of the target - such as screw holes - may also be detected. This feature of the system makes it possible to compare the results of the measurement to CAE (Computer Aided Engineering) data.

During the development of the system — in order to achieve the required measurement accuracy —, the following issues have been studied:

Since the proposed system is based on projecting markers onto the targeted surface acquired by a multi-camera system (see later in the upcoming sections), the characteristics of the markers were crucial. Numerous analysis have been performed to find the most suitable (most robust to noise) marker. An important consideration during the analysis was the careful inspection of the camera specifications. Based on the performed investigation a new type of gray level marker was proposed together with a new compensation technique aimed for compensating the time variability (due to different type of noise sources) of marker locations in the camera images. Furthermore, to speed up the processing the searching method for corresponding points was devised.

The paper is organized as follows: In Section 2 the architecture and working principle of the proposed 3D measurement system is described; Section 3 shows the achieved results and their evaluation. In Section 4 conclusions and future works are reported.

2 The Proposed System

2.1 Illustration of the Proposed System

Fig. 1 illustrates the architecture of the proposed 3D measurement system. Its main components are four high-resolution cameras and a projector to project a pattern composed of gray level markers onto the surface of the target. The primary application of the system is strongly related to the inspection of vehicle body parts during the various stages of their design and production. The main requirement was the real-time, high accuracy 3D measurement of car body parts such as car door or engine hood. In order to achieve high precision and real-time processing, the following issues have been considered:

- Improvement of the applied markers to reduce the error caused by the image sensor noise
- Compensation of errors caused by camera distortions
- Fast corresponding point search to support the real-time measurement

In the upcoming sections, the corresponding techniques are described in detail.

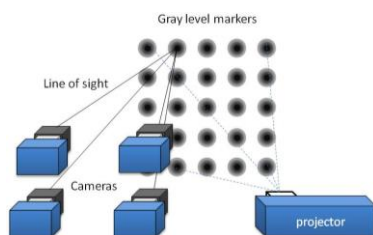


Figure 1

Components of the proposed system and the projected grid of gray level markers

2.2 Improvement of the “G-Marker”

In order to ensure precise detection of marker central points, many factors have to be taken into account, e.g. CCD (CMOS) image sensor noise, resolution, lens distortion, etc. When capturing the projected markers by camera, due to the mentioned factors the real properties of the markers may be corrupted - their shape properties for instance - and therefore it becomes difficult to accurately determine their exact central point. Usually the markers can easily be extracted by thresholding, however in case of a simple circular pattern - due to the above factors - the estimated center of gravity will not correspond to the exact central point of the marker. Although the related error is not reasonable, it is still important to consider it when high precision should be achieved.

Figs. 2 and 3 illustrate the gray level marker or “G-marker” proposed earlier by the authors. By using such type of markers - depending on the number of gray levels involved in the marker - several thresholded images have to be processed, i.e. the centre of gravity for each marker in each thresholded image are determined and the corresponding results are averaged. Usually this is a time consuming process, thus the “G-marker” in this form is less utilizable in real-time applications.



Figure 2

Illustration of the gray-level marker (“G-maker”)

To minimize the errors more efficiently and speedup the processing - based on numerous analyses - a new type of marker, the so called “new G” marker has been proposed by the authors (see Figs. 4). The marker is composed from concentric circles of different gray-levels similarly to its previous version. However, in this case the ratios of radiuses are different. The number of composing circles is less than previously and their radiuses are closer to the maximal one. The multi-stage binarization of this improved “G-marker” may contribute to realization of real-time applications. Based on our analysis, the proposed marker showed more robustness to noise overall.

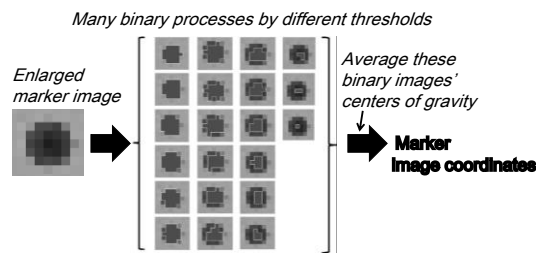


Figure 3

Illustration of marker extraction by thresholding. By modifying the threshold, the shape and size of markers will change accordingly. In order to reduce the error, the centers of gravities of corresponding markers are averaged

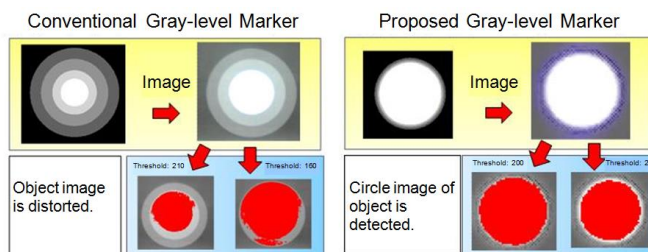


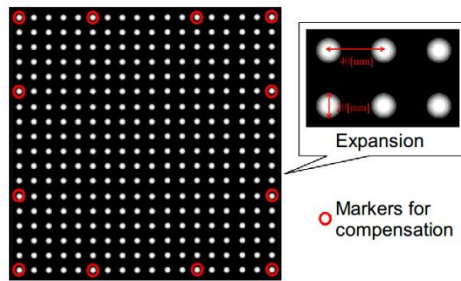
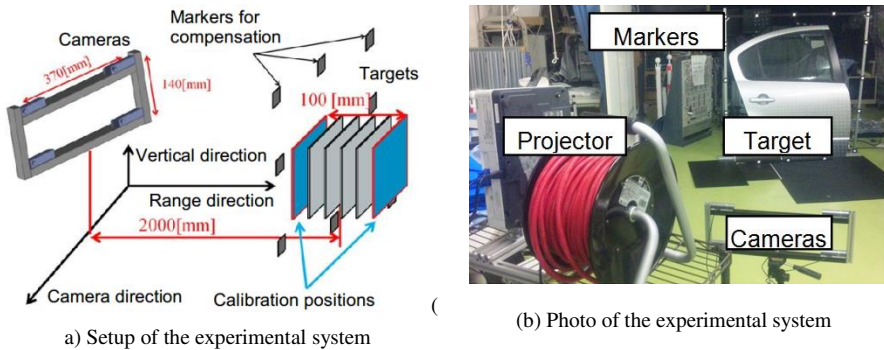
Figure 4

Illustration of the proposed gray-level marker and its efficiency

After the central point of each marker has been estimated, the correspondence problem has to be solved and finally based on triangulation the 3D coordinates are reconstructed. For the calibration of the cameras, the direct linear transformation (DLT) method was used [5].

2.3 Compensation of Camera Distortions

Almost each CCD (CMOS) image sensor is more or less sensitive to temperature variations, which has negative effect on the accuracy of the measurement. This phenomena can easily be recognized by placing a stable pattern composed for example from equidistant circular markers and starting to record the pattern by a camera. As the temperature in the device increases, difference in the sequentially acquired images can be observed. The detected centers fluctuate according to the temperature variation and depending on the location of the marker in the image. Various cameras of different types as well as their specifications were carefully inspected and the observed fluctuation as well as the influence of the pixel location on this variation have been identified for each type. According to the obtained data, the observed error is crucial when high accuracy should be achieved. As the temperature of the device becomes almost stable (according to our experiments this is few minutes after starting the recording) the fluctuation will remain in the range of ± 0.17 pixel.



(c) Projector pattern used for error compensation

Figure 5

Compensation of the error caused by the temperature variation of the CCD (CMOS) sensor. The setup of the system (a), the photo of the system (b) and the pattern used for the compensation (c).

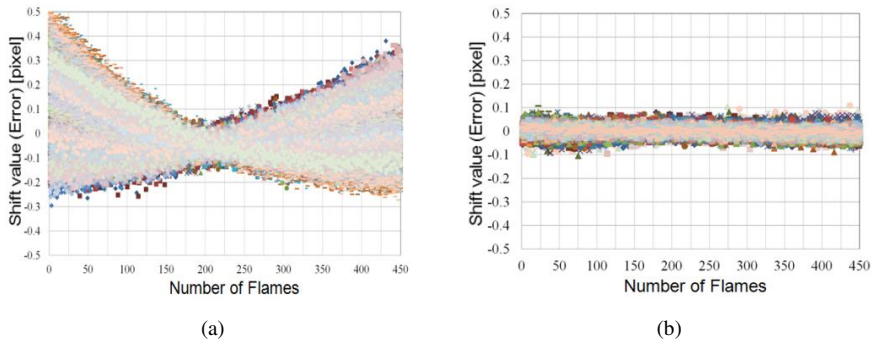


Figure 6

The measured variation in pixels: before compensation (a), after compensation by using the proposed method (b)

The minimal variation can be observed near the image centre and it increases according to the distance from it. The measured maximal variation was approximately the half of the pixel size that cannot be disregarded in high precision 3D measurement.

Based on the obtained data, the authors proposed a method to compensate the observed variation with the help of a calibration pattern illustrated by Fig. 5c.

As compensation technique for sensor distortion by heat the following equation was proposed and validated:

$$\begin{bmatrix} X \\ Y \end{bmatrix} = \begin{bmatrix} C_{11} & C_{12} & C_{13} & C_{14} & C_{15} & C_{16} & C_{17} & C_{18} & C_{19} & C_{110} \\ C_{21} & C_{22} & C_{23} & C_{24} & C_{25} & C_{26} & C_{27} & C_{28} & C_{29} & C_{210} \end{bmatrix} \begin{bmatrix} x \\ y \\ x^2 \\ xy \\ y^2 \\ x^3 \\ x^2y \\ xy^2 \\ y^3 \\ 1 \end{bmatrix},$$

where x, y stand for the marker coordinates before compensation while X and Y represent the coordinates of the marker after compensation. The C_{ij} values represent the compensation parameters.

In order to reduce the influence of the temperature change the camera temperature should be stabilized after startup.

During the calibration process based on numerous measurements first the characteristics of the fluctuation corresponding to the designated markers (red circles) in the pattern were identified (see Fig. 6a). By using such pattern the variation could efficiently be compensated. The achieved results can be followed in Fig. 6.

2.4 Fast Search for Corresponding Points

For cases when almost plain targets have to be measured, e.g. car door, engine hood, etc., a novel approach has been proposed by the authors to ensure the fast matching of corresponding markers. Fig. 7 illustrates the main concept of the matching principle. It can easily be recognized that an incorrectly identified marker yields a line of sight not crossing or being relatively distant from the intersection point of the other lines, i.e. the lines of sight corresponding to the correctly identified markers in the image planes of the other cameras.

There are many systems where the identification problem is solved by using active markers [13], structured lighting (3D scanning) [9] [14], etc. By these systems it is not necessary to search along epipolar lines and examine the neighboring pixels to find the corresponding one, so they are fast and robust. The proposed system has these properties, as well. The accuracy achieved by applying the above-described procedure has been compared to the case when epipolar line based searching technique was applied.

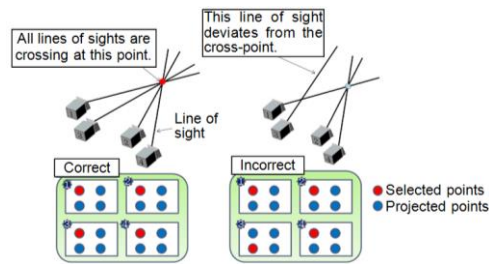


Figure 7

Successful identification of corresponding circles (left); incorrect identification of corresponding circles (right)

Fig. 8 shows the measured data obtained by the two different approaches. The accuracy achieved by the proposed technique is significantly higher than in case of applying the epipolar geometry. Due to the low complexity of the approach, the system can operate in real-time.

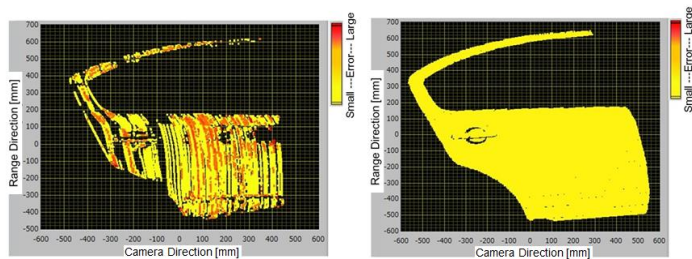


Figure 8

Searching for corresponding markers: the epipolar line based approach (left), the proposed approach (right)

The limitation of this matching technique is related to the shape characteristics of the target, i.e. the correspondence problem can be solved for limited depth changes only. The primary goal as already mentioned was to ensure the real-time measurement of car parts like door or engine hood, in which cases the requirements related to depth changes of the target are fulfilled.

After the identification of markers the 3D coordinates based on triangulation are estimated. Afterwards the projected pattern or the target is shifted and the whole procedure, i.e. detection, identification, reconstruction is repeated. Finally, a dense point cloud is obtained. In order to be able to measure larger depth differences, the density of the projected markers should be decreased. However, this would cause an increase in the duration of the whole reconstruction. This is because more shifts would be necessary to obtain a point cloud of same density. In the practical use, e.g. imagine the press line in the factory the targets are moved slowly to the next stages of processing. In this case the proposed system has the possibility to offer a dense point cloud, because the movement of the target is equivalent to the shift of the projected pattern.

3 Measurement Results

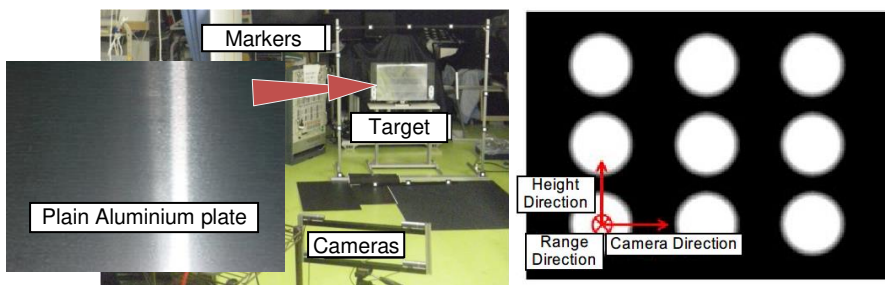
3.1 Target Measurement

The efficiency of the proposed techniques and the effectiveness of the marker have been validated through various measurements and consequent analysis. During the tests, targets selected by the factory were measured. First of all the 3D reconstruction of a car door has been performed in real-time. Due to its size, it was challenging to perform its real-time reconstruction at once with an accuracy of few dozen microns (see below the details). Based on the achieved results, the application of the method seems to be promising in many industry related fields.

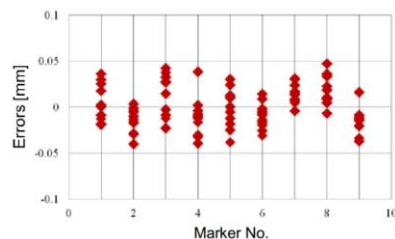
3.2 Verification of the Measurement Accuracy

In Fig. 9 the proposed gray level markers together with the achieved measurement accuracy can be followed. The target was a plain, non-painted aluminum plate (Fig. 9 (a)). The experimental setup can be followed in Fig. 5. During the experiment the location of each marker was examined. The error of the measurement was in the range ± 0.05 mm.

Due to reflectance properties of metal usually it is difficult to measure non-painted metal plates with high precision. The achieved results show that the proposed markers are suitable for inspecting the car body parts during the production.



(a) Experimental setup: the targeted plate and the projected markers



(b) Measurement error

Figure 9

Accuracy test of the marker central point estimation

3.3 An Example of Shape Measurement

Fig. 10 shows the results obtained by using the proposed approach. The target was a painted car door. In order to obtain a dense point cloud the projected markers had to be shifted in horizontal and vertical directions, as well. Fig. 10 (a) and (b) show the image of the target and its reconstructed model, respectively. Fig. 10 (c) shows the measured target from an oblique view. In this latter figure, a small rectangular segment is expanded twice to visualize the regularity of measured points. The specifications of the proposed measurement system can be followed in Table 1.

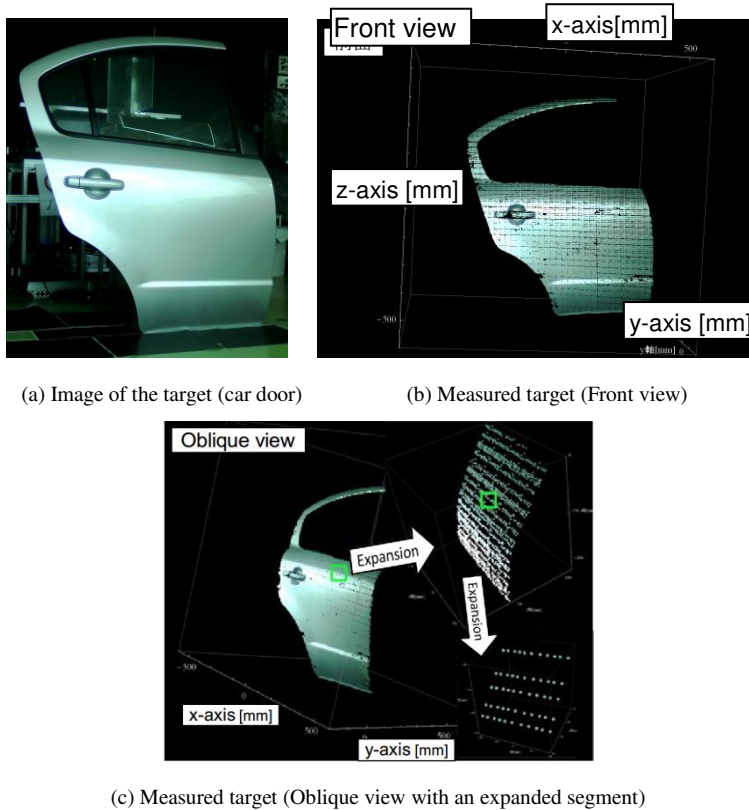


Figure 10

Measurement of a real car door: The data falling into the indicated rectangle are illustrated in more detail

3.3 Application of the Image-based Shape Measurement Method

In this section we point out the advantages of the image based shape measurement and show an application example.

Even if high-density point clouds are used, it is not trivial to extract feature-points from the point cloud. However images include features such as color, texture, etc., which can advantageously be applied to detect feature points on the target.

Product inspection and the related devices play important role in industrial applications where usually the result of the 3D measurement is compared to CAE data (CAD drawings). For such a comparison, feature points of drawings such as screw holes should be identified.

During this experiment the screw holes of the car door were measured. The results are shown in Fig. 11, where the 3D coordinates of four holes on the backside of the car door were measured. The absolute error was below 0.2 mm.

During the practical use in the factories, usually both sides of the pressed car door are measured. Since the camera positions are known, the holes on the backside are effective clues to match the front side of the car door with the CAE data.

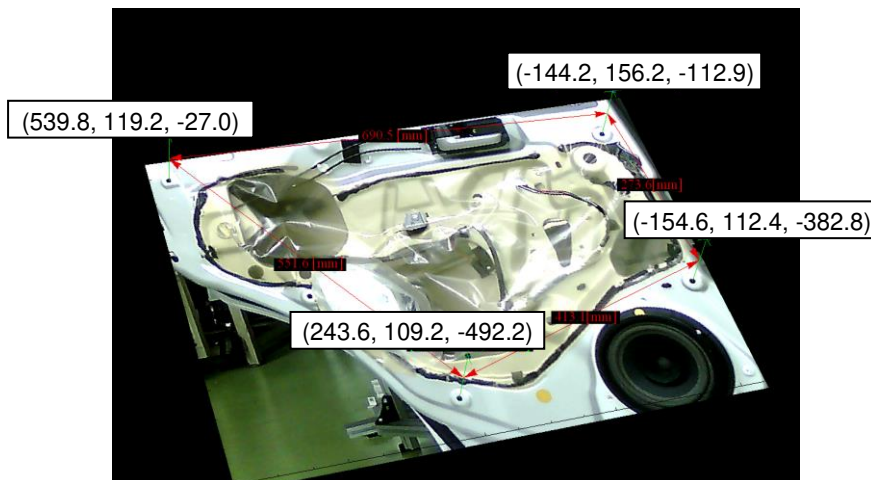


Figure 11

Testing the accuracy: measurement of a rectangular non painted aluminum plate attached to the car door

4 Summary

Discussions

In Table 1 the features of the proposed method are compared to other shape measurement techniques. As each method has good and bad points, suitable methods to measure targets are still welcome.

The features of the proposed method can be followed in the left column. The main advantage of the approach is the flexibility and the high speed operation. As disadvantage the relatively low density of the resulted point cloud can be mentioned.

Conclusions and Future Work

In the paper, a real-time measurement system has been proposed for measurement of nearly plain car body parts. The main advantage of the system is the high accuracy (minimum about 0.05 mm), the large measurement volume and the real-time processing. In order to achieve the mentioned features a new type of markers the so-called “new G” marker has been proposed by the authors.

Table 1
Comparison between the proposed method and other methods (representative value)

	Propose method	RANGE7 (KONICA MINOLTA HOLDINGS, Inc.)	ScanStation C10 (Leica Geosystems)	TDS-0216D (Pulstec Industrial Co., Ltd.)
Measurement area(horizonta l)	Approx. 1500 [mm]	79 or 267 [mm]	40[deg]	91[mm]
Measurement area (vertical)	Approx. 1500 [mm]	99 or 334 [mm]	40[deg]	80[mm]
Measurement area (range direction)	1 – 5[m]	450 or 800[mm]	0.1 – 300[m]	160 – 220[mm]
Errors [mm]	0.1	0.04	6	0.025
Number of measurement points	36,300 [points] with projected marker images shifted	Over 100 million[points]	Max 50,000[points/s]	200,000[points]
Scan time	1/30 [sec.] (1 projected marker image)	Approx. 2 [sec.](1 scan)	10[min.]	16[sec.]
Target move/still	Move and Still	Still	Still	Still
Advantages	Wide area, Real-time	Standard system of 3D shape measurement	For surveying outdoors	High precision, Possible of Metal surface shape measurement

During the measurement, the errors caused by the temperature variation of the camera were taken into account, as well. Due to the temperature the internal properties of the camera, especially the properties of the CCD (CMOS) image sensor are varying. The authors of this paper proposed a method for reducing the effect of this kind of error source. Accordingly an accuracy of few dozen microns could be achieved. As future work, the system is planned to be extended by mirrors in order to ensure the measurement of hidden parts, as well. The method can efficiently be applied to support cliff failure prediction by measuring the cliff deformation. In this case, the markers are attached to the cliff. Furthermore, thermal cameras are going to be applied to add an additional dimension, i.e. temperature to the measured data, as well as to ensure the measurement of transparent surfaces. In order to model the influence of the temperature variation of the camera more accurately and reduce the related errors, we are planning to measure the temperature distribution and its variation more accurately by high sensitive thermal cameras and create the corresponding mathematical models.

Acknowledgement

A part of this research was supported by Grants-in-Aid for Scientific Research, MEXT (No. 22560416) and partly realized through the assistance of the European Union, with the co-financing of the European Social Fund TÁMOP-4.2.1.B-11/2/KMR-2011-0001.

References

- [1] M. Young, E. Beeson, J. Davis, S. Rusinkiewicz and R. Ramamoorthi, "Viewpoint-Coded Structured Light", *IEEE Computer Society Conference on Computer Vision and Pattern Recognition*, pp. 1-8, June 2007
- [2] E. Lilienblum, B. Michaelis, "Optical 3D Surface Reconstruction by a Multi-Period Phase Shift Method," *Journal of Computers*, Vol. 2, No. 2, pp. 73-83, 2007
- [3] Yan Cui, Schuon, S., Chan, D., Thrun, S., Theobalt, C., "3D Shape Scanning with a Time-of-Flight Camera," *2010 IEEE Conference on Computer Vision and Pattern Recognition (CVPR)*, pp. 1173-1180, 13-18 June 2010
- [4] N. Karpinsky, S. Zhang, "High-Resolution, Real-Time 3D Imaging with Fringe Analysis," *Journal of Real-Time Image Processing*, Springer-Verlag, Vol. 7, Issue 1, pp. 55-66, 2010
- [5] Shapiro, R., "Direct Linear Transformation Method for Three-Dimensional Cinematography," *Research Quarterly*, 49(2), pp. 197-205, May 1978
- [6] H. Faraji, W.J. MacLean, "CCD Noise Removal in Digital Images," *IEEE Transactions on Image Processing*, Vol. 15, No. 9, pp. 2676-2685, Sept. 2006
- [7] Y. Wonpil; Y. Chung; "An Embedded Camera Lens Distortion Correction Method for Mobile Computing Applications," *IEEE International Conference on Consumer Electronics*, pp. 400-401, 17-19 June 2003
- [8] R. Cucchiara, C. Grana, A. Prati, R. Vezzani, "A Hough Transform-Based Method for Radial Lens Distortion Correction," *In Proc. of the 12th*

- International Conference on Image Analysis and Processing*, pp. 182-187, 17-19 Sept. 2003
- [9] Kai Liu, Yongchang Wang, Daniel L. Lau, Qi Hao, and Laurence G. Hassebrook, "Dual-Frequency Pattern Scheme for High-Speed 3-D Shape Measurement," *Optics Express*, 18(5), pp. 5229-5244, 2010
- [10] Gokturk, S. B.; Yalcin, H.; Bamji, C., "A Time-Of-Flight Depth Sensor - System Description, Issues and Solutions," *IEEE Conference on Computer Vision and Pattern Recognition Workshop*, p. 35, June 2004
- [11] Grubisic, I.; Gjenero, L.; Lipic, T.; Sovic, I.; Skala, T., "Active 3D Scanning Based 3D Thermography System and Medical Applications," *In Proc. of the 34th IEEE International Convention*, pp. 269-273, 23-27 May 2011
- [12] Li Yue, Xianyong Liu, "Application of 3D Optical Measurement System on Quality Inspection of Turbine Blade," *2009. IE&EM '09. 16th International Conference on Industrial Engineering and Engineering Management*, pp. 1089-1092, 21-23 Oct. 2009
- [13] Janssen, R.; Lou, E.; Durdle, N.G.; Raso, J.; Hill, D.; Liggins, A.B.; Mahood, S., "Active Markers in Operative Motion Analysis," *IEEE Transactions on Instrumentation and Measurement*, Vol. 55, No. 3, pp.854-859, June 2006
- [14] Gupta, M.; Agrawal, A.; Veeraraghavan, A.; Narasimhan, S.G., "Structured Light 3D Scanning in the Presence of Global Illumination," *2011 IEEE Conference on Computer Vision and Pattern Recognition (CVPR)*, pp. 713-720, 20-25 June 2011

Average Probability of Failure of Aperiodically Operated Devices

Krisztián Lamár, József Neszveda

Óbuda University, Kandó Kálmán Faculty of Electrical Engineering
Bécsi út 96/B, 1034 Budapest, Hungary
lamar.krisztian@kvk.uni-obuda.hu, neszveda.jozsef@kvk.uni-obuda.hu

Abstract: The aperiodically operated devices are typically non-operated or stored, usually in a powered-down state. The duration of being operated is much shorter than that of storage. These devices have to perform extremely reliably during usage, while the operation usually occurs under circumstances worse than the average. This paper proposes a calculation procedure of value jumps of failure rate caused by operating condition shifts, to determine the average probability of failure, based on the standards IEC 61511 and ANSI/ISA-84. In the suggested calculation method, a proposal is also made for taking the failure caused by the human factor during operation into account. It is known that the probability of successful operation is increasable with periodic diagnostic tests. The circumstances of diagnostic tests which interrupt the non-operated storage of the aperiodically operated devices differ from those described in the standards IEC 61511 and ANSI/ISA-84. As the repair rate given for the continuous technologies cannot be interpreted for diagnostic tests which interrupt the powered-down storage of the aperiodically operated devices, this paper suggests the implementation of the effect of tests into the calculation procedure as correction of state probabilities, and gives the required formulae. At last the article provides an easy algorithm for the suggested calculation method.

Keywords: Aperiodic Operation, Average Probability of Failure, Value Jumps of Failure Rate, Diagnostic Coverage, Reliability

1 Introduction

The standards IEC 61511 [1] and ANSI/ISA-84 [2] define the concepts of the safety integrity level (SIL) of the basic continuous technologies and their emergency/protective systems, thus enable the specialised authorities to determine or verify the reliability levels of devices and technologies.

The military and the disaster management use numerous devices containing electrical and mechanical components which are operated intermittently and are

stored powered down between two consecutive usages. The devices have to operate in continuous mode and extremely reliably during usage. In certain industries, such as manufacturing catalyst substances for the chemical industry, this kind of operation is also present, although in those cases the increased reliability is justified by the high expenses caused by failures. The intermittently operated, powered-down stored devices, technologies – furthermore aperiodically operated devices – have three distinguished operating conditions. These are:

- Mission period. The particularity of this condition is being relatively short (10–20 hours), and that the device or technology is operated in continuous mode. The devices of the military and the disaster management are often exposed to extreme strains (moving vehicle, outdoor operation) in this operating condition.
- Periodic diagnostic test. The particularity of this condition is being relatively short (less than 10 hours). The device or technology is operated similar to indoor continuous manufacturing technologies.
- Powered-down storage. In this condition, the operation of devices is somewhat similar to the emergency/protective devices as it is in standstill. On the other hand it differs, as the emergency/protective devices operate armed (in a standby condition), contrary to the aperiodically operated devices that do not function at all, thus their failures cannot be detected in this condition.

The aperiodic operation has numerous particularities that are not defined by the standards IEC 61511 and ANSI/ISA-84. The probability of failure values are various in different conditions. The duration of repairing the failures revealed by diagnostic tests which interrupt the powered-down storage state are not critical. It is practical to take the failure caused by the human factor into account during the mission period of the devices used by the military and the disaster management. The aim of this paper is to give a new investigation method that is in conform with the international standards and also takes the particularities of the aperiodic operation into account.

2 Average Probability of Failure

The standard IEC61511 has been worked out for continuous technologies. The continuous technologies can be split into high demand basic control and low demand emergency/protective control, based on the frequency of operation. The standard IEC 61511 separates strictly the concepts of the safety integrity level of the basic continuous technologies and their emergency/protective systems, and discusses them in two different time scales.

In low demand mode the failure appears when its operation is demanded. The probability of failure on demand (PFD [year⁻¹]) is the probability of the emergency system not working in accordance with standards in a potentially dangerous situation. The average probability of failure on demand is determined by the formula below, where “TI” stands for the period between the proof tests, which are the general overhauls of an device or technology in practice

$$PFD_{avg} = \frac{1}{TI} \int_0^{TI} PFD(t) dt \quad (1)$$

It occurs that the failure of the emergency/protective system indicates a spurious dangerous situation and this produces an unwanted safety operation that causes the spurious shutdown of the device. The probability of such shutdowns is called probability of failure to safety (PFS [year⁻¹]). The average probability of spurious shutdowns is:

$$PFS_{avg}^{spurious} = \frac{1}{TI} \int_0^{TI} PFS(t) dt \quad (2)$$

In high demand mode the devices are observed and taken care of continuously by operative personnel. In these cases the measure of reliability is the average of the probability of dangerous failures (PF_D [h⁻¹]).

$$PF_{Davg} = \frac{1}{T} \int_0^T PF_D(t) dt \quad (3)$$

The nature of aperiodically operated devices is that failures are critical only during the mission period, however, in those cases any kind of shutdown can be fatal therefore it is not adequate to take only dangerous failures and emergency shutdowns into consideration. This end, contrary to standard IEC 61511, the PF_{avg}^{sum} value should be calculated, which gives the average PF of every failure causing shutdown, during the T mission period starting from T_B moment for devices. Until T_B moment the devices were stored and interrupted with diagnostic tests.

$$PF_{avg}^{sum} = \frac{1}{T} \int_{T_B}^{T_B+T} PF(t) dt \quad (4)$$

3 Handling the Operating Condition Shifts

Currently there are internationally approved, standardised reliability calculation methods for the continuously operated and the emergency/protective devices and

technologies. Their principal [3] is that the λ failure rate is constant during operation. It is also common that the distribution of probability of failure (PF) is considered exponential [4].

$$PF(t) = 1 - e^{-\lambda t} \quad (5)$$

The λ failure rate of aperiodically operated devices and technologies varies in different operating conditions. FARADIP [5] database includes the probability of failure values for devices, subassemblies and components. According to the database the benchmark is the failure rate of devices installed indoor steadily, lacking any harmful vibration and temperature fluctuation, thus its coefficient is 1. The failure rate of inactive or powered-down storage condition is $\lambda_S = C_S \cdot \lambda$, where $C_S = 0.1$, as for the lack of mechanical and thermal effects decreases the λ failure rate, assuming that the storage is professional and the powered-down condition is shorter than one year. The failure rate of active devices used for outdoor and/or moving applications is $\lambda_A = C_A \cdot \lambda$, where $C_A = 4$.

The three operating conditions of aperiodically operated devices correspond with the classifications above. In figure 1.a, the probabilities of failure of individual operating conditions are shown; in figure 1.b the failure rate jumps can be seen with distorted time scale. Subscript “A” stands for the active operation of the mission period hereafter.

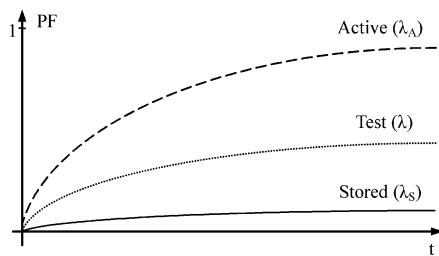


Figure 1a

Probability of failure of operating conditions

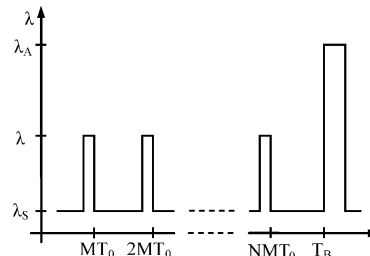


Figure 1b

Failure rate jumps

During mission period, the device can be investigated with any calculation method [3] developed for continuous technologies.

“ T_0 ” is a time base small enough that the time-discrete calculation of formula (4) results in a reasonably low error. “ N ” is the number of tests, and “ n ” is the ordinal number of the actual test. “ MT_0 ” is the duration of non-operated condition between two tests (including the test itself), and “ m ” is the m^{th} interval of this period. “ QT_0 ” is the duration between the last test and the beginning of the mission, and “ q ” is the q^{th} interval of this period. “ KT_0 ” is the mission period, and

“k” is the k^{th} interval of this period. Finally, $T_B = N \cdot M \cdot T_0 + Q \cdot T_0$ stands for the time elapsed until the beginning of the mission period. Now, formula (4) can be rewritten in time-discrete form:

$$PF_{\text{avg}}^{\text{sum}} = \frac{\sum_{k=N \cdot M + Q}^{N \cdot M + Q + K} PF(k \cdot T_0)}{K + 1} \quad (6)$$

For the correct determination of formula (6), it is necessary to calculate the initial probability of failure value $PF(N \cdot M \cdot T_0 + Q \cdot T_0)$.

The methods developed for continuous technologies are not able to take the effect of storage into account. When calculating the initial probability of failure the multiple jumps of λ failure rate during this period have to be minded. It also has to be taken into account that the repairing of failures revealed by diagnostic tests increase the probability of successful operation. From among the calculation methods of reliability, it is the Markov analysis that allows the temporal changes of λ failure rate to be calculated with [3]. The jumps of the λ failure rate can be handled with a time-discrete calculation method.

The Markov model is a graph (Figure 2). Its nodes represent the states of the system and its edges represent the probability of transition from one state to another at the end of the next T_0 period. The Markov model of 1oo2D structure of control systems [6] – which are efficient for both dangerous and safe failures – includes six states considering failures.

An aperiodically operating device with a 1oo2D control structure can get from faultless operation (1) into reduced (faulty yet operable) states (2), (3), (4), (5) or shutdown due to a failure (6). Based on the nature of failures [1], failure states are distinguished as safe and detected (SD), dangerous and detected (DD), safe but undetected (SU) finally dangerous and undetected (DU) ones.

The $\lambda_{x,y}$ failure rate, corresponding with the given state (x), defines the probability of transition into another state (y). The model shown in Figure 2 considers every shutdown by any reason dangerous, therefore the system can get into shutdown (6) from any reduced failure state or from the faultless state equally. The probability of transition into a yet operable failure state has to be taken into account with double coefficient because of the dual redundancy.

The model shown in Figure 2 does not include the μ repair rate defined by the standards [1] and [2], which in fact can be integrated into the Markov model easily. The reason is that the mission period of aperiodically operated devices is short and the operation often takes place on a previously unknown site, therefore it is assumed that during mission period, there is no chance or time to repair the device.

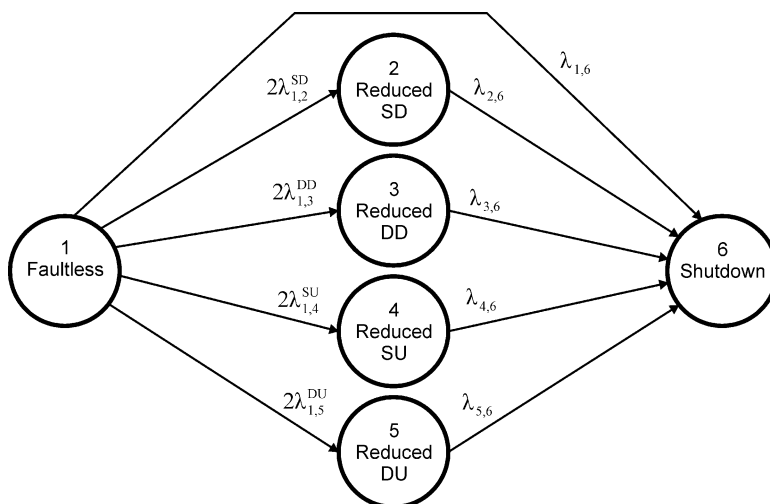


Figure 2

The simplified (contracted) Markov model of the 1oo2D structure

If the λ failure rate is constant, the \mathbf{S} vector of state probabilities at the (iT_0) moment is:

$$\mathbf{S}(iT_0) = \mathbf{S}(T_0) \cdot \mathbf{T}^{i-1} \quad (7)$$

where $\mathbf{S}(T_0)$ is the first row of the \mathbf{T} transition probability matrix, which can be written based on Figure 2.:

$$\mathbf{T} = \begin{pmatrix} 1 - \sum_{j=2}^6 \lambda_{1,j} & 2\lambda_{1,2}^{SD} & 2\lambda_{1,3}^{DD} & 2\lambda_{1,4}^{SU} & 2\lambda_{1,5}^{DU} & \lambda_{1,6} \\ 0 & 1 - \lambda_{2,6} & 0 & 0 & 0 & \lambda_{2,6} \\ 0 & 0 & 1 - \lambda_{3,6} & 0 & 0 & \lambda_{3,6} \\ 0 & 0 & 0 & 1 - \lambda_{4,6} & 0 & \lambda_{4,6} \\ 0 & 0 & 0 & 0 & 1 - \lambda_{5,6} & \lambda_{5,6} \\ 0 & 0 & 0 & 0 & 0 & 1 \end{pmatrix} \quad (8)$$

In case the device's $\mathbf{S}((i-1)T_0)$ state probabilities at the preceding $(i-1)T_0$ moment are known the recursive formula below may be applied instead of formula (7).

$$\mathbf{S}(iT_0) = \mathbf{S}((i-1)T_0) \cdot \mathbf{T} \quad (9)$$

The jumps of λ failure rate can be taken into account with constant coefficients $\lambda_S = C_S \cdot \lambda$ and $\lambda_A = C_A \cdot \lambda$ (Figure 1.b). \mathbf{T}_S shall stand for the transition probability matrix of the powered-down storage condition, \mathbf{T} for test mode among normal circumstances, and \mathbf{T}_A for mission period. Subtracting the \mathbf{I} unit matrix from the \mathbf{T} transition probability matrix yields the \mathbf{P} probability of failure matrix, which consists only of λ failure rate values, therefore the \mathbf{P} probability of failure matrix can be multiplied by constant values (C_S or C_A). Adding the \mathbf{I} unit matrix to the \mathbf{P}_S or the \mathbf{P}_A probability of failure matrix after the multiplication yields the new \mathbf{T}_S or \mathbf{T}_A transition probability matrix.

$$\mathbf{T}_S = (\mathbf{T} - \mathbf{I}) \cdot C_S + \mathbf{I}, \text{ and } \mathbf{T}_A = (\mathbf{T} - \mathbf{I}) \cdot C_A + \mathbf{I} \quad (10.1)$$

Of course the procedure can be inverted:

$$\mathbf{T} = (\mathbf{T}_S - \mathbf{I}) \cdot \frac{1}{C_S} + \mathbf{I}, \text{ and } \mathbf{T} = (\mathbf{T}_A - \mathbf{I}) \cdot \frac{1}{C_A} + \mathbf{I} \quad (10.2)$$

If λ_S failure rate jumps to λ_A value at $(i-1)T_0$ moment, then the $C_{SA} = \frac{C_A}{C_S}$ coefficient has to be applied in order to convert the \mathbf{T}_S transition probability matrix into the \mathbf{T}_A transition probability matrix.

If there are three interconvertible transition probability matrices assigned to the three operation conditions of the aperiodically operated devices, the condition shifts can be handled as transition probability matrix conversions.

$$\mathbf{S}((N \cdot M + Q + k)T_0) = \mathbf{S}(0) \cdot \mathbf{T}_S^M \cdot \mathbf{T}^P \cdot \mathbf{T}_S^M \cdot \mathbf{T}^P \dots \mathbf{T}_S^M \cdot \mathbf{T}^P \cdot \mathbf{T}_S^Q \cdot \mathbf{T}_A^k \quad (11)$$

“ PT_0 ” is the average value of the time needed for the test and the repair. N , M , Q and k are defined previously. Formula (11) still excludes the result of repair.

4 Human Factor

Since any shutdown of military or disaster management device may be fatal, the human factor has to be integrated into the probability of failure investigation. From among the numerous investigation methods [7], it is practical to choose one that is considerable with the jumps of the λ failure rate. The TESEO method is suitable, as it estimates by how much the human action raises the probability of failure, by empirically analysing the reasons leading to a failure caused by humans. TESEO defines carefully described categories for the competency of the

staff, the complexity of the task, the operability of the device as well as the time available for the decision, and assigns coefficients to them [8].

Table 1 presents some typical cases and gives the corresponding C_H factor that raises the failure rate.

Table 1
Conditions of carrying out the task during the mission period

Competency of the staff and the device	C_H
Well motivated and highly trained staff Totally familiar task, optimally maintained device	1.112
Highly trained staff without any stress or personal conflict Fairly simple task, well maintained device	1.224
Staff expanded with improperly trained persons Complex task, sufficiently maintained device	1.640
Staff is improperly trained but able to carry out the task Miscellaneous task, improperly maintained device	3.560

The C_H coefficient, which describes the competency of the staff and the device, can be taken into account with the formulae (10) where C_S has to be replaced by $C_S C_H$ and C_A by $C_A C_H$. The $C_{SAH} = \frac{C_A}{C_S} \cdot C_H$ coefficient converts the \mathbf{T}_S transition probability matrix into the \mathbf{T}_A transition probability matrix.

5 Periodic Diagnostic Tests

The purpose of periodic test is detecting and repairing the failures. The periodically executed diagnostic tests and repairs are capable of increasing the reliability of devices [9]. In diagnostic test condition which interrupts the non-operated storage condition of the aperiodically operated devices, the operative personnel carry out a prescribed sequence of actions. These actions are executed among normal circumstances, and mainly inspect the operation of the actuators in the control system. When the operative personnel detect a failure, the device is being repaired. The result of repair is reviewed by executing another prescribed sequence of actions. This method differs from the test mode carried out during continuous operation, as in reasonable time-limit the duration of test and repair is not critical.

The state probabilities, at starting the n^{th} diagnostic test in $n \cdot M \cdot T_0 = i$ moment, applying the model in Figure 2, is:

$$\mathbf{S}(i) = [s_1(i) \quad s_2(i) \quad s_3(i) \quad s_4(i) \quad s_5(i) \quad s_6(i)] \quad (12)$$

When analysing the effect of the interruptive test, it is assumed that the operative personnel are capable to reveal only the detectable – including shutdown causing – failure states; all the other states are presumed and documented as successful operation. In the moment of test, the device is either operating faultlessly or can get into a particular failure state.

Let the value of average probability of detected failures to be introduced. According the model in Figure 2, the operative personnel detect a failure in the average of tests with the probability given by formula (13).

$$s_{\text{avg}}(\mathbf{i}) = \frac{1}{3} \{s_2(\mathbf{i}) + s_3(\mathbf{i}) + s_6(\mathbf{i})\} \quad (13)$$

It is suitable to be calculated with in every further test, assuming that during the life cycle of the device the signed differences between the average and the real values are balanced, therefore the calculation error is negligible.

The efficiency of test is described with the diagnostic coverage. When calculating the diagnostic coverage (DC) for aperiodically operated devices, contrary to standards [1] and [2], not only the ratio of detected and all dangerous failures ($DC = \frac{\sum \lambda_{\text{DD}}}{\sum \lambda_{\text{Dtotal}}}$) has to be considered, but the ratio of all detected and all

failures, as during mission period a shutdown of any reason can be fatal. Therefore the modified diagnostic coverage is:

$$DC_M = \frac{\sum \lambda_{\text{0D}}}{\sum \lambda_{\text{total}}} \quad (14)$$

Assuming that the initial state is recovered during repairs, the repair of revealed failures may reset the state probabilities to the $S(1)$ values succeeding the commissioning [10]. However, this value is reduced by the DC_M value of diagnostic coverage. If the operative personnel reveal and repair the failures with the average probability of detected failures s_{avg} , the result of repairs is the average probability of recovery (v_{avg}), which, according to the model in Figure 2, is:

$$v_{\text{avg}}(\mathbf{i}) = \frac{DC_M}{3} \{s_2(\mathbf{i}) - s_2(1) + s_3(\mathbf{i}) - s_3(1) + s_6(\mathbf{i}) - s_6(1)\} \quad (15)$$

In the $i+1$ moment following the test, the probability of successful operation is increased by the value of average probability of recovery caused by repair. Accordingly, the probability of detectable failure states decrease. The failure states can be repaired with the probability of their occurrence, therefore the distribution of the average probability of recovery (v_{avg}) among the individual failure states is carried out weighted by the failure states' probability of occurrence. For example the probability of recovery from the (2) failure state in the model of Figure 2 is:

$$v_{\text{avg}}(\mathbf{i}) \frac{s_2(\mathbf{i})}{s_2(\mathbf{i}) + s_3(\mathbf{i}) + s_6(\mathbf{i})} = v_{\text{avg}}(\mathbf{i}) \frac{s_2(\mathbf{i})}{3s_{\text{avg}}(\mathbf{i})} \quad (16)$$

As a result of repairs, the device's state probabilities change, thus the elements of the $\mathbf{S}(\mathbf{i})$ vector corresponding the successful operation and detectable failure states have to be corrected. In the model of Figure 2, these values are $s_1(\mathbf{i})$, $s_2(\mathbf{i})$, $s_3(\mathbf{i})$ and $s_6(\mathbf{i})$.

The probability of successful operation is increased by the value of average probability of recovery caused by the repair.

$$s_1(\mathbf{i}+1) = s_1(\mathbf{i}) + v_{\text{avg}}(\mathbf{i}) \quad (17.1)$$

The values of detectable failures have to be corrected:

$$s_2(\mathbf{i}+1) = s_2(\mathbf{i}) - v_{\text{avg}}(\mathbf{i}) \frac{s_2(\mathbf{i})}{3s_{\text{avg}}(\mathbf{i})} = s_2(\mathbf{i}) \left\{ 1 - \frac{v_{\text{avg}}(\mathbf{i})}{3s_{\text{avg}}(\mathbf{i})} \right\} = s_2(\mathbf{i})w(\mathbf{i}) \quad (17.2)$$

$$s_3(\mathbf{i}+1) = s_3(\mathbf{i}) - v_{\text{avg}}(\mathbf{i}) \frac{s_3(\mathbf{i})}{3s_{\text{avg}}(\mathbf{i})} = s_3(\mathbf{i}) \left\{ 1 - \frac{v_{\text{avg}}(\mathbf{i})}{3s_{\text{avg}}(\mathbf{i})} \right\} = s_3(\mathbf{i})w(\mathbf{i}) \quad (17.3)$$

The non-detected failure states keep their original values.

$$s_4(\mathbf{i}+1) = s_4(\mathbf{i}) \quad (17.4)$$

$$s_5(\mathbf{i}+1) = s_5(\mathbf{i}) \quad (17.5)$$

The value of detectable failure causing shutdown has to be corrected:

$$s_6(\mathbf{i}+1) = s_6(\mathbf{i}) - v_{\text{avg}}(\mathbf{i}) \frac{s_6(\mathbf{i})}{3s_{\text{avg}}(\mathbf{i})} = s_6(\mathbf{i}) \left\{ 1 - \frac{v_{\text{avg}}(\mathbf{i})}{3s_{\text{avg}}(\mathbf{i})} \right\} = s_6(\mathbf{i})w(\mathbf{i}) \quad (17.6)$$

At first approach, the T_0 time base was considered as unit. As the repair is considered as a correction of state probabilities, the actual time has no meaning, because it is assumed that it is much shorter than the period of powered-down storage and the repair is not carried out during the mission period.

For algorithmizability, the $\mathbf{v}(\mathbf{i})$ vector-variable including the average increase of the probability of successful operation is introduced.

$$\mathbf{v}(\mathbf{i}) = [v_{\text{avg}}(\mathbf{i}) \ 0 \ 0 \ 0 \ 0 \ 0] \quad (18.1)$$

For handling the $w(\mathbf{i}) = 1 - \frac{v_{\text{avg}}(\mathbf{i})}{3s_{\text{avg}}(\mathbf{i})}$ factor the $\mathbf{w}(\mathbf{i})$ vector-variable is introduced:

$$\mathbf{w}(\mathbf{i}) = [1 \ w(\mathbf{i}) \ w(\mathbf{i}) \ 1 \ 1 \ w(\mathbf{i})] \quad (18.2)$$

The corrected state probabilities following the repair of failures detected during the tests can be calculated with the vector operation below:

$$\mathbf{S}_{\text{corr}}(\mathbf{i}) = \left\{ \text{Diag}(\mathbf{w}^T(\mathbf{i})\mathbf{S}(\mathbf{i})) + \mathbf{v}^T(\mathbf{i}) \right\}^T \quad (19)$$

6 Algorithmization

The values of the state probabilities from commissioning till the beginning of the mission period are necessary for determining the required frequency of periodic diagnostic tests and/or the required value of diagnostic coverage. The effect of repairs, which is excluded in formula (11), has to be taken into account at this point. If the duration of the test and the repair is still considered as unit (T_0), the steps of calculating the state probabilities before, during and after the test mode are as follows:

T_0 period preceding the test (storage condition):

$$\mathbf{S}((M-1)T_0) = \mathbf{S}((M-2)T_0) \cdot \mathbf{T}_S \quad (20.1)$$

T_0 period of the test (normal mode):

$$\mathbf{S}(MT_0) = \mathbf{S}((M-1)T_0) \cdot \mathbf{T} \quad (20.2)$$

The result of the test, thus the correction:

$$\mathbf{S}_{\text{corr}}(MT_0) = \left\{ \text{Diag}(\mathbf{w}^T(MT_0)\mathbf{S}(MT_0)) + \mathbf{v}^T(MT_0) \right\}^T \quad (20.3)$$

T_0 period following the test (storage condition):

$$\mathbf{S}((M+1)T_0) = \mathbf{S}_{\text{corr}}(MT_0) \cdot \mathbf{T}_S \quad (20.4)$$

The formulae (20) describe the effect of the test executed in the MT_0 moment, but of course any test carried out at any $n \cdot MT_0$ moment can be handled similarly.

Standards [1] and [2] give the safety integrity level (SIL) values referring to $T_0=1$ [hour] time base when investigating continuous operation, and referring to $T_{\text{year}}=1$ [year] when investigating emergency/protective systems. The storage condition interrupted with periodical tests differs from the operation modes above.

The λ failure rates of the Markov model (Figure 2) are presented for normal, continuous mode in the [5] databases, therefore primarily the \mathbf{T} transition probability matrix is determined where the λ failure rate values correspond with the $T_0=1$ [hour] time base. In formulae (11) and (20) the \mathbf{T} , \mathbf{T}_S , \mathbf{T}_A transition probability matrices are shown corresponding with the $T_0=1$ [hour] time base. In the case of $T_0=1$ [hour] time base, the period of the diagnostic test and the repair is

being realistically considered PT_0 long. The determination of the first $N(M-1+P)+Q-1$ set of state probabilities requires significant computing resources.

If the result of the test mode is taken as correction of state probabilities into account, the duration of the test, as far as it is much shorter than the non-operated condition, is irrelevant. Choosing a $T_{10}=10$ [hours] period is useful, because the test and the repair are executable in such term, the number of calculation operations is reduced and it does not add further rounding problems, as follows.

If $\lambda_S = C_S \cdot \lambda = 0.1 \cdot \lambda$ and $T_{10} = 10 \cdot T_0$, then:

$$\lambda_S \cdot T_{10} = \lambda \cdot T_0 \quad (21)$$

Thus calculating with $T_{10}=10$ [hours] time base in the case of powered-down condition converts the T_S transition probability matrix right into the T transition probability matrix, and this does not imply any further rounding error. The introduction of the ten-hour (T_{10}) time base modifies the duration between two tests to $M_{10}T_{10}$, and the duration between the last test and the beginning of the mission period to $Q_{10}T_{10}$.

T_{10} period preceding the test (storage condition):

$$\mathbf{S}((M_{10}-1)T_{10}) = \mathbf{S}((M_{10}-2)T_{10}) \cdot \mathbf{T} \quad (22.1)$$

Assuming that the average duration of the test and the repair is $PT_0 = T_{10} = 10$ [hours]. The T_{10} period of the test:

$$\mathbf{S}(M_{10}T_{10}) = \mathbf{S}((M_{10}-1)T_{10}) \cdot \mathbf{T} \quad (22.2)$$

The result of the test, thus the correction:

$$\mathbf{S}_{\text{corr}}(M_{10}T_{10}) = \left\{ \text{Diag}(\mathbf{w}^T(M_{10}T_{10})\mathbf{S}(M_{10}T_{10})) + \mathbf{v}^T(M_{10}T_{10}) \right\}^T \quad (22.3)$$

T_{10} period following the test:

$$\mathbf{S}((M_{10}+1)T_{10}) = \mathbf{S}_{\text{corr}}(M_{10}T_{10}) \cdot \mathbf{T} \quad (22.4)$$

During mission period, it is still recommended to determine the state probabilities referring to the $T_0=1$ [hour] time base, therefore the primarily determined T transition probability matrix has to be converted into T_A transition probability matrix. The value of C_H can be picked out of Table 1 according to the particular situation.

$$\mathbf{T}_A = (\mathbf{T} - \mathbf{I}) \cdot C_A \cdot C_H + \mathbf{I} \quad (23)$$

After that, with the recursive operations of formulae (24), the time-discrete sequence of the vectors of state probabilities, during the KT_0 mission period can

be figured out. The initial values at the $T_B = (N \cdot M_{10} + Q_{10}) \cdot T_{10}$ beginning of the mission period are:

$$\mathbf{S}((N \cdot M_{10} + Q_{10}) \cdot T_{10}) = \mathbf{S}((N \cdot M_{10} + Q_{10} - 1) \cdot T_{10}) \cdot \mathbf{T} \quad (24)$$

Restoring $T_0=1$ [hour] time base, formula (24) is rewritten as:

$$\mathbf{S}((N \cdot M + Q) \cdot T_0) = \mathbf{S}((N \cdot M_{10} + Q_{10}) \cdot T_{10}) \quad (25.0)$$

The first two steps of the recursive operations are:

$$\mathbf{S}((N \cdot M + Q + 1) \cdot T_0) = \mathbf{S}((N \cdot M + Q) \cdot T_0) \cdot \mathbf{T}_A \quad (25.1)$$

$$\mathbf{S}((N \cdot M + Q + 2) \cdot T_0) = \mathbf{S}((N \cdot M + Q + 1) \cdot T_0) \cdot \mathbf{T}_A \quad (25.2)$$

The k^{th} step of the recursive operations is:

$$\mathbf{S}((N \cdot M + Q + k) \cdot T_0) = \mathbf{S}((N \cdot M + Q + k - 1) \cdot T_0) \cdot \mathbf{T}_A \quad (25.k)$$

Now, the average probability of failure applied for the aperiodically operated devices according to formula (6) can be determined. The sixth (S6) state probabilities of the KT_0 mission period, which stand for the shutdown, are sufficient for the calculation.

$$PF_{\text{avg}}^{\text{sum}} = \frac{\sum_{k=N \cdot M + Q}^{N \cdot M + Q + K} s_6(k \cdot T_0)}{K + 1} \quad (26)$$

Conclusion

The concept of aperiodically operated devices and the characteristics of their operation have been defined. It has been shown that if the operation mode shifts are taken into account by the jumps of the λ failure rate, the time-discrete Markov model is applicable. Different transition probability matrices belong to the different operation conditions. The rule of conversion between these matrices has been given. This rule is capable of taking the failure caused by the human factor also into account. By analysing the effect of diagnostic test and repair interrupting the non-operated condition, a proposal for the modified interpretation of the diagnostic coverage has been given. Also by analysing the effect of diagnostic test and repair, it has been recommended that the increase of the probability of successful operation should be taken into account with correction of state probabilities. Finally, – due to their recursive nature – a well-programmable algorithm of the equations has been given, and the average probability of failure applied for the aperiodically operated devices was determined. In order to decrease the need of computing resources, a proposal has been given for a time base conversion that does not affect the calculation accuracy. Based on this work further investigations may be performed, i.a. a computer simulation program can be written for the analysis of diagnostic coverage and the impact of the test

frequency. These results will be published later, and can be the basis of a commercial product, that will support the military and the disaster management to determine and improve the reliability of their aperiodically operated devices.

References

- [1] IEC 61511, International Standard, Functional safety – Safety instrumented systems for the process industry sector, International Electrotechnical Commission (IEC), 2002
- [2] ANSI/ISA-84.00.01-2004, American National Standard, Functional Safety: Safety Instrumented Systems for the Process Industry Sector, International Society of Automation (ISA), 2004
- [3] ISA-TR84.00.02-2002, Safety Instrumented Functions (SIF) – Safety Integrity Level (SIL) Evaluation Techniques, International Society of Automation (ISA), 2002
- [4] Goble, W., M., Cheddie, H. L., Safety Instrumented System Verification: Practical Probabilistic Calculation, International Society of Automation (ISA), 2005
- [5] <http://www.technis.org.uk> (Available: 03-02-2013)
- [6] Scott, M., Adler, B., How to select a safety PLC, On-line Technical Paper, http://www.isa.org/Content/Microsites838/Safety_Division/Home818/ISA_2004_Safety_Papers/How_to_Select_a_Safety_PLC.pdf, International Society of Automation (ISA), 2004 (Available: 03-02-2013)
- [7] Humphreys. P. (editor), Human Reliability Assessor's Guide: A Report by the Human Factors in Reliability Group (Reports: SRDA-R11), AEA Technology, 1995
- [8] Smith, D. J., Reliability, Maintainability, and Risk: Practical Methods for Engineers, 8th edition. Butterworth-Heinemann, 2011
- [9] Bukowski, J. V., Modeling and Analyzing the Effects of Periodic Inspection on the Performance of Safety-Critical Systems. IEEE Transactions on Reliability, Vol. 50, No. 3, pp. 321-329, 2001
- [10] Goble, W. M., Bukowski, J. V., Brombacher, A. C., How Diagnostic Coverage improves safety in programmable electronic systems, ISA Transactions, Vol. 36, No. 4, pp. 345-350, 1997
- [11] Jadlovská, A., Jajčíšin, Š., Predictive Control Algorithms Verification on the Laboratory Helicopter Model, Acta Polytechnica Hungarica, Vol. 9, No. 4, pp. 221-245, 2012
- [12] Bokor, Z., Integrating Logistics Cost Calculation into Production Costing, Acta Polytechnica Hungarica, Vol. 9, No. 3, pp. 163-181, 2012
- [13] Sárosi J., New Force Functions for the Force Generated by Different Fluidic Muscles, Transactions on Automatic Control and Computer

- Science, Scientific Bulletin of the "Politehnica" University of Timisoara, Vol. 57(71), No. 3, pp. 135-140, 2012
- [14] Varga, A., Rácz, E., Kádár, P., New Experimental Method for Measuring Power Characteristics of Photovoltaic Cells at Given Light Irradiation, Proceedings of 8th IEEE International Symposium on Applied Computational Intelligence and Informatics, SACI 2013, Timisoara, Romania, pp. 405-409, 2013
- [15] Pachter, M., State Estimation for Discrete Systems, Military Operations Research, Vol.16, No. 3, pp. 23-31, 2011
- [16] Rădac, M.-B., Precup R.-E., Petriu, E. M., Preitl, S., Experiment-based Performance Improvement of State Feedback Control Systems for Single Input Processes, Acta Polytechnica Hungarica, Vol. 10, No. 3, pp. 5-24, 2013
- [17] Sven Guzman, M., Pohl, E. A., Schneider, K., Rainwater, C., Application of Reliability Methods to Social Networks, Military Operations Research, Vol. 17, No. 4, pp. 51-58, 2012
- [18] Grosselin, K., Bayesian Estimates of the Rideshare Reliability Effect, Military Operations Research, Vol. 17, No. 4, pp. 39-49, 2012
- [19] Novak-Marcincin, J., Janak, M., Barna, J., Torok, J., Novakova-Marcincinova, L., Fecova, V., Verification of a Program for the Control of a Robotic Workcell with the use of AR, International Journal of Advanced Robotic Systems, Vol. 9, Art. No. 54, 2012
- [20] Kolozsi, G., Changes of "UT" Specifications, Korrozios Figyelo, Vol. 51, No. 1, pp. 15-19, 2011
- [21] Durovsky, F., Fedak, V., Integrated Mechatronic Systems Laboratory, Proceedings of the 14th International Power Electronics and Motion Control Conference (EPE-PEMC 2010), pp. S51-S55, 2010
- [22] Horváth, L., Rudas, I. J., New Method of Knowledge Representation and Communication for Product Object Modeling, Proceedings of the 12th WSEAS International Conference on Applied Computer Science ACS-12, pp. 75-80, 2012

High Speed Hard Turning of AISI S1 (60WCrV8) Cold Work Tool Steel

Alaattin Kaçal¹, Ferhat Yıldırım²

^{1*} Department of Manufacturing Engineering, Faculty of Simav Technology, Dumlupınar University, 43500, Simav – Kütahya / Turkey
e-mail: akacal@dumlupinar.edu.tr

² Department of Machine Educational, Faculty of Simav Technical Education, Dumlupınar University, 43500, Simav – Kütahya / Turkey

Abstract: This study deals with experimental results of high speed hard turning of hardened AISI S1 cold work tool steel with ceramic and CBN cutting tools. Ceramic and CBN tools performance were evaluated based on machining force, surface roughness and tool wear. Cutting speed, feed rate, depth of cut and tool types were determined as processes parameters. Evaluating tool wear type and wear mechanism by tool makers' microscope and SEM analysis. Analysis of variance (ANOVA) was used for observing that the most influencing machining parameters on the quality characteristics in terms of the statistically. CBN cutter exhibited a better performance than the ceramic cutter. For CBN and ceramic inserts, the increase in cutting speed increased the flank wear. After the turning of hardened workpiece, surfaces at grinding quality were obtained. It was predicted that, with the choice of appropriate cutting parameters, its hazardous effects of grinding operation on the environment and humans shall be decreased for such processes.

Keywords: Hard turning; cold work tool steel; cutting force; tool wear; surface roughness

1 Introduction

Especially, finishing of hardened steel parts using extra hard cutting tools offers manufacturers an alternative to grinding. Hard machining includes turning, milling and broaching. This machining method covers generally semi-finishing and finishing, operations [1]. The materials such as tool steels, die steels, bearing steel, alloys steels, case-hardened steels, white cast irons, and alloy cast irons are widely machining in hard machining operations.

In manufacturing industry, hard turning is a turning operation performed on hard or high strength alloy steels to reach high surface quality as grinding operations [2]. Lubricant can be eliminate, efficiency can be increasing and less energy than

conventional methods by using hard turning operations. Manufacturing of the complex parts without the need for a second operation is another important characteristic of hard turning. Because of hard turning performed in dry machining condition, the harmful effect of cooling on environment can be eliminated. Due to very high hardness, high thermal hardness, wear resistance and very high strength level Ceramic, CBN and PCD cutting inserts are used in hard turning of hardened materials. [2, 3, 4, 5,6]. CBN tools exhibit low solubility, and satisfactory fracture toughness [6]. These cutting tools generate a better surface finish and lower flank wear on machining of hardened steel [7]. Ceramic tools can be used for the machining of hardened components in the manufacturing industry. Ceramic insert has high melting point, excellent hardness and good wear resistance. Ceramic inserts based on Al_2O_3 are used for machining the hardened materials [8]. Due to the high hardness and high strength of the work pieces, occur high temperatures on the cutting edge, diffusion tool and the chips interface, and wear on tool nose. It could be said that wear resistance and chemical stability are the most important properties of tool materials used for hard turning [6].

Although heavy catastrophic effect and reduction of tool lifetime, high speed machining (HSM) for hard turning has several advantages such as improvement of the surface roughness and increasing of productivity, achieve high removal rate [9, 10]. HSM has been developed as an eminent technology in rapid tooling and manufacturing applications. For the effective high speed manufacturing of materials which are poor machinability require advanced tooling such as coated carbides, ceramics and poly crystalline cubic boron nitride (PCBN) [11]. Sai [12] researched realization of a wear model in relation to time and to cutting speed. Sai obtained that it is possible to set optimal cutting speed to achieve the maximum tool life. Pawade *et. al* [13] presents an experimental investigation to assess the effect of machining process and cutting edge geometry related parameters on surface integrity in the high-speed turning of Inconel 718. Fang and Wu [14] investigated a comparative experimental study of high speed machining of two materials–titanium alloy Ti–6Al–4V and Inconel 718–have been performed. The results show that for both materials: as the cutting speed increases, the cutting force, the thrust force, and the result force all decrease; however, the force ratio increases. Thakur *et. al* [10] experimentally investigated on high-speed machining of Inconel 718 using cemented tungsten carbide insert tool. Chou *et. al* [15] investigated the performance and wear behavior of different cubic boron nitride (CBN) tools finish turning of hardened AISI 52100 steel. Experimental results revealed that low CBN content tools perform better than high CBN content. In spite of the low CBN content tools have subordinate mechanical properties. Additionally, Diniz and Oliveira [16] pointed out same results related to the effect of CBN content on machining of hardened steel.

Gaitonde *et. al* [17] investigated the relationships between the cutting conditions (cutting speed, feed rate, and machining time) on machinability aspects (machining force, power, specific cutting force, surface roughness, and tool wear).

The machining force is highly sensitive to feed rate variations and the maximum tool wear occurs at a cutting speed of 150 m/min for all values of feed rate. Lima et. al [18] experimentally studied the machinability of hardened steels at different hardness and cutting tool materials. AISI 4340 steel was conducted using of 42 and 48 HRC hardness. Firstly, coated carbide insert was used. Then, a PCBN insert was employed. The experimental tests on the hardened AISI D2 steel (58 HRC) were performed with a mixed alumina-cutting tool. According to the machining tests, obtained surface finish as good as that produced by cylindrical grinding. Davim and Figueira [19] studied using ceramic cutting inserts in surface finish operations on cold work tool steel AISI D2 heat treated to a hardness of 60 HRC. Experimental results revealed that with an appropriate cutting parameters choice is possible to obtain a surface roughness ($R_a < 0.8 \mu\text{m}$). Cakir et. al [20] investigated the effects of cutting parameters on to the surface roughness using the mathematical model developed by using the data gathered from turning experiments. Higher feed rate leads to poor surface roughness, whereas cutting speed has an opposite effect and depth of cut has no significant effect. Işık [21] were performed a study to determine the machinability of tool steels. Results; Cutting speed is the most effective parameter on tool life, feed rate is the second and depth of cut is the least. Flank wear was the most encountered wear type. Increases in feed rate and cutting depth affect the surface quality negatively, while the increase of nose radius affects it positively. The different studies related to the machinability assessments on hard turning can be found in published scientific literature [7, 22, 23, 24, 25, 26].

In this study, machinability characteristics were investigated in hard turning of AISI S1 cold work tool steel widely used in manufacturing industry. Machining force, surface roughness, tool wear, evaluating of tool wear mechanism using Scanning Electron Microscope (SEM) and analysis of variance (ANOVA) were conducted in order to achieve the objective of the study.

2 Experimental Set-up

The AISI S1 (1.2550) cold work tool steel (hardened 60 HRC) which made by Dörrenberg Edelstahl in form of 100 mm diameter and 300 mm length was used as a work piece material. The chemical composition of work piece material is shown in Table 1. The AISI S1 has been using in cold shear knives, paper and wood cutting knives, cutting tools for plates up to 10 mm, ejector pins and air hammers, because of the excellent wear resistance, high surface hardness and very good toughness, dimensionally stable, impact resistant and high hardening capacity [27].



Table 1
Chemical composition of AISI S1 experimental work piece (wt%)

C	Si	Mn	P	S	Cr	W	V
0.6	0.74	0.33	0.012	0.007	1.01	1.88	0.16

The PVD TiN coated ceramic and CBN inserts which produced by SANDVIK Coromant were used in turning tests. The mixed alumina ceramic inserts designation code is SNGA 120408 S01525 6050 and low CBN content inserts code is SNGA 120408 S01030 A 7015. The inserts were clamped onto with a designation of DSBNR-2525-M12 (approach angle: 75°) tool holder. The geometry and properties of inserts is shown in Table 2.

The turning tests were performed (Figure 1-a) on JOHNFORD T35 CNC lathe having a maximum spindle speed of 4000 rpm and a maximum power of 10 kW (Figure 1-b) in dry conditions. A KISTLER 9257B piezoelectric dynamometer and its equipments were used to measure three components of forces (cutting force (F_c), feed force (F_f) and passive force (F_p)) (Figure 1-c). Surface roughness (R_a) was measured by using a Mahr Perthometer M1 with a cut-off length of 0.8 mm. After each turning test, surface roughness was measured at intervals of 120° on outer diameter surface (Figure 1-d).

Table 2
Properties of cutting inserts and tool holder

Cutting Inserts	SNGA 120408 S01525	SNGA 120408 S01030
		
Nose radius, mm	0.8	0.8
Edge geometry	Chamfered and honed	Chamfered and honed
Chamfer width, mm	0.15	0.10
Chamfer angle	25°	30°
Grade	6050 (Sandvik Coromant)	7015 (Sandvik Coromant)
Tool holder	DSBNR-2525-M12	
Approach angle (Kr)	75°	

The flank wear formed on cutting inserts was measured by Mitutoyo TM-500 tool makers' microscope with 40x magnification. Flank wear which occurring in constant chip removal volume was used in order to evaluating of the tool wear.

The machining force (F_m) was determined by using the following equations:

$$F_m = \sqrt{F_c^2 + F_f^2 + F_p^2} \quad (1)$$

Machining parameters and their levels used in the machining tests are given in Table 3. Design of experiment was determined by full-factorial experimental design.

Table 3
Experimental machining parameters

Machining Parameters	Levels		
	1	2	3
Cutting tool	Ceramic	CBN	---
Cutting Speed, V_c (m/min)	150	225	300
Feed rate, f (mm/rev)	0.05	0.1	0.15
Depth of Cut (mm)	0.2	0.4	0.6



a) Performing of the tests



b) CNC lathe



c) KISTLER 9257B dynamometer



d) Surface roughness measurement

Figure 1
Experimental setup

3 Results and Discussion

Obtaining results after the tests were detailed under titles of surface roughness, cutting forces and tool wear respectively as follows.

3.1 Surface Roughness

After each cutting experiment carried out according to the experiment parameters, the R_a roughness values were measured over the machined surfaces. The graphs showing the correlations between the measured values and the cutting parameters are given in Figure 2.a and Figure 2.b. The curves are placed based on cutting depths on the graphics.

As seen in Figure 2.a, in experiments carried out with ceramic cutting inserts, it is observed that the R_a values increase in parallel with the increase in the feed rate values for all the three cutting speeds. With the raise of the feed rate value from 0.1 mm/rev. to 0.15 mm/rev., a significant increase is observed in the R_a value. Furthermore, when evaluated with regards to cutting speeds, the roughness value obtained at the cutting speed of 150 m/min. is observed to be slightly higher in comparison with others. It was observed that the R_a curves obtained at cutting speeds of 225 and 300 m/min. were close to each other. There, some improvement may be seen in roughness since the temperature increasing with the increasing cutting speed makes chip formation relatively easier. The effect of the increase in the cutting speed is low on R_a . However, it may cause a negative effect on R_a after a point depending on the increase of the cutting speed and the tool wear. Especially, it is inevitable the fact that the machined material is hardened at a very high value shall worsen this situation.

When the graphs given in Figure 2.b and related to the experiments carried out with CBN cutting inserts are studied, significant increases in the R_a value have been observed. Here, it is seen that feed rate has a significant effect on R_a . The increase in the cutting speed has displayed an improvement on R_a similar to the ceramic inserts. Furthermore, with regards to cutting depths at low feed rate (0.05 mm/rev), there was change in the R_a value; however, as the progress increased, an increase was displayed at high cutting depths. This situation may be explained through the negative effect that the combination of the increased chip cross-section with the hardness of the workpiece makes on the machined surfaces. When the R_a values obtained under the same cutting conditions are compared with regards to cutting inserts, it may be said that the CBN cutting insert exhibits a better performance in relation to the ceramic cutting inserts. Considering that the ceramic cutting inserts are used in experiments with a hardness above the recommended maximum piece hardness and that they are cheaper than the CBN cutting inserts, it may be considered that this improvement obtained with CBN cutting insert may be small. The best R_a value was obtained under conditions at low feed rate and high cutting speeds for both cutting inserts. Lima *et al.* also suggested similar results [18].

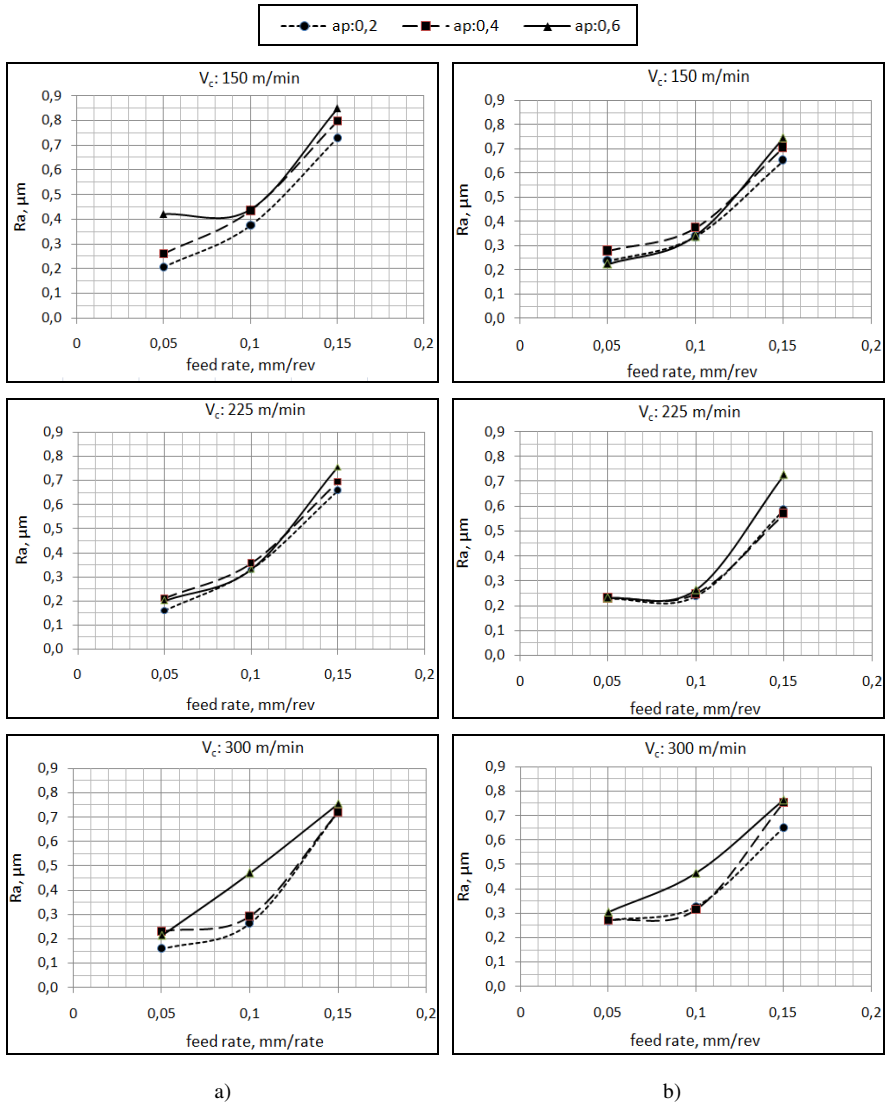


Figure 2

a) Variation at value of R_a depending on feed rate in hard turning of AISI S1 with ceramic inserts in different cutting speed

b) Variation at value of R_a depending on feed rate in hard turning of AISI S1 with CBN inserts in different cutting speed

3.2 Cutting Forces

The machining force (F_m) established as the evaluation criterion for the cutting forces was obtained via calculation (in accordance with Equation 1) from the force values measured in three directions via a dynamometer during the experiments.

In Figure 3.a, the change of the machining force depending on feed rate for the machining of AISI S1 steel at different cutting speeds with ceramic cutting inserts. When the graph is studied, it can be seen that the machining force increases in parallel with the increase in the feed rate. Since the increase of the feed rate value increases the chip cross-section, more force shall be required for chip formation. In this case, the cutting forces shall increase [28, 17]. Furthermore, similar increase rates were exhibited dependent on the increase of the depths of cut. Since the increases in the amounts of feed rate and depth of cut increase the chip cross-section, it is inevitable that this increases the force required for chip formation. When the results of the machining forces in the three graphs in Figure 3.a are evaluated, the machining force exhibited a trend to decrease in parallel with the increase in the cutting speed. It was observed that the trend to decrease is more distinctive at high feed rate and depths of cut (increasing chip cross-section). This situation may be related to the fact that the increase in the cutting speed improves the formation and removal of chips at the cutting region.

In Figure 3.b, the change of the machining force at different cutting speeds with CBN cutting inserts is shown depending on the feed rate. The increase in feed rate increased the machining force also in the cutting experiments carried out with CBN cutting tools. The increase in all the three graphs in the figure displayed parallelism to each other. With regards to depths of cut, it was observed that the machining force increases with increasing cutting depth. It is also observed that the increasing cutting speed decreases the processing speed in general. When the ceramic and CBN inserts are evaluated with regards to machining forces, it is seen that slightly lower machining forces are obtained in the cutting experiments carried out with CBN cuttings tools. The machining force, which is 127.399 N at a cutting speed of 300 m/min., at a feed rate of 0.05 mm/rev. and at a depth of cut of 0.2 for CBN cutting inserts, was 150.661 N with the same parameters for ceramic inserts. These values are the lowest values obtained for both inserts. The fact that CBN cutting inserts perform better on hardened steels has an influence on this situation.

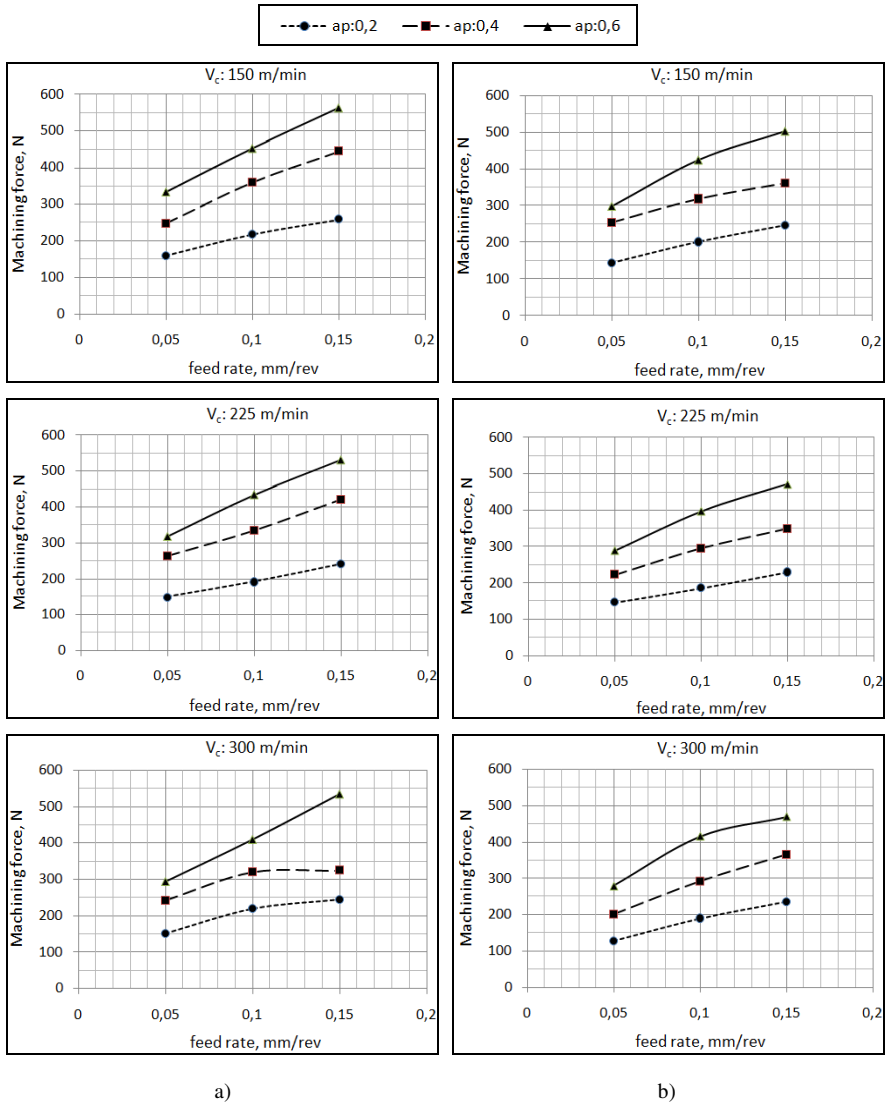


Figure 3

- a) Variation at machining force depending on feed rate in hard turning of AISI S1 with ceramic inserts in different cutting speed
- b) Variation at machining force depending on feed rate in hard turning of AISI S1 with CBN inserts in different cutting speed

3.3 Tool Wear

The flank wears were measured and evaluated as the result of the experiments carried out under fixed chip conditions for the wear criterion that is an important factor for the evaluation of the machining performance of hardened steels. Poulachon *et. al* [4] stated that the back-shift of the cutting edge as a result of wear has an important effect on the geometrical dimension of the work piece. Therefore, they suggested flank wear should be preferred with priority in the measurement and classification of tool wears [4]. The change of the flank wear on the cutting speed for AISI S1 steel with ceramic cutting inserts at different depths of cut is given in Figure 4.a. In all the three graphs, the increase in the cutting speed increased the flank wear. In general, in turning and milling operations, the factors affecting the toll wear are ordered, with regards to significance, as cutting speed, feed rate and depth of cut [29]. With the increasing of the cutting speed, the high-speed deformation and friction at the interface of the tool and the chip increases the temperature at the cutting region [2, 19, 29, 30]. When turning hard pieces, the high hardness and strength of the work piece plays an important role in formation of high heat at the cutting side and between the tool and the chip [6]. It is observed that the increase amount of the flank wear is relatively low at depth of cut of 0.4 and 0.6 mm, and distinctively high at the depth of cut of 0.2 mm. The highest wear values are observed at a cutting speed of 300 m/min., a cutting depth of 0.2 mm, and a feed rate of 0.015 mm/rev. Almost the same results are mentioned in other studies [8, 10, 18].

In Figure 4.b, the change of flank wear vs. cutting speed is given for different depths of cutting with CBN cutting inserts. When the graphs given in the figures are studied, the flank wear values exhibit an increase with the increase in the depth of cut. Increasing cutting speeds increase the deformation on the tool at places where the cutting tool contacts the chips at the cutting region. Furthermore, looking at the graphs, it can be seen that the occurring tool wears are close to each other. Accordingly, it may be said that cutting depth does not have much more effect on the tool wear for the cutting experiments carried out with CBN cutter compared to ceramic cutters.

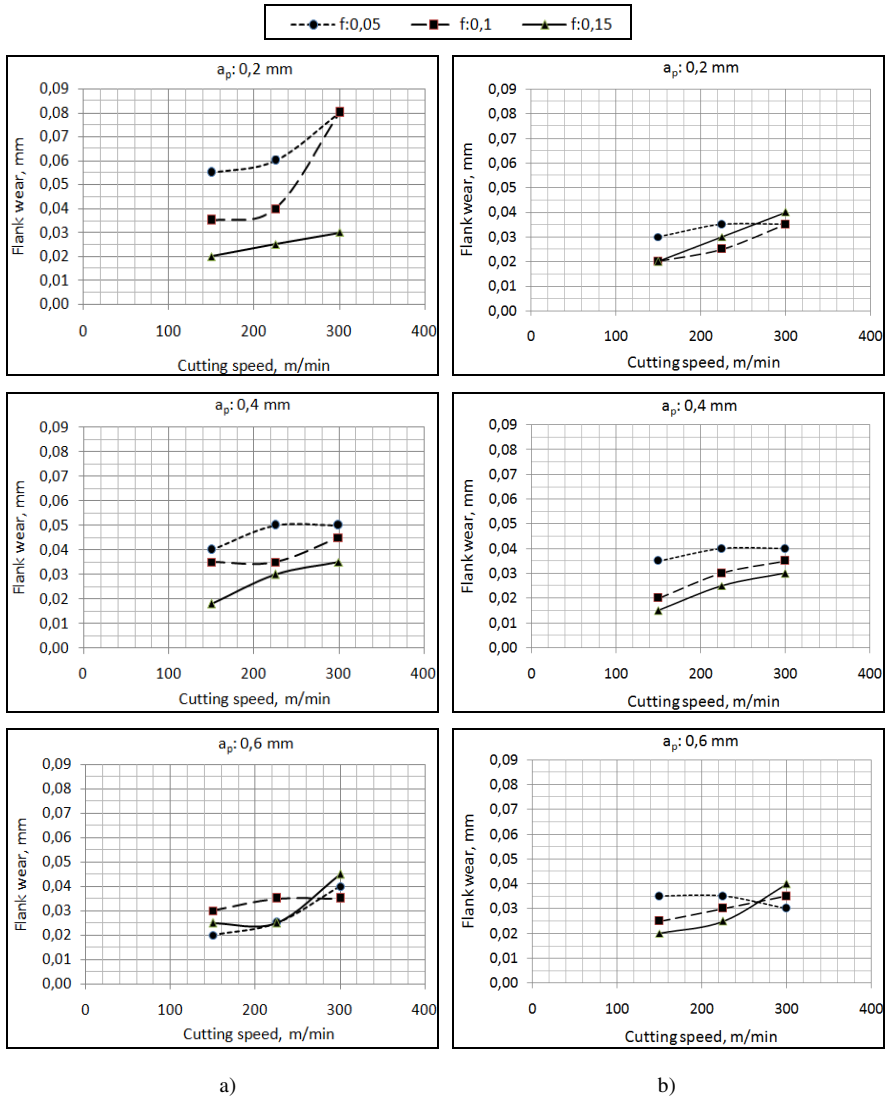


Figure 4

- a) Variation at flank wear depending on cutting speed in hard turning of AISI S1 with ceramic inserts in different depth of cut
- b) Variation at flank wear depending on cutting speed in hard turning of AISI S1 with CBN inserts in different depth of cut

When ceramic and CBN cutting inserts are compared for the same cutting parameters, it is seen that the CBN cutting insert displays a better performance than ceramic cutter with regards to flank wear.

3.4 Wear Mechanism

SEM images of the cutting inserts were taken and evaluated to assess more effectively the determination of wear mechanisms occurring in the cutting experiments and establishing wear types and consequent better evaluation of tool performance.

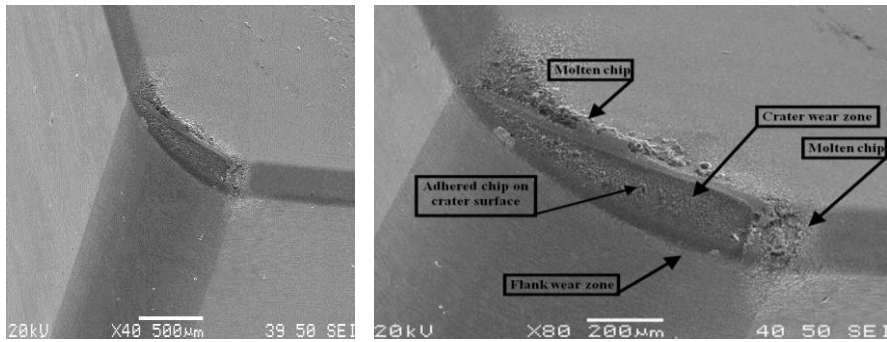


Figure 5

SEM photos of wears on ceramic insert (V_c : 300 m/min., f : 0.15 mm/rev. a_p : 0.4 mm)

In Figure 5, the wear status of the ceramic insert with cutting parameters of V_c : 300 m/min., f : 0.15 mm/rev., and a_p : 0.4 mm. In the figure, flank wear, crater wear, notch wear, and the molten chip and adhered chip on to the crater surface at the region where the chip surface and the insert diameter ends (where the contact of the chip with the cutting insert ends) can be seen clearly. In other studies on the turning of hard pieces, similar results are seen [10, 9]. When the figure is studied, it seems possible that some indent wear shall occur after some more cutting on this area. Abrasion marks that are the result of the abrasive wear mechanism caused by the hard martensite particles inside the work piece were small [5]. The flank wear occurrence is quite small. When the crater wear at the chamfer area of the cutting insert is studied, it can be said that the crater size shall grow if the cutting process is continued. The main reason for crater wear is the sliding of the chip on the chip surface of the tool. The sliding movement abrades the rises and decreases the waviness of the surface [5]. Also, the presence of chip pieces adhering on the crater surface can be observed. These adhering pieces break during the ongoing cutting process and new pieces adhere to the emptied area. Abrasion gains acceleration after this point. However, the contact inside the crater at high cutting speeds is evaluated through the combination of very high temperature, great chip sliding speed and the adhering and accumulation of chips [9]. The adhering layers may also have a protective effect [9]. Looking at the wear area in general, it can be said that effects of slightly abrasive and intensely adhesive and diffusion wear mechanism are seen in the ceramic cutter.

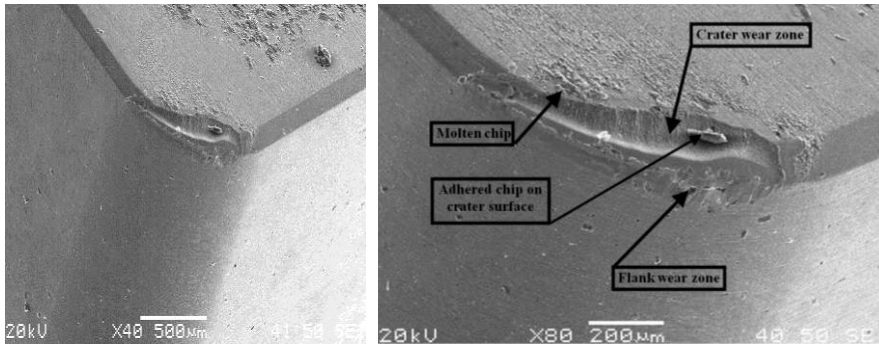


Figure 6

SEM photos of wears on CBN insert V_c : 300 m/dak., f : 0.15 mm/dev., a_p : 0.4 mm)

In Figure 6 is given the SEM image taken after the experiment carried out with CBN cutting insert at cutting conditions of V_c : 300 m/min., f : 0.15 mm/rev., and a_p : 0.4 mm. Flank wear, crater wear, newly developing notch wear, molten chip, and adhered chip on to the crater surface are observed. When the flank wear areas are studied, chips smeared under the effects of friction and pressure can be seen as well as abrasion wear marks formed in the cutting direction cutting. Crater wear is observed at high cutting speeds. The reason for this may be the fact that the carbides in the hardened work piece separate the bonds of the CBN binder and abrade the tool [2]. The main reason for crater wear is the sliding of the chip on the chip surface of the tool. The sliding movement abrades the rises and decreases the waviness of the surface [5]. At the small cutting area, the crater wear occurred at the chamfer zone of the cutting tool. The shape of the crater wear on the tool is related to the distribution of the pressure along the chip surface [9]. The crater wear occurring consequently can change the geometry of the cutting area suddenly [5, 9]. While the fact that the cutting process is carried out on hardened pieces and at high cutting speed values is useful with regards to economy or quality, it also causes the formation of high temperatures at the cutting region. The increasing temperature increases the diffusion effect that facilitates crater formation. Furthermore, high cutting speeds give rise to serious tribological condition at the tool-chip interface, causes the tool coating to peel and the tool to act consequently as an uncoated tool [9]. When the figure is studied, the presence of chip can be seen that occurs at the region the contact of the chip with the tools ends and contact with air starts with a trend to develop. As a result, it can be said that effects of abrasive and intensely adhesive and diffusive wear mechanism are seen in the CBN cutter.

3.5 ANOVA Results of the AISI S1

The effects of the cutting parameters on surface roughness, flank wear, and machining force were evaluated statistically using variance analysis. The obtained results were investigated under the titles of surface roughness, machining force and flank wear. ANOVA is a method most widely used and aims at determining significant parameters on response and measuring their effects [31]. The results of the variance analysis for R_a values are given in Table 4. As can be understood from the table, it is seen that, with regards to P values, the cutting speed, feed rate and cutting depth have a significant effect on R_a and that the effect of the cutter type is insignificant. With the value of $F=455.19$, it was seen that the change in the feed rate levels is the most effective parameter on R_a . According to the variance analysis results for the machining force (F_m), it is observed that, at 95% confidence level, the effects of all the parameters on F_m are significant. It was observed that the change in the cutting levels of the depth of cut with $F=298.36$ is the most effective parameter on F_m . Feed rate is the second significant parameter with the value of 141.31 F.

Table 4
ANOVA results of surface roughness, machining force and flank wear

Surface roughness					
Source	DoF	SS	MS	F	P
Tool type	1	0.00904	0.00904	3.71	0.060
Cutting speed	2	0.05597	0.02798	11.49	0.000
Feed rate	2	2.21635	1.10818	455.19	0.000
Depth of cut	2	0.05344	0.02672	10.98	0.000
Residual error	46	0.11199	0.00243		
Total	53	2.44678			
Machining force					
Tool type	1	10222	10222	14.51	0.000
Cutting speed	2	6675	3338	4.74	0.013
Feed rate	2	1999140	99570	141.31	0.000
Depth of cut	2	420457	210229	298.36	0.000
Residual error	46	32412	705		
Total	53	668906			
Flank wear					
Tool type	1	0.0038845	0.0038845	10.04	0.003
Cutting speed	2	0.0059364	0.0029682	7.67	0.001
Feed rate	2	0.0021681	0.0010841	2.80	0.071
Depth of cut	2	0.0044481	0.0022241	5.75	0.006
Residual error	46	0.0178008	0.0003870		
Total	53	0.0342380			

When the variance analysis results of flank wear values is studied, it is seen that the changes in tool type, cutting speed and depth of cut have a significant effect on flank wear and that the effect of progress at 95% confidence level is insignificant. It was observed that tool type is the most effective parameter with $F=10.04$.

When the experimental findings are studied in general, the smallest ideal R_a value was found with CBN cutting insert at the cutting conditions of $V_c=225$ m/min., $f=0.05$ mm/rev. and $a_p=0.2$ mm; the most ideal result at cutting conditions of $V_c=300$ m/min, $f=0.05$ mm/rev. and $a_p=0.2$ mm; the lowest flank wear with CBN cutting insert at cutting conditions of $V_c=150$ m/min., $f=0.15$ mm/rev. and $a_p=0.6$ mm. With regards to all the three environment criteria, CBN tool displayed a better performance. It is seen that the greatest problem encountered in turning of hard pieces is the rapid wear of the tool in a short time. Therefore, when determining the ideal cutting conditions, cutting speed may be increases to a degree. Since the first expectations in turning of hard pieces are a good surface smoothness and also enabling the longest lifetime for the tool, this correlation should be kept at an optimum level when determining the cutting parameters.

Conclusions

The experiments of AISI S1 material are carried out satisfactorily and the results obtained from the experiments were evaluated graphically and using ANOVA, which is one of the statistical techniques.

During the high-speed finishing turning of hardened AISI S1 material, the best results with regards to surface roughness were obtained with CBN cutters. The increase in the feed rate value increased the roughness for both cutters. With regards to turning operations, a roughness value of approximately $0.2 \mu\text{m}$ was obtained, which is very good.

For both cutters, while the machining force increased depending on the increase of the feed rate and cutting depth, it decreased depending on the increase of the cutting speed. With regards to machining force, CBN cutting inserts exhibited better performance than ceramic inserts.

For CBN and ceramic inserts, the increase in cutting speed increased the flank wear. With regards to flank wear, CBN cutter exhibited a better performance than the ceramic cutter for the same cutting parameters.

According to the study of the SEM images, it was determined that effects of slightly abrasive and intensely adhesive and diffusive wear mechanism are seen in the ceramic cutter. For CBN cutting inserts, abrasive and intensely adhesive and diffusive wear mechanisms are seen for the CBN cutters.

According to the ANOVA results, it was seen the change in progress levels is the most effective parameter on surface roughness (R_a) statistically. It was shown that the change of tool types did not lead to much change.

It was observed that the change in the cutting levels of the cutting depth with $F=298.36$ is the most effective parameter on F_m .

According to the ANOVA results, it was determined that the effects of the changes in tool type and the values of the cutting speed and the depth of cut are significant and that the effect of feed rate is insignificant. It was seen that the tool type is the most effective parameter with the value of $F=10.04$.

After the turning of both hardened materials investigated within the scope of the study, surfaces at grinding quality were obtained. It was predicted that, with the choice of appropriate cutting parameters, grinding operation and its hazardous effects on the environment and humans shall be decreased for such processes.

Acknowledgement

The authors would like to thank the Dumlupinar University, Department of Scientific Research Projects for funding this research (Project code: 2010/5). Besides, the authors thank the Gazi University Faculty of Technology Manufacturing Engineering Department and Dr. Yakup Turgut because of contribution in performing of machining tests.

References

- [1] Grzesik W., Influence of Tool Wear on Surface Roughness in Hard Turning Using Differently Shaped Ceramic Tools, *Wear*, 265, 2008, 327-335
- [2] Poulachon G., Moisan A. and Jawahir I. S., Tool-Wear Mechanisms in Hard Turning with Polycrystalline Cubic Boron Nitride Tools, *Wear*, 250, 2001, 576-586
- [3] Chou Y. K., Song H., Tool Nose Radius Effects on Finish Hard Turning, *J. Mater. Process. Technology*, 148, 2004, 259-268
- [4] Poulachon G., Bandyopadhyay B. P., Jawahir I. S., Pheulpin S. and Seguin E., Wear behavior of CBN Tools while Turning Various Hardened Steels, *Wear*, 256, 2004, 302-310
- [5] More A. S., Jiang W., Brown W. D. and Malshe A. P., Tool Wear and Machining Performance of CBN-TiN-coated Carbide Inserts and PCBN Compact Inserts in Turning AISI 4340-hardened Steel, *J. Mater. Process. Technology*, 180, 2006, 253-262
- [6] Derakhshan E. D. Akbari A. A., Experimental Investigation on the Effect of Workpiece Hardness and Cutting Speed on Surface Roughness in Hard Turning with CBN Tools, *Proceeding of The World Congress on Engineering*, 2009, Vol:2, London
- [7] Tamizharasan T., Selvaraj T. and Noorul Haq A., Analysis of Tool Wear and Surface Finish in Hard Turning, *Int. J. Adv. Manuf. Technol.*, 2006, 28:671-679

- [8] Horng J. T., Liu N. M. and Chiang K. T., Investigating the Machinability Evaluation of Hadfield Steel in the Hard Turning with $\text{Al}_2\text{O}_3/\text{TiC}$ Mixed Ceramic Tool Based on the Response Surface Methodology, *J. Mater. Process. Technology*, 208, 2008, 532-541
- [9] Mahfoudi F., List G., Molinari A., Moufki A. and Boulanour L., High Speed Turning for Hard Material with PCBN Inserts: Tool Wear Analysis, *Int. J. Machining and Machinability of Materials*, Vol:3 Nos. ½ 2008
- [10] Thakur D. G., Ramamoorthy B. and Vijayaraghavan L., Machinability Investigation of Inconel 718 in High Speed Turning, *Int. J. Adv. Manuf. Technol.*, 2009, 45:421-429
- [11] Umer U., Butt S. I., Askari S. J., Danish S. N. and Xie L., Comparative Analyses for Different Modeling Methods in High Speed Turning Operations for Hardened Steel, *J. Mech. Engng.*, 54, 2008, 12, 850-854
- [12] Sai W. B., An Investigation of Tool Wear in High Speed Turning of AISI 4340 Steel, *Int. J. Adv. Manuf. Technology*, 2005, 26:330-334
- [13] Pawade R. S., Joshi S. S. and Brahmanekar P. K., Effect of Machining Parameters and Cutting Edge Geometry on Surface Integrity of High Speed Turned Inconel 718, *International Journal of Machine Tools and Manufacture*, 48, 2008, 15-28
- [14] Fang W., Wu Q., A Comparative Study of the Cutting Forces in High Speed Machining of Ti-6Al-4V and Inconel 718 with a Round Cutting Edge Tool, *J. Mater. Process. Technology*, 209, 2009, 4385-4389
- [15] Chou Y. K., Evans C. J. and Barash M. M., Experimental Investigation on CBN Turning of Hardened AISI 52100 Steel, *J. Mater. Process. Technology*, 124, 2002, 274-283
- [16] Diniz A. E., Oliveira A. J., Hard Turning of Interrupted Surfaces Using CBN Tools, *J. Mater. Process. Technology*, 195, 2008, 275-281
- [17] Gaitonde V. N., Karnik S. R., Figueira L. and Davim P., Analysis of Machinability During Hard Turning of Cold Work Tool Steel (Type:AISI D2), *Materials And Manufacturing Processes*, 24:2009, 1373-1382
- [18] Lima J. G., Avila R. F., Abrao A. M., Faustino M. and Davim J. P., Hard Turning: AISI 4340 High Strength Low Alloy Steel and AISI D2 Cold Work Tool Steel, *J. Mater. Process. Technology*, 169, 2005, 388-395
- [19] Davim J. P., Figueira L., Machinability Evaluation in Hard Turning of Cold Work Tool Steel (D2) with Ceramic Tools Using Statistical Techniques, *Mater. Des*, 28, 2007, 1186-1191
- [20] Çakır M. C., Ensarioğlu C. and Demirayak I., Mathematical Modeling of Surface Roughness for Evaluating the Effects of Cutting Parameters and Coating and Coating Material, *J. Mater. Process. Technology*, 209, 2009, 102-109

- [21] Işık Y., Investigating the Machinability of Tool Steels in Turning Operations, *Materials and Design*, 28, 2007, 1417-1424
- [22] Huang Y., Liang S. Y., Force Modeling in Shallow Cuts with Large Negative Rake Angle and Large Nose Radius Tools-Application to Hard Turning, *Int. J. Adv. Manuf. Technology*, 2003, 22:626-632
- [23] Zhou J. M., Walter H., Andersson M. and Stahl J. E., Effect of Chamfer Angle on Wear of PCBN Cutting Tool., *International Journal of Machine Tools and Manufacture*, 43, 2003, 301-305
- [24] Kundrak J., Karpuschewski B., Gyani K. and Bana V., Accuracy of Hard Turning, *J. Mater. Process. Technol.*, 202, 2008, 328-338
- [25] Singh D., Rao P. V., Improvement in Surface Quality with Solid Lubrication in Hard Turning, *Proceeding of The World Congress on Engineering*, 2008, Vol:3, London
- [26] Qian L., Hossain M. R., Effect on Cutting Force in Turning Hardened Tool Steels with Cubic Boron Nitride Inserts, *J. Mater. Process. Technology*, 191, 2007, 274-278
- [27] <http://www.doerrenberg.de/>
- [28] Fnides B., Aouici H. and Yaltese M. A., Cutting Forces and Surfaces Roughness in Hard Turning of Hot Work Steel X38CrMoV5-1 Using Mixed Ceramic, *Mechanika*, 2008, Nr:2, 70
- [29] Davim J. P., Maranhao C., Faria P., Abrao A., Rubio J. C. and Silva L.R., Precision Radial Turning of AISI D2 Steel, *Int. J. Adv. Manuf. Technol.*, 2009, 42:842-849
- [30] Sahin Y., Comparison of Tool Life between Ceramic and Cubic Boron Nitride (CBN) Cutting Tool when Machining Hardened Steels, *J. Mater. Process. Technology*, 209, 2009, 3478-3489
- [31] Kacal, A and Gulesin, M., Determination of Optimal Cutting Conditions in Finish Turning of Austempered Ductile Iron Using Taguchi Design Method. *Journal of Scientific & Industrial Research*, 2011, 70, 278-283

Should Codification Emerge in IFRS? Does Form of Regulation Matter?

György Andor and Ildikó Rózsa

Budapest University of Technology and Economics (BME), Department of Finance, Magyar tudósok körútja 2, H-1117 Budapest, Hungary, rozsa@finance.bme.hu; andor@finance.bme.hu

Abstract: The International Financial Reporting Standards (IFRS) is in the process of becoming globally recognised in stock exchanges alongside the Generally Accepted Accounting Principles in the United States (US GAAP). The IFRS and US GAAP have evolved based on the GAAP encompassed by the list of standards that constitute the structure of both accounting literatures. The structure that this article refers to as “standard-based” has been a traditional format for the IFRS and US GAAP in the past. Whereas the IFRS still maintains a standard-based literature structure, US GAAP standard setters of the Financial Accounting Standards Board (FASB) decided to depart from the standard-based tradition of editing accounting literature by redesigning the existing authoritative US GAAP literature into a single codified text, titled the Accounting Standards Codification (ASC). This paper focused on the structures of IFRS and US GAAP to understand whether the ASC enhances the application of US GAAP by professionals. The objective of this paper was to determine whether the structure of the ASC offers an appropriate alternative to the standard-based structure of IFRS – making IFRS a user-friendly accounting literature in Central Europe. We administered a survey as a tool to foster discussion and to identify the features offered by the ASC, which is similar in structure to statutory accounting traditionally adopted in Central Europe.

Keywords: IFRS; US GAAP; Codification; standard-based structure; stock exchange

1 Introduction

The International Financial Reporting Standards (IFRS) and the Generally Accepted Accounting Principles in the United States (US GAAP) have played a significant role in improving financial reporting information on an international scale. The International Accounting Standards Board (IASB) and the Financial Accounting Standards Board (FASB), which are the standard setters of the IFRS and US GAAP, respectively, have made important efforts to converge the respective accounting literatures with the objective of reducing the existing differences between the IFRS and US GAAP. As part of this convergence endeavour, the IFRS has gradually achieved global recognition along with the US GAAP. For example, approximately 120 countries encourage or require the

application of the IFRS. Other countries have adopted the IFRS by drafting local accounting legislation in line with IFRS, resulting in further acceptance of the IASB by the international community [2]. In particular, the European Union has imposed the application of the IFRS by public companies.

This progress provides an exciting opportunity to compare recent developments in the way the IFRS and US GAAP are being communicated to the public. Both the IFRS and US GAAP have evolved based on generally accepted accounting principles embodied in thoroughly documented conceptual statements that provide solid ground in developing accounting standards. The standard-based approach to accounting is common and traditional to the IFRS and US GAAP. Under a standard-based approach, the structure of the accounting literature refers to the chronological sequence of standards issued over time. The reference numbers of the standards do not particularly refer to the sequence of financial statement components or name any particular financial statement components. For example, intangible assets are listed among the first lines in the balance sheet, whereas the reference number of the relevant standard is IAS 38. Additionally, the standard titled “Construction contracts” does not refer to any particular financial statement line item. Some countries in Europe apply standard-based accounting principles, for example, the UK, where the structure of the accounting literature is very similar to that of the IFRS or US GAAP prior to codification (see section 2 for more information about the Accounting Standards Codification). In most of Europe, however, accounting is subject to legislation, where accounting conventions are driven by statute and enacted by law. The structure of legislative accounting literature has a different approach to the documentation of accounting rules. If the IFRS and US GAAP can be considered “standard-based”, then legislative accounting documentation can be referred to as being “analog” instead. In Hungary, for example, accounting law holds that the rules be listed in a sequence consistent with the sequence of financial statement line items as they appear on balance sheets and income statements. That is, if intangible assets appear in line 1 of a balance sheet, then the first paragraph will refer to the accounting treatment of intangibles in the section regarding balance sheet regulations.

Because of the differences experienced in the way standard-based and legislative accounting structures are designed, most European entities encounter severe difficulties in applying the IFRS or US GAAP prior to codification. Professionals who are not confident in handling standard-based accounting structures will need further knowledge to perform advanced searches of the IFRS or US GAAP to find answers to particular accounting issues. The extensive cross-referencing between accounting standards create further difficulties for professionals used to the legislative structure in ensuring whether all items in a subject are adequately covered when performing a search of the IFRS or US GAAP prior to codification. As a result, experience shows that as requirements to adopt the IFRS have become more widespread in Europe, significant resistance has been triggered at the same time by entities in countries where accounting rules adopt a legislative structure.

The analog structures of accounting legislation in most European countries provide a lean approach to obtaining a comprehensive overview of accounting regulation. In addition to the structural differences experienced in standard-based accounting literatures, the language and the approach used have made companies reluctant to adopt the IFRS. In the paper, we considered the difficulties that most countries in Europe encounter in the process of becoming familiar with the standard-based approach to accounting structure with the introduction of the IFRS.

In the course of events, the FASB implemented a substantive change in the structure of the US GAAP with the objective of gathering all relevant existing GAAP literatures into a uniform structure, known today as the Accounting Standards Codification (or the Codification). Because the new structure of the Codification (discussed in section 2) agrees with the analog approach of most legislative accounting structures, the Codification inspired us to challenge the existing structure of the IFRS. The purpose of this paper was to examine the implications of the Codification to understand whether users enjoy the benefits of the new US GAAP structure and determine whether users would welcome a similar change to the IFRS structure.

2 The Development of Accounting standards Codification

2.1 Accounting Standards Codification

The US GAAP authoritative literature includes a large number of publications issued over the past fifty years by various professional bodies. The publications, including standards, interpretations, position statements, and opinions, have been published in a relatively uncoordinated manner. Each professional body has applied a unique method for coding the publications, which are very much inconsistent from one another. By 2009, the literature comprised over 2,000 publications. The large amount of literature maintained under relative disintegration could not facilitate efficient research based on the publications. The FASB alone issued 168 standards, accompanied by further publications adding to the total. In addition, the standards themselves had features similar to those of the IFRS, such as extensive cross-references between standards; the coverage of a single topic by more than one standard; and a sequential numbering of standards based on chronological order rather than any order of financial statement components. As a result, criticism began to focus on the lack of a consistent and concise approach inherent to the standard-based US GAAP structure. Professional bodies believed that the US GAAP structure was unwieldy and difficult to follow [11]. Criticism also noted risks associated with the structure, such as the possible incompleteness of research work given the wide range of relevant publications available for review. Consequently, the existing standard-based structure was

discouraging to professionals in maintaining timely knowledge in a cost-effective manner. In response, the FASB took action and announced its project to target the weaknesses identified above.

To initiate the project, the FASB first surveyed the opinions of users of the US GAAP through questionnaires. Companies and practicing professionals were invited to the survey, representing a total of 1,400 participants who received questionnaires featuring the following questions [8]:

Q-1: Do you find the current US GAAP literature confusing?

Q-2: Does research in the current system require considerable time?

Q-3: Would codification make the system more understandable?

Q-4: In your opinion, will codification make searching in the system easier?

Q-5: In your opinion, should FASB pursue codification?

The results of the survey were favourable, and the Accounting Standards Codification (ASC or, Codification) project was launched with over 200 professionals from different entities being involved. The Codification structure intended to differ significantly from the existing standard-based US GAAP structure. The objective of the Codification project was to facilitate access to the complete authoritative US GAAP literature. The Codification did not change existing accounting principles but rearranged the existing and relevant publications into a user-friendly structure to facilitate consistency and completeness in accounting research. Ultimately, the existing authoritative literature was organised under approximately 90 different topics, each dedicated to separate areas of concentration, such as assets, liabilities, equity, expenses, and revenue accounts in financial statements. In this context, it is important to underline that the FASB moved toward a structure that was much different from what was previously known as a standard-based structure.

The Accounting Standards Codification was effective on June 30, 2009 as the single authoritative US GAAP literature, and former publications were no longer authoritative subsequent to that date. Review and update processes take place within the Codification platform on an annual basis. Any change or revision is documented and announced in the Accounting Standards Updates (ASU), which is the exclusive forum used to communicate amendments to the Codification.

2.2 Experience in Europe after Inception of Accounting Standards Codification

We reviewed the results of the FASB survey three years after the Codification was implemented. We were interested in determining whether the Codification provided effective solutions to previous difficulties and whether the properties of the former standard-based structure still remain. We reissued the initial survey to compare how users feel about the Codification three years after. We invited 100

US GAAP users, including practicing professionals with considerable experience, from several European countries: Austria, Bulgaria, the Czech Republic, France, Germany, Hungary, Poland, Romania, Slovakia, Slovenia, and Spain.

The sample was composed of 100 individual European entities that are subsidiary undertakings of companies headquartered and listed in the United States. The companies under survey are, therefore, continuously involved in the preparation of quarterly and annual financial reporting in compliance with SEC requirements. Such requirements include the filing of form 10-Q and 10-K reports quarterly and at year end, respectively. In a group structure, subsidiaries deliver the quarterly and annual reports to the headquarters for consolidation purposes at the group level. In the sample, we avoided selecting foreign security issuers and overseas companies that are directly listed in the US because such companies are subject to annual reporting only. The SEC requires foreign companies to submit form 20-F once at year end, and it may be prepared in accordance with the IFRS. Since 2008, the SEC has no longer required foreign companies to reconcile their local financial statements to US GAAP accounts. Foreign companies, therefore, would not have been representative of the sample because such companies exhibit limited use of the US GAAP.

We achieved a 74 percent survey response rate, i.e., 74 questionnaires out of 100 were accepted as complete for evaluation purposes. The number of responses by country were as follows: 7 from Austria, 9 from Bulgaria, 8 from the Czech Republic, 5 from France, 11 from Germany, 16 from Hungary, 8 from Poland, 4 from Romania, 2 from Slovakia, 1 from Slovenia, and 3 from Spain.

The questions we designed for our survey were based on the questions initially posed by the FASB:

Q-1: Do you find the current US GAAP literature confusing?

Q-2: Does research in the current system require considerable time?

Q-3: In your opinion, has the Codification made the literature more understandable?

Q-4: In your opinion, has the Codification made research in the literature easier?

Q-5: In your opinion, was the Codification worth launching?

Table 1 compares the results of our survey with those of the previous FASB survey conducted in 2008.

Table 1

Survey of demand for US GAAP codification (by FASB; N=1400; source: Finance Accounting Foundation 2008) and experiences with US GAAP codification (N=74)

	Survey (2008)	Survey (2012)
Believe the current system of US GAAP regulation is confusing	80%	31%
Believe searching the current system requires considerable time	85%	38%
Believe codification makes / has made the US GAAP more understandable	87%	81%
Believe codification will make / has made searching in the system easier	96%	79%
Believe it would be / was worth launching codification	95%	82%

It should be noted that the population surveyed by the FASB was different from the population we surveyed, and the sample we selected was not statistical. Nevertheless, the sampling technique was sufficient to understand whether users welcomed the Codification overall. It appears that Europeans working in legislative accounting environments could identify with the structure outlined in the Codification because of its direct relationship to financial statement accounts represented by areas of concentration, as mentioned earlier. The survey results indicate that the Codification made the US GAAP transparent and clear to follow for European users.

3 Demand for IFRS Codification in Europe

3.1 Existing IFRS Structure

The following section will focus on the existing structure and properties that characterise the IFRS as the other significant representative of accounting literature on a global level along with the US GAAP. The IFRS includes three authoritative texts: the Framework, Standards, and Interpretations. Readers of the IFRS must continuously consider the interrelations between standards and interpretations that cover a number of accounting topics that reference one another across different standards and interpretations.

In an effort to globalise the IFRS, the IASB amended or superseded a number of standards and issued new standards in recent years. In addition, the IASB is looking forward to issuing further standards in the future. Nevertheless, the IFRS literature included fewer publications than the US GAAP prior to the codification due to the history and organisational background of the IASB. The IASB is a younger organisation than the FASB and its surrounding organisations but is also the ultimate body governing the IFRS. In contrast, various professional bodies

contributed to the US GAAP, leading to a number of different publications before the codification. In this context, we discovered opinions indicating that the IFRS is currently in a stage where the US GAAP was 30 years ago in terms of exhibiting a standard-based structure. Even if there are fewer IFRS publications than pre-codified US GAAP publications, the existing structure of the IFRS is alien to users working in legislative accounting environments. The extensive cross-references between standards and specific editing matters make the IFRS difficult to oversee. Additionally, the numbering of IFRS publications is based on chronological order rather than any particular sequence of financial statement components, similarly to the US GAAP prior to codification. In light of the existing IFRS structure, which shares much in common with the pre-codified US GAAP, it may be worth considering whether the codification of the IFRS would lead to favourable results similar to those observed for the codification of the US GAAP.

Table 2 presents a summary of the cross-references between standards effective on January 1, 2012. The table indicates that the standard number of cross-references is 6 on average. Common or mandatory standards such as IAS 1, IAS 12, and IAS 16 indicate a greater number of cross-references, whereas industry-specific standards such as IAS 29 and IFRS 6 indicate fewer cross-references relative to the average. From a statistical point of view, the standard deviation of references from one particular standard towards other standards is 6.13, whereas the standard deviation of references towards one particular standard from other standards is 3.84. Considering solely cross-references between standards and omitting other references to interpretations and limitations in scope, the total number of cross-references is 6 on average based on the number of effective standards in place.

Table 2

Relationships among IFRS standards (Only includes standards in force as of January 1, 2012)

Standard	Its refer-ences	References to it	Ex-ceptions	Standard	Its refer-ences	References to it	Ex-ceptions
IAS 1	36	12	1	IAS 31	4	3	3
IAS 2	2	6	3	IAS 32	6	10	6
IAS 7	2	3	-	IAS 33	6	2	-
IAS 8	7	14	1	IAS 34	4	1	-
IAS 10	8	4	-	IAS 36	5	12	9
IAS 11	2	3	-	IAS 37	4	14	8
IAS 12	10	6	1	IAS 38	10	9	13
IAS 16	10	11	5	IAS 39	6	10	10
IAS 17	7	6	3	IAS 40	10	4	1
IAS 18	2	5	7	IAS 41	7	4	4
IAS 19	4	7	2	IFRS 1	14	1	1
IAS 20	2	5	2	IFRS 2	1	5	4
IAS 21	5	9	3	IFRS 3	13	10	1
IAS 23	1	4	2	IFRS 4	8	2	11

IAS 24	1	4	-	IFRS 5	4	12	6
IAS 26	-	2	2	IFRS 6	6	2	-
IAS 27	4	7	1	IFRS 7	4	3	7
IAS 28	5	4	1	IFRS 8	2	6	-
IAS 29	1	1	-				
Subtotal	109	113	34		114	110	83
Total					223	223	117
Average					6	6	3
Standard deviation					6,13	3,84	3,52

Table 3 illustrates the complexity of cross-references in a network of interrelations between standards. The network excludes cross-references between interpretations and limitations in scope for simplicity. Still, the diagram indicates that the network of interrelations between standards is extensive and topics are difficult to follow. The chart shows a positive correlation between standards only. It is clear that the number of references between standards is significant, and to study a topic requires comprehensive knowledge of all standards.

The continuous revisions of existing standards and issuances of new standards may further complicate the IFRS literature in future. Under these conditions, the opportunity to evaluate the viability of a possible codification of the IFRS has been welcome. Codification efforts should therefore commence in due course to implement a structure that provides a user-friendly approach to readers of the IFRS.

3.2 IFRS Presence in Europe

The extent to which the IFRS is applied in Europe varies by country. In some European countries, the application of the IFRS is optional under certain conditions. For example, in Hungary, companies may opt to use the IFRS in preparing consolidated financial statements. Additionally, the mandatory use of the IFRS may vary by industry sector. For example, financial institutions must issue annual consolidated financial statements in compliance with the IFRS. Private companies are free to use the IFRS, whereas publicly listed companies in the European Union must report under the IFRS on a consolidated basis [18]. Because local accounting regulations are mandatory by statute, businesses within the scope of the IFRS must comply with both accounting requirements in turn. Additionally, there are certain countries where the IFRS has replaced local accounting legislations in a specific manner. Such inconsistent expectations regarding when and how the IFRS should be applied makes financial reporting difficult to compare between industries [10].

Table 3
Links and references between standards

	IAS 1	IAS 2	IAS 7	IAS 8	IAS 10	IAS 11	IAS 12	IAS 16	IAS 17	IAS 18	IAS 19	IAS 20	IAS 21	IAS 23	IAS 24	IAS 26	IAS 27	IAS 28	IAS 29	IAS 31	IAS 32	IAS 33	IAS 34	IAS 36	IAS 37	IAS 38	IAS 39	IAS 40	IAS 41	IFRS 1	IFRS 2	IFRS 3	IFRS 4	IFRS 5	IFRS 6	IFRS 7	IFRS 8			
IAS 1	-	1	1	1	1	1	1	1	1	1	1	1	1	1	1	1	1	1	1	1	1	1	1	1	1	1	1	1	1	1	1	1	1	1	1	1	1	1		
IAS 2		-	1	1	1	1	1			1																		1	1										1	
IAS 7			-	1									1									1						1												
IAS 8				-	1	1	1	1	1	1	1	1	1	1	1	1	1	1	1	1	1	1	1	1	1	1	1	1	1	1	1	1	1	1	1	1	1	1	1	
IAS 10					-		1																	1	1			1								1				
IAS 11						-				1																														
IAS 12							-	1	1	1	1	1	1	1	1											1	1	1	1			1	1	1						
IAS 16								-	1				1	1	1										1	1	1	1	1	1	1	1	1			1	1		1	
IAS 17																							1					1											1	
IAS 18																	1											1												1
IAS 19																		1										1												
IAS 20																									1	1														
IAS 21																																								1
IAS 23																																								
IAS 24																																								
IAS 26																																								
IAS 27																																								
IAS 28																																								
IAS 29																																								
IAS 31																																								
IAS 32																																								
IAS 33																																								
IAS 34																																								
IAS 36																																								
IAS 37																																								
IAS 38																																								
IAS 39																																								
IAS 40																																								
IAS 41																																								
IFRS 1																																								
IFRS 2																																								
IFRS 3																																								
IFRS 4																																								
IFRS 5																																								
IFRS 6																																								
IFRS 7																																								
IFRS 8																																								

Table 4
Summary of use of IFRS in some European countries [4]

	Austria	Bulgaria	Czech Republic	France	Germany	Hungary	Poland	Romania	Slovakia	Slovenia
Is the use of IFRS obligatory in standalone statements?	No	Yes (except for SME-s)	No	No	No	No	No	No	No ^{a)}	No ^{b)}
Is the use of IFRS obligatory in consolidated statements?	No	Yes (except for SME-s)	No	No	No	No	No ^{c)}	No ^{c)}	Yes	No ^{b)}
Can the use of IFRS be chosen for standalone statements?	No	Yes	No	No	No	No	No ^{d)}	No	No	Yes ^{e)}
Can the use of IFRS be chosen for consolidated statements?	Yes	Yes	Yes	Yes	Yes	Yes	No ^{d)}	Yes	No	Yes ^{e)}
Do they use statutory accounting regulation or standards?	Statutory regulation ^{f)}	Statutory regulation ^{g)}	Statutory regulation ^{h)}	Statutory regulation ^{p)}	Statutory regulation ^{o)} /trends on standard-based	Statutory regulation ⁱ⁾	Statutory regulation ^{j)}	Statutory regulation ^{k)}	Statutory regulation ^{l)}	Standards ^{m)}

a) Except for financial institutions, insurance companies, asset managers, and large enterprises (which exceed 2 from 3 indicators in two successive years: assets of 150 million EUR, annual revenue of 150 million EUR, and a staff size of 2000); b) Except for financial institutions and insurance companies; c) Except for financial institutions; d) Except for companies listed on the stock market and companies with a parent company abroad; e) Yes, but the domestic accounting report cannot be chosen for 5 years after decision; f) Austrian Commercial Code (UGB); g) SG 4/15.01.1991, but already standards today; h) Accounting Directives Law (Act No. 563/1991); i) Hungarian Accounting Law (Act No. C); j) Act of 29 September 1994 on Accounting (“AA”); k) Accountancy Law No.82/1991; l) Accounting Act No. 431/2002. as amended by Act no. 562/2003 Coll. and Act no. 561/2004 Coll.; m) Slovenian Accounting Standards, Source: (IFRS Foundation, 2011); o) Bilanzrechtsmodernisierungsgesetz (German Act on the Modernisation of Accounting Law), p) Plan Comptable Général (PCG)

From the survey, we highlight the case in Slovenia and Bulgaria, where the IFRS has been imposed for all types of financial statements, including stand-alone statements of private companies. We paid special attention to Bulgaria to study the effects of IFRS application. Despite the fact that the IFRS superseded the former accounting law in Bulgaria, resulting in the general requirement of the IFRS in financial reporting, there has been criticism regarding the completeness and consistency of IFRS application in Bulgaria. In 2008, the World Bank reported that Bulgaria has in fact not adapted the IFRS in its complete form. World Bank analyses indicate that there were significant inconsistencies regarding the scope of IFRS application in Bulgaria compared to the scope of EU adoption. The World Bank reviewed 15 company reports and revealed 9 companies whose consolidated financial statements were not in compliance with the IFRS in full. The conclusion drawn by the World Bank required Bulgaria to extend the scope of the IFRS in local accounting regulations [19].

The overall results of our survey with respect to IFRS presence in Europe indicate in Table 4 that financial reporting in most countries is still subject to statutory legislation.

3.3 Survey of the Demand for IFRS Codification

To assess the viability of IFRS codification, a survey similar to that initiated by the FASB prior to the codification of the US GAAP should be administered to IFRS users as well. As a start, we submitted 300 questionnaires to practicing professionals in different multinational companies, of which 218 responses were received, representing a 73% response rate. Not all responses were complete; incomplete responses were considered inadequate for processing. We considered 194 responses appropriate for evaluation. The questionnaire addressed the following questions, which are consistent with the questions designed by the FASB in preparation of the ASC project:

- Q-1: Do you find the current IFRS literature confusing?
- Q-2: Does research in the current IFRS require considerable time?
- Q-3: Would IFRS codification make the system more understandable?
- Q-4: In your opinion, will IFRS codification make searching the system easier?
- Q-5: In your opinion, should the IASB pursue IFRS codification?

3.3.1 Sample Selected

For the sample, we selected multinational companies because of the predominant use of the IFRS in this sector in Europe due to public listings or foreign ownerships. Table 5 is a summary of the 194 companies evaluated in the survey, by sector; the number of companies publicly listed is indicated in a separate column. We considered it important to include publicly listed companies in the survey sample as well because such companies must prepare financial statements under the IFRS.

3.3.2 Evaluation of the Survey

Responses to the five questions listed above are summarised in Table 6. The results indicate that the codification of IFRS might be a possible alternative to the current system.

Table 5
Number of respondents and listed companies by sector

Sector	Number of responses	Listed on stock exchange
Energy and services	31	18
Building industry	18	11
Automobile industry	29	20
Telecommunication	18	18
Pharmaceutical industry	19	17
Media	7	4
Merchandising	28	13
Transportation and delivery	15	10
Bank and insurance	29	29
Total	194	140

Table 6
Survey of demand for US GAAP codification (by FASB; N=1400; source: FASB 2008) and demand for IFRS codification (N=194)

	US GAAP (2008)	IFRS (2012)
Believe the system of the US GAAP / the IFRS regulation is confusing	80%	39%
Believe searching the current system requires considerable time	85%	73%
Believe codification would make the US GAAP / the IFRS more understandable	87%	69%
Believe codification will make searching in the system easier	96%	71%
Believe it would be worth launching codification	95%	77%

To draw a fair conclusion from the results of the survey, we identified the following three factors for consideration.

First, it is important to note that the sample surveyed regarding IFRS codification consisted users unlike those initially surveyed by the FASB with respect to US GAAP codification. Although both groups of users are involved in accounting, the environment in which they practice and the challenges they encounter are inherently different. The background and structure of the US GAAP before codification and the existing IFRS literature exhibit different features (see sections 2.1 and 3.1), which may have affected the ways in which the participants in the two groups interpreted the questions in the surveys.

The second factor considered is the sizes of the samples selected by the FASB and by us for the purpose of this paper. The FASB survey results were gathered from 1,400 questionnaires, as opposed to the results of our survey, which were gathered from 300 questionnaires. We acknowledge that the scope of our survey may appear limited compared with the scope of the FASB survey. To compensate for any possible adverse effects the relative sample size may have had on the results, we focused on the composition of the companies invited to the survey (Table 5). We expected that the variety of sectors presented in our sample would, to a favourable extent, offset the shortcomings attributable to the sample size.

Third, the different approaches applied in carrying out the surveys may have also caused deviations in interpreting the percentages presented in Table 6. The results of the US GAAP survey were used in this paper as readily available source of data. We had no background details available regarding the methodology applied by the FASB in deriving the results of its survey. Therefore, we cannot conclude whether our approach for evaluating the results of our survey was in any way identical to that employed by the FASB. In our approach, we asked the participants to answer the questions on a scale of 10, where 1 represented the lowest satisfaction and 10 the highest satisfaction in response to the questions. We then calculated the average score of the responses and weighted the average based on the scale. Finally, we related the weighted averages to the total number of responses received, by question, to calculate the percentages. The percentages, therefore, are considered to represent the relative expectations and attitudes of the participants towards the five issues addressed by the questions.

The evaluation of the survey results is sensitive to the factors described above. The results derived from our survey are affirmative to the extent that we acknowledge possible differences between the features of the two groups of samples; the way they have been selected; and the approach used to evaluate the responses gathered from the participants. Although the percentages regarding the demand for IFRS codification seem less promising than those indicated by the FASB survey, our results remain above marginal, indicating that IFRS codification may be a timely proposal for a certain group of professionals. However, regarding the question whether the codification of the IFRS would represent an important contribution to the profession, we considered further conditions, as discussed in Section 3.4.

3.4 Further Considerations Regarding IFRS in Europe

The objective of this section is to consider others factors that explain why most countries in Europe may be unwilling to adopt the IFRS in its existing form unless codification of the IFRS literature takes place.

Previous assessments mentioned in this article indicate that traditionally accounting is subject to statutory legislation in most of Europe, where users are

familiar with the content of accounting laws and favour the customary approach to structuring rules and regulations. Today, the Accounting Standards Codification in the United States shares many aspects in common with legislations favoured in Europe in terms of structuring accounting literature. The ASC proposed a consistent approach to editing and updating accounting requirements oriented toward areas of concentration, including individual financial statement components – a very similar approach observed in legislative environments in Europe. In contrast to the ASC, the IFRS structure is driven by a list of standards that do not accommodate users in legislative environments to conduct research easily.

In most European countries, entities must comply with charts of accounts predefined in local accounting legislations. The IFRS, in turn, does not outline such distinct procedures [15]. If local legislations were to remove mandatory requirements similarly to the chart of accounts, then practicing professionals would lose reference and comfort in the application [17].

Despite the successful distribution of IFRS publications, the IFRS has been released in a limited number of languages. As a consequence, a number of studies have concluded that the lack of available languages in which the IFRS is published [14] and the lack of timely revisions of IFRS publications issued in languages other than English make it difficult for users to follow the relevant literature [1] [7].

Because statutory accounting rules are often driven by taxation, some countries in Europe oppose the introduction of the IFRS overall [5] [6] [10] [12] [13] [16]. Others have observed that the different national tax regimes represent the primary obstacles to imposing the IFRS in local accounting environments [9].

Continuing professional development is another area of controversy [3]. Professional IFRS training courses vary in timing and quality by country. Because IFRS knowledge is not a prerequisite to obtaining local accounting certificates, candidates do not appreciate such courses.

Having reviewed the structures of the ASC and IFRS, as well as the characteristics of local legislations, we believe that the structures attributable to national accounting legislations have conceptually more in common with the Codification than with the standard-based IFRS. Therefore, we anticipate that the structure of the Codification is a suitable reference to use for the possible codification of the IFRS. In the following section, we discuss a possible alternative to IFRS codification based on the existing ASC structure.

4 Possible Way to Codify IFRS

Following our discussions with respect to the difficulties users encounter in applying the IFRS in Europe, in this section, we encourage the initiative to rearrange the IFRS to overcome this obstacle. The primary difficulty with the existing structure of the IFRS is that many practicing professionals in Europe find it unusual compared to the structures followed by local legislations. Therefore, we recommend a structure very similar to what was developed under the ASC in the United States. The codification approach should lead to a structure with which users will be able to more easily identify, in contrast to any possible revised versions of the standard-based approach to the IFRS.

Having observed the codification process in the United States, we are convinced that traditional standard-based structures are not necessarily practical in the long term. Therefore, the time to initiate the codification of the IFRS may well be now. We expect the codified structure to ease the review of standards and the monitoring of amendments to standards in the IFRS literature. Additionally, we expect that the large number of IFRS opponents will be assuaged once a codified structure replaces the existing standard-based structure. Certainly, a codification of the IFRS will not overcome the conflict with the various taxation regimes in Europe governing local accounting rules. To date, taxation has been considered one of the strongest arguments against IFRS introduction. In evaluating the merits and possible demerits of IFRS codification, we propose to carry forward and initiate a codification structure based on the ASC implemented in the United States. That is, all standards and interpretations effective to date will be rearranged into a new codified structure to enable readers to follow IFRS literature in a user-friendly form. Finally, the codified IFRS should represent the sole authoritative reference for practicing professionals.

Table 7 demonstrates the way IFRS can be codified.

Conclusions

Today's accounting environment is in an inevitable result of globalisation. The standard setters of the IFRS and US GAAP have significant influence over financial reporting requirements at the international level. Current trends indicate that the IFRS will take a leading position in global accounting in the near future. The developments in this area inspired us to investigate and examine the merits and possible demerits of, as well as the arguments for and against, the IFRS. We focused primarily on the differences between the ways in which the IFRS and US GAAP are structured, rather than discussing differences in accounting conventions that have already converged in recent years. Briefly, we challenged the current standard-based structure of the IFRS using the well-received Codification in the United States.

Table 7
Draft of a possible IFRS codification based on the US codification structure

US GAAP codification structure	Classification of IFRS standards
General Principles	Framework, IAS 1
Presentation	
205-Presentation of Financial Statements	IAS 1, IAS 34, IFRS 1, IFRS 8
210-Balance Sheet	IAS 1
215-Statement of Shareholder Equity	IAS 1
220-Comprehensive Income	IAS 1
225-Income Statement	IAS 1
230-Statement of Cash Flows	IAS 1, IAS 7
235-Notes to Financial Statements	IAS 1, IAS 34
250-Accounting Changes and Error Corrections	IAS 8, IFRS 1, Framework
255-Changing Prices	IAS 21, IAS 29, IFRIC 7, SIC 7
260-Earnings per Share	IAS 33, IFRS 2
270-Interim Reporting	IAS 34, IFRIC 10
275-Risks and Uncertainties	IAS 8, IAS 10, IAS 37
280-Segment Reporting	IFRS 8
Assets	
305-Cash and Cash Equivalents	IAS 7, IAS 32, IAS 39, IFRS 7
310-Receivables	IAS 11, IAS 18, IAS 32, IAS 39, IFRS 7, IFRIC 13, SIC 31
32X-Investments	IAS 27, IAS 28, IAS 31, IAS 32, IAS 39, IFRS 7, IFRIC 12, IFRIC 16, IFRIC 17, SIC 29
330-Inventory	IAS 2, IAS 11, IFRIC 15
340-Deferred Costs and Other Assets	IAS 23, IAS 32, IAS 39
350-Intangibles-Goodwill and Other	IAS 38, IFRS 3, IFRIC 12, SIC 29, SIC 32
360-Property, Plant and Equipment	IAS 16, IAS 17, IAS 20, IAS 23, IAS 36, IAS 40, IFRS 5, IFRIC 18
Liabilities	
405-Liabilities	IAS 32, IAS 37, IAS 39, IFRIC 4, IFRIC 14
410-Asset Retirement and Environmental Obligations	IAS 16, IAS 37, IFRIC 1, IFRIC 5
420-Exit or Disposal Cost Obligations	IAS 37, IFRS 5, IFRIC 1, IFRIC 5
430-Deferred Revenue	IAS 11, IAS 18, IAS 37, IFRIC 15, SIC 10
440-Commitments	IAS 10, IAS 37, IAS 39, IFRIC 14
450-Contingencies	IAS 10, IAS 37
460-Guarantees	IAS 10, IAS 37
470-Debt	IAS 32, IAS 39, IFRS 7
480-Distinguishing Liabilities from Equity	IAS 32, IFRS 2, IFRIC 2, IFRIC 19
Equity	IAS 1, IAS 32, IFRS 2, IFRIC 2, IFRIC 16, IFRIC 17, IFRIC 19
Revenue	IAS 11, IAS 18, IFRIC 12, IFRIC 13, IFRIC 15, SIC 31
Expenses	
705-Cost of Sales and Services	IAS 2, IAS 11
71X-Compensation	IAS 19, IFRS 2
720-Other Expenses	IAS 16, IAS 20, IAS 26, IAS 36, IAS 37, IAS 39, SIC 15
730-Research and Development	IAS 38
740-Income Taxes	IAS 12, SIC 21, SIC 25
Broad Transactions	
805-Business Combinations	IFRS 3
810-Consolidation	IAS 27, IAS 28, IAS 31, IFRS 3, SIC 12, SIC 13
820-Fair Value Measurements and Disclosures	IAS 32, IAS 39, IAS 40, IFRS 7, IFRIC 9
825-Financial Instruments	IAS 32, IAS 39, IFRS 7, IFRIC 9
830-Foreign Currency Matters	IAS 21, IAS 29, IAS 32, IAS 39, IFRS 7
835-Interest	IAS 32, IAS 39, IFRS 7
840-Leases	IAS 17, IAS 32, IAS 39, IFRIC 4, SIC 15, SIC 27
845-Nonmonetary Transactions	IAS 21, SIC 10

Our results were based on a sample of entities surveyed and analysed through questionnaires. The entities represented operational ASC and IFRS users. From the US GAAP perspective, we analysed the results of the FASB survey initially designed to assess the practical need for codification. Next, we addressed questions, consistent with those previously formulated by the FASB, to a sample of ASC users (post implementation) with the objective of determining the success of codification. Later, we selected a sample of IFRS users to determine whether codification of the IFRS literature would be rational in the future. A considerable number of respondents favoured IFRS codification.

Because users appeared to welcome the idea of IFRS codification, we directly proposed a codified structure of the IFRS similar to the ASC implemented in the United States. Because the ASC has proved to function, we have not considered any further alternative to the future structure of the IFRS other than codification. The proposed method for codification is based on the principles applied in the United States during the ASC project.

The globalisation of financial reporting has been spectacular for the accounting profession. The IFRS is foreseen as becoming a global accounting standard, and listed companies in the United States will be expected to convert financial reporting from the US GAAP to the IFRS. We believe that the codification of the existing IFRS structure may further contribute to its globalisation, as users will most likely be more willing to accept the IFRS literature in a codified structure, which is consistent with ASC or other European legislations, than in its current standard-based format.

References

- [1] Aisbitt, S. and C. Nobes, 2001. The True and Fair View Requirement in Recent National Implementations, *Accounting and Business Research*, 31(2): 83-90
- [2] Choi, F.D.S., C.A. Frost and G.K. Meek, 2002. *International Accounting* (4th ed.), Upper Saddle River, NJ: Prentice Hall, Pearson Education
- [3] Christensen, HB, 2012. Why do Firms Rarely Adopt IFRS Voluntarily? Academics Find Significant Benefits and the Costs Appear to be Low. *Review of Accounting Studies* 17(3): 518-525
- [4] Deloitte Global Services Limited, 2010. IAS Plus Implementation of the IAS Regulation (1606/2002) in the EU and EEA, Available at <http://www.iasplus.com/europe/1007ias-use-of-options.pdf>
- [5] Eberhartinger, E. L. E., 1999. The Impact of Tax Rules on Financial Reporting in Germany, France, and the U.K., *The International Journal of Accounting*, 34(1): 93-119
- [6] Eilifsen, A., 1996. The Relationship between Accounting and Taxation in Norway, *The European Accounting Review*, 5 (Suppl.): 835-844

- [7] Evans, L., 2003. The True and Fair View and the 'Fair Presentation' Override of IAS 1, *Accounting and Business Research*, 33(4): 311-325
- [8] FASB (Finance Accounting Standards Board), 2008. Accounting Standards Codification Notice to Constituents (v1.05), Available at <http://asc.fasb.org/imageRoot/10/5724610.pdf>
- [9] Guenther, D. A. and M. E. A. Hussein, 1995. Accounting Standards and National Tax Laws: The IASC and the Ban on LIFO, *Journal of Accounting and Public Policy*, 14: 115-141
- [10] Haller, A., 2002. Financial Accounting Developments in the European Union: Past Events and Future Prospects, *The European Accounting Review*, 11(1): 153-190
- [11] Herz, R. H., 2003. A Year of Challenge and Change for the FASB, *Accounting Horizons*, 17(3): 247-255
- [12] Holeckova, J., 1996. Relationship between Accounting and Taxation in the Czech Republic, *The European Accounting Review*, 5 (Suppl.): 859-869
- [13] Hoogendoorn, M. N., 1996. Accounting and Taxation in Europe – A Comparative Overview, *The European Accounting Review*, 5 (Suppl.): 783-794
- [14] IFRS Foundation, 2011. Available Translations, Available at <http://www.ifrs.org/Use+around+the+world/IFRS+translations/Available+translations.htm>
- [15] Jaruga, A. A. and A. Szychta, 1997. The Origin and Evolution of Charts of Accounts in Poland, *The European Accounting Review*, 6(3): 509-526
- [16] Lamb, M., C. Nobes and A. Roberts, 1998. International Variations in the Connections Between Tax and Financial Reporting, *Accounting and Business Research*, 28: 173-188
- [17] Nobes, C, 2011. IFRS Practices and the Persistence of Accounting System Classification. *Abacus – a Journal of Accounting Finance and Business Studies*, 47: 267-283
- [18] Street, D.L. and R.K. Larson, 2004. Large Accounting Firms' Survey Reveals Emergence of „Two Standard” System in the European Union, *Advances in International Accounting*, 17: 1-29
- [19] World Bank, 2008. Report on the Observance of Standards and Codes (ROSC) Bulgaria, Available at: http://www.worldbank.org/ifa/rosc_aa_bgr_eng_08.pdf

The Non Linear Controller for Terminal Voltage and Power Angle of Power Systems

Moulay Fatima¹, Ramdani Youcef², Habbati Assia², Hamdaoui Habib², Bendaoud Abdelber³

¹LMSR Laboratory; Djilali Liabes University of Sidi Bel-Abbes; Tlemcen street, Sidi Bel-Abbes (22000), Algeria. E-mail: babelber@univ-sba.dz

²IRECOM Laboratory; Djilali Liabes University of Sidi Bel-Abbes; Algeria Tlemcen street, Sidi Bel-Abbes (22000), Algeria. E-mail: ramdani@univ-sba.dz

³APELEC Laboratory; Djilali Liabes University of Sidi Bel-Abbes; Algeria Tlemcen street, Sidi Bel-Abbes (22000), Algeria. E-mail: babelber@gmail.com

Abstract: The purposed work is the design of a nonlinear voltage and rotor angle controller to improve the stability properties of a system which comprises a synchronous generator connected to an infinite bus and hydraulic turbine. The controller is based on the feedback linearization scheme. The advantage of this systematic nonlinear controller design is that the control system is liberalized in a wider domain. A linear control can then be used to stabilize the linear system. The performances of the linear voltage and rotor angle regulators are compared with those of the standard linear voltage and speed regulators in the presence of short circuits at the generators. The infinite bus and the non-linear regulator improved considerably the stability and the transient dynamic performance of the generator.

Keywords: Nonlinear control; hydraulic turbine; synchronous generator; voltage regulation; rotor angle stability; feedback linearization

1 Introduction

The control equipment of synchronous generators, such as an automatic voltage regulator, a speed governor and a power system stabilizer, are normally designed for a liberalized model of a power system around a given operating conditions. Therefore, when the operating condition or the network configuration changes widely, it may become less effective because of the non linearity of the power system. This became a very important problem in power systems. To solve this problem and to realize efficient control performance, many advanced studies have been done on generator control systems, such as adaptive generator controllers based on linear control theory[1] and self-tuning power system stabilizers based

on adaptive control theory. The technique of input-output feedback linearization is now well known because it gives a good solution for tracking control problems [2]. This later one has been successfully applied to the control of AC motors and synchronous generators. The main goal of this paper is to investigate the application of a nonlinear control technic to a detailed multi-input, multi-output nonlinear model of a power system in order to improve both, its stability and damping properties even under large and sudden disturbances and to insure good post-fault voltage regulation [3].

2 Model of the System

The generator is connected to an infinite bus through a transmission line having resistance R_e and inductance L_e . We applied classical Park's transformation, and the model takes into account both field effects and damper-winding effects introduced by the different rotors circuits as follows:

In the axe d:

$$\begin{bmatrix} i_d \\ i_{fd} \\ i_{kd} \end{bmatrix} = \frac{\begin{bmatrix} -(L_{fd} \cdot L_{kd} - L_{md}^2) & (L_{md} \cdot L_{kd} - L_{md}^2) & (L_{fd} \cdot L_{md} - L_{md}^2) \\ -(L_{md} \cdot L_{kd} - L_{md}^2) & (L_d \cdot L_{kd} - L_{md}^2) & -(L_d \cdot L_{md} - L_{md}^2) \\ -(L_{fd} \cdot L_{md} - L_{md}^2) & (L_d \cdot L_{md} - L_{md}^2) & (L_{fd} \cdot L_d - L_{md}^2) \end{bmatrix}}{L_d \cdot L_{fd} \cdot L_{kd} - L_{md}^2 \cdot (L_d + L_{fd} + L_{kd}) + 2 \cdot L_{md}^3} \begin{bmatrix} \Phi_d \\ \Phi_{fd} \\ \Phi_{kd} \end{bmatrix} \quad (1)$$

In the axe q:

$$\begin{bmatrix} i_q \\ i_{kq} \end{bmatrix} = \frac{\begin{bmatrix} -L_{kq} & L_{mq} \\ -L_{mq} & L_q \end{bmatrix}}{L_q \cdot L_{kq} - L_{mq}^2} \cdot \begin{bmatrix} \Phi_q \\ \Phi_{kq} \end{bmatrix} \quad (2)$$

$$\begin{aligned} \frac{d(\Phi_q)}{dt} &= v_q + R_s \cdot i_q - \omega \cdot \Phi_d \\ \frac{d(\Phi_d)}{dt} &= v_d + R_s \cdot i_d + \omega \cdot \Phi_q \\ \frac{d(\Phi_{kd})}{dt} &= -R_{kd} \cdot i_{kd} \\ \frac{d(\Phi_{kq})}{dt} &= -R_{kq} \cdot i_{kq} \\ \frac{d(\Phi_{fd})}{dt} &= v_{fd} - R_{fd} \cdot i_{fd} \end{aligned} \quad (3)$$

Where: $v_d(t)$, $v_q(t)$ and $v_{fd}(t)$ are respectively the direct-axis, quadrature-axis terminal voltages, and excitation control input.

And :

$i_d(t)$, $i_q(t)$: direct-axis and quadrature-axis currents

$i_{kd}(t)$, $i_{kq}(t)$: direct-axis and quadrature-axis damper windings currents

$i_{fd}(t)$: field winding current

R_s , R_{kd} , R_{kq} and R_{fd} : stator resistance, damper windings resistances, and field resistance

L_d , L_q , L_{fd} : direct and quadrature self-inductances, rotor self-inductance

L_{kd} , L_{kq} : direct and quadrature damper windings self-inductances

L_{md} inductance, L_{mq} : direct and quadrature magnetizing.

The mechanical dynamics of the machine rotor are given in these equations:

$$2H\omega_R \frac{d\omega}{dt} = T_m - T_e - T_f$$

$$T_m = \frac{P_m}{\omega}$$

$$T_e = (L_q - L_d)i_d i_q + L_{md}i_{fd}i_q + L_{md}i_{kd}i_q - L_{mq}i_d i_{kq}$$

$$T_f = F.\omega$$

$$H = \frac{\omega_R}{S_R}$$

$$2H.\omega_R \frac{d\omega}{dt} = \frac{P_m}{\omega} - (L_q - L_d)i_d i_q - L_{md}i_{fd}i_q - L_{md}i_{kd}i_q + L_{mq}i_d i_{kq} - F.\omega$$

$$\frac{d\delta}{dt} = (\omega - 1) \quad (4)$$

Where: T_e is the electromagnetic torque, and T_f is the resistant torque

T_m : mechanical torque, H : inertia constant, ω : speed of the generator,

F : the coefficient of friction, δ : power angle of the generator P_m , S_R mechanic power and nominal power.

The model of the synchronous machine connected to an infinite bus, the d-q terminal voltages v_d and v_q are given by the load equations. After using the Park's transformation, we can write:

$$\begin{bmatrix} v_q \\ v_d \\ v_o \end{bmatrix} = R_e \begin{bmatrix} i_q \\ i_d \\ i_o \end{bmatrix} + L_e \frac{d}{dt} \begin{bmatrix} i_q \\ i_d \\ i_o \end{bmatrix} - \omega.L_e \begin{bmatrix} -i_d \\ i_q \\ 0 \end{bmatrix} + v \begin{bmatrix} \sin(-\delta + a) \\ \cos(-\delta + a) \\ 0 \end{bmatrix} \quad (5)$$

Where v is the rms value of the bus voltage and a is its phase angle.

2.1 Model of the Hydraulic Turbine

The hydraulic turbine can be modeled by:

$$\frac{dq}{dt} = \frac{1}{T_w} \left(1 - \frac{q^2}{A_t^2 g^2}\right) \quad (6)$$

$$P_m = \frac{q^3}{A_t^2 \cdot g^2}$$

Where: q , g , T_w and A_t : flow in the conduit, gate opening ,water time constant, constant proportionality factor

$$\frac{dq}{dt} = \frac{-2}{T_w G_0} q + \frac{2A_t}{T_w G_0} g \quad (7)$$

$$P = 3q - 2A_t g$$

2.2 Model of the Servomotor

The servomotor is modeled by the block diagram of Fig. 1:

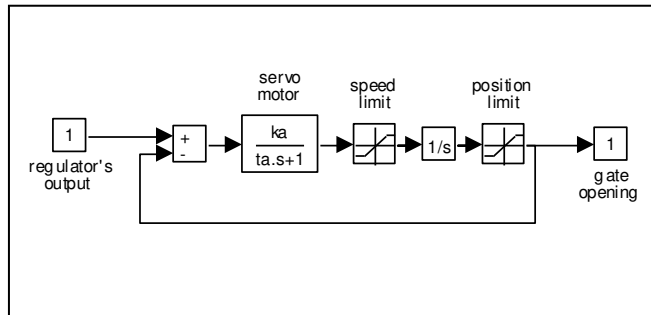


Figure 1

Model of the servomotor

Where k_a and t_a successively the gate servomotor gain and time constant the regulator of voltage has as a role to maintain the final voltage of the generator in its face value of 1 per unit (p.u). It uses the seven state variables of the controlled system, which is the generator on the infinite bar, the measure of mechanical potency and reference of voltage. They assume of course that they can have state variables of the system. Otherwise, the non measurable variables can be estimated by observation.

The generator linked to an infinite network is a system of order 7 state variables of which are currents i_d , i_q , i_{fd} , i_{kd} and i_{kq} , speed and internal angle. The input of the control is the voltage.

State equations of our system in p.u. in plan d-q are:

$$\frac{dx}{dt} = F(x) + G(x) * u_1$$

$$= \begin{bmatrix} A_{11}x_1 + A_{12}x_2 + A_{13}x_3x_6 + A_{14}x_4 + A_{15}x_6x_5 + A_{16} \cos(-x_7 + a) \\ A_{21}x_1 + A_{22}x_2 + A_{23}x_3x_6 + A_{24}x_4 + A_{25}x_6x_5 + A_{26} \cos(-x_7 + a) \\ A_{31}x_1x_6 + A_{32}x_2x_6 + A_{33}x_3 + A_{34}x_4x_6 + A_{35}x_5 + A_{36} \sin(-x_7 + a) \\ A_{41}x_1 + A_{42}x_2 + A_{43}x_3x_6 + A_{44}x_4 + A_{45}x_6x_5 + A_{46} \cos(-x_7 + a) \\ A_{51}x_1x_6 + A_{52}x_2x_6 + A_{53}x_3 + A_{54}x_4x_6 + A_{55}x_5 + A_{56} \sin(-x_7 + a) \\ A_{61}x_1x_3 + A_{62}x_2x_3 + A_{63}x_1x_5 + A_{64}x_3x_4 + A_{65}x_6 + \frac{p}{x_6} \\ \omega_R(x_6 - 1) \end{bmatrix} + \begin{bmatrix} g_1 \\ g_2 \\ 0 \\ g_4 \\ 0 \\ 0 \\ 0 \end{bmatrix} u_1 \quad (8)$$

$$y = v_t(x) = \sqrt{v_d^2(x) + v_q^2(x)}$$

$$v_d(x) = c_{11}x_1 + c_{12}x_2 + c_{13}x_3x_6 + c_{14}x_4 + c_{15}x_5x_6 + c_{16} \cos(-x_7 + a) \quad (9)$$

$$v_q(x) = c_{21}x_1x_6 + c_{22}x_2x_6 + c_{23}x_3 + c_{24}x_4x_6 + c_{25}x_5 + c_{26} \sin(-x_7 + a)$$

$$x = [x_1 \ x_2 \ x_3 \ x_4 \ x_5 \ x_6 \ x_7]^T = [i_d \ i_{fd} \ i_q \ i_{kd} \ i_{kq} \ \omega \ \delta]^T$$

p_m and y are the vector of state variables, u_1 is the vector of control inputs. A_{ij} and C_{kl} are constants which depend on the generator's parameters [3].

3 Feedback Linearization of the System

The first output to be chosen is the terminal voltage v_t

$$y = v_t(x) = \sqrt{v_d^2(x) + v_q^2(x)} \quad (10)$$

The expressions of v_d and v_q as a function of the state variables can be obtained by combining equations (1) and (5) which gives equation (9)

In order to obtain the nonlinear controller u_1 , we compute the time derivative of the output y .

$$\dot{y} = \dot{v}_t(x) = \frac{\partial v_t}{\partial x} \dot{x} = \frac{1}{v_t} (v_d \frac{\partial v_d}{\partial x} + v_q \frac{\partial v_q}{\partial x}) (F(x) + G(x)u_1) \quad (11)$$

$$\frac{\partial v_d}{\partial x} = [c_{11} \quad c_{12} \quad c_{13}x_6 \quad c_{14} \quad c_{15}x_6 \quad c_{13}x_3 + c_{15}x_5 \quad c_{16} \sin(-x_7 + a)] \quad (12)$$

$$\frac{\partial v_q}{\partial x} = [c_{21}x_6 \quad c_{22}x_6 \quad c_{23} \quad c_{24}x_6 \quad c_{25} \quad c_{21}x_1 + c_{22}x_2 + c_{24}x_4 \quad -c_{26} \cos(-x_7 + a)]$$

$$\dot{y} = a(x) + b(x) * u_1 \quad (13)$$

Where:

$$a(x) = \frac{1}{v_t} (v_d \frac{\partial v_d}{\partial x} + v_q \frac{\partial v_q}{\partial x}) F(x) \quad (14)$$

$$b(x) = \frac{1}{v_t} (v_d \frac{\partial v_d}{\partial x} + v_q \frac{\partial v_q}{\partial x}) G(x)$$

We choose u_1 that:

$$u_1 = \frac{(-a(x) + v)}{b(x)}, b(x) \neq 0 \quad (15)$$

We obtain the linear differential equation in first order between the output and the new input.

$$\dot{y} = v \quad (16)$$

The relative degree corresponding to the output is:

$$y = v_t \quad \text{is } r_t = 1$$

$$v = -k_t (y - y_{ref}) = -k_t (v_t - v_{ref}) \quad k_t > 0 \quad (17)$$

v_{ref} is the reference to terminal voltage. So that the linear control is low, the dynamic system feedback is:

$$\dot{y} + k_t y = k_t y_{ref} \quad (18)$$

$$\frac{y}{y_{ref}} = \frac{v_t}{v_{ref}} = \frac{1}{s * \tau + 1} \quad (19)$$

$$\tau = \frac{1}{k_t} \quad \text{is the time constant}$$

$$v = -k_t (y - y_{ref}) + \dot{y}_{ref} = -k_t (v_t - v_{ref}) + \dot{v}_{ref}, k_t > 0 \quad (20)$$

In case the dynamic tracking error “e” is:

$$\dot{e} + k_t e = 0 \quad (21)$$

A judicious choice of k_t is necessary to assure a good tracking.

$$\dot{x} = \begin{bmatrix} \dot{x}_1 \\ \dot{x}_2 \\ \dot{x}_3 \\ \dot{x}_4 \end{bmatrix} = \begin{pmatrix} \omega_R(x_2 - 1) \\ P_e + \frac{x_3^3}{(A_t x_4)^2} \\ \frac{1}{T_w} \left(1 - \frac{x_3^2}{A_t^2 x_4^2}\right) \\ -\frac{1}{T_g} x_4 \end{pmatrix} + \begin{pmatrix} 0 \\ 0 \\ 0 \\ \frac{1}{T_g} \end{pmatrix} u$$

$$y = \delta$$

$$x = [\delta \quad \omega \quad q \quad g]^T \quad (22)$$

Successive derivations of the output give:

$$\dot{y} = \dot{\delta} = \omega_R(x_2 - 1)$$

$$\ddot{y} = \omega_R \dot{\omega} = \left(P_e + \frac{q^3}{A_t^2 g^2}\right) \cdot \omega_R$$

$$y^{(3)} = \frac{\omega_R q^2}{A_t^2 g^2} \left(3\dot{q} - \frac{2q \cdot \dot{g}}{g}\right) = \frac{\omega_R q^2}{A_t^2 g^2} \left\{ \frac{3}{T_w} \left(1 - \frac{q^2}{A_t^2 g^2}\right) + \frac{2q}{T_g g} \dot{g} \right\} - \frac{2\omega_R q^2}{A_t^2 g^3 T_g} u$$

$$y^{(3)} = a(x) + b(x)u \quad (23)$$

$$a(x) = \frac{\omega_R q^2}{A_t^2 g^2} \left\{ \frac{3}{T_w} \left(1 - \frac{q^2}{A_t^2 g^2}\right) + \frac{2q}{T_g} \dot{g} \right\} \quad (24)$$

$$b(x) = \frac{-2\omega_R q^2}{A_t^2 g^3 T_g}$$

$$u = \frac{v - a(x)}{b(x)} \quad \text{if } b(x) \neq 0 \quad (25)$$

$$y^{(3)} = v \quad (26)$$

The relative degree corresponding to the output $y_2 = \delta$ is $r_2 = 3$.

$$v = -k_1(y - y_{ref}) - k_2(\dot{y} - \dot{y}_{ref}) - k_3(\ddot{y} - \ddot{y}_{ref}) =$$

$$-k_1(\delta - \delta_{ref}) - k_2\omega_R(\omega - 1) - k_3\omega_R\dot{\omega} \quad (27)$$

k_1 , k_2 and k_3 are real positive numbers, δ_{ref} the reference of the rotor angle.

The implementation of control v requires that stemming of the speed (acceleration) be available. It can seem problematic. Indeed, it is not always easy to have an accelerometer. However, it is necessary to point out that control v is no more and no less than P.I.D., the implementation of which is very well-known and well-controlled.

The dynamic equation of the system in a continuous closed loop is:

$$y^{(3)} + k_3 \ddot{y} + k_2 \dot{y} + k_1 y = k_1 y_{ref} \quad (28)$$

The equation which characterises it given by:

$$s^3 + k_3 s^2 + k_2 s + k_1 = 0 \quad (29)$$

$$s^3 + (p_3 + p_1 + p_2)s^2 + (p_2 p_3 + p_1 p_2 + p_1 p_3)s + p_1 p_2 p_3 \quad (30)$$

By identification, constants k_i are easily determined as follows:

$$\begin{aligned} k_3 &= p_3 + p_1 + p_2 \\ k_2 &= p_2 p_3 + p_1 p_2 + p_1 p_3 \\ k_1 &= p_1 p_2 p_3 \end{aligned} \quad (31)$$

It is necessary to note that p_3 must be a negative real pole and p_1 and p_2 two negative or complex real poles conjugated in negative real part. A way to choose poles p_1 , p_2 and p_3 is to make sure that the system in a continuous closed loop acts as a system of second control, having a time of stabilization t_r and an overtaking d . The third pole is then chosen 10 times as big as the real part of poles.

So:

$$\begin{aligned} \xi &= \frac{1}{\sqrt{1 + \left(\frac{\pi}{\log(1/d)}\right)^2}} \\ \omega_n &= \frac{5}{\xi t_r} \\ p_1 &= -\xi \omega_n - j \omega_n \sqrt{1 - \xi^2} \\ p_2 &= -\xi \omega_n + j \omega_n \sqrt{1 - \xi^2} \\ p_3 &= -10 \xi \omega_n \end{aligned} \quad (32)$$

3.1 Study of the Stability of the System

The stability of the system in a closed loop depends on the internal dynamic which is determined from the dynamic of zero. In fact, the dynamic of zero is the internal dynamic when the system's output is equal to zero. In our case, the output will be considered equal to the reference value.

The proposed method consists in proving the stability of the dynamic of zero. If it is unstable, it should be offered a variant of the linear control which stabilizes the system in closed loop.

3.2 Study of Internal Dynamics

Since the relating degree of the system is 3, so, internal dynamic is first rate. The variable of this dynamic must verify the next equation:

$$L_{G(x)}\eta(x) = 0 \Rightarrow \frac{1}{T_g} \frac{\partial \eta}{\partial g} = 0 \quad (33)$$

And it must also be linearly independent of external variables z_i ($i= 1, \dots, 0$).

A resolution is to choose:

$$\eta = q \quad (34)$$

Therefore expressions of new state variables according to previous assumptions are:

$$\begin{aligned} z_1 &= \delta \\ z_2 &= \omega_R(\omega - 1) \\ z_3 &= \omega_R \left(P_e + \frac{q^3}{A_t^2 g^2} \right) \end{aligned} \quad (35)$$

$$\eta = q$$

Then, they lead to deduce easily initial variables with respect to the new state variables.

$$\begin{aligned} \delta &= z_1 \\ \omega &= 1 + \frac{z_2}{\omega_R} \\ q &= \eta \\ g &= \frac{\eta}{A_t} \sqrt{\frac{\eta}{\frac{z_3}{\omega_R} - P_e}} \end{aligned} \quad (36)$$

One can already point out that if internal dynamic is not stable (or if q tightens towards infinity) then state variable g will also strive towards infinity and vice versa. Even if g converges, then q also will converge. So, if it is unstable, the dynamic can be stabilized by a control which stabilizes state variable g .

The derivate of internal variable allows us to acquire the equation of internal dynamics.

$$\dot{\eta} = \dot{q} = \frac{1}{T_w} \left(1 - \frac{q^2}{A_t^2 g^2} \right) = \frac{1}{T_w} \left(1 - \frac{\left(\frac{z_3}{\omega_R} - P_e \right)}{\eta} \right) \quad (37)$$

With P_e negative.

The dynamic of the zero is determined by putting the external variables equal to zero. By considering these variables constants, it doesn't change final conclusion. Therefore, the dynamic of zero is:

$$\dot{\eta} = f(\eta) = \frac{1}{T_W} \left(1 + \frac{P_e}{\eta}\right) \quad (38)$$

The point of equilibrium of this equation is $\eta_0 = -P_e$

One can conclude on stability or instability of the dynamics of zero by examining the derivative of $f(\eta)$ at the equilibrium point. If it is negative, the system is stable. If it is positive, the system is unstable.

$$f'(\eta_0) = -\frac{P_e}{T_W \eta_0^2} = \frac{1}{T_W \eta_0} > 0 \quad (39)$$

The internal dynamic is therefore unstable. So, it can be concluded that the system is unstable in a closed loop. The next stage is to offer a control which stabilizes the system in a closed loop.

3.3 In a Continuous Closed Loop Stability

The main purpose of the closed loop study of the system is to determine the condition stability of the state variable g . The stabilization of g will generate the stabilization of state variable q and consequently, the stabilization of internal dynamic. To this end, the expression of control is substitute in the dynamic equation of variable g .

$$\dot{g} = \frac{-1}{T_g} g + \frac{1}{T_g} u \quad (40)$$

With:

$$u = \frac{-A_t^2 g^3 T_g}{2\omega_R q^2} v + \frac{3T_g}{2T_w} \left(1 - \frac{q^2}{A_t^2 g^2}\right) g + g \cdot q \quad (41)$$

v being a variant of the linear control equation (26) which will allow us to stabilize the system. After substitution of equation (41) in equation (40) and simplification, we obtain:

$$\dot{g} = \left(-\frac{1}{T_g} + \frac{q}{T_g} + \frac{3}{2T_w}\right) g - \frac{3q^2}{2T_w A_t^2} \cdot \frac{1}{g} - \frac{A_t^2 g^3}{2\omega_R q^2} v \quad (42)$$

$$\begin{aligned} v = v_1 - k_4(g - g_{ref}) &= -k_1(y - y_{ref}) - k_2(\dot{y} - \dot{y}_{ref}) \\ &- k_3(\ddot{y} - \ddot{y}_{ref}) - k_4(g - g_{ref}) \end{aligned} \quad (43)$$

The previous dynamic equation becomes:

$$\begin{aligned} \dot{g} = m(g, q) = & \\ & \left(-\frac{1}{T_g} + \frac{q}{T_g} + \frac{3}{2T_W}\right)g - \\ & \frac{3q^2}{2T_W A_t^2} \cdot \frac{1}{g} - \frac{A_t^2 g^3}{2\omega_R q^2} v_1 + \frac{A_t^2 g^3 k_4}{2\omega_R q^2} (g - g_{ref}) \end{aligned} \quad (44)$$

With g_{ref} as constant.

It is then enough to choose k_4 so that g is stable and converges towards g_{ref} . It is necessary to note that the choice of gains k_1 , k_2 and k_3 assures that v_1 will converge on zero.

To determine k_4 , equation (44) is linearized around a functioning point (g_0, q_0) and the condition $\frac{\partial m(g, q)}{\partial g} \Big|_{(g_0, q_0)} < 0$, is put.

$$\begin{aligned} \frac{\partial m(g, q)}{\partial g} \Big|_{(g_0, q_0)} = & \\ & \frac{-1}{T_g} + \frac{q_0}{T_g} + \frac{3}{2T_W} + \frac{3q_0^2}{2T_W A_t^2 g_0^2} \\ & + \frac{A_t^2 (4g_0^3 - 3g_0^2 g_{ref}) k_4}{2\omega_R q_0^2} \end{aligned} \quad (45)$$

To assure the stability of the system whichever the point of operation is, it is necessary to choose k_4 according to the following relation:

$$\begin{aligned} k_4 \gg & \\ & -\left(\frac{-1}{T_g} + \frac{q_0}{T_g} + \frac{3}{2T_W} + \frac{3q_0^2}{2T_W A_t^2 g_0^2}\right) \frac{2\omega_R q_0^2}{A_t^2 (4g_0^3 - 3g_0^2 g_{ref})} \end{aligned} \quad (46)$$

The very upper condition (\gg) allows to make k_4 independent of the point (g_0, q_0)

3.4 Stabilizing Control

The new linear control which stabilizes external and internal dynamics is therefore

$$v = -k_1(y - y_{ref}) - k_2(\dot{y} - \dot{y}_{ref}) - k_3(\ddot{y} - \ddot{y}_{ref}) - k_4(g - g_{ref}) \quad (47)$$

Gains k_i ($i=0, \dots, 4$) are determined according to (31) and (46).

In this work, we start with a first resolution in which a simplifying hypothesis was taken into consideration, this hypothesis is based on two models acquired after decoupling of the total system, and therefore the controlled system will be on the order of 7. The input of its control is the excitation voltage and its output is the terminal voltage. As shown, in sequence resolution, this system is linearized by the linearization method by return of state, and then stabilized by a linear order, and the effectiveness of such strategy will be tested by simulation.

4 Simulation

This test consists in forcing at zero the voltage across the generator or infinite bus for 100 ms. The generator is initially charged to 60% at nominal power and not decoupled during the short-circuit from the network, which leads to important changes of the electric power. The role of power controller and rotor angle controller is to quickly maintain the terminal voltage and internal angle at their nominal values with minimum overshoot after the short-circuit.

Here, we test the performance of the proposed SISO controller, which was tested on the complete 7th order model of the turbine-generator system in a single machine infinite bus. The parameters are chosen from [1]. The stability of the system which is validated by simulating a short-circuit at the secondary of the generator's transformer for a period of 100 ms. We compare the performance of both the non-linear controller and the linear controller [5]. In Figures 2 to 5 we show the response of the terminal voltage v_t after a short-circuit in which it is shown the stabilization of v_t .

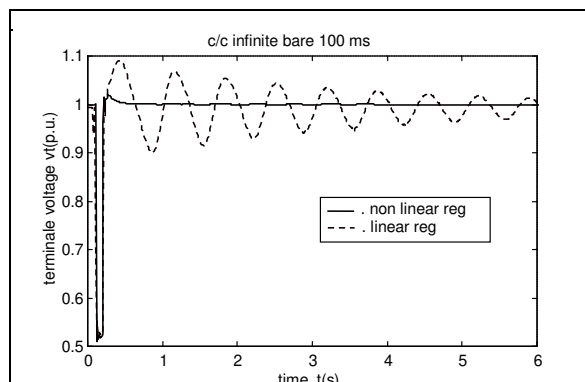


Figure 2
Terminal voltage v_t

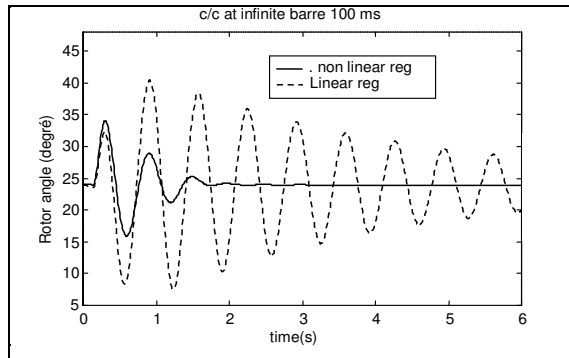


Figure 3
Rotor Angle δ

After using the non-linear controller, it is observed that the dynamics of the rotor angle has a much shorter time for the oscillations. The same remarks are made for the Figures 4 and 5.

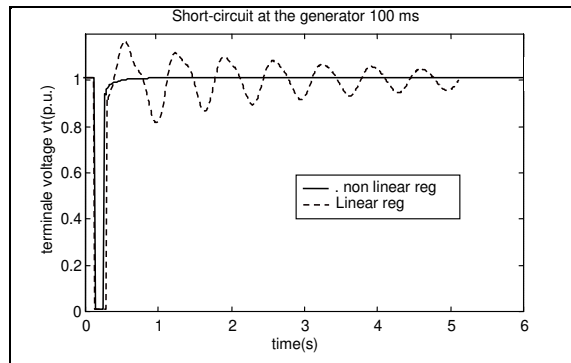


Figure 4
Terminal voltage v_t

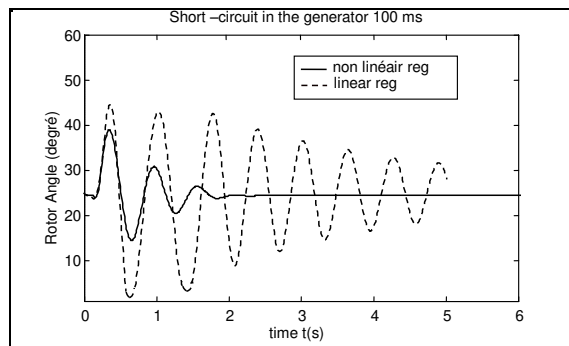


Figure 5
Rotor Angle δ

After the short-circuit the bus frequency and the rotor angle of generator stabilized 2 to 4 times more rapidly and the terminal voltage came back at the first position twenty times more quickly than with the non-linear regulator. These performances assure for the network to resist at the important disturbance without losing its synchronism.

Conclusion

The considered machine in this work comprises synchronous generator and hydraulic turbine. We used for control the nonlinear regulator based on the feedback linearization. The controller is tested in simulation and compared with classical linear scheme. In conclusion, the controller is able to power system damping and the post fault regulation of the generator terminal voltage even after a large fault [6]. All these performance compensating nonlinear meet standard linear regulators are due to the fact that the linearization by feedback state ensures the validity of a priori linear control around the state space. The superiority of non-linear regulators is largely due to the inclusion of nonlinearities. However, the price is that with nonlinear control regulators efforts are bigger and the control laws are much more complex. Their implementation requires faster processors and are therefore more expensive [7], [8].

References

- [1] Ouassima Akhrif, Francis-Aimé Okou, "Application of a Multivariable Feedback Linearization Scheme for Rotor Angle Stability and Voltage Regulation of Power Systems" IEEE Transactions on Power Systems, Vol. 14, No. 2, May 1999
- [2] Anderson, M and Fouad, A, "Power System Control and Stability", IEEE Press, 1993
- [3] H. F. Wang, Y. S. Hao, "An Adaptive Power System Stabilizer Based on Turbine Governor Control" IEEE 2nd international conference on advances in power system control, operation and management, Dec. 1993, Hong Kong
- [4] Do-Kwan Lee, Tae-Woong Yoon, "Adaptive Nonlinear Control of a Power System" Proceeding of the 1998 IEEE, International Conference on Control Applications, Trieste, Italy, 1-4 Sept. 1998
- [5] Okou, A. F. "Conception d'un régulateur non linéaire de tension et d'angle de charge pour un générateur synchrone", MS.Thesis, ETS, Montreal, 1996
- [6] M. Labben ben Braick, F. Fnaiech, "Feedback Linearization Control Technique Applied to a Three Phase Shunt Active Power Filter" IEEE, 2003
- [7] Yang Han et al., "Control Strategies, Robustness Analysis, Digital Simulation and Practical Implementation for a Hybrid APF with a Resonant AC-link." Acta Polytechnica Hungarica, Vol. 7, N°5, 2010
- [8] Belabbès B, "Commande Non Linéaire Robuste d'une Machine Synchrone à Aimants Permanents sans capteur Mécanique" Doctorat en ETT, Sidi Bel Abbès, Algérie 2007

Quantitative Characterization of Derivatization Effects in Separations Techniques

I. Derivatization of Ibuprofen

Anca-Gabriela Cârje¹, Zoltán Juvancz², Béla Tőkés¹

¹University of Medicine and Pharmacy, Tirgu Mureş, Physical Chemistry Laboratory, Romania

²Department of Environmental Engineering, Óbuda University, Budapest, Hungary, juvancz.zoltan@rkk.uni-obuda.hu

Abstract: Quantitative relations were studied between chiral separation parameters and chemical forms of ibuprofen. The structure, partition coefficients, enthalpy, entropy and free enthalpy change of inclusion complex formations of enantiomers have been established. Results of different methods were compared. The authors emphasis distinguished study of chiral recognition and the derivatization procedures.

Keywords: chiral separation methods; ibuprofen; derivatization; structure – selectivity relationship

1 Introduction

In this paper the authors perform a study of chemical structure dependence of separation methods' parameters among different conditions. Special attention was paid to effects of derivatization processes of analytes for the chiral recognition of permethylated β -cyclodextrin.

The chiral or asymmetric molecules cannot superimpose with molecules which are their mirror images [1]. A chiral molecule and its mirror image isomer are together called an enantiomeric pair. The members of enantiomer pairs are distinguished with (*R*) and (*S*) prefix according to Chan-Ingold-Prelog rules [2]. An old assignment of enantiomer pairs are the (+) and (-) symbols. Negative and positive symbols show the direction of torsion of polarized light (486 nm) in the solution of given enantiomer.

Enantiomeric pairs can show rather different biological effects, in spite of their very similar structures [3, 4]. The Contergan Scandal was a tragic example for the different effects of enantiomers. The Contergan (Thalodimide) a sedative pill was

sold as mixtures of members of enantiomers. The (*R*) isomer was harmless, but the (*S*) caused serious birth defects [5]. The possible biological difference between members of enantiomeric pairs has forced the authorities to introduce the directives of enantiomeric pure medicines [6]. These directives expect to commercialize only one member of an enantiomeric pair. A product can contain less than 0.1% of the other members of the enantiomeric pair. The requirement of chiral pure medicines makes the chiral selective analyses necessary.

Enantiomeric separations or chiral selective separations are a very challenging branch of chromatography [7]. The members of enantiomeric pairs are indistinguishable in homogeneous space. Their separations require a chiral separation agent: chiral stationary phase (CPS) or chiral mobile phase additives (CMA). The chiral separations need simultaneous three point interactions between the selectors and selectands [8]. It is not enough to have appropriate types of interaction groups in selector and selectand, but their appropriate steric arrangements are also required for the three point interactions. The separation of a given enantiomeric pair needs “tailor made” separation agents, which has its three interaction groups in appropriate steric arrangements. Trial and error method are used in several occasions to find the appropriate separation agent for the required chiral separation.

An efficient chromatographic system can separate enantiomeric pairs having only 0.1 kJ/mol interaction energy difference toward to the chiral separation media [9].

The chiral separations can be improved to choose appropriate derivatives of enantiomeric pairs and selectors [10, 11].

Our aim is to flash the theoretical background of successful chiral separations. This paper shows that the acidic hydrogen of acids can improve their chiral recognition via hydrogen bonds comparing the methyl ester derivatives of the these acids. Using our results may help to find the appropriate combinations of selector-selectand pairs for chiral separations in a more effective way than only the application of trial and error method.

Ibuprofen was chosen as model compound and starting material for further studies. Ibuprofen is an important nonsteroidal anti-Inflammatory drug (NSAID) used in the treatment of pain and inflammation in a variety of musculoskeletal and rheumatic disorders [12]. Ibuprofen, like other 2-arylpropionate derivatives (including ketoprofen, flurbiprofen, naproxen, etc.), does contain an asymmetric stereo center in the α -position of the propionate moiety. As such, there are two possible enantiomers of ibuprofen, with the potential for different biological effects and metabolism for each enantiomer [13, 14]. Indeed, the (*S*)-(+)-ibuprofen was found to be the active form both *in vitro* and *in vivo*. It was logical, then, that there was the potential for improving the selectivity and potency of ibuprofen formulations by marketing ibuprofen as a single-enantiomer product (dexibuprofen) [15]. Further *in vivo* testing, however, revealed the existence of an

isomerase (*alpha-methylacyl-CoA racemase*), which converted (*R*-)-ibuprofen to the active (*S*+)-enantiomer [16].

Enantiospecific analytical methodology is suitable for the determination of the enantiomeric ratio of the drug and its metabolites. The determination of enantiomeric ratio is essential in order to evaluate the significance of stereoselectivity both in terms of drug action and disposition. Enantiomer selective GC [17], HPLC [18], SFC [19] and CE [20] methods have been developed for the ibuprofen. Many of these methods use cyclodextrins as chiral selective agents. In this study, the stereo selective separation mechanism of ibuprofen has been studied using permethylated- β -cyclodextrin as chiral selective agent. The sterical arrangements and thermodynamic parameters of interactions between the permethylated- β -cyclodextrin and enantiomers of ibuprofens have been established. The methodology of our report is same as the one used in our previous studies [21, 22]. It was established, that ibuprofen and its methyl ester derivatives have different chiral recognition mechanism among GC conditions. These results were compared and interpreted with the literature data. Our data was compared to literature data of CE separations referring to the selectivity differences between undissociated and the dissociated forms of ibuprofens toward to β -cyclodextrin.

2 Experimental

2.1 Compounds

The (*R,S*)-Ibuprofen or (*R,S*)-2-(4-(2methylpropyl)-phenyl)-propionic acid, Nitroso(N)-methyl-carbamide methylation agent, n-hexane and diethyl ether are product of Sigma-Aldrich.

2.2 Instrumental

The samples were measured on Shimadzu QP5000 GC/MS instrument (Shimadzu Inc., Kyoto, Japan). The experimental conditions were the following: column, 25 m x 0.22 mm FSOT; stationary phase, Cydex-B (0.25 μ m); (SGE); carrier, He. The used chiral selective stationary phase (Cydex-B) is a mixture of silicone polymer and permethylated- β -cyclodextrin.

2.3 Procedures

Methyl ester of ibuprofen was synthesized by standard methylation procedure with Nitroso(N)-methyl-carbamide via diazomethane intermediate [23]. The retention times of free acid and methyl esters of ibuprofen were measured at least 4 times in different temperatures. This data was sufficient for thermodynamic calculations.

3 Results

The structural formulas of enantiomers of ibuprofen (*RS*)-2-(4-(2methylpropyl)-phenyl)-propionic acid are presented in Figure 1.

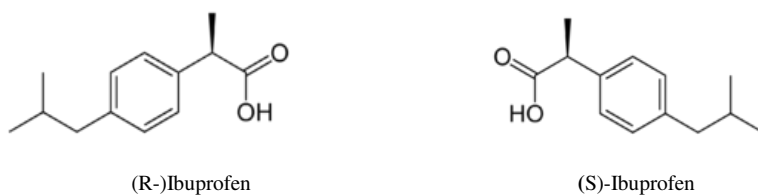


Figure 1

Structures of ibuprofen enantiomers. Figures show how the enantiomers of ibuprofen are mirror images of each other, but are not superimposable.

Figure 2 is a representative chromatogram of ibuprofen enantiomeric pairs in free acid forms among GC conditions.

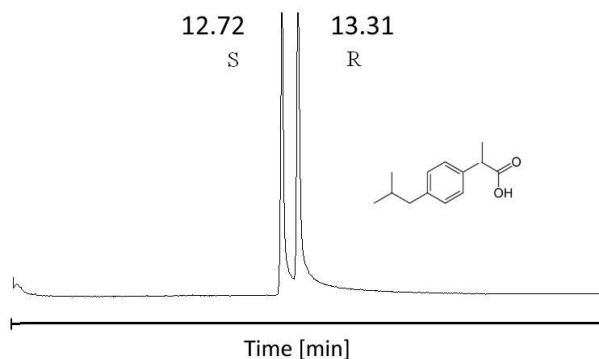


Figure 2

The separation of ibuprofen enantiomers in acid form with GC.

Parameters: Instrument, Shimadzu QP5000 GC/MS; column, 25 m x 0.22 mm FSOT; stationary phase, Cydex-B (0.25 μ m); carrier, He (50 cm/sec); analysis temperature, 180°C.

Table 1
Raw data of selectivity- analysis relationship for ibuprofen (free acid)*

t°C	(1/T)10 ³	α	ln α
170	2.257	1.06601	0.06392
180	2.208	1.05548	0.05399
190	2.160	1.04501	0.04403
200	2.114	1.03458	0.03399

*Symbols: t , temperature (°C); T , absolute temperature (K); α , selectivity

The (ln α , 1/T) linear correlation is describable by the following equation:

$$\ln \alpha = (0.2091 \pm 0.0025)10^3/1/T - (0.4078 \pm 0.0054) \quad \text{Eq. 1.}$$

$$R = 0.99986, N = 4, SD = 0.00026$$

The excellent linearity of the equation 1 shows that the interaction processes allowing the chiral recognition of ibuprofen belonging to one mechanism, because the equation 1 is linear. The high regression value also underlines that the measurements have high precision values.

As we have demonstrated before [21, 22]:

$$\ln \alpha = \ln (K_B/K_A) = \Delta(\Delta\mu_{BA}^{\circ})/RT = \Delta_{BA}\Delta G^{\circ}/RT \quad \text{Eq. 2}$$

In these relations the symbols are the following: K_B and K_A show the distribution ratios of A and B compounds between the stationary phase and mobile phase; ΔG° , ΔH° and ΔS° represent the normal free enthalpy, enthalpy and entropy changes respectively of the participant chemical processes. The notations $\Delta_{BA}\Delta$ refer to the difference between two forms proposed for separation. In this case the questionable compounds are the enantiomers R , S . The signs of differences are conditioned by the relative values of enantiomer parameters, so hereinafter will appear only with absolute values.

Thermodynamic parameters of chiral selective interactions between ibuprofen (free acids) enantiomers are the following:

$$\Delta_{RS}\Delta H^{\circ} = 0.209 \times 10^3 R = 1.738 \text{ kJ/mol K}$$

$$\Delta_{RS}\Delta S^{\circ} = 0.408 \times R = 3.392 \text{ J/mol}$$

$$\Delta_{RS}\Delta G^{\circ} = \Delta_{RS}\Delta H^{\circ} - T\Delta_{RS}\Delta S^{\circ} = 0.812 \text{ kJ/mol K}$$

The corresponding methyl esters of ibuprofen were graphically illustrated (Fig. 3), chromatograms were measured (Figure 4), calculations (Table 2) were done and equations established (Table 2) with similar to free acids.

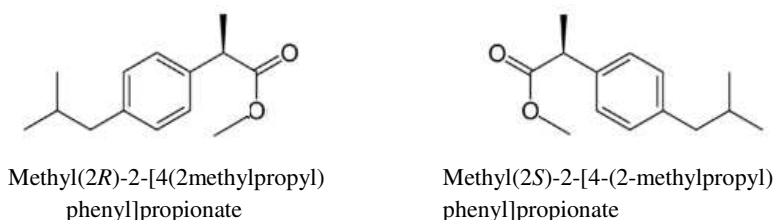


Figure 4

Structure of methyl ester derivatives of ibuprofen enantiomers

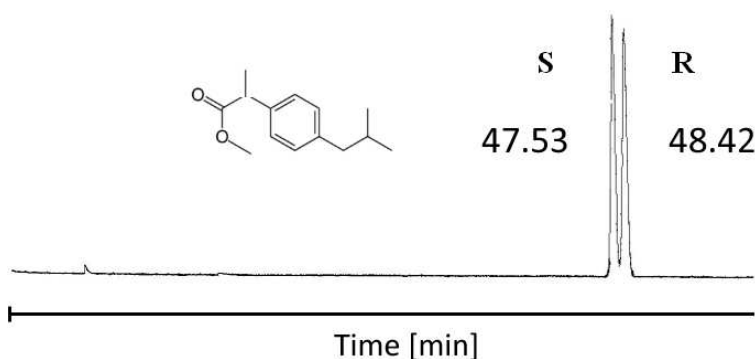


Figure 3

The separation of ibuprofen enantiomers in methyl ester forms with GC.

Parameters: Instrument, Shimadzu QP5000 GC/MS; column, 25 m x 0.22 mm FSOT; stationary phase, Cydex-B (0.25 μm); carrier, He (50 cm/sec); analysis temperature, 110°C.

The peaks of ibuprofen-methyl ester had excellent symmetrical peak shapes. The quantitative determination of secondly eluting isomer can be done without difficulties even if it had only 0.1 % ratio at 100°C. The symmetrical peaks of methyl esters showed high efficiency (4570 theoretical plates/meter), but the tailings of free acids produced broader, less efficient peaks (2150 theoretical plates/meter).

Table 2

Raw data of selectivity- analysis relationship for ibuprofen methyl ester

$t^{\circ}\text{C}$	$(1/T)10^3$	α	$\ln \alpha$
100	2.681	1.02829	0.02790
110	2.611	1.02170	0.02147
120	2.545	1.01700	0.01686
130	2.481	1.01260	0.01252

$$\ln \alpha = (0.0763 \pm 0.0042)10^3/T - (0.177 \pm 0.011) \quad \text{Eq. 3}$$

$$R = 0.9971 \quad N = 4 \quad SD = 0.00060$$

Thermodynamic parameters of chiral selective interactions between ibuprofen methyl esters enantiomers are the following:

$$\Delta_{RS}\Delta H^{\circ} = 0.0763 \times 10^3 R = 0.634 \text{ kJ/mol K}$$

$$\Delta_{RS} \Delta S^{\circ} = 0.0772 R = 0.642 \text{ J/mol}$$

$$\Delta_{RS}\Delta G^{\circ} = \Delta_{BA}\Delta H^{\circ} - T\Delta_{BA} \Delta S^{\circ} = 0.459 \text{ kJ/m}$$

Comparing the results, the free acid shows much higher selectivity ($\Delta_{RS}\Delta G^{\circ} = 0.812 \text{ kJ/mol K}$) than in the case of methyl ester ($\Delta_{RS}\Delta G^{\circ} = 0.459 \text{ kJ/mol K}$). Similar relative values are also observed at the thermic effects and entropic phenomena. But, at comparison, it must observe that the working temperatures differ to a great extent (nearly to 100°C). The differing polarity of free acid and ester is decisive. Most likely, the H-bridge interactions of free acids with the cyclodextrins are supplementary key interactions from the point of view of chiral recognitions.

Esters with longer alky chains or branching (e.g. ethyl, propyl, isopropyl) probably result in less selectivity than methyl ester, similar to amino acids, and pyrethroid acids [24].

Other derivatives of cyclodextrins have been also applied for chiral GC separation of ibuprofen [25, 26, 27]. Comparing the results of different separations, the permethylated- β -cyclodextrin based stationary phases show the highest selectivity toward the free acid of ibuprofen.

It is very edifying to compare the results to those from the literature by CE obtained for the same enantiomer pairs [28]. The effect of temperature on the electrophoretic chiral separation of ibuprofen with β -CD was investigated. Ibuprofen has a temperature independent pK_a value of 4.36. At that same temperature ($t = 25^{\circ}\text{C}$), formation constants K_1 for the uncharged enantiomers (at pH 4.20) are approximately just the same ($10^4 M$). The formation constant K_2 for the charged form, determined at pH 6.55, where only interaction between the fully charged ibuprofen and β -CD takes place, is $5.10^3 M$ for both isomers. From the temperature dependence of these chiral formation constants, we have calculated the corresponding thermodynamic parameters, and the results obtained we have compared to our results (Table 3).

Table 3

The effect of temperature on the chiral interaction parameters between ibuprofen and β -CD at ionic strength 10.0 mMol / L [28]

t ($^{\circ}\text{C}$)	(1/T)* 10^3 (K^{-1})	K_1^* (M)	ln K_1	K_2^* (M)	ln K_2	d K_1^* (M)	ln d K_1
25	3,354	10124	9.223	5256	8.567	339	5.826
32	3,277	6089	8.714	3550	8.175	213	5.361
40	3,193	3692	8.244	2139	7.668	112	4.718
50	3,095	3011	8.010	1675	7.424	78	4.357

* K_1 denotes the formation constant for the uncharged enantiomer, K_2 represents the formation constant for the charged form, and d K_1 is the difference of the stability constants for the uncharged compound.

In the case of undissociated (uncharged) ibuprofen we have obtained the following regression equation:

$$\ln K_1 = (4,72 \pm 0,71)10^3/T - (6,69 \pm 2,30) \quad \text{Eq. 4}$$

$$R = 0.978 \quad N = 4 \quad SD = 0.137$$

The thermodynamic parameters were calculated from van't Hoff relation:

$$\ln K_1 = -\Delta G^0/RT = -\Delta H^0/R \cdot 1/T + \Delta S^0/R \quad \text{Eq. 5}$$

Wherein the notation is the same as explained earlier.

$$\Delta H^0 = 4.72 \cdot 10^3 R = 39.22 \text{ kJ/mol K}$$

$$\Delta S^0 = -6.69 R = -55.59 \text{ J/mol} = -0.056 \text{ kJ/mol K}$$

$$\Delta G^0 = \Delta H^0 - T \Delta S^0 = 39.22 + 273 \times (-0.056) = 54.51 \text{ kJ/mol K}$$

The dissociated (charged) ibuprofen has the following characteristics:

$$\ln K_2 = (4,54 \pm 0,56)10^3/T - (6,69 \pm 1,80) \quad \text{Eq. 6}$$

$$R = 0.985 \quad N = 4 \quad SD = 0.108$$

The thermodynamic parameters:

$$\Delta H^0 = 4.53 \times 10^3 R = 37695.68 \text{ J/mol K} = 37.70 \text{ kJ/mol K}$$

$$\Delta S^0 = -6.69 R = -55.60 \text{ J/mol K} = -0.056 \text{ kJ/mol K}$$

$$\Delta G^0 = \Delta H^0 - T \Delta S^0 = 37.70 - 273 \times (-0.056) = 52.98 \text{ kJ/mol K}$$

As it is visible, the values obtained for K_1 are higher, as was the case with K_2 . It can be seen that both K_1 and K_2 decrease monotonously with increasing temperature. The negative sign of ΔH (exothermic effect) indicates a decrease of enthalpy, due to the release of high energy water out of the cyclodextrin cavity, and forming of more stable bonds with complexants. The negative sign of ΔS alludes to a decrease of entropy, due to complex formation, which consequently results in a decrease of the degree of freedom of the components involved in the interaction. As expected, the dominant force for analyte binding arises from enthalpy changes.

There is a similarity between derivatization by ester-formation and the dissociation equilibrium of ibuprofen. The ester and the uncharged forms are most apolar and consequently give rise to most stable inclusion complexes. This conclusion is demonstrated by in the Table 3 recapitulated experimental results.

As expected, the selectivity grows with increasing β -CD concentration and dropping temperature in the measured range. The calculated selectivity maximum in the function of concentration of selector is higher than the saturation concentration of β -CD. In CE, the maximum of the resolution of enantiomers

show a maximum curve in the function of selector concentration according to the Wren equation [29]. Namely the concentration values of selector are in first degree in the numerators, but they are in the second degree in the denominators.

Other derivatives of cyclodextrins have been also applied for chiral separation of ibuprofen in CE [30-33]. Good separations were achieved using amino substituted permethylated 6-monoamino-6-monodeoxy- β -cyclodextrin and heptakis(2,3-dimethyl-6-amino-6-deoxy)- β -cyclodextrin, because the oppositely charged selectors and selectand can show high resolutions in CE [29].

The heptakis(2,3-di-O-methyl-6-amino)- β -CD proved the best selector (Figure 3). Even 0.5 mMol concentration of this selector produced R_s 2.18 value.

The retention or migration orders of the enantiomers are a very important factor in the determination of trace impurities [34, 35]. The tailing of the major peak can mask that of the minor compounds if the minor is coming later. The *S* isomers of ibuprofen elutes first in every instance using cyclodextrin base stationary phases in GC. On the other hand, the migration orders of enantiomers can be reverse in CE according to which isomers the minor components are. The first migrating peak is *R* isomer of ibuprofen using permethylated 6-monoamino-6-monodeoxy- β -cyclodextrin selector [32, 33]. The *S* isomer of ibuprofen is the first migrating peak using heptakis(2,3-dimethyl-6-amino-6-deoxy)- β -cyclodextrin [32]. The selectivity mechanism of the two selectors are the same, but migration directions are opposite with these selector, because the electroosmotic flow is reverse in the case of heptakis(2,3-dimethyl-6-amino-6-deoxy)- β -cyclodextrin.

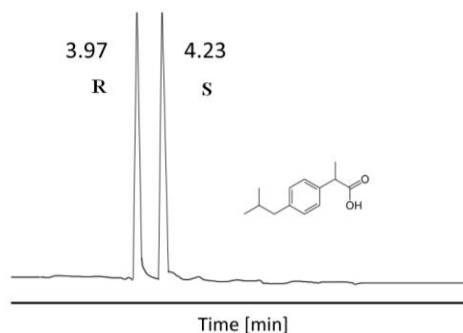


Figure 4

Separation of enantiomers of ibuprofen in free acid form with CE. Parameters: Instrument Hewlett Packard ^{3D}CE; column, 48.5 cm x 50 μ m I.D. FSOT; background electrolyte, Britton Robinson 50 mM (pH5); selector, 0.5 mMol heptakis(2,3-di-O-methyl-6-amino)- β -CD; analysis temperature, 20°C [32].

Conclusion

There is a visible analogy between the derivatization (esterification) and the acid-base dissociation equilibrium. In the both cases the undissociated acid forms give birth with cyclodextrins more selective inclusion complexes, although the fine mechanism of complex formation differs.

Specifically for the chiral separation parameters, it was observed that the stability constant and the selectivity values decrease with increasing temperature, with negative values for both free energy and entropy changes. This means that when optimizing a chiral separation, using the present model, a different operating temperature may lead to different optimized conditions: selectivity will generally be lower at elevated temperatures.

The general rule can be drawn from our results. High resolution can be achieved for enantiomer of nonsteroidal anti-inflammatory drugs using permethylated- β -cyclodextrin containing chiral stationary phase in GC. The free acids show higher selectivity than methyl ester derivatives, but show significant tailing of the peaks. Methyl esters of these enantiomers are recommended derivatives for their GC analysis.

Very high resolutions can be achieved for the nonsteroidal anti-inflammatory drugs using aminosubstituted derivatives of cyclodextrins among CE conditions.

Acknowledgement

This research was partly sponsored by OTKA K72861 grant. The valuable consultations are highly appreciated by Dr. R. Iványi.

References

- [1] R. K. Sharma: Stereochemistry, Discovery Publishing House, New Delhi, 2008
- [2] Sudhir Chandra Pal, Nomenclature of Organic Compounds, Alpha Science International, Pangbourne, 2008
- [3] S. M. Batra, M., A. P. Bhaduri: Chirality and Future Drug Design, Progress in Drug Research 41 (1994) 191
- [4] M. Simonyi, G. Maksay: Stereochemical Aspects of Drug Action II: Optical Isomerism, The practice of Medicinal Chemistry, Academic Press Budapest 1996
- [5] W. Freitag: Contergan, Waxmann Verlag GmbH, Münster 2005
- [6] Department of Health and Human Service of the USA, Food and Drug Administration's Policy Statement for the Development of New Stereoisomeric Drugs, Fed. Regist. 57/ 2 May (1992) 102
- [7] F. Toda (Editor): Enantiomer Separation: Fundamentals and Practical Methods, Kluwer Academic Publisher, Dordrecht 2010
- [8] V. R. Meyer, M. Rais: A Vivid Model of Chiral Recognition, Chirality 1 (1989) 167
- [9] V. Schurig: Enantiomer Separation by Gas Chromatography on Chiral Stationary Phases, J. Chromatogr. A 666 (1994) 111

- [10] Z. Juvancz, V. Kiss, J. Schindler and J. Bálint: Use of Achiral Derivatization to Increase Selectivity and Reverse the Order of Elution of Enantiomers on Chirasil-Dex, *Chromatographia* 60S (2004), S161
- [11] S. Fanali, C. Desiderio, Z. Aturk: Enantiomeric resolution study by capillary electrophoresis: Selection of the appropriate chiral selector, *J. Chromatogr. A* 772 (1997) 185
- [12] P. C. Gøtzsche: Non-steroidal anti-inflammatory drugs, *British Medical J.* 320 (2000) 1058
- [13] M. A. Hamman, G.A. Thompson, S.D. Hall: Regioselective and stereoselective metabolism of ibuprofen by human cytochrome P450, *Biochem. Pharmacol.* 54 (1997) 33
- [14] M. Niemi, P. Neuvonen, Janne Backman: Stereoselective interaction between the CYP2C8 inhibitor gemfibrozil and racemic ibuprofen, *Eur. J. Clin Pharmacol.* 27 (2007) 463
- [15] G. Leising, R. Resel, F. Stelzer, *et al.*: Physical aspects of dexibuprofen and racemic ibuprofen, *J. Clin. Pharmacol.* 36 (1996) 3
- [16] V. Wsól, L. Skálová, B. Szotáková: Chiral inversion of drugs: coincidence or principle?, *Curr. Drug Metab.* 5 (2004) 517
- [17] G. Cretu, M. Ionică, A. F. Dănet, *et al.*: Separation of the enantiomers of ibuprofen by a gas chromatographic–mass spectrometric method, *Acta Chromatographica* 15 (2005) 315
- [18] Jincui Ye, W. Yu, G. Chen, *et al.*: Enantiomeric separation of 2-arypropionic acid nonsteroidal anti-inflammatory drugs by HPLC with hydroxypropyl-beta-cyclodextrin as chiral mobile phase additive, *Biomed. Chromatogr.* 24 (2009) 17
- [19] M. Johannsen: Separation of enantiomers of ibuprofen on chiral stationary phases by packed column supercritical fluid chromatography, *J. Chromatogr. A* 937 (2001) 135
- [20] F. Główka, M. Kraźniewicz: Enantioselective CE method for pharmacokinetic studies on ibuprofen and its chiral metabolites with reference to genetic polymorphism, *Electrophoresis.* 28 (2007) 2726
- [21] B. Tóké, Z. Juvancz, R. Iványi, S. Vancea, G. Donáth-Nagy, V. Schurig, A. Cârje: Temperature Dependence of Enantiomer Separation Parameters by Gas-Chromatographic and Supercritical Fluid Chromatographic Methods, *Studia Universitatis Babeş-Bolyai Chemia* 54 (2009) 93
- [22] B. Tóké, Z. Juvancz, R. Iványi, G. Donáth-Nagy, S. Vancea, V. Schurig, A. Cârje: Chemical Structure Dependence of Separation Methods Parameters, *Studia Universitatis Babeş-Bolyai, Chemia* 54 (2009) 103
- [23] K. Blau, G.S. King (Eds.): *Handbook of derivatives for chromatography*, Heyden & Son, N.Y. 1977

- [24] Z. Juvancz, P. Petersson: Enantioselective Gas Chromatography, *J. Microcol. Sep.* 8 (1996) 99
- [25] G. Cretu, M. Ionica, A.F. Daner, H. Aboul-Enein, R. Macover, M. Buleandra: Separation of the enantiomers of ibuprofen by gas chromatographic-mass spectrometric method, *Acta Chromatographica* 15 (2005) 315
- [26] http://www.restek.com/chromatogram/view/GC_PH00242 (22.04.2013)
- [27] H. Hühnerfuss, S. Selke, R. Kallenborn, J. Kuhlmann, S. Weigel: Enzymatic transformation of chiral pharmaceuticals in the environment as revealed by enantioselective chromatography, *Natural halogenated and chiral compounds* 68 (2006) 17
- [28] J. C. Reijnga, B. A. Ingelse, F. M. Everaerts: Thermodynamics of chiral selectivity in capillary electrophoresis: separation of ibuprofen enantiomers with β -cyclodextrin, *Journal of Chromatography A*, 792 (1997) 371
- [29] S.A. Wren, R.C. Rowe: Theoretical aspects of chiral separation in capillary electrophoresis: I. Initial evaluation of a model, *J. Chromatogr. A* 603 (1993) 235
- [30] B. K. Patel, M. Hanna-Brown, M. R. Hadley, A. J. Hutt: Enantiomeric resolution of 2-arylpropionic acid nonsteroidal anti-inflammatory drugs by capillary electrophoresis: Methods and applications, *Electrophoresis* 25 (2004) 2625
- [31] R. Hamoudova, M. Pospisilova: Determination of ibuprofen and flurbiprofen in pharmaceuticals by capillary zone electrophoresis, *J. Pharm. and Biomed. Anal.* 41 (2006) 1463-1467
- [32] R. Iványi, L. Jicsinszky, Z. Juvancz: Single isomer permethylated amino cyclodextrins for chiral selective capillary electrophoresis 24th Int. Symp. on Cap. Chromatogr. Las Vegas (2001)
- [33] J. Olsson: New Techniques for Chiral Separations, Dissertation Karlstadt University 2008
- [34] V. Schurig: Separation of enantiomers by gas chromatography, *J. Chromatogr. A* 906 (2001) 275
- [35] L.G. Blomberg, H. Wan: Determination of enantiomeric excess by capillary electrophoresis, *Electrophoresis* 21 (2000) 1940